

# Sheffield Hallam University

*The effect of fictional and thermal forces upon sea bed pipeline buckling behaviour.*

GAN, Aik Ben.

Available from the Sheffield Hallam University Research Archive (SHURA) at:

<http://shura.shu.ac.uk/19217/>

## A Sheffield Hallam University thesis

This thesis is protected by copyright which belongs to the author.

The content must not be changed in any way or sold commercially in any format or medium without the formal permission of the author.

When referring to this work, full bibliographic details including the author, title, awarding institution and date of the thesis must be given.

Please visit <http://shura.shu.ac.uk/19217/> and <http://shura.shu.ac.uk/information.html> for further details about copyright and re-use permissions.

POLYTECHNIC LIBRARY  
POND STREET  
SHEFFIELD S1 1WB

6798

100 453 801 4

TELEPEN



**Sheffield City Polytechnic Library**

**REFERENCE ONLY**

ProQuest Number: 10694097

All rights reserved

INFORMATION TO ALL USERS

The quality of this reproduction is dependent upon the quality of the copy submitted.

In the unlikely event that the author did not send a complete manuscript and there are missing pages, these will be noted. Also, if material had to be removed, a note will indicate the deletion.



ProQuest 10694097

Published by ProQuest LLC (2017). Copyright of the Dissertation is held by the Author.

All rights reserved.

This work is protected against unauthorized copying under Title 17, United States Code  
Microform Edition © ProQuest LLC.

ProQuest LLC.  
789 East Eisenhower Parkway  
P.O. Box 1346  
Ann Arbor, MI 48106 – 1346

FOR USE IN LIBRARY  
ONLY

1/22



SHEFFIELD CITY POLYTECHNIC  
ERIC MENSFORTH LIBRARY  
POND STREET  
SHEFFIELD  
S1 1WB

THESIS

'D' NO:

FOR USE IN THE LIBRARY ONLY

AUTHOR ...GAN, A.B:.....

TITLE ..Effect.. of.. Fractional + thermal forces.....  
upon sealed pipeline buckling behaviour:..

CONDITIONS

OF LOAN/CONSULTATION: ...Reference only.....

---

I undertake that neither the whole nor any part of the above-mentioned thesis shall be copied, quoted or published without the consent of the Author and of the Sheffield City Polytechnic.

This undertaking is to be signed by the reader consulting the thesis.

---

Name

Organisation

Signature

Date

THE EFFECT OF FRICTIONAL AND THERMAL FORCES  
UPON SEA BED PIPELINE BUCKLING BEHAVIOUR

AIK BEN GAN BSc.

A thesis submitted to the Council for National  
Academic Awards in partial fulfilment of the  
requirements for the degree of Doctor of Philosophy.

Sponsoring Establishment

SHEFFIELD CITY POLYTECHNIC

Department of Civil Engineering

Collaborating Establishments

University of Surrey

and

J.P. KENNY AND PARTNERS

Pipeline Consultants

December 1985



100 11538

The Effects of Frictional and Thermal Forces  
upon Sea Bed Pipeline Buckling Behaviour

The objective of the research programme has been to develop design parameters applicable to in-service submarine pipeline buckling behaviour. The programme has involved experimental and theoretical studies and computer graphics are widely employed throughout. Initially, as detailed in Chapter 1, the necessary buckling mechanisms in pipelines subjected to axial compression have been identified and analysed in the form of relatively basic fully mobilised studies. In addition, errors and limitations contained within these studies have been determined and delineated. Consequently, geotechnical experimentation as reported in Chapter 2 was deemed necessary particularly given the dearth of information available relating to the nature of the friction resistance force between the pipeline and its supporting medium. Full scale values for the axial and lateral friction coefficients together with their respective fully mobilised displacements have been deduced upon the basis of model tests. A semi-empirical formula has thereby been produced for use in design practice. Further, a novel interpretation of sea bed recovery, or the pipeline's submerged self-weight inertial characteristics associated with vertical buckling, has also been determined.

Following on from the above geotechnical study, more refined quasi-idealised analyses, dealt with in Chapter 3, have been undertaken incorporating the appropriate full scale deformation-dependent axial and lateral friction-response loci together with the respective sea bed recovery characteristics. These analyses enable, for the first time, definition of the appropriate critical temperature rise at which axial-flexural bifurcation occurs. Finally, noting that previous buckling analyses have been based on quasi-idealised buckling phenomena, attempts have also been made to incorporate practical submarine pipeline imperfections. Pipelines are not perfectly straight in field conditions and, consequently, the imperfection studies denoted in Chapter 4 have attempted to model the appropriate behaviour. Design charts have been produced accordingly and suggestions made regarding further studies.

# CONTENTS

Advanced Studies Undertaken	4	
List of Tables	5	
List of Figures	6	
Acknowledgements	9	
Abstract	10	
CHAPTER 1	INITIAL CONSIDERATIONS	11
1.1	Introduction	11
1.2	Elastic Buckling - The Phenomenon	13
1.3	Submarine Pipeline Buckling	20
1.3.1	Historical Résumé	20
1.3.2	The Buckling Mechanism	25
1.3.3	Boundary Conditions	29
1.3.4	Derivation of Field Equations	35
1.3.5	Interface Compatibility	39
1.3.6	Primary Parameters	41
1.3.7	Geotechnical Factors	42
1.4	Fully Mobilised Quasi-Idealised Analyses	42
1.4.1	Introduction	42
1.4.2	Lateral Mode 1 Analysis	43
1.4.3	Lateral Mode 2 Analysis	50
1.4.4	Lateral Mode 3 Analysis	53
1.4.5	Lateral Mode 4 Analysis	58
1.4.6	Lateral Mode $\infty$ Analysis	63
1.4.7	Vertical Mode Analysis	66
1.4.8	Discussion	73

1.5	Summary	81
CHAPTER 2	GEOTECHNICAL EXPERIMENTATION	83
2.1	Introduction	83
2.2	Friction Force Characteristics	84
2.3	Experimental Programme	88
2.4	Experimental Procedure	90
2.5	Experimental Observations and Results	91
2.6	Axial and Lateral Friction Force Characteristics - Assimilation	103
2.7	Sea Bed Recovery	108
2.8	Preliminary Design Considerations	116
2.9	Summary	125
CHAPTER 3	QUASI-IDEALISED CRITICAL STATE STUDIES	127
3.1	Introduction	127
3.2	Essential Structural Relationships	132
3.3	Lateral Mode Analyses: Deformation- Dependent Axial Resistance in Conjunction with Fully Mobilised Lateral Resistance	138
3.3.1	Lateral Mode 1	138
3.3.2	Lateral Modes 2, 3 and 4	141
3.3.3	Assimilation - Lateral Modes	143
3.4	Vertical Mode Analysis: Deformation- Dependent Axial Resistance in Conjunction with Fully Mobilised Submerged Self-Weight	144
3.5	Lateral Mode 1: Deformation-Dependent Axial and Lateral Friction Resistances	149
3.6	Vertical Mode: Deformation-Dependent Axial Resistance in Conjunction with Sea Bed Recovery Characteristics	154

3.7	Summary	164
CHAPTER 4	IMPERFECTION STUDIES	170
4.1	Introduction	170
4.2	Lateral Mode 1 Analysis	176
4.3	Lateral Mode 2 Analysis	184
4.4	Vertical Mode Analysis	191
4.5	Assimilation	196
4.6	Summary	207
CHAPTER 5	COMMENTS AND CONCLUSIONS	211
5.1	Primary Assessments	211
5.2	Associated Factors	215
5.3	Suggestions for Further Studies	216
CHAPTER 6	APPENDICES	
I	Publications	A1
II	Geotechnical Results	A36
III	Programme Listings	A58
IV	Notation	A66
V	References	A70

ADVANCED STUDIES UNDERTAKEN

1983	Fortran Programming Course
Autumn Term	Computer Services
	Sheffield City Polytechnic
1983-84	Advanced Structures Course
October-March	Department of Civil Engineering
	Sheffield City Polytechnic
1984	Computer Graphics Course
Spring Term	Computer Services
	Sheffield City Polytechnic

## LIST OF TABLES

Table	Title	Page
1.1	Boundary Conditions	34
1.2	Pipeline Parameters	44
1.3	Action-Response Data at $T_{\min}$ State for Lateral Mode 4	77
2.1	Friction Coefficients	98
3.1	Constants for All Buckling Modes	133
3.2	Percentage of Region Subjected to Fully Mobilised Resistance Employing the Fully Mobilised Friction Force Criterion	136
3.3	c - Dependent Output Data	160
3.4	Quasi-Idealised Post-Buckling Data	166
4.1	Quasi-Idealised/Fully Mobilised Analyses - Stress Trends at $T_{\min}$	171
4.2	Maximum Temperature Rise, $T_m$	198
4.3	Temperature Rise at First Yield, $T_y$	199

LIST OF FIGURES

Figure	Title	Page
1.1	Idealised Linear Axial Compression System	14
1.2	Quasi-Idealised Buckling System	16
1.3	Combined Plate and Column Buckling- Imperfection Snap	21
1.4	Rail Track Friction Model	23
1.5	Lateral Buckling Mode Topologies	24
1.6	Lateral Mode 1 Buckling Topology	26
1.7	Slip Length Detail	31
1.8	Flexural Topology	36
1.9	Interface Compatibility	40
1.10	Fully Mobilised Lateral Mode 1 Model	45
1.11	Vertical Mode - Details of Fully Mobilised Model	67
1.12	Comparison of Lateral Modes ( $\phi_A = \phi_L = 0.5$ )	74
1.13	Lateral Mode 4 - $\phi_A = 0.1$	75
1.14	Lateral Mode 4 - $\phi_A = 0.3$	75
1.15	Lateral Mode 4 - $\phi_A = 0.5$	76
1.16	Lateral Mode 4 - $\phi_A = 0.7$	76
1.17	Results for Vertical Mode	79
2.1	Simplified Vertical Mode Topology	85
2.2	Simplified Lateral Mode 1 Topology	85
2.3	Slip Length Characteristics	86
2.4	Sieve Analysis	86

Figure	Title	Page
2.5	Schematic (Plan) View of Pipe under Arbitrary/Lateral Forces ( $0^\circ \leq \theta < 90^\circ$ )	89
2.6	Schematic (Side) View of Pipe under Axial Force ( $\theta = 90^\circ$ )	89
2.7	Force-Displacement Relationships $\theta = 0^\circ$	92
2.8	Force-Displacement Relationships $\theta = 15^\circ$	92
2.9	Force-Displacement Relationships $\theta = 30^\circ$	93
2.10	Force-Displacement Relationships $\theta = 45^\circ$	93
2.11	Force-Displacement Relationships $\theta = 60^\circ$	94
2.12	Force-Displacement Relationships $\theta = 75^\circ$	94
2.13	Force-Displacement Relationships $\theta = 90^\circ$	95
2.14	Graphs of Friction Coefficient against $\theta$	99
2.15	Generalised Axial Friction Characteristics	104
2.16	Generalised Lateral Friction Characteristics	105
2.17	Sea Bed Loading and Unloading Loci	110
2.18	Stress-Strain Loci	112
2.19	Sea Bed Foundation Stiffness Topology	113
2.20	Sea Bed Recovery Loci	115
2.21	Axial Force-Displacement Characteristics	121
2.22	Slip Length Ratio Characteristics	121
3.1	Post-Buckling Characteristics	129
3.2	Revised Buckling Topology - Lateral Mode 1	139
3.3	Comparison of Lateral Buckling Modes	142
3.4	Revised Buckling Topology - Vertical Mode	145
3.5	Individual Rational Modelling Loci - Vertical Mode	148
3.6	Rational Modelling for Lateral Mode 1	153

Figure	Title	Page
3.7	Vertical Mode - Details of Rational Model	155
3.8	Composite Rational Modelling Locus - Vertical Mode	159
3.9	Critical Temperature Rise Assessment	162
3.10	Post-Buckling Mechanism	165
4.1	Pin-Ended Strut - Imperfection Topology	175
4.2	Details of Lateral Mode 1	177
4.3	Thermal Action Characteristics - Lateral Mode 1	185
4.4	Dependent Parameter Characteristics - Vertical Mode and Lateral Mode 1	186
4.5	Details of Lateral Mode 2	187
4.6	Thermal Action Characteristics - Lateral Mode 2	192
4.7	Dependent Parameter Characteristics - Lateral Mode 2	193
4.8	Details of Vertical Mode	194
4.9	Thermal Action Characteristics - Vertical Mode	197
4.10	Permissible Temperature Rise/ Imperfection Ratio Graph	205
4.11	Qualitative Imperfection Ratio Relationships	206
5.1	Lateral Submarine Buckling - Enhanced Action-Response Loci (Mode 1)	213
5.2	Vertical Submarine Buckling - Enhanced Action-Response Loci	214

## ACKNOWLEDGEMENTS

The author would like to take this opportunity to express his appreciation to Dr N Taylor, Director of Studies, and Professor A C Walker, External Supervisor, for their help and guidance.

Appreciation is also expressed to Mr D A Richardson for his invaluable contribution to the Geotechnical Experimentation.

# ABSTRACT (A B GAN)

## The Effects of Frictional and Thermal Forces upon Sea Bed Pipeline Buckling Behaviour

The objective of the research programme has been to develop design parameters applicable to in-service submarine pipeline buckling behaviour. The programme has involved experimental and theoretical studies and computer graphics are widely employed throughout. Initially, as detailed in Chapter 1, the necessary buckling mechanisms in pipelines subjected to axial compression have been identified and analysed in the form of relatively basic fully mobilised studies. In addition, errors and limitations contained within these studies have been determined and delineated. Consequently, geotechnical experimentation as reported in Chapter 2 was deemed necessary particularly given the dearth of information available relating to the nature of the friction resistance force between the pipeline and its supporting medium. Full scale values for the axial and lateral friction coefficients together with their respective fully mobilised displacements have been deduced upon the basis of model tests. A semi-empirical formula has thereby been produced for use in design practice. Further, a novel interpretation of sea bed recovery, or the pipeline's submerged self-weight inertial characteristics associated with vertical buckling, has also been determined.

Following on from the above geotechnical study, more refined quasi-idealised analyses, dealt with in Chapter 3, have been undertaken incorporating the appropriate full scale deformation-dependent axial and lateral friction-response loci together with the respective sea bed recovery characteristics. These analyses enable, for the first time, definition of the appropriate critical temperature rise at which axial-flexural bifurcation occurs. Finally, noting that previous buckling analyses have been based on quasi-idealised buckling phenomena, attempts have also been made to incorporate practical submarine pipeline imperfections. Pipelines are not perfectly straight in field conditions and, consequently, the imperfection studies denoted in Chapter 4 have attempted to model the appropriate behaviour. Design charts have been produced accordingly and suggestions made regarding further studies.

# CHAPTER 1

## INITIAL CONSIDERATIONS

### 1.1 INTRODUCTION

The increase in demand for (offshore) oil and natural gas in many parts of the world has greatly increased the need for the installation of submarine pipelines. During the past two decades, the offshore industry has moved into deeper water for oil and gas production, involving water depths of up to 2,000 m.<sup>(1)</sup> Pipelines installed at such depths require the utmost care in engineering design. Construction methods and pipe-laying techniques<sup>(2-5)</sup> are both sophisticated and expensive. Investment in submarine pipelines is substantial. Failure of a pipeline is costly both in terms of lost production and repair costs.

A typical submarine pipeline consists of a steel pipe of high strength and ductility, including a wall thickness sufficient to withstand high stresses during installation and routine operation. It is also coated to give protection against external corrosion and concrete coated to provide weight. The pipeline can be either completely buried or partially buried<sup>(6-10)</sup> to some depth in marine soils or it can rest on the sea bed, accordingly exposed to the hydrodynamic and inertia forces of the sea.

Of particular interest to the present study is that care should be taken when designing a submarine pipeline to ensure its stability during the period of installation and lifetime use. Indeed, the pipeline should have sufficient vertical, longitudinal and lateral resistance to overcome the internal and environmental actions which could otherwise induce unstable behaviour. The magnitudes of the forces associated with such behaviour in a submarine pipeline depend on many factors, including,

- (i) gravitational (weight of pipeline and its protective coating),
- (ii) environmental (buoyancy, hydrodynamic and inertial forces),
- (iii) constructional (longitudinal, torsional and bending stresses when pipelaying), and,
- (iv) operational or in-service (internal operating pressure and constrained thermal expansion).

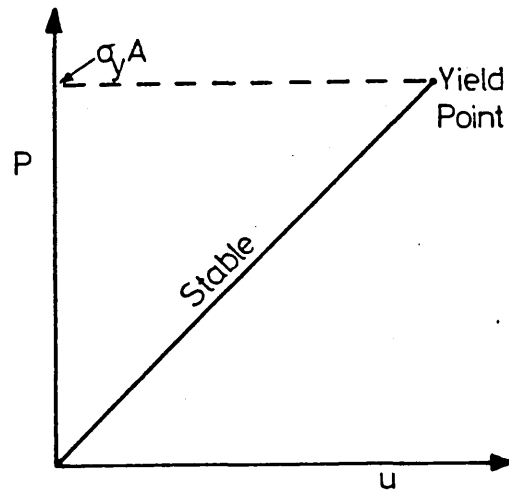
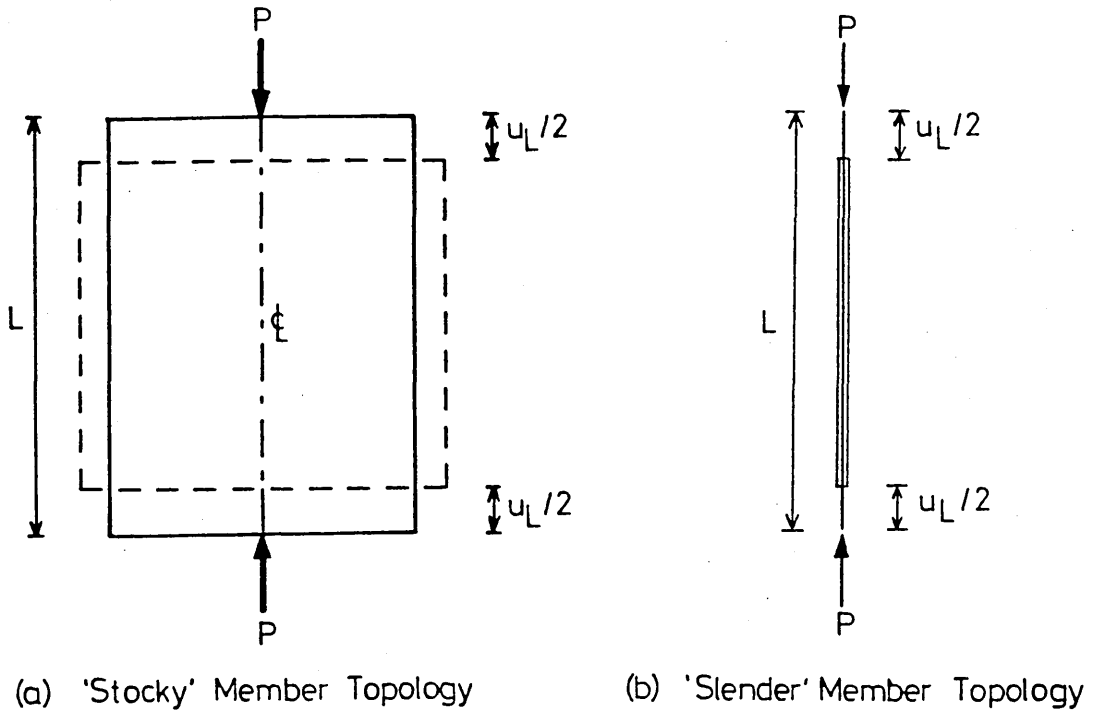
It is with the last set of parameters that this study is concerned. The two major sources of operational compressive force can be identified as being that centred on the internal operating pressure and that concerning the constrained thermal expansion caused by hot oil or gas flowing in the pipeline. Of particular relevance to submarine conditions is the

necessity of determining not only the buckling force but also the probable location of the pipeline should buckling occur. Another important feature of pipeline buckling behaviour concerns the resistance to movement caused by the interaction between the pipeline and the sea bed.

Most published literature to-date regarding submarine pipeline behaviour has been directed at stresses caused during laying<sup>(11-15)</sup> and modification or repair<sup>(16-19)</sup> operations. Relatively little previous research has been undertaken with regard to the pipeline buckling behaviour during routine operation<sup>(20-21)</sup>, that is, under in-service conditions.

## 1.2 ELASTIC BUCKLING - THE PHENOMENON

Within the field of elastostatics<sup>(22)</sup>, general idealised structural behaviour can be typified by reference to the 'stocky' and 'slender' axial compression systems depicted in Figs. 1.1 (a) and (b) respectively. As action parameter  $P$ , equivalent to the axial force in the respective member, is gradually increased, the primary response parameter, axial deformation  $u$ , represented herein by the overall axial shortening  $u_L$ , also increases gradually. All structural response parameters, including axial stress for example, afford a similar behavioural pattern.



(c) Action-Response Locus

Fig. 1.1 Idealised Linear Axial Compression System

For systems involving linear constitutive properties and vanishingly small deformations,  $u_L$  is given by

$$u_L = \frac{PL}{AE} \quad (1.1)$$

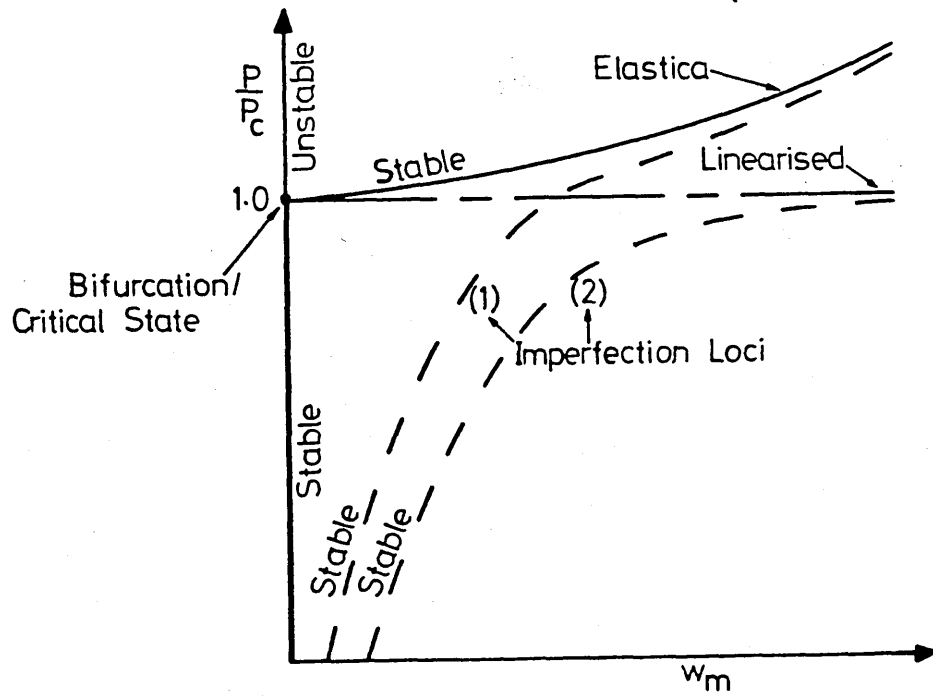
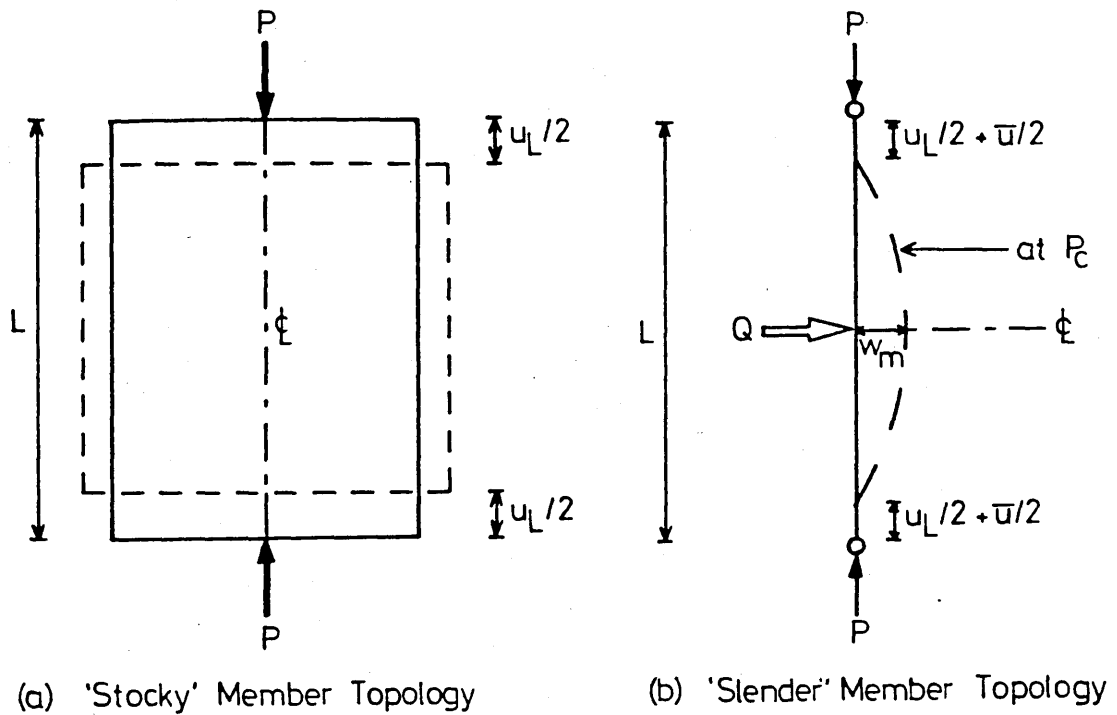
where  $L$  is the member length,  $A$  is the cross-sectional area and  $E$  is the Young's modulus of the member.

The governing action-response locus is of linear form as depicted in Fig. 1.1 (c). The axial stress induced in the member,  $\sigma_A$ , takes the form

$$\sigma_A = P/A \quad (1.2)$$

System linearity will cease upon the onset of either constitutive non-linearity, that is the onset of yield in ductile steel structures for example, or finite deformations which, with respect to the present system, refers to the state at which the induced change in cross-sectional area becomes significant; in flexural studies, of particular relevance to this study, finite deformations are typified by slopes in excess of 0.1 radians. (23)

If, however, a relatively small transient force  $Q$  is introduced into each of the above idealised axial compression systems in the manner denoted in Figs. 1.2 (a) and (b), by means of which the systems concerned become only quasi-idealised compression systems, the responses of the 'stocky' and 'slender' systems become



(c) Action - Response Loci

Fig. 1.2 Quasi-Idealised Buckling System

quite distinct; the behaviour of the former is effectively unchanged whilst the latter will undergo elastic instability. As opposed to the foregoing purely axial compression systems, elastic instability studies<sup>(24,25)</sup> relate to systems in which structural response undergoes a singular and sudden change despite the action parameter  $P$  again being only gradually and uniformly increased. The basic nature of the instability studies can be couched in terms of Thom's Catastrophe Theory.<sup>(26,27)</sup>

Quasi-idealised elastic instability can be typified by reference to the 'slender' compression system depicted in Fig. 1.2 (b). Noting the presence of the small transient force  $Q$ , then, as the action parameter  $P$  is gradually increased, axial response in terms of  $u_L$  is again witnessed. However, at some singular loading state  $P_c$ , a dramatic change in structural response is observed, and flexural deformation, typically represented by the central and maximum transverse deflection parameter  $w_m$  is statically incurred. Further, a flexurally induced end shortening  $\bar{u}$  is also set up. That is, an apparently axial system is replaced by a predominantly flexural system at and beyond a singular state. This singular state can be represented by the critical load  $P_c$ , where  $P_c$  is given by<sup>(24)</sup>

$$P_C = \pi^2 EI/L^2 \quad (1.3)$$

where  $I$  is the second moment of area of the member. The appropriate behaviour is depicted in Fig. 1.2 (c). The overall end shortening,  $u_L + \bar{u}$ , takes the form

$$u_L + \bar{u} = \frac{P_C L}{AE} + \frac{1}{2} \int_0^L (w, x)^2 dx \quad (1.4)$$

whilst the appropriate maximum stress induced in the member,  $\sigma_m$ , can be represented by

$$\sigma_m = P_C/A + M_m/Z \quad (1.5)$$

where  $M_m$  is the maximum bending moment and  $Z$  is the section modulus of the member. The critical load  $P_C$  represents, in linearised terms, the limiting load carrying capacity of the member. Experimentation has shown that such members can carry loads higher than the buckling load  $P_C$ , the necessary modelling requiring a non-linear finite deformation study (the 'Elastica' (28)), the appropriate behavioural locus being shown in Fig. 1.2 (c). It is to be noted that in fully idealised terms, the parameter  $Q$  is not present and both stocky and relatively slender members would afford purely axial behaviour. The foregoing slender analysis with the incorporation of the parameter  $Q$  is therefore deemed to be quasi-

idealised; in practice, physical imperfections in the structural system cannot be avoided and  $Q$  serves to represent this fact.

Clearly, the engineer has to be able to discern whether or not a system is likely to undergo unstable behaviour as the respective analyses, typified by Figs. 1.1 and 1.2, are clearly distinct. Two basic factors are involved. The degree of slenderness monitored by the so-called slenderness ratio<sup>(24)</sup>, is clearly of importance with regard to the possible onset of flexural behaviour. The second important factor relates to the unavoidable presence of structural imperfections. Physical imperfections can be grouped under three major headings; initial curvature, eccentric loading and residual stresses. Action-response loci corresponding to slender systems possessing such imperfections are depicted in Fig. 1.2 (c). Imperfection locus (1) relates to the path of certain members capable of carrying loads higher than  $P_c$ . This locus has no theoretical maximum load (except due to plasticity onset) and the effects of any initial imperfections have largely disappeared as  $w_m$  gets larger. It can therefore be concluded that the locus is imperfection insensitive. Imperfection locus (2) appertains to that quasi-linear systems with the maximum load converging

with the critical load  $P_c$  as  $w_m$  increases. It is essentially unaffected by the presence of imperfections and is therefore, effectively, imperfection insensitive. Imperfection sensitive systems can be represented by the case of combined plate and column buckling.<sup>(29)</sup> A typical quasi-idealised locus and the appropriate imperfection loci are depicted in Fig. 1.3. It can be seen that any slight increase in initial imperfection will significantly reduce the maximum load and any attempt to increase the load further will result in a dynamic snap buckling; such systems are therefore extremely imperfection sensitive.

### 1.3 SUBMARINE PIPELINE BUCKLING

#### 1.3.1 Historical Résumé

The earliest published work on the effect of axial loads upon the submarine pipeline buckling behaviour was undertaken by Hobbs<sup>(20)</sup> and subsequently corrected by Taylor and Gan.<sup>(21)</sup> Their studies relied heavily on similar work established in the related field of rail track and crane rail buckling.<sup>(30-45)</sup> It is to be noted, however, that substantial differences exist. The primary difference between submarine pipeline and rail track buckling studies lies in the nature of the axial and lateral friction resistances of the structure/supporting medium

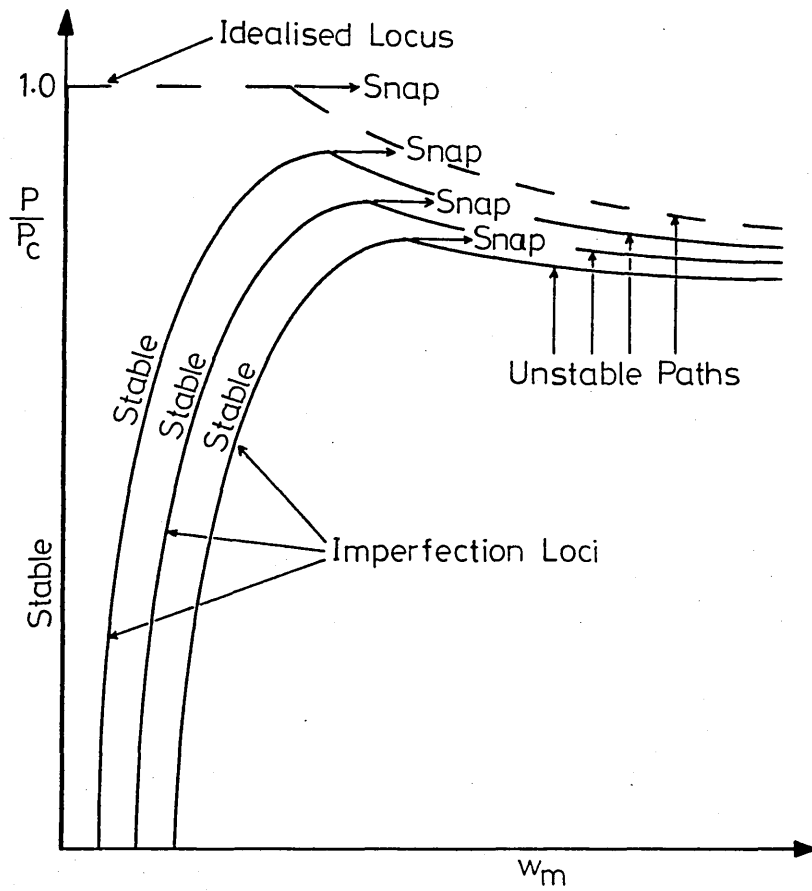
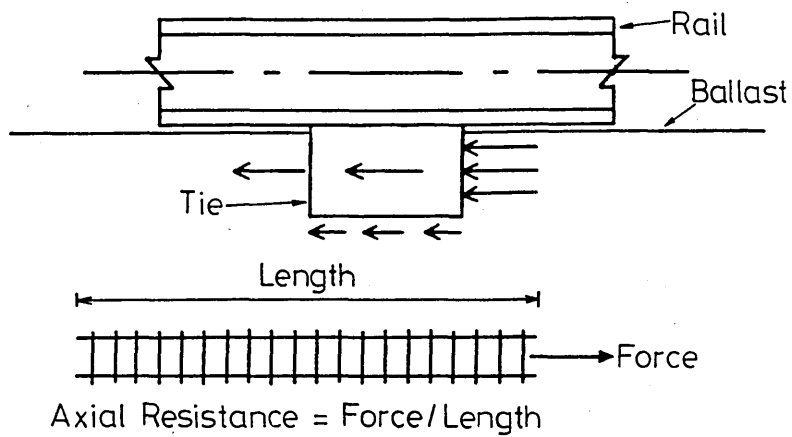


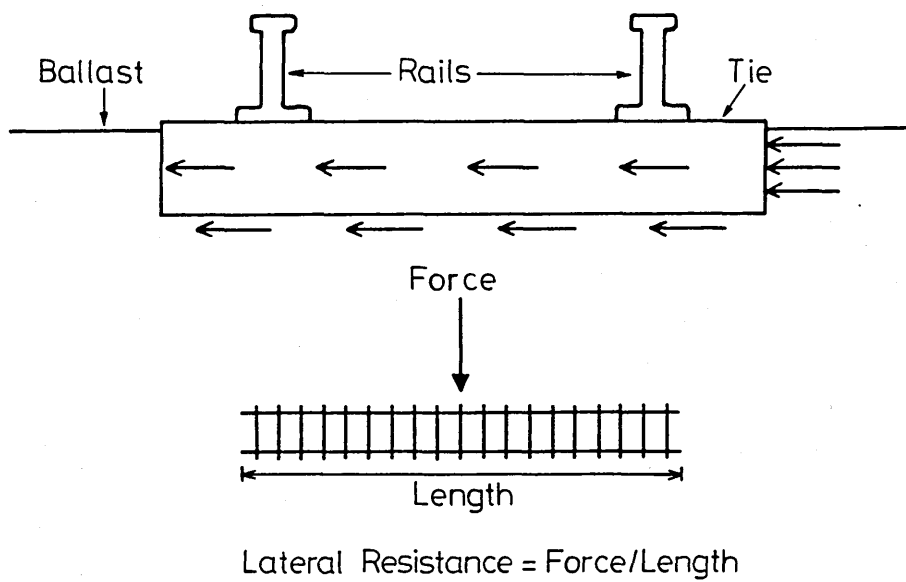
Fig.1.3 Combined Plate and Column Buckling  
-Imperfection Snap

interface. While it can be said that the axial and lateral friction resistance forces between the submarine pipeline and the sea bed foundation are effectively continuous, the friction resistance forces between the rail track and the ballast foundation are of discrete form. The axial friction resistance exerted by the ballast on the rail-tie structure, as depicted in Fig. 1.4 (a), consists of the friction forces between the ballast and the bottom surface of the ties, and the pressure on the vertical tie surface. In the case of the lateral friction resistance, the friction forces occur between the bottom surface and the two long sides of the ties and the ballast, as well as the pressure on the front surface of the ties, as shown in Fig. 1.4 (b). In the rail track analyses, however, it is assumed that the resulting axial and lateral friction resistances are continuous and the rail-tie structure is replaced by an equivalent beam of uniform cross-section. Such interpretations are superfluous in submarine pipeline studies.

With regard to these latter buckling studies, the five established lateral buckling modes which relate to snaking movements across the sea bed are illustrated in Fig. 1.5.<sup>(20,21)</sup> Axial and lateral displacements are denoted by  $u$  and  $w$  respectively. The appropriate buckling lengths are denoted by  $L$ ,  $L_1$  and  $L_2$ , whilst  $L_s$  represents the so-called slip length.

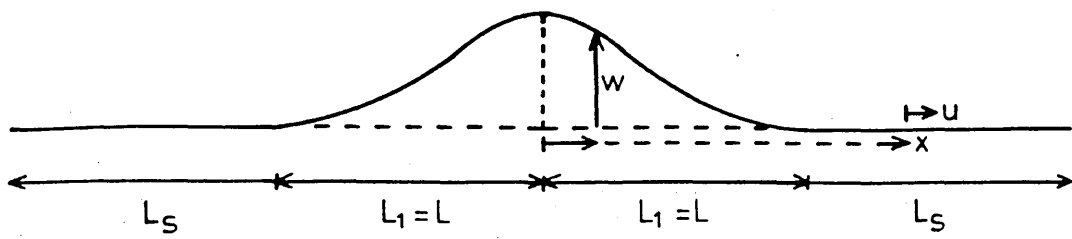


(a) Axial Resistance

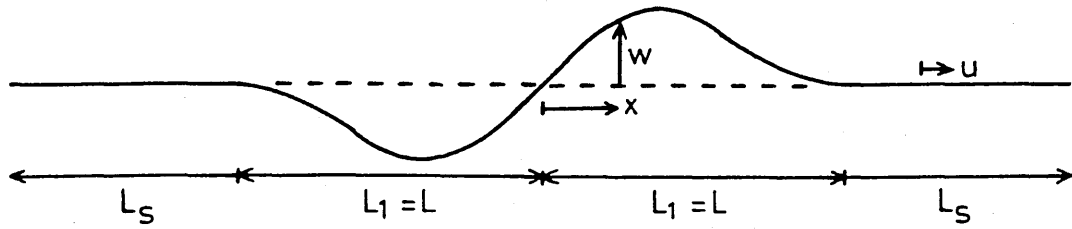


(b) Lateral Resistance

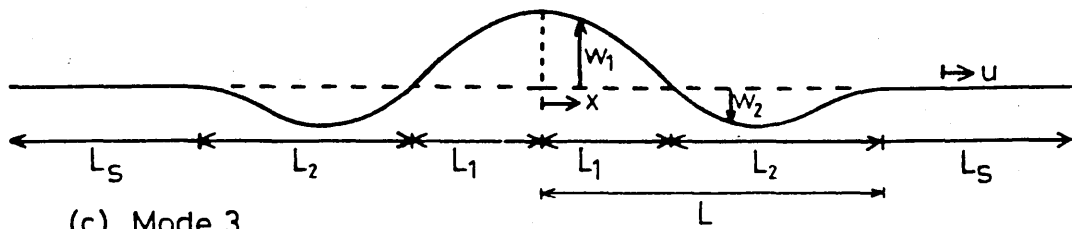
Fig. 1-4 Rail Track Friction Model



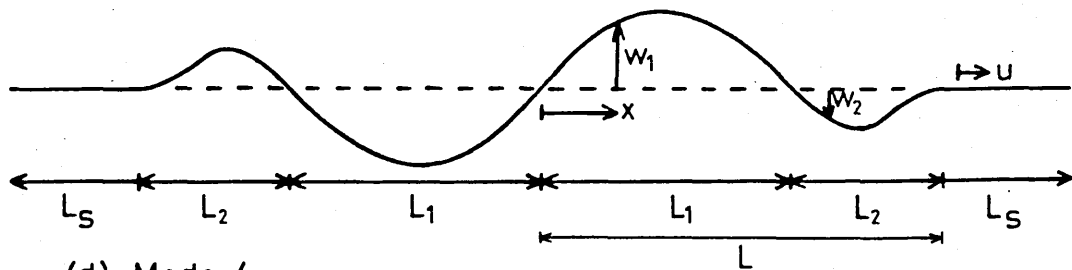
(a) Mode 1



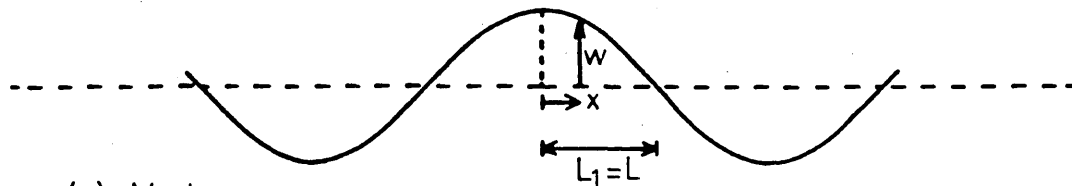
(b) Mode 2



(c) Mode 3



(d) Mode 4



(e) Mode  $\infty$

Fig.1.5 Lateral Buckling Mode Topologies

Axial friction resistance is generated through the slip lengths whilst lateral friction resistance occurs through the buckling lengths. The vertical buckling mode which involves part of the pipeline buckling out of the sea bed can also be represented by Fig. 1.5 (a) except that  $w$  is now replaced by  $v$ , the appropriate vertical displacement.

### 1.3.2 The Buckling Mechanism

As previously inferred, stability analyses of submarine pipelines may be grouped into two main categories: pipelines buckling laterally across the sea bed and pipelines buckling vertically up from the sea bed. Although actual pipeline buckling may proceed in a more complicated manner, the choice of these two special modes of deformation is made in order to reduce the problem to two dimensions and thus to simplify the resulting analysis. Modal interaction can then be considered as required.

It is proposed, initially, to discuss the essential features of the mechanism involved; the mathematical features of the appropriate field and functional equations will then ensue. A typical submarine pipeline buckling topology is given in Fig. 1.6 which depicts the essential details of lateral mode 1 before and after buckling. A uniform temperature rise,  $T$ , in a perfectly straight pipeline will create an axial compression force due to constrained

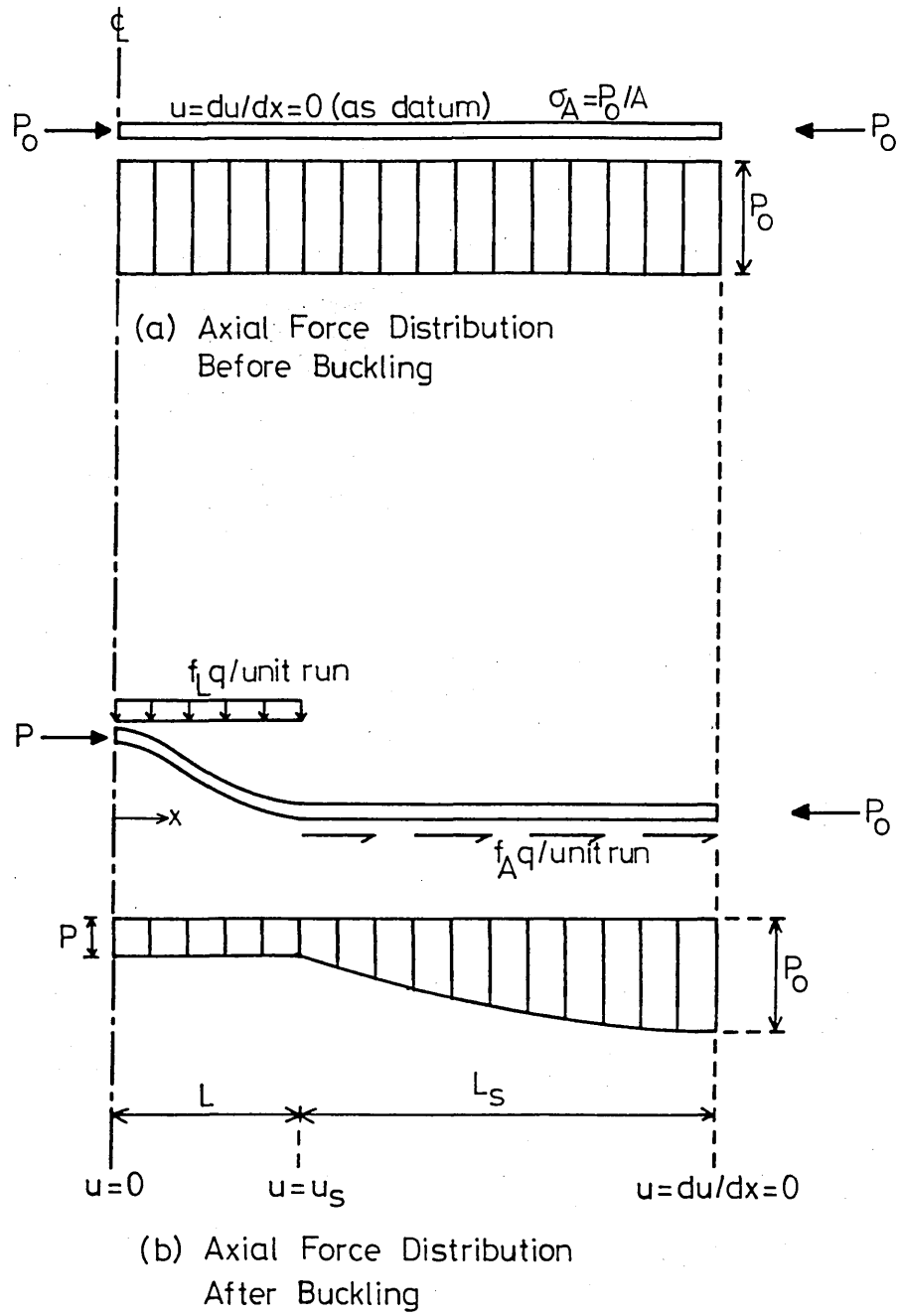


Fig. 1-6 Lateral Mode 1 Buckling Topology

thermal expansion as illustrated in Fig. 1.6 (a). Taking the structural response, at least initially, to be within the elastic range of the pipeling response (gross sectional distortion as associated with laying operations<sup>(17)</sup> is not a factor here), this force can be represented by

$$P_o = AE\alpha T \quad (1.6)$$

where  $\alpha$  is the respective coefficient of linear thermal expansion of the pipe. Whilst thermal effects are presently of primary concern to this study, it should be noted that  $P_o$  can also be created by the pressure difference  $p$  across the wall of the pipe which produces a free axial strain<sup>(46)</sup>

$$\epsilon = \frac{pr}{Et} (0.5 - \nu) \quad (1.7)$$

where  $\nu$  is the Poisson's ratio,  $r$  is the radius and  $t$  is the wall thickness of the pipe. If this free axial strain  $\epsilon$  is fully restrained, the axial compression force generated,  $P_o$ , noting equation (1.7), takes the form

$$P_o = AE\epsilon = \frac{Apr}{t} (0.5 - \nu) \quad (1.8)$$

With oil and gas temperatures potentially ranging up to 100°C above that of the water environment and operating pressures over 10 N/mm<sup>2</sup>, these effects can produce very significant axial compression forces,  $P_o$ .

Fig. 1.6 (a) indicates that this pre-buckling force  $P_0$  is set up in the absence of any permitted straining.

At the onset of buckling, as shown in Fig. 1.6 (b), part of the constrained expansion is released in the buckled region which, taken together with the friction resistance of the sea bed/pipeline interface, results in a reduction in the axial compression to some buckling force  $P$ . Axial friction resistance  $f_A q$  is generated per unit length of pipe through the slip length  $L_S$  whilst lateral friction resistance  $f_L q$  occurs per unit length of pipe through the buckling length  $2L$ . The nature of these friction forces, together with that of the similar sea bed recovery parameter  $f_M q$  introduced in Section 1.3.4, are of major importance to this study. They relate to the proportion of the pipeline's self-weight per unit length,  $q$ , which is frictionally active at any state of deformation; that is,  $f_A$  and  $f_L$  (together with  $f_M$ ), are such that

$$\left. \begin{aligned} 0 &\leq f_A \leq \phi_A \\ 0 &\leq f_L \leq \phi_L \\ 0 &\leq f_M \leq 1 \end{aligned} \right\} \quad (1.9)$$

where  $\phi_A$  and  $\phi_L$  are the respective axial and lateral friction coefficients. To-date, the established fully mobilised analyses have employed the simplifying

non-conservative assumption that

$f_A = \phi_A$ ,  $f_L = \phi_L$ ,  $f_M = 1$ . The non-linear, deformation dependent nature of these parameters is suggested in Fig. 1.6 (b) by virtue of the non-linear axial force distribution attributed to the slip length  $L_S$ . Detailed definition and discussion of these three parameters is given in Chapter 2.

### 1.3.3 Boundary Conditions

Submarine pipeline stability analyses involve, with one notable exception denoted below, five distinct behavioural regions; the flexural region of buckling length  $2L$ , the two adjoining slip length regions, each of length  $L_S$  and subject to axial friction resistance, and two 'quasi-infinite' regions for  $|x| \geq L + L_S$  which are only subject to prebuckling axial compression  $P_0 = AE\alpha T$ . Lateral mode  $\infty$  is unique in as much as the entire run of pipe is taken to be subject to buckling action, with  $L_S = 0$ . The symmetrical nature of the vertical mode and lateral modes 1 and 3 and the skew-symmetrical nature of lateral modes 2 and 4 are to be noted. These features will be exploited in the ensuing analyses. Lateral mode  $\infty$  is also taken to be symmetrical. The aforementioned behavioural regions are delineated by the boundary conditions appertaining to the respective modes. Consideration of these conditions is initially given in the context of lateral mode 1.

Referring to Figs. 1.5 (a) and 1.6 (b), then, at the centreline,  $x = 0$ , symmetry logic demands

$$w, x|_0 = -EIw, xxx|_0 = 0 \quad (1.10)$$

Physical or, rather, kinematic conditions take the form

$$w|_L = w, x|_L = u|_{L+L_s} = 0 \quad (1.11)$$

The conditions given in equation (1.11) can be termed 'variable matching conditions',<sup>(32)</sup> as the respective locations  $x = L, L + L_s$  are variable; that is,  $L$  and  $L_s$  are variable. This is due to the fact that the pipeline is not physically attached to the sea bed foundation.<sup>(47,48)</sup> The axial strain can also be prescribed at location  $x = L$ . Noting the slip length details given in Fig. 1.7, then

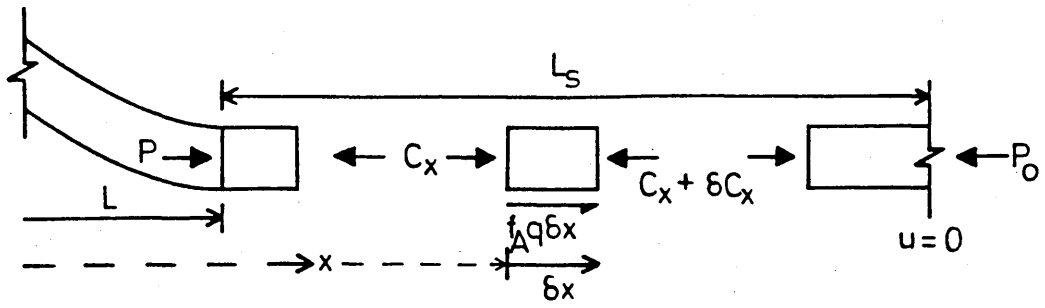
$$-u = \alpha T(L_s + L - x) - \int_x^{L_s + L} \frac{C_x}{AE} dx \quad (1.12)$$

in which

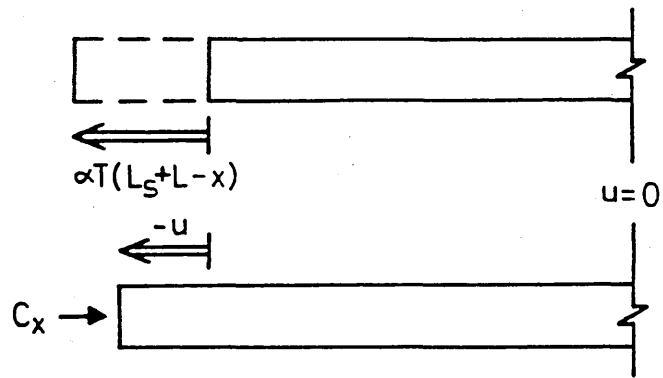
$$C_x = P_o - \int_x^{L_s + L} f_A q dx \quad (1.13)$$

Differentiating equation (1.12) with respect to  $x$ , noting equation (1.13), gives

$$u, x = \alpha T - (P_o - \int_x^{L_s + L} f_A q dx) / AE \quad (1.14)$$



(a) Equilibrium



(b) Compatibility

Fig.1.7 Slip Length Detail

Noting equation (1.6), the axial strain at the buckling length/slip length interface takes the form

$$u',x|_L = \int_L^{L_S+L} \frac{f_{Aq}}{AE} dx = \frac{(P_0 - P)}{AE} \quad (1.15)$$

Again noting the variable nature of  $L$  and  $L_S$ , then in addition to the usual boundary and matching conditions for fixed matching points, two additional 'transversality' conditions<sup>(32)</sup>, at  $x = L$  and at  $x = L_S$ , are needed for the determination of the unknowns  $L$  and  $L_S$ . A requirement of the slip length is that behaviour is purely axial with

$$M|_x = w|_x = 0 \quad \text{for } L \leq x \leq L+L_S \quad (1.16)$$

consequently, there can be no flexural moment at  $x = L$ . The required condition is therefore

$$EIw',_{xx}|_L = w',_{xx}|_L = 0 \quad (1.17)$$

This condition is often termed to be a 'transversality' condition and can be alternatively derived employing the Calculus of variations<sup>(32)</sup> with subsidiary conditions<sup>(49)</sup> introduced in the form of Lagrange multipliers. These involve, for example, stipulation of the condition given in equation (1.16). A further 'transversality' equation is available from equation (1.14) with  $x = L + L_S$  such that

$$u',x|_{L+L_S} = 0 \quad (1.18)$$

With regard to the remaining buckling modes, the necessary expressions are delineated in Table 1.1. The only condition which perhaps requires additional consideration is that relating to the shear force at the ends of each buckle length in lateral mode  $\infty$ . The problems involved in determining the nature of any concentrated reaction being provided by the sea bed supporting medium have been discussed elsewhere.<sup>(20, 32, 45)</sup> With regard to lateral mode 1, a lateral shearing concentrated reaction of  $\int_0^L f_L q dx$  will be provided in order that lateral equilibrium be maintained. This reaction is not developed, however, without an internal shear force of this magnitude first being provided within the pipe - this feature is observed from the appropriate analysis although it is unnecessary for it to be a prescribed boundary condition (note Section 1.4.2). Similar situations apply to all modes at the respective buckle length/slip length interface. Further, lateral modes 2, 3 and 4 provide for continuation of shear force with no generated shear reaction from the supporting medium at all discrete buckle length interface locations or buckling nodes ( $w = 0$ ). In the exceptional lateral mode  $\infty$  case, however, self-equilibrating concentration of contact pressures<sup>(32)</sup> are generated as support reactions in the vicinity of the buckling nodes such that the internal shear force is null.

BUCKLING MODES					
Lateral 1	Lateral 2	Lateral 3	Lateral 4	Lateral $\infty$	Vertical
$w_{,x} _0=0$ $w_{,xxx} _0=0$	$w _0=0$ $w_{,xx} _0=0$	$w_{1,x} _0=0$ $w_{1,xxx} _0=0$	$w_1 _0=0$ $w_{1,xx} _0=0$	$w_{,x} _0=0$ $w_{,xxx} _0=0$	$v_{,x} _0=0$ $v_{,xxx} _0=0$
		$(w_1=w_2) _{L_1}$ $(w_{1,x}=w_{2,x}) _{L_1}$ $(w_{1,xx}=w_{2,xx}) _{L_1}$ $(w_{1,xxx}=w_{2,xxx}) _{L_1}$ $w_2 _{L_1}=0$ (transversality)			
$w _L=0$ $w_{,x} _L=0$ $w_{,xx} _L=0$ (transversality)		$w_2 _L=0$ $w_{2,x} _L=0$ $w_{2,xx} _L=0$ (transversality)		$w _L=0$ $w_{,xx} _L=0$ $w_{,xxx} _L=0$ (unique)	$v _L=0$ $v_{,x} _L=0$ $v_{,xx} _L=0$ (transversality)
		$u _{L+L_s}=0$ $u_{,x} _{L+L_s}=0$ (transversality)			
		$u_{,x} _L=(P_o-P)/AE$			$u_{,x} _L=(P_o-P-P_a)/AE$

Table 1.1 Boundary Conditions

#### 1.3.4 Derivation of Field Equations

The five regions appertaining to submarine pipeline stability analyses have been delineated in Section 1.3.3. The appropriate field equations can be most conveniently derived in the ensuing novel manner. With regard to the flexural region, Fig. 1.8 depicts the topology appertaining to a typical flexural element of a lateral buckling mode. Bending moment and shear force are denoted by  $M$  and  $F$  respectively. Considering the transverse equilibrium of the elemental pipe  $\delta x$ , then  $\delta F = f_L q \delta x$ , so that

$$F'_{,x} = f_L q \quad (1.19)$$

Taking moment about point O gives

$$M + \delta M - M = -(F + \delta F) \delta x - P \delta w + f_L q (\delta x)^2 / 2 \quad (1.20)$$

which yields, ignoring second order differentials  $(\delta F \delta x)$  and  $(\delta x)^2 / 2$ ,

$$-F = M'_{,x} + Pw'_{,x} \quad (1.21)$$

Differentiating equation (1.21) with respect to  $x$ , noting the appropriate linearised moment-curvature expression  $M = EIw_{,xx}$ , affords

$$F'_{,x} = -EIw_{,xxxx} - Pw_{,xx} \quad (1.22)$$

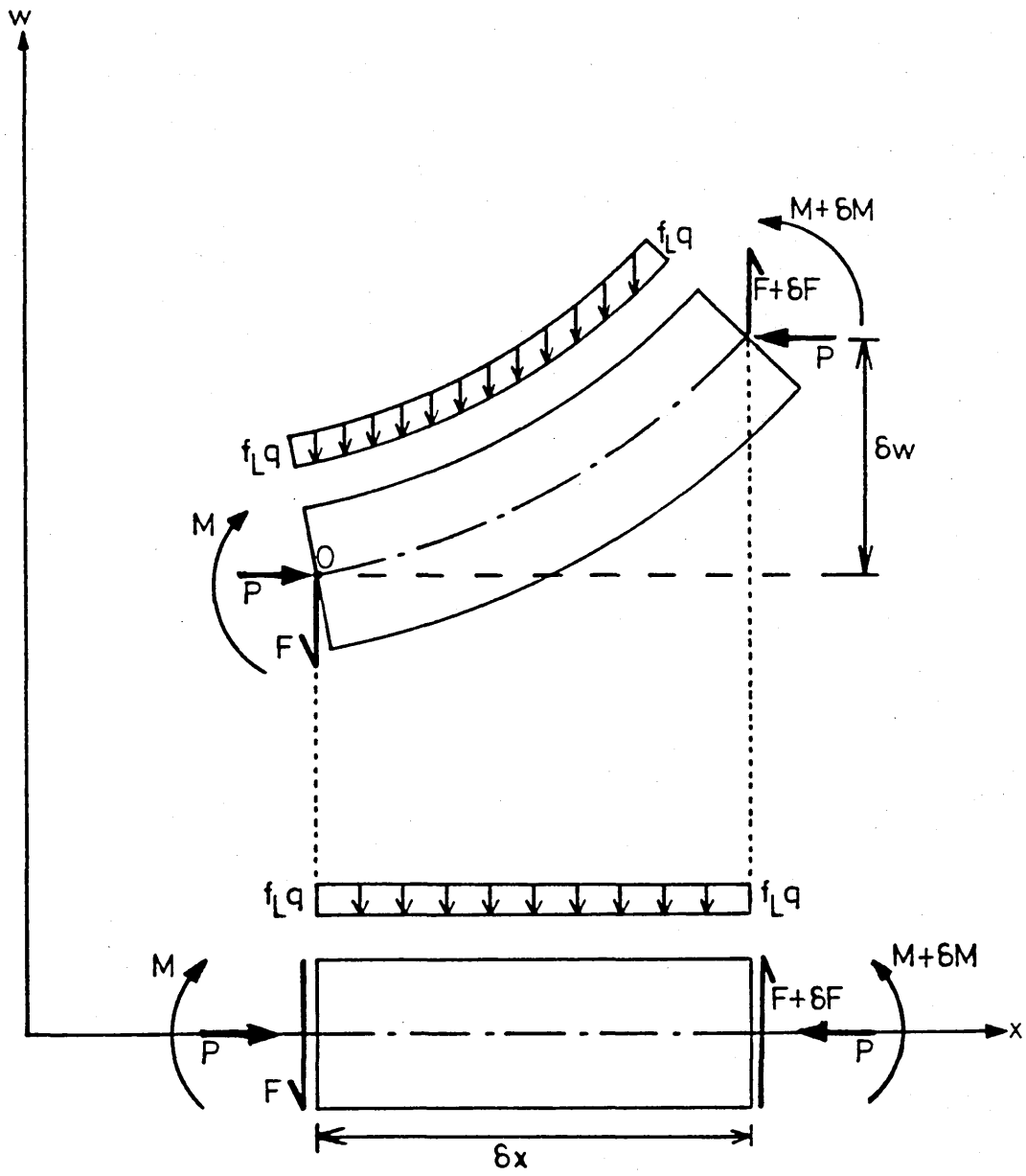


Fig.1.8 Flexural Topology

Finally, equating equation (1.22) with equation (1.19) yields the linearised flexural field equation

$$EIw_{,xxxx} + Pw_{,xx} = -f_L q \quad 0 \leq x \leq L \quad (1.23)$$

As a corollary, the appropriate linearised flexural field equation for the vertical buckling mode can be similarly derived, with  $w$  and  $f_L q$  being replaced by  $v$  and  $f_M q$  respectively. Hence the vertical mode equivalent to equation (1.23) can be rewritten

$$EIV_{,xxxx} + Pv_{,xx} = -f_M q \quad 0 \leq x \leq L \quad (1.24)$$

The parameter  $f_M$  is such that  $f_M q$  is the effective self-weight per unit length of the pipeline at any given state of deformation, such that, as previously mentioned,  $0 \leq f_M \leq 1$ . The reasoning behind the introduction of  $f_M$  is that as the pipe lifts off the sea bed, some component of the self-weight is taken up by the recovery, on unloading, of the sea bed medium.

With regard to both lateral and vertical buckling cases, the topology of the slip length region,  $L \leq x \leq L + L_S$ , is depicted in Fig. 1.7. Axial compression is denoted by  $C_x$ . Considering the

longitudinal equilibrium of the elemental pipe  $\delta x$ , as shown in Fig. 1.7 (a), then  $\delta C_x = f_A q \delta x$ , so that

$$C_{x,x} = f_A q \quad (1.25)$$

Incorporating the appropriate thermal effect detailed in Fig. 1.7 (b), compatibility yields the expression given in equation (1.12). Differentiating equation (1.12) with respect to  $x$  affords

$$C_x = AE(\alpha T - u_{,x}) \quad (1.26)$$

Substituting equation (1.26) into equation (1.25) yields the linearised slip length field equation

$$AEu_{,xx} = -f_A q \quad L \leq x \leq L+L_s \quad (1.27)$$

The above formulations represent a novel vectorial mathematical interpretation of the submarine pipeline buckling system. Elsewhere, derivation is made using a rather more lengthy Calculus of Variations approach.<sup>(32)</sup> The foregoing considers the submarine pipeline buckling system to be of quasi-linearised elastic form and deformations requiring that checks be made upon the appropriate limiting stresses. As discussed previously, established analyses<sup>(20,21,50)</sup> have employed the simplifying assumption that  $f_L/\phi_L = f_A/\phi_A = f_M = 1$ ; that is, the frictional and self-weight forces are taken to be fully-mobilised throughout. Solution schemes are thereby more readily determined but consequently suffer distinct

limitations. It is proposed to set out the established analyses, suitably corrected, employing the equations delineated as above in order that the developed studies given later may be placed in context.

### 1.3.5 Interface Compatibility

Having established the appropriate boundary conditions and field equations for both the buckling and slip length regions, it is now necessary to set up a matching compatibility expression at the interface of the buckling and slip lengths, that is at  $x = L$ , in order to combine the buckling length and slip length analyses. Noting Fig. 1.9, the axial movement of the pipe within the buckling region can be expressed in the form

$$u = \alpha T x - P x / A E - \frac{1}{2} \int_0^x (w_{,x})^2 dx \quad 0 \leq x \leq L \quad (1.28)$$

Noting Fig. 1.5 (a), then with regard to lateral mode 1, at the buckle length/slip length interface ( $x = L$ ), equation (1.28) becomes

$$u|_L = u_s = \frac{(P_o - P)L}{AE} - \frac{1}{2} \int_0^L (w_{,x})^2 dx \quad (1.29)$$

Equation (1.29) remains valid for lateral mode 2 and, substituting  $v$  for  $w$ , the vertical mode. For lateral modes 3 and 4, then, noting Figs. 1.5 (c) and

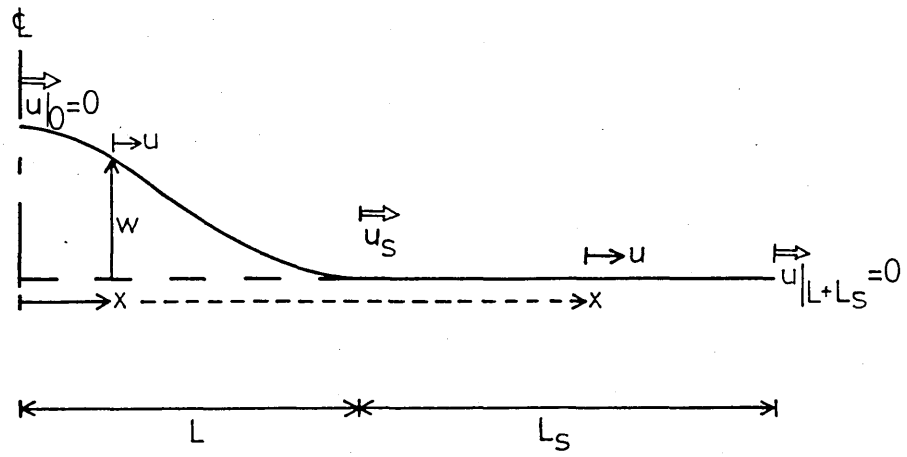


Fig.1-9 Interface Compatibility

(d), equation (1.29) takes the form

$$u_s = \frac{(P_o - P)L}{AE} - \frac{1}{2} \left[ \int_0^{L_1} (w_{1,x})^2 dx + \int_{L_1}^L (w_{2,x})^2 dx \right] \quad (1.30)$$

Equation (1.29) is also valid for lateral mode  $\infty$ , although it is of trivial form ( $u_s = L_s = 0$ ). Either equation (1.29) or (1.30) can now be used in conjunction with equation (1.27) subject to the necessary integration.

### 1.3.6 Primary Parameters

Essentially, the displacements  $u$  and  $w$  ( $v$  in the vertical mode) represent the basic analytical parameters in the study - note Fig. 1.5. Given this and the previous discourse on the boundary conditions, then, for engineering purposes, the structural response is defined in terms of  $P$ ,  $w$ ,  $L$  and  $\sigma_m$ , where  $\sigma_m$  represents the maximum stress induced in the pipe, for any given action  $T(P_o)$ . Noting equation (1.5), the maximum stress can be expressed in the form

$$\sigma_m = P/A + M_m r/I \quad (1.31)$$

where  $M_m$  is the maximum bending moment for any given temperature rise  $T$ . Parameters  $u_s$  and  $L_s$  can also be obtained but they are of secondary importance.

### 1.3.7 Geotechnical Factors

The nature of the pipeline/sea bed interface has been shown to be both important and complex. The geotechnical parameters  $f_A$ ,  $f_L$  and  $f_M$  have been introduced and defined. Further study of these crucial parameters is given in the following chapter. In addition, the employment of simple beam theory<sup>(32)</sup> in conjunction with an effectively rigid sea bed has led to the existence of transversality and associated conditions and the compatibility statement. It is also to be noted that the eccentricity of  $f_A q \delta x$  and  $f_L q \delta x$  from the pipe centreline is neglected as is the effect of axial friction force resistance within the buckling region for the lateral mode studies.<sup>(32)</sup> Considerable effort is necessary to mathematically model the various geotechnical effects but, prior to such incorporation, it is proposed to set out the established analyses which avoid the associated complexities by means of employing the corresponding fully mobilised forces.

## 1.4 FULLY MOBILISED QUASI-IDEALISED ANALYSES

### 1.4.1 Introduction

As noted previously, the following quasi-linearised

analyses employ fully mobilised geotechnical/frictional forces with  $f_A/\phi_A = f_L/\phi_L = f_M = 1$ . Further, the pipeline's material or constitutive response is taken to be of linear elastic form. Topologically, linear kinematic behaviour is assumed, with, for example, pipeline slopes in excess of 0.1 radians implying violation of the respective analysis. Most of the ensuing expressions relate to work initially carried out in the field of rail track buckling. However, noting the previous studies given in Sections 1.3.3 - 1.3.5, the basic expressions given herein are presented in terms of the appropriate vectorial field equations rather than as derivative expressions of the Calculus of Variations.

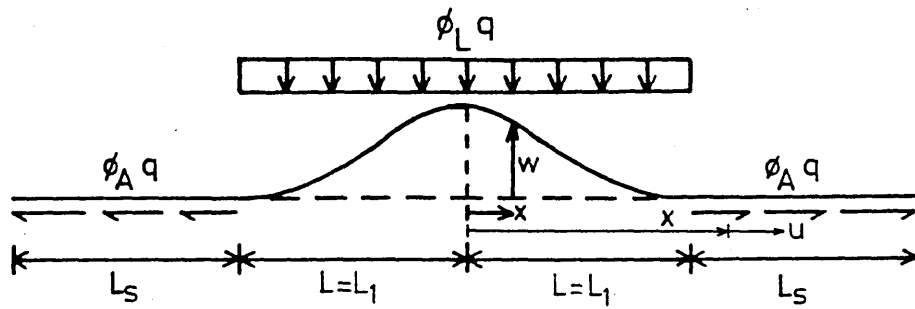
The numerical values for the various parameters involved are given in Table 1.2 together with a variety of  $\phi_A$  and  $\phi_L$  values between 0.1 and 0.7. (20, 50)

#### 1.4.2 Lateral Mode 1 Analysis

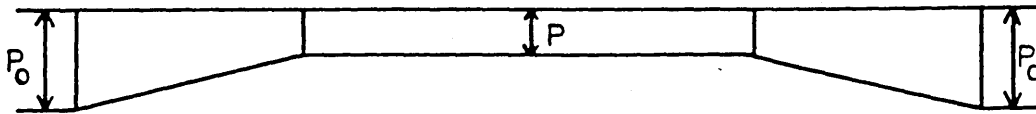
The essential features of lateral mode 1 are shown in Figs. 1.10 (a) and (b) which depict the fully mobilised topology and axial force distribution respectively. The submerged self-weight of the pipe per unit length is denoted by  $q$  whilst  $\phi_A q$  and  $\phi_L q$  represent the respective fully mobilised

Parameter	Symbol	Value
External Radius	r	325 mm
Wall Thickness	t	15 mm
Sectional Area	A	29920 mm <sup>2</sup>
Young's Modulus	E	206 kN/mm <sup>2</sup>
Second Moment	I	1.509 x 10 <sup>9</sup> mm <sup>4</sup>
Self-weight	q	3.8 kN/m
Yield Stress	$\sigma_y$	448 N/mm <sup>2</sup>
Thermal Coefficient	$\alpha$	11 x 10 <sup>-6</sup> /°C

Table 1.2 Pipeline Parameters



(a) Fully Mobilised Topology



(b) Axial Force Distribution

Fig.1-10 Fully Mobilised Lateral Mode 1 Model

axial and lateral friction resistance forces per unit length. The linearised flexural field equation, noting equation (1.23), can be given by

$$w_{,xxxx} + n^2 w_{,xx} = -m \quad 0 \leq x \leq L \quad (1.32)$$

where  $n^2 = P/EI$  and  $m = \phi_L q/EI$ . The appropriate boundary conditions within the buckling region take the form

$$w_{,x}|_0 = 0 \quad (1.33)$$

$$-EI w_{,xxx}|_0 = 0 \quad (1.34)$$

$$w|_L = 0 \quad (1.35)$$

$$w_{,x}|_L = 0 \quad (1.36)$$

$$w_{,xx}|_L = 0 \quad (\text{transversality}) \quad (1.37)$$

The general solution of equation (1.32) is

$$w = A_1 \cos nx + A_2 \sin nx + A_3 x + A_4 - \frac{mx^2}{2n^2} \quad (1.38)$$

where  $A_i$ ,  $i = 1, 2, 3, 4$ , are constants of integration.

Substituting the boundary conditions given in equations

(1.33) through (1.36) into equation (1.38) gives the lateral displacement expression

$$w = \frac{mL^4}{2(nL)^2} \left[ 1 - \frac{x^2}{L^2} - \frac{2(\cos nx - \cos nL)}{nL \sin nL} \right] \quad (1.39)$$

Equating this expression with the transversality boundary condition given in equation (1.37) yields

$$\tan nL = nL \quad (1.40)$$

with the lowest non-trivial root affording

$$nL = 4.4934 \quad (1.41)$$

Hence, the buckling force is evaluated by substituting for  $n$ , with

$$P = 20.19 EI/L^2 \quad (1.42)$$

The maximum amplitude occurs at  $x = 0$ , noting equations (1.39) and (1.41), such that

$$w_m = 3.8512 \times 10^{-2} \frac{\phi_L q L^4}{EI} \quad (1.43)$$

and the maximum slope, at  $x = 0.398L$ , is given by

$$w_{,xm} = 0.06926 \frac{\phi_L q L^3}{EI} \quad (1.44)$$

while the maximum bending moment, at  $x = 0$ , is

$$M_m = EI w_{,xxm} = -0.27751 \phi_L q L^2 \quad (1.45)$$

the negative sign correctly indicating flexural compression to be acting on the lower part of the pipeline section. Further, the maximum compressive stress  $\sigma_m$  induced in the pipe, noting equations (1.31), (1.42) and (1.45), takes the form

$$\sigma_m = \frac{20.19EI}{AL^2} + 0.27751\phi_L q r L^2 / I \quad (1.46)$$

Having established the relationships between  $w$  and  $L$ , incorporating  $w_m$ ,  $w_{,xm}$  and  $\sigma_m$ , and the buckling force  $P$ , it is now necessary to determine the dependence of  $P$  upon  $T(P_0)$ . This is achieved by considering the slip length characteristics. The linearised slip length field equation, noting equation (1.27), can be given by

$$AEu_{,xx} = -\phi_A q \quad L \leq x \leq L+L_s \quad (1.47)$$

which yields the general solution, for the fully mobilised modelling,

$$u = -\left(\frac{\phi_A q}{AE}\right) \frac{x^2}{2} + B_1 x + B_2 \quad (1.48)$$

where  $B_i$ ,  $i = 1, 2$ , are constants of integration.

The appropriate slip length boundary conditions take the form

$$u|_{L+L_s} = 0 \quad (1.49)$$

$$u',x|_{L+L_S} = 0 \quad (\text{transversality}) \quad (1.50)$$

$$u',x|_L = \frac{(P_O - P)}{AE} \quad (1.51)$$

Substituting equations (1.49) and (1.50) into equation (1.48) gives the axial displacement expression

$$u = - \frac{\phi_A q}{2AE} \left[ (L+L_S)^2 + x(x-2L-2L_S) \right] \quad (1.52)$$

Differentiating equation (1.52) with respect to  $x$  and employing equation (1.51) affords

$$L_S = (P_O - P) / \phi_A q \quad (1.53)$$

Substituting for  $L_S$  in equation (1.52) and incorporating the identity  $u|_L = u_S$ , then, for  $x = L$ , equation (1.52) yields

$$u_S = - \frac{(P_O - P)^2}{2AE\phi_A q} \quad (1.54)$$

The matching compatibility condition at the buckle/slip length interface, noting equation (1.29), takes the form

$$u_S = (P_O - P)L/AE - 0.5 \int_0^L (w',x)^2 dx \quad (1.55)$$

in which the integral term, noting equations (1.39) and (1.41), affords

$$0.5 \int_0^L (w, x)^2 dx = 1.0225 \times 10^{-3} \left( \frac{\phi_L q}{EI} \right)^2 L^7 \quad (1.56)$$

Equating equation (1.55) with equation (1.54), noting equations (1.42) and (1.56), yields, upon manipulation,

$$P_0 = \frac{20.19EI}{L^2} + \phi_A q L \left[ \left( 1 + 2.045 \times 10^{-3} \frac{AE}{\phi_A q} \left[ \frac{\phi_L q}{EI} \right]^2 L^5 \right)^{\frac{1}{2}} - 1 \right] \quad (1.57)$$

Solutions for  $P_0$  are thereby obtained in terms of discrete values of  $L$  and substituted into equation (1.6) to determine  $T$ . Effectively, therefore, for any given action  $T$ , structural response in terms of  $w$ ,  $P$ ,  $L$ ,  $w_m$ ,  $w_{xm}$ ,  $\sigma_m$ ,  $u$ ,  $L_S$  and  $u_S$  can be determined noting equations (1.39), (1.42), (1.43), (1.44), (1.46), (1.52), (1.53) and (1.54).

### 1.4.3 Lateral Mode 2 Analysis

The topology of lateral mode 2 is depicted in Fig. 1.5 (b). The formulation is similar to that for lateral mode 1 with the linearised flexural field equation given in equation (1.32) which yields the general solution

$$w = A_1 \cos nx + A_2 \sin nx + A_3 x + A_4 - \frac{mx^2}{2n^2} \quad (1.58)$$

where  $A_i$ ,  $i = 1,2,3,4$ , are constants of integration. The appropriate boundary conditions within the buckling region take the form

$$w|_0 = 0 \quad (1.59)$$

$$w'_{,xx}|_0 = 0 \quad (1.60)$$

$$w|_L = 0 \quad (1.61)$$

$$w'_{,x}|_L = 0 \quad (1.62)$$

$$w'_{,xx}|_L = 0 \quad (\text{transversality}) \quad (1.63)$$

Employing the boundary conditions given in equations (1.59), (1.60), (1.61) and (1.62) on equation (1.58) affords the lateral displacement expression

$$w = \frac{mL^4}{(nL)^4} \left[ 1 - \cos nx + \frac{nL}{2} \sin nx - \frac{(nL)^2}{2} \left( \frac{x^2}{L^2} - \frac{x}{L} \right) \right] \quad (1.64)$$

Equating this expression with the transversality boundary condition given in equation (1.63) yields

$$\tan nL/2 = 0 \quad (1.65)$$

with the lowest non-trivial root affording

$$nL = 2\pi \quad (1.66)$$

Hence the buckling load is evaluated by substituting for  $n$ , with

$$P = 4\pi^2 EI/L^2 \quad (1.67)$$

The maximum amplitude occurs at  $x = 0.3464 L$ , noting equations (1.64) and (1.66), such that

$$w_m = 5.532 \times 10^{-3} \frac{\phi_L q L^4}{EI} \quad (1.68)$$

and the maximum slope, at  $x = 0$ , is given by

$$w_{,xm} = \frac{\phi_L q L^3}{4\pi^2 EI} \quad (1.69)$$

while the maximum bending moment, at  $x = 0.299L$ , is

$$M_m = EI w_{,xxm} = -0.10884 \phi_L q L^2 \quad (1.70)$$

Further, the maximum compressive stress induced in the pipe, noting equations (1.31), (1.67) and (1.70), takes the form

$$\sigma_m = \frac{4\pi^2 EI}{AL^2} + 0.10884 \phi_L q r L^2 / I \quad (1.71)$$

The formulation appertaining to the slip length region is identical to that of lateral mode 1; equations (1.47) through (1.55) remain valid,

except that the integral term in equation (1.55), noting equations (1.64) and (1.66), is now given by

$$0.5 \int_0^L (w, x)^2 dx = 8.715 \times 10^{-5} \left( \frac{\phi_L q}{EI} \right)^2 L^7 \quad (1.72)$$

As previously, equating equation (1.55) with equation (1.54), noting equations (1.67) and (1.72), yields, upon manipulation,

$$P_0 = \frac{4\pi^2 EI}{L^2} + \phi_A q L \left[ \left( 1 + 1.743 \times 10^{-4} \frac{AE}{\phi_A q} \left[ \frac{\phi_L q}{EI} \right]^2 L^5 \right)^{\frac{1}{2}} - 1 \right] \quad (1.73)$$

the full solution set being determined as previously.

#### 1.4.4 Lateral Mode 3 Analysis

The topology of lateral mode 3 is detailed in Fig. 1.5 (c). It can be seen that the linearised flexural field equation for the buckling region,  $0 \leq x \leq L_1$ , is similar to that given in equation (1.32) with  $w$  now replaced by  $w_1$ , that is

$$w_1'_{xxxx} + n^2 w_1'_{xx} = -m \quad 0 \leq x \leq L_1 \quad (1.74)$$

For the buckling region,  $L_1 \leq x \leq L$ , in which the lateral friction resistance acts in the opposite direction to that of the above buckling region, the appropriate linearised flexural field equation is given by

$$w_2'_{xxxx} + n^2 w_2'_{xx} = m \quad L_1 \leq x \leq L \quad (1.75)$$

The respective general solutions of equations (1.74) and (1.75) are

$$w_1 = A_1 \cos nx + A_2 \sin nx + A_3 x + A_4 - \frac{mx^2}{2n^2} \quad (1.76)$$

and

$$w_2 = A_5 \cos nx + A_6 \sin nx + A_7 x + A_8 + \frac{mx^2}{2n^2} \quad (1.77)$$

where  $A_i$ ,  $i = 1, 2, 3, 4, 5, 6, 7, 8$ , are constants of integration. The appropriate boundary and matching conditions take the form

$$w_1'_{x|0} = 0 \quad (1.78)$$

$$w_1'_{xxx|0} = 0 \quad (1.79)$$

$$w_1|_{L_1} = w_2|_{L_1} \quad (1.80)$$

$$w_1'_{x|L_1} = w_2'_{x|L_1} \quad (1.81)$$

$$w_1'_{xx|L_1} = w_2'_{xx|L_1} \quad (1.82)$$

$$w_1'_{xxx}|_{L_1} = w_2'_{xxx}|_{L_1} \quad (1.83)$$

$$w_2|_L = 0 \quad (1.84)$$

$$w_2'_{x}|_L = 0 \quad (1.85)$$

$$w_2|_{L_1} = 0 \quad (\text{transversality}) \quad (1.86)$$

$$w_2'_{xx}|_L = 0 \quad (\text{transversality}) \quad (1.87)$$

Substituting all the boundary and matching conditions given in equations (1.78) through (1.87) into equations (1.76) and (1.77) yields

$$nL_1 = 2.918 \quad (1.88)$$

and

$$nL = 7.551 \quad (1.89)$$

as the lowest non-trivial roots, with

$$A_1 = 5.3809 \times 10^{-2} \text{ mL}_1^4 \quad (1.90)$$

$$A_2 = 0 \quad (1.91)$$

$$A_3 = 0 \quad (1.92)$$

$$A_4 = 0.11121 \text{ mL}_1^4 \quad (1.93)$$

$$A_5 = 2.6905 \times 10^{-2} \text{ mL}_1^4 \quad (1.94)$$

$$A_6 = 6.2778 \times 10^{-3} \text{ mL}_1^4 \quad (1.95)$$

$$A_7 = -0.23567 \text{ mL}_1^3 \quad (1.96)$$

$$A_8 = 0.20089 \text{ mL}_1^4 \quad (1.97)$$

It can be seen that buckling region  $L_1$  involves larger lateral displacements than that of buckling region  $L_2$ . Consequently, the appropriate buckling force is evaluated by substituting equation (1.88) for  $n$ , with

$$P = 8.515 \text{ EI/L}_1^2 \quad (1.98)$$

The maximum amplitude occurs at  $x = 0$ , noting equations (1.76), (1.88), (1.90), (1.91), (1.92) and (1.93), such that

$$w_{1m} = 0.16512 \frac{\phi_L q L_1^4}{EI} \quad (1.99)$$

and the maximum slope, at  $x = 0.627L_1$ , is given by

$$w_{1'xm} = 0.22542 \frac{\phi_L q L_1^3}{EI} \quad (1.100)$$

while the maximum bending moment, at  $x = 0$ , is

$$M_m = EI w_{1'xxm} = -0.57562 \phi_L q L_1^2 \quad (1.101)$$

Further, the maximum compressive stress induced in the pipe, noting equations (1.31), (1.98) and (1.01), takes the form

$$\sigma_m = \frac{8.515EI}{AL_1^2} + 0.57562 \phi_L q r L_1^2 / I \quad (1.102)$$

The formulation appertaining to the slip length region is analogous to that of lateral mode 1 with equations (1.47) through (1.54) remaining valid. Noting the appropriate lateral mode 3 topology depicted in Fig. 1.5 (c), the matching compatibility condition at the buckle/slip length interface, given in equation (1.30), now takes the form

$$u_s = \frac{(P_o - P)L}{AE} - 0.5 \left[ \int_0^{L_1} (w_1', x)^2 dx + \int_{L_1}^L (w_2', x)^2 dx \right] \quad (1.103)$$

Noting equations (1.76), (1.77), and (1.88) through (1.97), equation (1.103) can be rewritten

$$u_s = \frac{2.588(P_o - P)L_1}{AE} - 1.7878 \times 10^{-2} \left( \frac{\phi_{Lq}}{EI} \right)^2 L_1^7 \quad (1.104)$$

Equating the expression with equation (1.54) yields

$$P_o = \frac{8.515EI}{L_1^2} + 2.588 \phi_{Aq} L_1 \left[ \left( 1 + 5.3397 \times 10^{-3} \frac{AE}{\phi_{Aq}} \left[ \frac{\phi_{Lq}}{EI} \right]^2 L_1^5 \right)^{\frac{1}{2}} - 1 \right] \quad (1.105)$$

The full solution set being determined as previously.

#### 1.4.5 Lateral Mode 4 Analysis

The topology of lateral mode 4 is illustrated in Fig. 1.5 (d). The formulation is similar to that of lateral mode 3 with the linearised field equations given in equations (1.74) and (1.75) yielding the appropriate general solutions

$$w_1 = A_1 \cos nx + A_2 \sin nx + A_3 x + A_4 - \frac{mx^2}{2n^2} \quad (1.106)$$

and

$$w_2 = A_5 \cos nx + A_6 \sin nx + A_7 x + A_8 + \frac{mx^2}{2n^2} \quad (1.107)$$

where  $A_i$ ,  $i = 1, 2, 3, 4, 5, 6, 7, 8$ , are constants of integration. The appropriate boundary and matching conditions take the form

$$w_1|_0 = 0 \quad (1.108)$$

$$w_1'_{xx}|_0 = 0 \quad (1.109)$$

$$w_1|_{L_1} = w_2|_{L_1} \quad (1.110)$$

$$w_1'_{x}|_{L_1} = w_2'_{x}|_{L_1} \quad (1.111)$$

$$w_1'_{xx}|_{L_1} = w_2'_{xx}|_{L_1} \quad (1.112)$$

$$w_1'_{xxx}|_{L_1} = w_2'_{xxx}|_{L_1} \quad (1.113)$$

$$w_2|_L = 0 \quad (1.114)$$

$$w_2'_{x}|_L = 0 \quad (1.115)$$

$$w_2|_{L_1} = 0 \quad (\text{transversality}) \quad (1.116)$$

$$w_2'_{xx}|_L = 0 \quad (\text{transversality}) \quad (1.117)$$

Substituting all the boundary and matching conditions given in equations (1.108) through (1.117) into equations (1.106) and (1.107) yields

$$nL_1 = 5.31 \quad (1.118)$$

and

$$nL = 8.54 \quad (1.119)$$

as the lowest non-trivial roots, with

$$A_1 = -1.271 \times 10^{-3} \text{ mL}_1^4 \quad (1.120)$$

$$A_2 = 3.814 \times 10^{-3} \text{ mL}_1^4 \quad (1.121)$$

$$A_3 = 2.034 \times 10^{-2} \text{ mL}_1^3 \quad (1.122)$$

$$A_4 = 1.271 \times 10^{-3} \text{ mL}_1^4 \quad (1.123)$$

$$A_5 = 1.338 \times 10^{-4} \text{ mL}_1^4 \quad (1.124)$$

$$A_6 = 1.740 \times 10^{-3} \text{ mL}_1^4 \quad (1.125)$$

$$A_7 = -5.059 \times 10^{-2} \text{ mL}_1^3 \quad (1.126)$$

$$A_8 = 3.425 \times 10^{-2} \text{ mL}_1^4 \quad (1.127)$$

It can be seen that buckling region  $L_1$  involves larger lateral displacement than that of buckling region  $L_2$ . Consequently, the appropriate buckling force is evaluated by substituting equation (1.118) for  $n$ , with

$$P = 28.20 \text{ EI/L}_1^2 \quad (1.128)$$

The maximum amplitude occurs at  $x = 0.40L_1$ , noting equations (1.106), (1.118), (1.120), (1.121), (1.122) and (1.23), such that

$$w_{1m} = 1.047 \times 10^{-2} \frac{\phi_L q L_1^4}{\text{EI}} \quad (1.129)$$

and the maximum slope, at  $x = 0$ , is given by

$$w_{1,xm} = 0.04059 \frac{\phi_L q L_1^3}{EI} \quad (1.130)$$

while the maximum bending moment, at  $x = 0.359L_1$ , is

$$M_m = EI w_{1,xxm} = -0.14880 \phi_L q L_1^2 \quad (1.131)$$

Further, the maximum compressive stress induced in the pipe, noting equations (1.31), (1.128) and (1.131), takes the form

$$\sigma_m = \frac{28.20EI}{AL_1^2} + 0.14880 \phi_L q r L_1^2 / I \quad (1.132)$$

The formulation appertaining to the slip length region is similar to that of lateral mode 3, that is, equations (1.47) through (1.54) remain valid. Further, the matching compatibility condition at the buckle/slip length interface given in equation (1.103), noting equations (1.106), (1.107) and (1.118) through (1.127), yields

$$u_s = 1.608 \frac{(P_o - P)L_1}{AE} - 2.7716 \times 10^{-4} \left( \frac{\phi_L q}{EI} \right)^2 L_1^7 \quad (1.133)$$

Equating this expression with equation (1.54) affords

$$P_0 = \frac{28.20EI}{L_1^2} + 1.608\phi_A q L_1 \left[ \left( 1 + 2.143 \times 10^{-4} \frac{AE}{\phi_A q} \left[ \frac{\phi_L q}{EI} \right]^2 L_1^5 \right)^{\frac{1}{2}} - 1 \right] \quad (1.134)$$

the full solution set being determined as previously.

#### 1.4.6 Lateral Mode $\infty$ Analysis

The topology of lateral mode  $\infty$  is depicted in Fig. 1.5 (e). The formulation is similar to that of lateral mode 1 with the linearised field equation being as given in equation (1.32) yielding the general solution

$$w = A_1 \cos nx + A_2 \sin nx + A_3 x + A_4 - \frac{mx^2}{2n^2} \quad (1.135)$$

where  $A_i$ ,  $i = 1, 2, 3, 4$ , are constants of integration.

The appropriate boundary conditions within the buckling region take the form

$$w, x|_0 = 0 \quad (1.136)$$

$$-EIw, xxx|_0 = 0 \quad (1.137)$$

$$w|_L = 0 \quad (1.138)$$

$$w,_{xx}|_L = 0 \quad (1.139)$$

$$-EIw,_{xxx}|_L = 0 \quad (\text{unique condition}^{(20)}) \quad (1.140)$$

Substituting the boundary conditions given in equations (1.136), (1.137), (1.138) and (1.139) into equation (1.135) affords the lateral displacement expression

$$w = \frac{m}{n^4} \left[ 1 + \frac{n^2 L^2}{2} - \frac{n^2 x^2}{2} - \frac{\cos nx}{\cos nL} \right] \quad (1.141)$$

Equating this expression with the unique condition given in equation (1.140) yields

$$\tan nL = 0 \quad (1.142)$$

with the lowest non-trivial root affording

$$nL = \pi \quad (1.143)$$

Hence, the buckling force is evaluated by substituting for  $n$ , with

$$P = \pi^2 EI/L^2 \quad (1.144)$$

The maximum amplitude occurs at  $x = 0$ , noting equations (1.141) and (1.143), such that

$$w_m = 7.1192 \times 10^{-2} \frac{\phi_L q L^4}{EI} \quad (1.145)$$

and the maximum slope, at  $x = L$ , is given by

$$w'_{,xm} = 0.10132 \frac{\phi_L q L^3}{EI} \quad (1.146)$$

while the maximum bending moment, at  $x = 0$ , is

$$M_m = EI w'_{,xxm} = -0.20264 \phi_L q L^2 \quad (1.147)$$

Further, the maximum compressive stress induced in the pipe, noting equation (1.31), (1.144) and (1.147), takes the form

$$\sigma_m = \frac{\pi^2 EI}{AL^2} + 0.20264 \phi_L q r L^2 / I \quad (1.148)$$

It is to be noted that this mode is unique in as much as the entire run of the pipe is taken to be subject to buckling action with  $u_S = L_S = 0$ .

Consequently, the compatibility expression given in equation (1.29) can be rewritten

$$\frac{(P_0 - P)L}{AE} = 0.5 \int_0^L (w'_{,x})^2 dx \quad (1.149)$$

which yields, noting equations (1.141), (1.143) and (1.144),

$$P_0 = \frac{\pi^2 EI}{L^2} + 3.0112 \times 10^{-3} AE \left( \frac{\phi_L q}{EI} \right)^2 L^6 \quad (1.150)$$

the full solution set being determined as previously except that  $u$ ,  $u_s$  and  $L_s$  do not exist in this mode.

#### 1.4.7 Vertical Mode Analysis

The essential features of vertical mode are depicted in Figs. 1.11 (a) and (b) which show the fully mobilised topology and axial force distribution respectively. The linearised flexural field equation, noting equation (1.24), can be given by

$$v_{,xxxx} + n^2 v_{,xx} = -m \quad 0 \leq x \leq L \quad (1.151)$$

where  $n^2 = P/EI$  and  $m = q/EI$ . The appropriate boundary conditions within the buckling region take the form

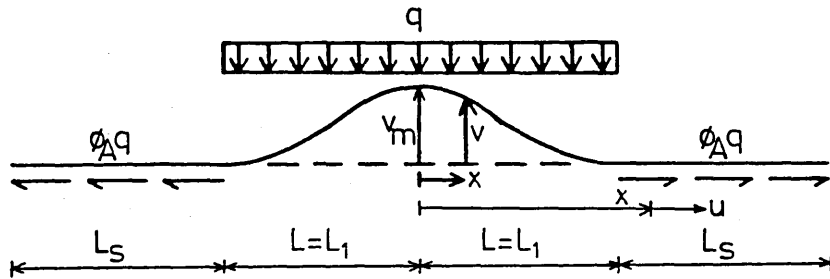
$$v_{,x}|_0 = 0 \quad (1.152)$$

$$-EIV_{,xxx}|_0 = 0 \quad (1.153)$$

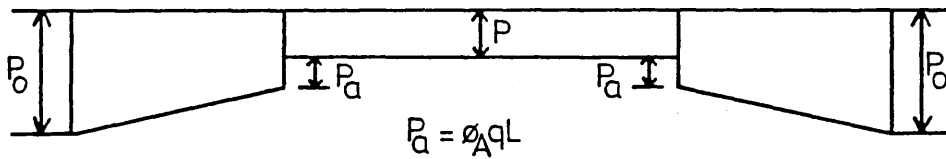
$$v|_L = 0 \quad (1.154)$$

$$v_{,x}|_L = 0 \quad (1.155)$$

$$v_{,xx}|_L = 0 \quad (\text{transversality}) \quad (1.156)$$



(a) Topology



(b) Axial Force Distribution

Fig.111 Vertical Mode - Details of Fully Mobilised Model

The general solution of equation (1.151) is

$$v = A_1 \cos nx + A_2 \sin nx + A_3 x + A_4 - \frac{mx^2}{2n^2} \quad (1.157)$$

where  $A_i$ ,  $i = 1, 2, 3, 4$ , are constants of integration. Substituting the boundary conditions given in equations (1.152) to (1.155) into equation (1.157) affords the vertical displacement expression

$$v = \frac{mL^4}{2(nL)^2} \left[ 1 - \frac{x^2}{L^2} - \frac{2(\cos nx - \cos nL)}{nL \sin nL} \right] \quad (1.158)$$

Equating this expression with the transversality boundary condition given in equation (1.156) yields

$$\tan nL = nL \quad (1.159)$$

with the lowest non-trivial root affording

$$nL = 4.4934 \quad (1.160)$$

Hence, the buckling force is evaluated by substituting for  $n$ , with

$$P = 20.19 EI/L^2 \quad (1.161)$$

The maximum amplitude occurs at  $x = 0$ , noting equations (1.158) and (1.160), such that

$$v_m = 3.8512 \times 10^{-2} \frac{qL^4}{EI} \quad (1.162)$$

and the maximum slope, at  $x = 0.398L$ , is given by

$$v_{,xm} = 0.06926 \frac{qL^3}{EI} \quad (1.163)$$

while the maximum bending moment, at  $x = 0$ , is

$$M_m = EIv_{,xxm} = -0.27751 qL^2 \quad (1.164)$$

Further, the maximum compressive stress induced in the pipe, noting equations (1.31), (1.161) and (1.164), takes the form

$$\sigma_m = \frac{20.19EI}{AL^2} + 0.27751 qrL^2/I \quad (1.165)$$

The linearised slip length field equation, noting equation (1.27), can be given by

$$AEu_{,xx} = -\phi_A q \quad L \leq x \leq L+L_s \quad (1.166)$$

which yields the general solution, for the fully mobilised modelling,

$$u = -\left(\frac{\phi_A q}{AE}\right) \frac{x^2}{2} + B_1 x + B_2 \quad (1.167)$$

where  $B_i$ ,  $i = 1, 2$ , are constants of integration.

The appropriate slip length boundary conditions take the form

$$u|_{L+L_s} = 0 \quad (1.168)$$

$$u, x|_{L+L_s} = 0 \quad (\text{transversality}) \quad (1.169)$$

$$u, x|_L = \frac{(P_o - P) - P_a}{AE} \quad (1.170)$$

It is to be noted that the parameter  $P_a$  occurs only in the vertical mode slip length modelling - note equation (1.15).  $P_a$  is, essentially, the axial force component frictionally induced on the pipe by the vertical shear reaction at the buckle/slip length interface. Noting Fig. 1.11, this force can be represented by

$$P_a = \phi_A qL \quad (1.171)$$

Substituting equations (1.168) and (1.169) into equation (1.167) gives the axial displacement expression

$$u = - \frac{\phi_A q}{2AE} \left[ (L+L_s)^2 + x(x-2L-2L_s) \right] \quad (1.172)$$

Differentiating equation (1.172) with respect to  $x$  and employing equations (1.170) and (1.171) affords

$$L_s = \frac{(P_o - P) - \phi_A qL}{\phi_A q} \quad (1.173)$$

Substituting for  $L_S$  in equation (1.172) and incorporating the identity  $u|_L = u_S$ , then for  $x = L$ , equation (1.172) yields

$$u_S = - \frac{(P_O - P - \phi_A q L)^2}{2AE\phi_A q} \quad (1.174)$$

The appropriate matching compatibility condition at the buckle/slip length interface, noting equation (1.29), takes the form

$$u_S = \frac{(P_O - P)L}{AE} - 0.5 \int_0^L (v_{,x})^2 dx \quad (1.175)$$

which can be rewritten, noting equations (1.158) and (1.160),

$$u_S = \frac{(P_O - P)L}{AE} - 1.0225 \times 10^{-3} \left( \frac{q}{EI} \right)^2 L^7 \quad (1.176)$$

Equating this expression with equation (1.174) affords

$$(P_O - P)^2 = 2.045 \times 10^{-3} \frac{\phi_A q^3 AEL^7}{(EI)^2} - (\phi_A q L)^2 \quad (1.177)$$

which can be further simplified, noting equation (1.161), to

$$P_o = \frac{20.19EI}{L^2} + \frac{qL}{EI} \left[ 2.045 \times 10^{-3} AE \phi_A q L^5 - (\phi_A EI)^2 \right]^{\frac{1}{2}} \quad (1.178)$$

the full solution set being obtained as previously.

It should be noted that as a result of assuming fully mobilised axial friction resistance, the vertical mode modelling can be shown to be invalid at small values of vertical displacement. Clearly, noting Fig. 1.11 (b),

$$(P_o - P) \geq P_a \quad (1.179)$$

whereupon, substituting equations (1.171) and (1.179) into equation (1.177), there is the requirement

$$L \geq \left[ \frac{978 \phi_A q}{AE} \left( \frac{EI}{q} \right)^2 \right]^{1/5} \quad (1.180)$$

which affords the corresponding maximum amplitude, noting equation (1.162), such that

$$v_m \geq \frac{9.5031q}{EI} \left[ \frac{\phi_A q}{AE} \left( \frac{EI}{q} \right)^2 \right]^{4/5} \quad (1.181)$$

It can be noted, however, that the above restrictions do not apply when  $v_m = L = 0$  since  $(P_o - P) = P_a = 0$  at this state - note equations (1.171) and (1.177) - although the asymptotic behaviour of the present model

precludes this from being of value to the analyst. Further, these restrictions on the established fully mobilised vertical modelling<sup>(20, 31, 36, 37, 50)</sup> as denoted in equations (1.180) and (1.181) have not been previously reported.

#### 1.4.8 Discussion

Results are presented for a variety of axial ( $\phi_A$ ) and lateral ( $\phi_L$ ) friction coefficients between 0.1 and 0.7.<sup>(20, 50)</sup> Considering first the lateral modes, Fig. 1.12 shows the comparison of all the lateral modes with  $\phi_A = \phi_L = 0.5$ . Minimum 'safe' temperature rise,  $T_{\min}$ , is defined as the minimum temperature rise at which buckling occurs. It can be shown that lateral mode 4 has the lowest value of  $T_{\min}$ . Other combinations of friction coefficients, using a range of  $\phi_A$  and  $\phi_L$  between 0.1 and 0.7, have been analysed (not shown) to ensure that lateral mode 4 is indeed the critical lateral mode. Figs. 1.13-1.16 depict the graphs for lateral mode 4 using various combinations of  $\phi_A$  and  $\phi_L$ . The appropriate values of  $T_{\min}$ , together with the corresponding values of maximum amplitude,  $w_{1m}$  and buckling length  $L_1$  at the minimum safe temperature rise state, are given in Table 1.3. It can be seen that an increase in  $\phi_A$  results in an increase in  $T_{\min}$  and decrease in the

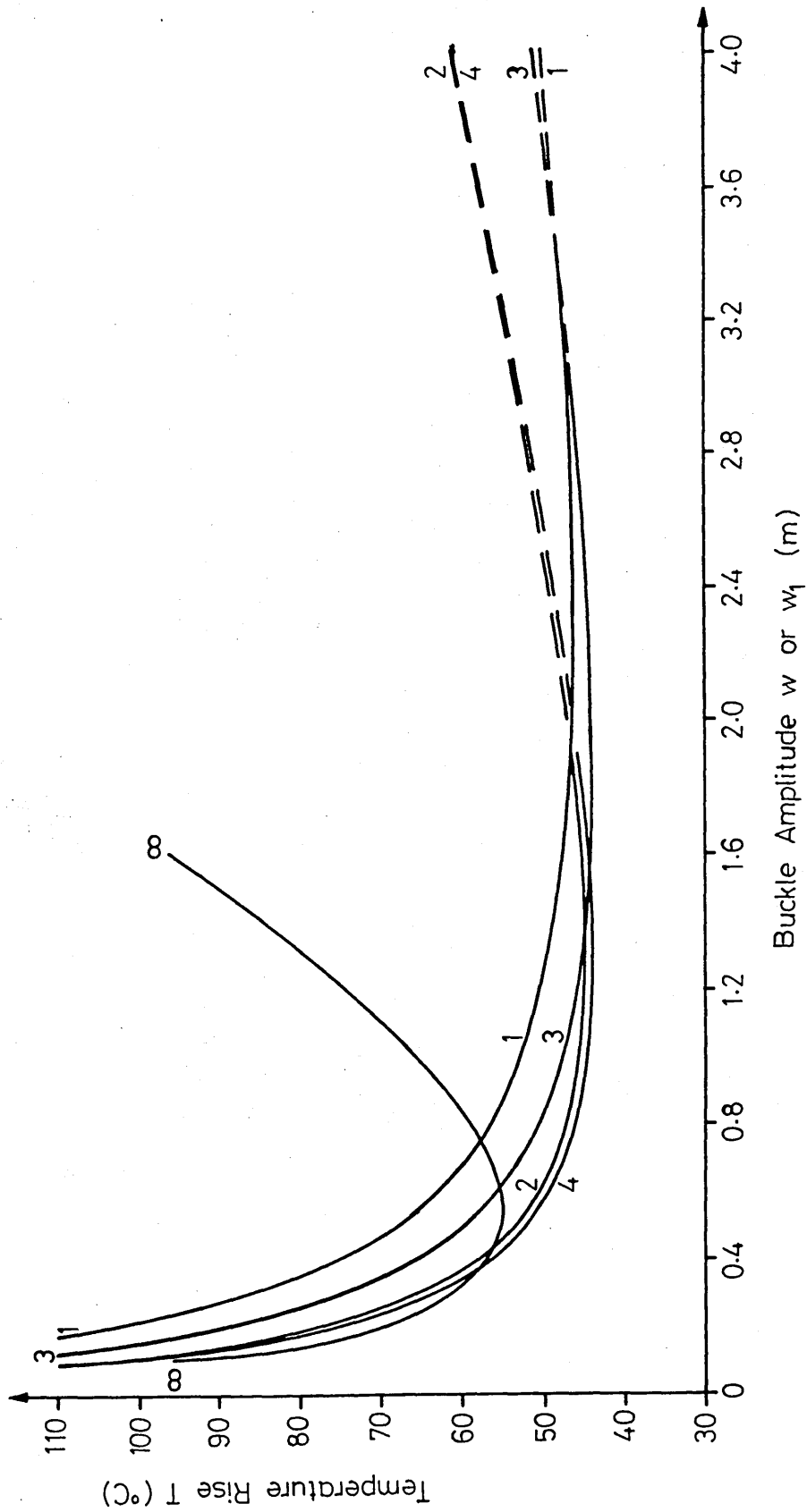


Fig. 1.12 Comparison of Lateral Modes ( $\varphi_A = \varphi_L = 0.5$ )

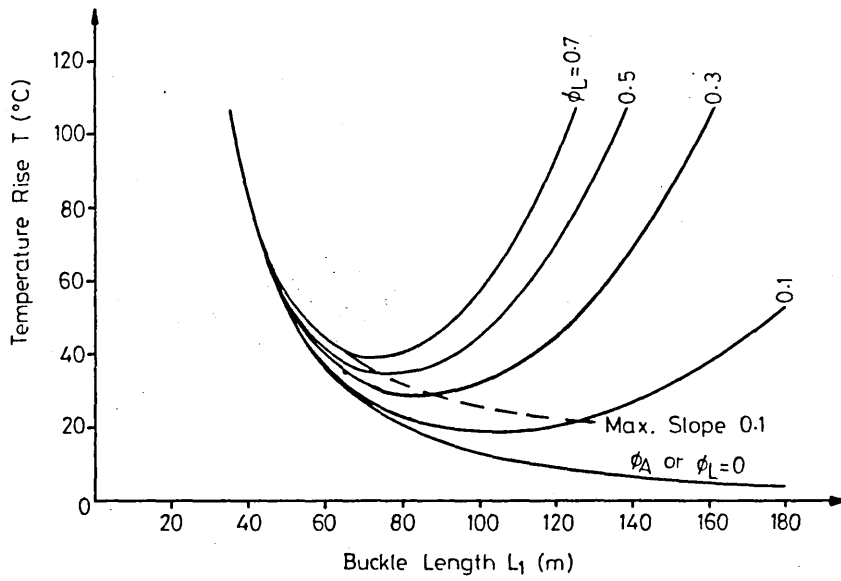


Fig.1-13 Lateral Mode 4 -  $\phi_A = 0.1$

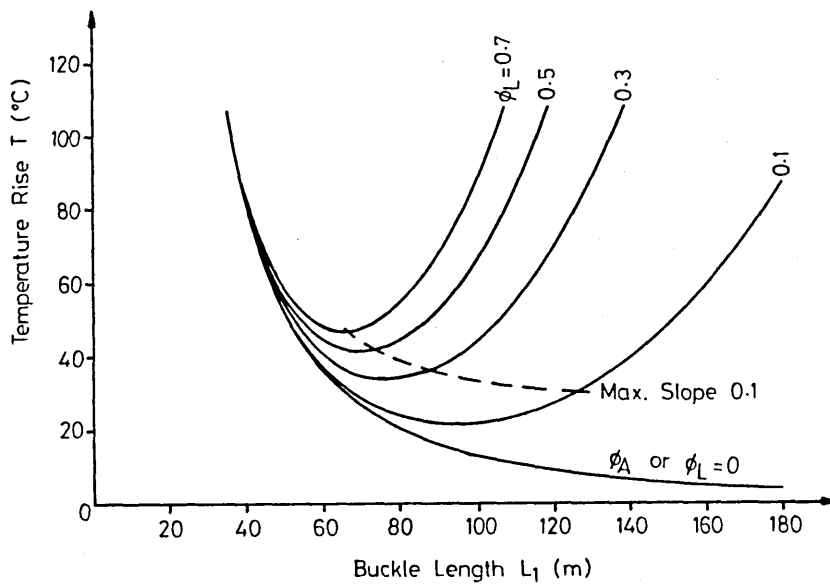


Fig.1-14 Lateral Mode 4 -  $\phi_A = 0.3$

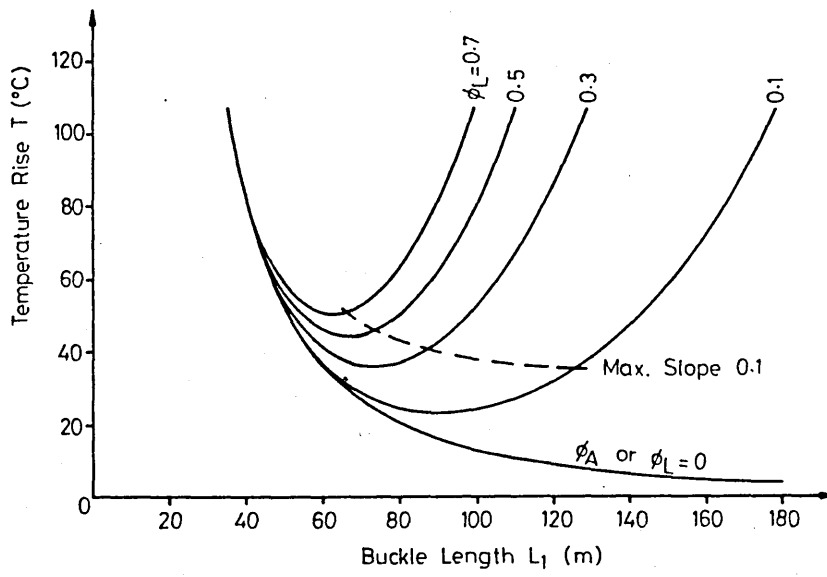


Fig. 1.15 Lateral Mode 4 -  $\phi_A = 0.5$

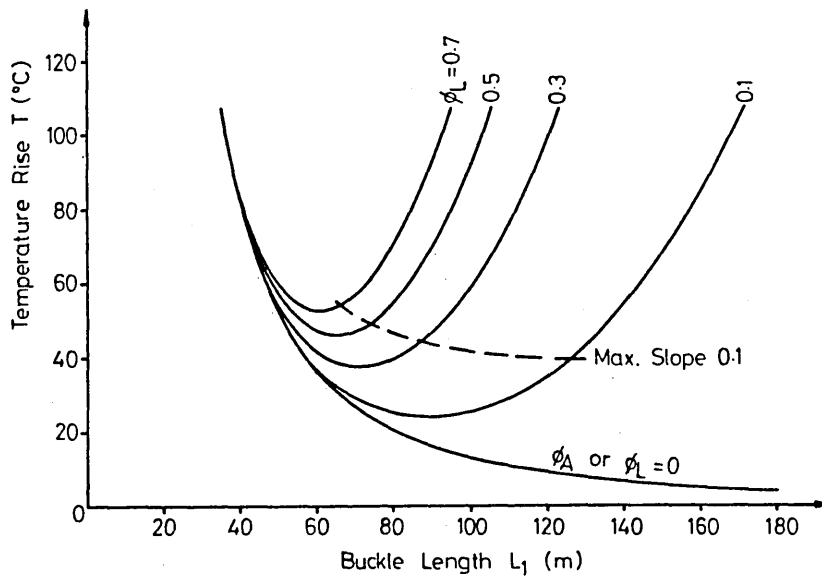


Fig. 1.16 Lateral Mode 4 -  $\phi_A = 0.7$

$\phi_L \backslash \phi_A$	0	0.1	0.3	0.5	0.7	
0	0	0	0	0	0	$T_{\min} (^{\circ}\text{C})$
	$\infty$	$\infty$	$\infty$	$\infty$	$\infty$	$w_{1m} (m)$
	$\infty$	$\infty$	$\infty$	$\infty$	$\infty$	$L_1 (m)$
0.1	0	18.5	21.5	22.7	23.4	$T_{\min} (^{\circ}\text{C})$
	$\infty$	1.45	1.01	0.87	0.80	$w_{1m} (m)$
	$\infty$	103.1	94.3	90.9	88.9	$L_1 (m)$
0.3	0	28.2	33.4	35.8	37.4	$T_{\min} (^{\circ}\text{C})$
	$\infty$	1.93	1.32	1.11	1.00	$w_{1m} (m)$
	$\infty$	84.2	76.6	73.4	71.5	$L_1 (m)$
0.5	0	34.1	40.8	43.9	46.0	$T_{\min} (^{\circ}\text{C})$
	$\infty$	2.20	1.50	1.27	1.14	$w_{1m} (m)$
	$\infty$	76.6	69.6	66.7	64.9	$L_1 (m)$
0.7	0	38.7	46.4	50.1	52.6	$T_{\min} (^{\circ}\text{C})$
	$\infty$	2.41	1.64	1.38	1.23	$w_{1m} (m)$
	$\infty$	72.0	65.4	62.6	60.9	$L_1 (m)$

Table 1.3 Action-Response Data at  $T_{\min}$  State for Lateral Mode 4

corresponding values of  $w_{1m}$  and  $L_1$ ; an increase in  $\phi_L$ , however, results in increasing  $T_{min}$  and  $w_{1m}$  but decreasing  $L_1$ . With regard to the vertical mode, Fig. 1.17 depicts the temperature rise against buckling length for a set of axial friction coefficients,  $\phi_A$ . All the loci in this figure possess deformations beyond their respective invalid lower ranges; note equations (1.180) and (1.181). These lower ranges of invalidity are subject to the geotechnical and pipeline parameters employed. The 0.1 radian limit<sup>(51)</sup> appertaining to linearised analyses is indicated on Figs. 1.13-1.17 and shown by the dashed loci in Fig. 1.12. The important minimum safe temperature rise,  $T_{min}$ , states of all the lateral modes depicted in Fig. 1.12 are within this limit. It is apparent from Figs. 1.12-1.17 that all the lateral modes, except lateral mode  $\infty$  which can be considered to be of academic interest only<sup>(50)</sup>, occur at a lower temperature rise than the vertical mode. The lateral modes are therefore dominant unless lateral restraint is provided by trenching. Modal interaction also becomes possible noting this latter consideration.

At this stage, an overview is essential. The results given in Fig. 1.12 are at variance with those given by Hobbs<sup>(20)</sup>, wherein lateral mode  $\infty$  is claimed to be the critical mode. It could be argued that as action (temperature rise) is a distributive action,

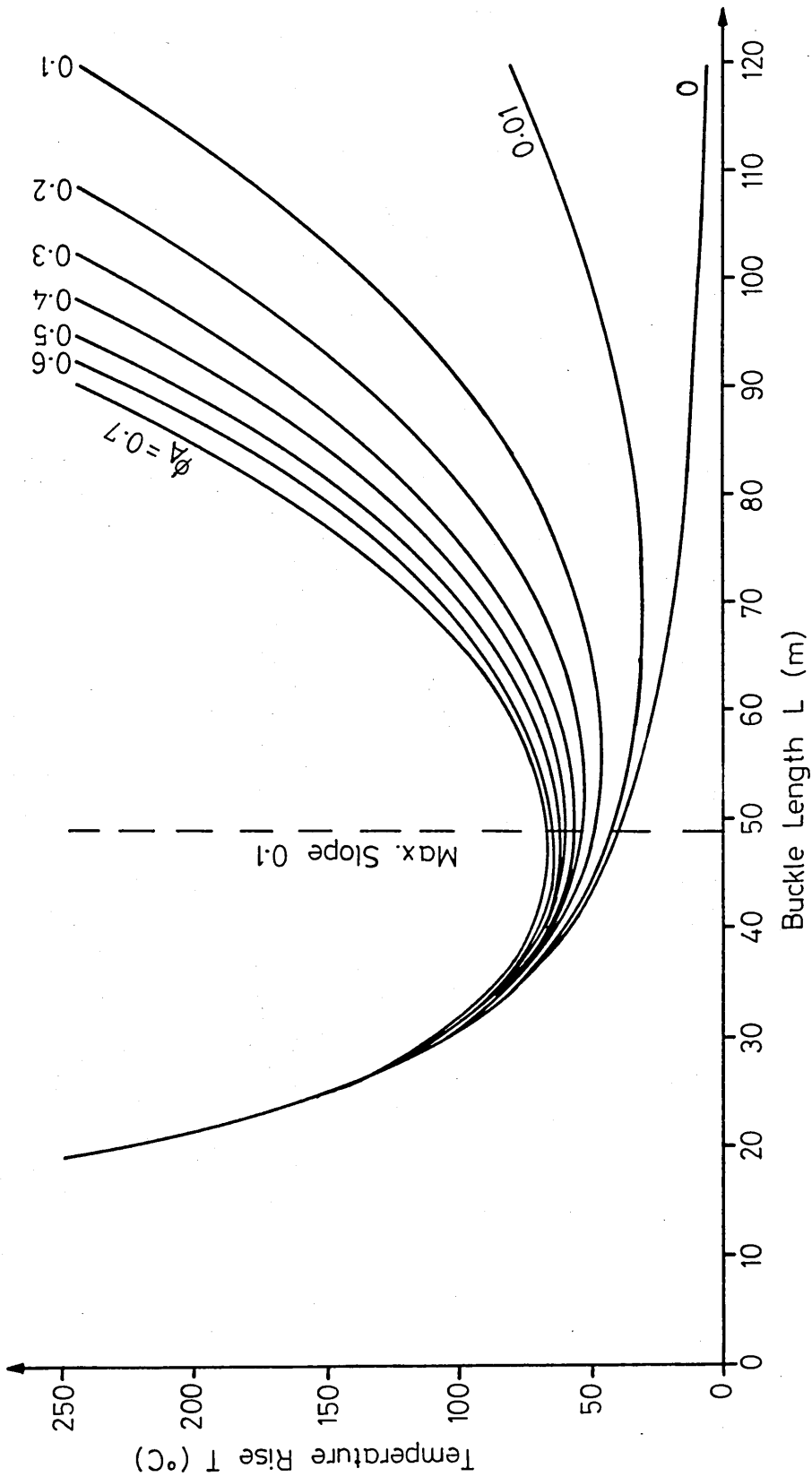


Fig. 1.17 Results for Vertical Mode

a distributive response (that is, lateral mode  $\infty$  wherein the pipeline buckles fully along its length) is to be anticipated. However, the modelling employed, in no way at variance with that employed by Hobbs<sup>(20)</sup>, does not afford this to be the critical response. This finding has subsequently been verified and acknowledged by Hobbs<sup>(50)</sup> in later work. Indeed, lateral mode 4 could be argued to be a semi-infinity mode - note Fig. 1.5. Lateral modes 1 to 4 can be considered to be localised buckling mode<sup>(38)</sup> forms of lateral mode  $\infty$ ; indeed, perhaps this is the only practical role for this singular case.

Further, all the lateral mode action-response loci depicted in Figs. 1.12-1.16 approach the thermal axis asymptotically; this is a consequence of assuming fully mobilised lateral friction resistance even for vanishingly small lateral displacements. This can be observed from consideration of, for example, equation (1.32), wherein, applying the critical state criterion

$$w_{,xx} \equiv 0 \quad (1.182)$$

affords the loading intensity to be

$$w_{,xxxx} = -\phi_L q/EI \neq 0 \quad (1.183)$$

Regarding the vertical mode, asymptotic behaviour is similarly caused by assuming the self-weight to be

fully mobilised. There is also the additional problem of defining the axial friction resistance force in a manner which overcomes the previously denoted inherent limitations involved when using a fully mobilised axial resistance force modelling ( $v > 0$ ). As in lateral buckling, the invalidity of the vertical mode analysis can be observed from consideration of equation (1.151), wherein, applying the critical state criterion

$$v_{,xx} \equiv 0 \quad (1.184)$$

affords the loading intensity to be

$$v_{,xxxx} = -q/EI \neq 0 \quad (1.185)$$

Indeed, only the minimum safe temperature rise,  $T_{\min}$ , is of immediate use in the established fully mobilised modellings. A published technical article<sup>(21)</sup> concerning the foregoing discussion is given in Appendix I (A).

## 1.5 SUMMARY

The essential factors involved in submarine pipeline buckling have been set out and the established analyses detailed and corrected as necessary. These analyses have been set out in a novel field equation format and a set of appropriate limits, errors and forward path developments discussed.

With regard to the developments detailed in the following, it is first proposed to establish the nature of the necessary geotechnical parameters.

This is because definition of the critical state at which axial-flexural bifurcation occurs requires that geotechnical experimentation be undertaken in order that data relating to the appropriate axial and lateral friction resistance characteristics, as well as to the pipeline's submerged self-weight inertial characteristics associated with the vertical buckling mode, be established. The appropriate analyses will then ensue.

## 2.1 INTRODUCTION

An important feature of the submarine pipeline buckling behaviour concerns the resistance to movement of pipelines provided by the supporting medium. Assumptions previously made included that axial and lateral friction resistance forces were taken to be fully mobilised throughout. (20,21,50) Despite an intensive literature search, little information relating to the nature of frictional resistance force was forthcoming. (52-58) Experimentation was therefore required in order to provide data relating to fully mobilised frictional coefficient values, sub-fully mobilised frictional coefficient values and to the corresponding displacements to which they appertain.

Another important feature with regard to the buckling region of the vertical mode concerns the gradual nature by means of which the pipeline's submerged self-weight is incurred at the onset of buckling. Effectively, this feature concerns the recovery of the sea bed upon unloading. The established modelling assumes this force to be fully mobilised, that is, the sea bed is taken to be rigid. Initially, however, attention is focussed upon the friction resistance force characteristics.

## 2.2 FRICTION FORCE CHARACTERISTICS

The vertical and lateral system topologies are given in Figs. 2.1 and 2.2 respectively. It is apparent that in the vertical buckling mode, the pipe will, with regard to the interface frictional forces, involve only axial coefficient action. The established fully mobilised modelling<sup>(20,21,50)</sup> employs, noting equations (1.53) and (1.173), a resultant axial friction force  $F_A$  given by

$$F_A = \phi_A q L_S \quad (2.1)$$

where

$$F_A = P_O - P - \phi_A q L \quad (2.2)$$

for the vertical mode, and

$$F_A = P_O - P \quad (2.3)$$

for all the lateral modes except lateral mode  $\infty$  in which axial friction force does not exist. The revised deformation-dependent axial friction modelling is illustrated in Fig. 2.3. The axial friction resistance force is denoted therein by  $f_A q$  per unit length where parameter  $f_A$  is, in formal terms, some variable in  $x$  for  $L \leq x \leq L + L_S$ . Equilibrium affords the slip length friction resistance force to be more formally given by

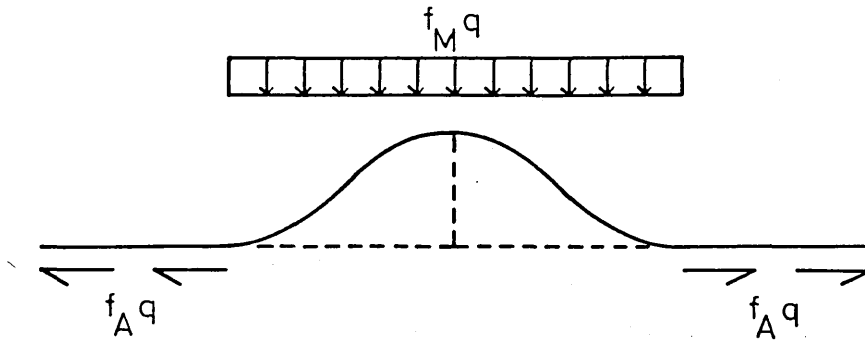


Fig. 2-1 Simplified Vertical Mode Topology

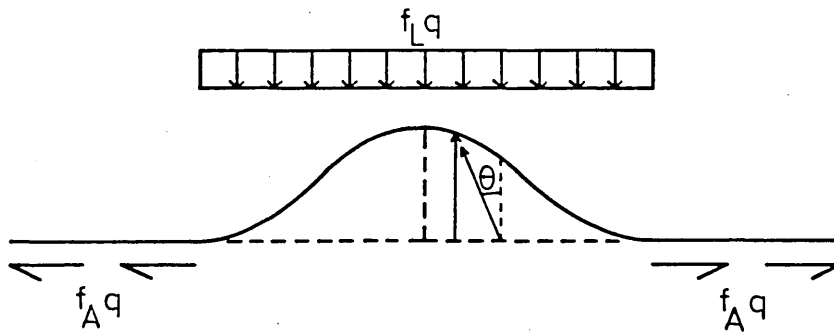


Fig. 2-2 Simplified Lateral Mode 1 Topology

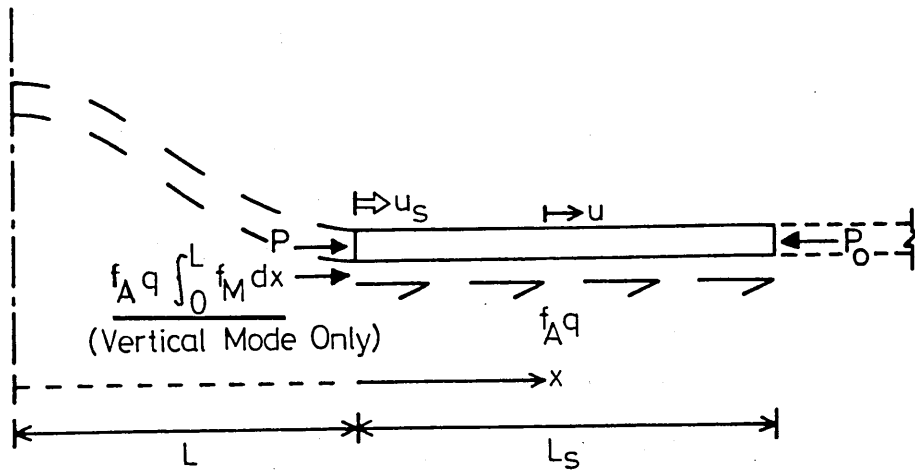


Fig. 2.3 Slip Length Characteristics

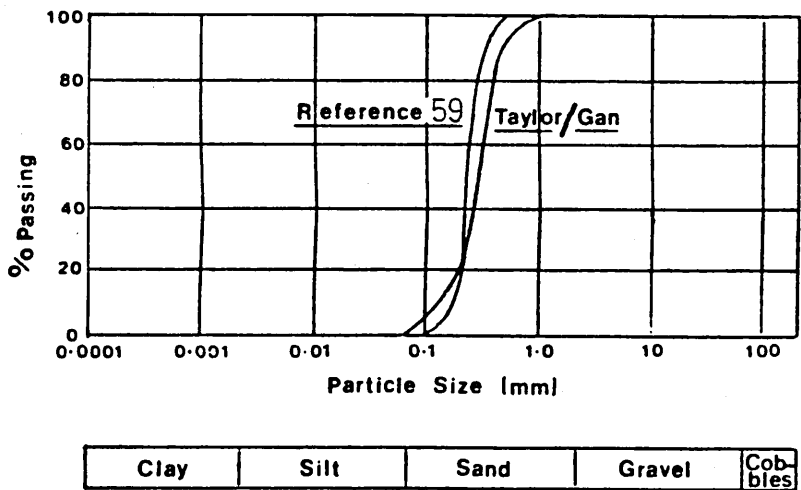


Figure 2.4 Sieve Analysis

$$F_A = \int_L^{L+L_s} f_A q \, dx \quad (2.4)$$

It can be seen from equations (2.1) and (2.4) that the established modelling therefore assumes  $f_A$  to be a constant ( $\phi_A$ ) throughout the slip length. Further, in the case of lateral buckling, the pipe will incur not only both axial and lateral friction resistances, but, in addition, the motion involved will give rise to friction resistance occurring in relatively arbitrary orientations. This is denoted by angle  $\theta$  in Fig. 2.2. The roles played by the axial and lateral friction resistance forces have already been delineated in Chapter 1, and Figs. 1.7 and 1.8 serve to illustrate the generalised axial and lateral friction parameters  $f_A$  and  $f_L$ .

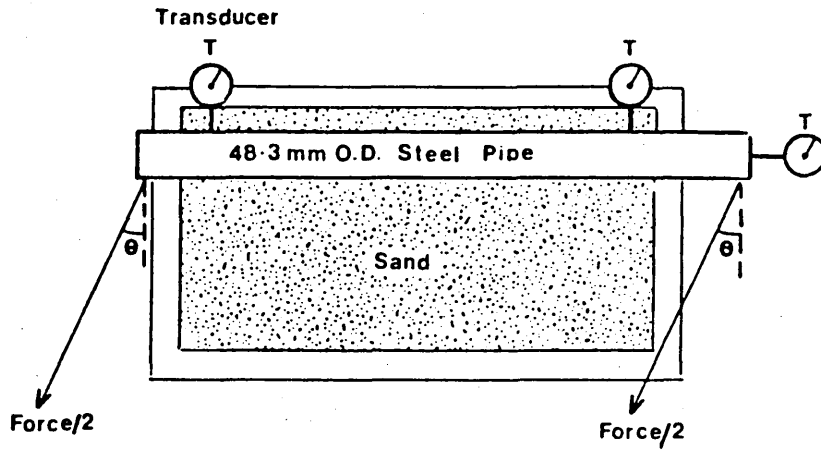
The problem therefore centred on determining the values of the friction coefficients for arbitrary orientations of force-displacement. Further, some assessment of the displacements at which these coefficients become fully established was to be sought. The objective was, therefore, to investigate the force-displacement relationships for a pipe subject to laterally, axially and arbitrarily oriented action when in contact with a sand foundation. Sand was chosen in view of North Sea conditions<sup>(59)</sup>, and a sieve analysis enabled the requisite fine to medium

sand to be determined; the sieve analysis results are depicted in Fig. 2.4 with the appropriate data given in Appendix II (A). Three typical frictional interface configurations are considered. Model tests were deemed to offer sufficient insight at this stage and dry testing was employed for convenience noting that a Coulomb medium was involved. That is, dry testing for determining saturated fine to medium sand behaviour is acceptable given that in both conditions the sand is cohesionless and that the angle of internal friction is unchanged. (60)

Finally, drained triaxial tests upon the material were undertaken in order to determine the respective modulus. This parameter has a bearing upon vertical lift-off characteristics, this feature being discussed following delineation of the frictional force experimentation.

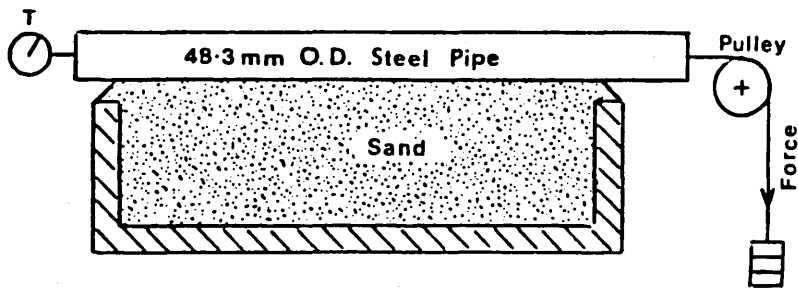
### 2.3 EXPERIMENTAL PROGRAMME

A 1 m long steel pipe of outer diameter 48.3 mm, thickness 3.2 mm and a self-weight of 34.92 N/m was used for all the tests. Fig. 2.5 depicts the line diagram of the pipe section under arbitrarily oriented force ( $0 < \theta < \pi/2$ ); this arrangement was also employed for the application of lateral force ( $\theta = 0$ ). Fig. 2.6 depicts the line diagram of the pipe



Schematic (Plan) View of Pipe under Arbitrary/Lateral Forces  
 $10^\circ \leq \theta < 90^\circ$

Figure 2.5



Schematic (Side) View of Pipe under Axial Force ( $\theta = 90^\circ$ )

Figure 2.6

under axial force ( $\theta = \pi/2$ ). The pipe possessed a 150 mm overhang with respect to the sand flume employed in order to prevent the pipe from digging into the sand when undergoing axial movement. Further equipment included weights, wires, pulleys and transducers for measuring the longitudinal and transverse displacement components of the pipe. Three frictional interface configurations were considered as trenching will clearly affect buckling response. The configurations chosen were that with the pipe simply resting on the supporting medium ( $\bar{R}$ ), a basic entrenched topology ( $\bar{E}$ ) and an entrenched arrangement involving compaction of the supporting medium ( $\bar{P}$ ). Trenching constituted a quarter pipe diameter penetration of the supporting medium and compaction studies were primarily for qualitative purposes. Quasi-static behaviour is stipulated throughout.

#### 2.4 EXPERIMENTAL PROCEDURE

The disturbing force was applied to the pipe in the horizontal plane at values of  $\theta$  ranging from zero through to  $\pi/2$  in increments of  $\pi/12$ . The three interface configurations were thereby considered in each of these seven orientations. The disturbing force was applied in the form of two equal component forces acting at the ends of the pipe except in the axial case studies in which the disturbing force was

only applied to the respective end of the pipe. It was considered that a long pipeline on the sea bed would slide rather than roll along its longitudinal axis under lateral force, hence the transducer readings were subject to the prevention of any significant rolling movement. The onset of full mobilisation for each of the twenty-one cases considered was taken as being the state at which displacement continued without any further increase in the respective disturbing force. Each test was undertaken four times, average results being finally recorded.

## 2.5 EXPERIMENTAL OBSERVATIONS AND RESULTS

The results are given in Figs. 2.7 to 2.13 in the form of resistance force-displacement loci. For the lateral ( $\theta = 0$ ) cases, a sand wedge was formed in front of the pipe as the force was applied, the wedge gradually growing in height. Full mobilisation was preceded by the pipe rising over the respective wedge. Both trenched cases initially required the pipe to rise out of the respective trench, and this effect is clearly displayed in Fig. 2.7 by virtue of the appropriately stiffer force-displacement loci obtained. Further, the maximum resistance values obtained, also denoted in Fig. 2.7, reflect the greater inertia possessed by the trenched cases. With regard

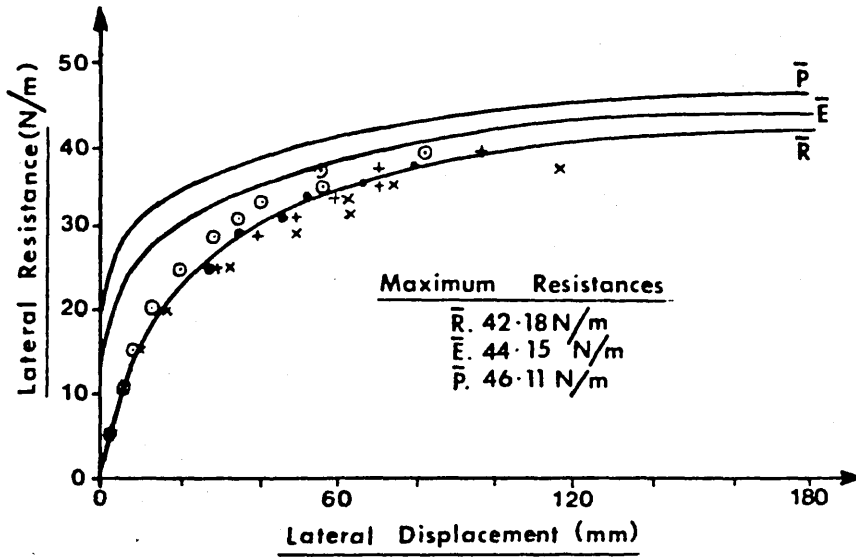


Figure 2.7 Force - Displacement Relationships  $\theta = 0^\circ$

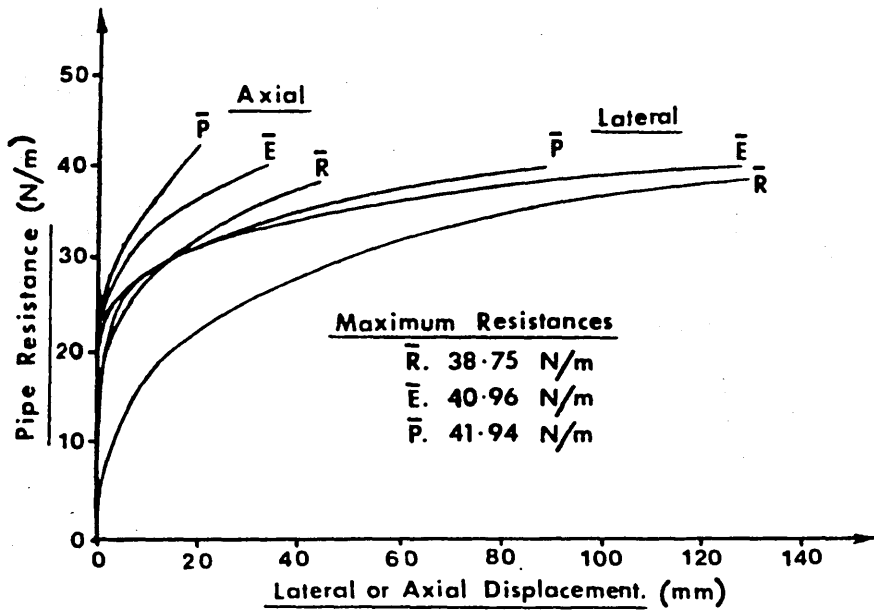


Figure 2.8 Force - Displacement Relationships  $\theta = 15^\circ$

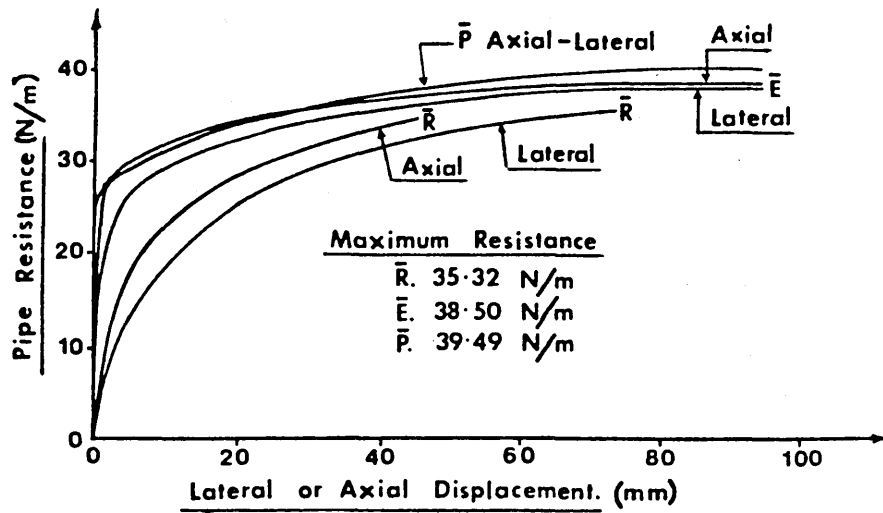


Figure 2.9 Force - Displacement Relationships  $\theta = 30^\circ$

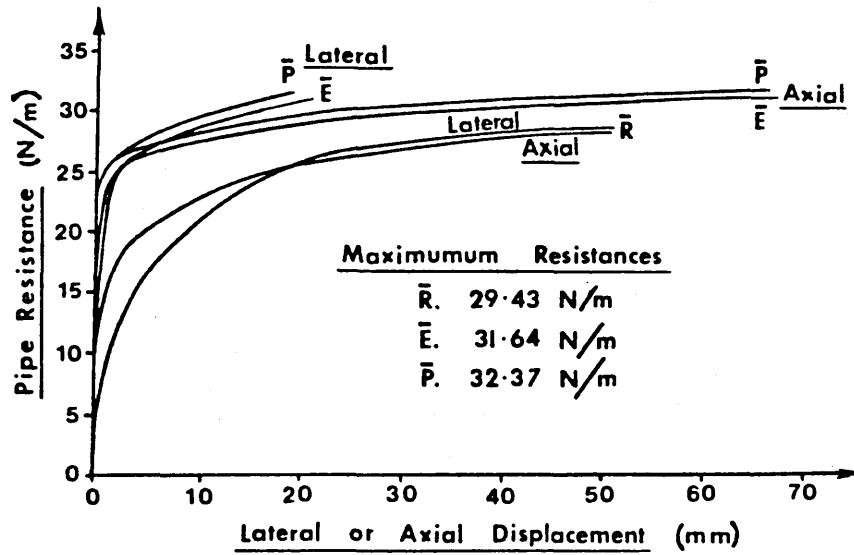


Figure 2.10 Force - Displacement Relationships  $\theta = 45^\circ$

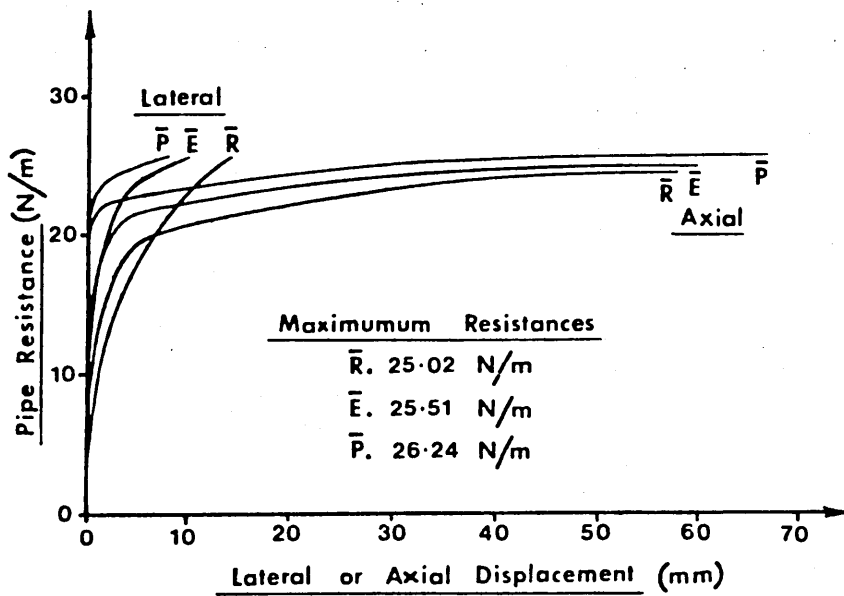


Figure 2.11 Force - Displacement Relationships  $\theta = 60^\circ$

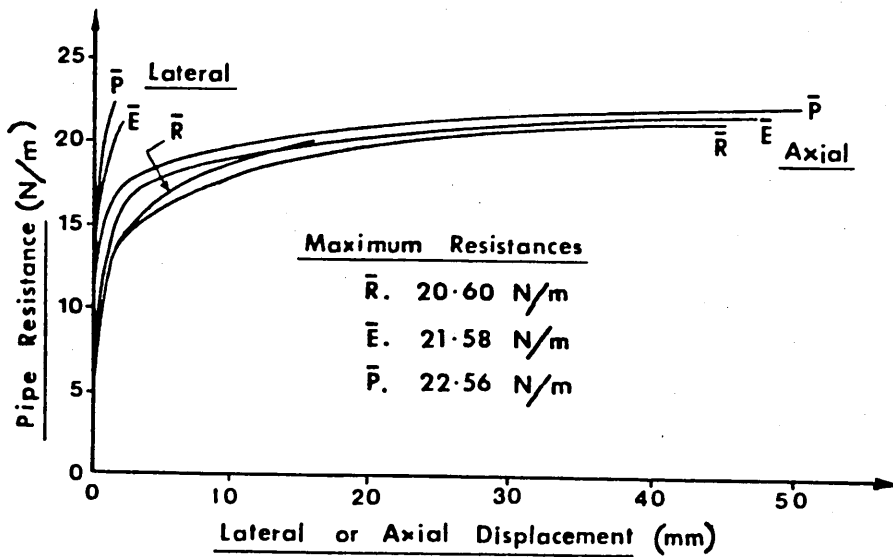


Figure 2.12 Force - Displacement Relationships  $\theta = 75^\circ$

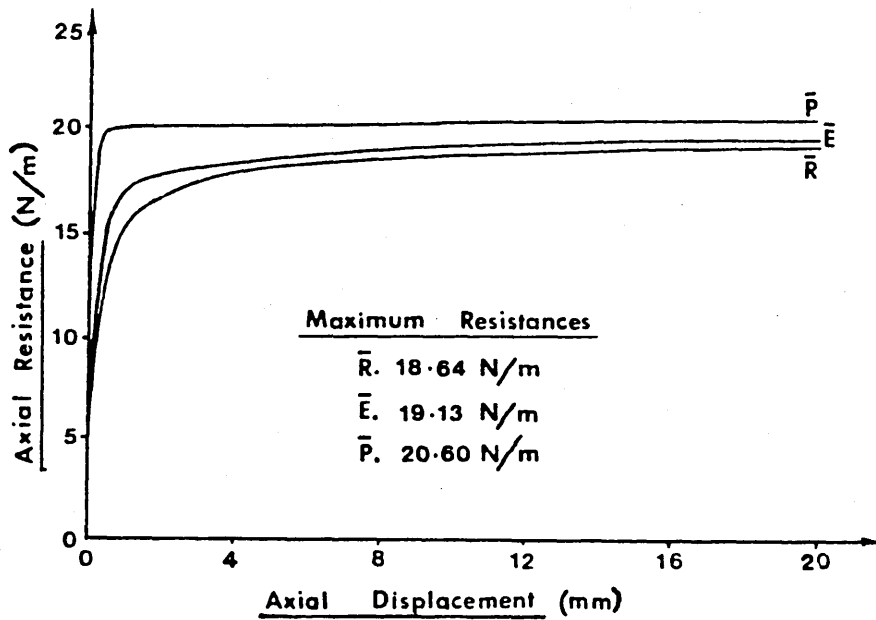


Figure 2.13 Force - Displacement Relationships  $\theta = 90^\circ$

to both of these characteristics, and as is to be anticipated given the respective degrees of sand compaction involved, the compacted case is to be particularly noted. Experimental data points, included in Fig. 2.7 ( $\bar{R}$ ) for information, are suppressed for clarity in the remaining force-displacement figures. Axial movement was negligible throughout.

For each of the remaining force orientation cases, illustrated in Figs. 2.7 to 2.13, maximum frictional resistance was again attributable to the depressed configuration. All but the axial case set generated a sand wedge, this being, relatively, of decreasing magnitude as  $\theta$  was increased. For the resting configuration, full lateral mobilisation signified maximum resistance for values of  $\theta < \pi/4$ , whilst full axial mobilisation signified maximum resistance for values of  $\theta > \pi/4$ . Simultaneous mobilisation occurred for  $\theta = \pi/4$ . The trenching effect caused simultaneous mobilisation to occur as precipitately as  $\theta = \pi/6$ , full axial mobilisation governing maximum resistance thereafter. For each interface configuration set, values of the maximum resistance force decreased as orientation was increased through to  $\theta = \pi/2$ , at which state lateral movement became negligible. In the cases governed by full axial mobilisation, the maximum resistance state occurred

more abruptly with significantly less displacement. Tables of results for the force-displacement relationships are given in Appendix II (B).

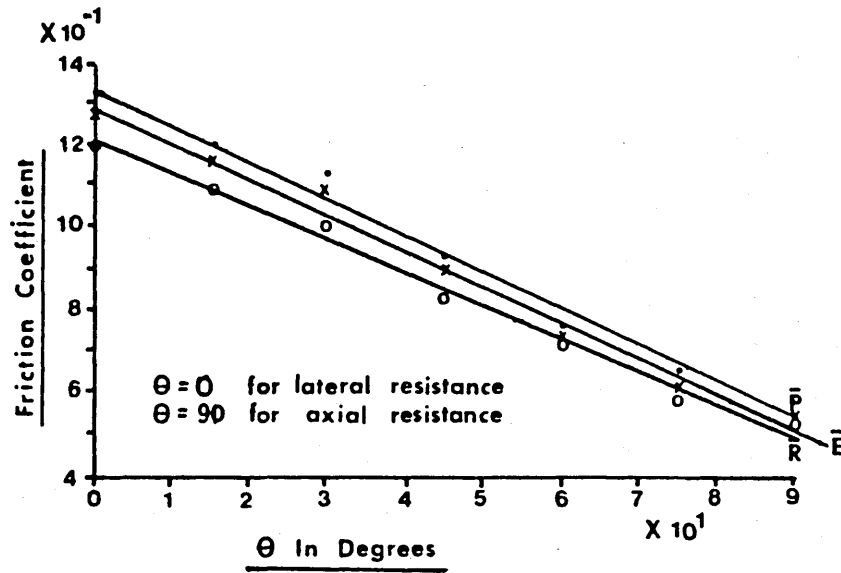
Table 2.1 summarizes the values of friction coefficient determined from the force-displacement loci. The resting configuration, involving a relatively small interface area, exhibits the lowest value of friction coefficient for each force orientation, whilst the compacted configuration, involving a higher angle of internal friction, exhibits the highest value of friction coefficient for each force orientation. The respective friction coefficients decrease as the disturbing force orientation  $\theta$  increases. The relationships between force orientation, interface configuration and friction coefficient are displayed by means of computer graphics in Fig. 2.14, together with the appropriate linear and cubic interpolation curves. The equations of these least square fit computer-generated formulae, written in terms of  $\theta$  and  $\phi$ , the pertinent abscissa and ordinate parameters, take the form;

$$\phi = 1.220 - 8.024 \times 10^{-3} \theta \quad (2.5)$$

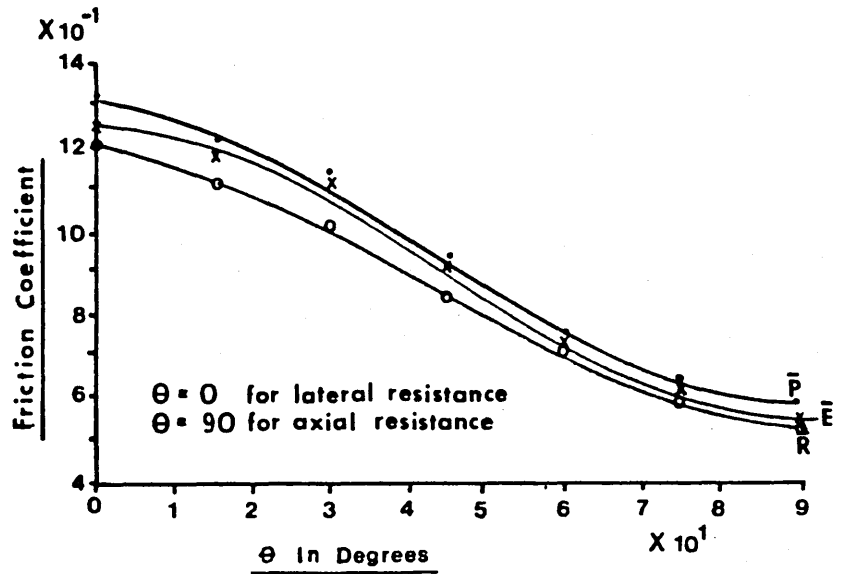
$$\phi = 1.291 - 8.571 \times 10^{-3} \theta \quad (2.6)$$

$\theta$	FRICTION COEFFICIENT ( $\phi$ )		
(DEGREES)	$\bar{R}$	$\bar{E}$	$\bar{P}$
0	1.21	1.26	1.32
15	1.11	1.17	1.20
30	1.01	1.10	1.13
45	0.84	0.91	0.93
60	0.72	0.73	0.75
75	0.59	0.62	0.65
90	0.53	0.55	0.59

Table 2.1 Friction Coefficients



a) Linear interpolation



b) Cubic interpolation

Figure 2.14 Graphs of Friction Coefficient against  $\theta$

$$\phi = 1.332 - 8.738 \times 10^{-3} e \quad (2.7)$$

for the linear resting ( $\bar{R}$ ), entrenched ( $\bar{E}$ ) and compacted ( $\bar{P}$ ) cases respectively with;

$$\phi = 1.208 - 4.094 \times 10^{-3} e - 1.312 \times 10^{-4} e^2 + 1.030 \times 10^{-6} e^3 \quad (2.8)$$

$$\phi = 1.252 - 6.105 \times 10^{-4} e - 2.315 \times 10^{-4} e^2 + 1.682 \times 10^{-6} e^3 \quad (2.9)$$

$$\phi = 1.311 - 2.428 \times 10^{-3} e - 2.062 \times 10^{-4} e^2 + 1.061 \times 10^{-6} e^3 \quad (2.10)$$

for the cubic resting ( $\bar{R}$ ), entrenched ( $\bar{E}$ ) and compacted ( $\bar{P}$ ) cases respectively.

The maximum variation between interface configuration friction coefficient values for any of the orientations considered is of the order of 10%. The displacements corresponding to the attainment of fully mobilised resistance do not show great variation with interface configuration. These values range from 180 mm in the lateral orientation to 5 mm in the axial orientation. It is to be noted that the frictional

resistance-displacement loci produced are of inelastic form.

Clearly, the foregoing data relates to model tests. In practice, submarine pipelines possess, typically, diameters in excess of 200 mm. With regard to this matter, the values for  $\phi_L$  ( $\theta = 0$ ) follow the trend set by Lyons<sup>(52)</sup> and Gulhati et al<sup>(53)</sup>, indicating that values for  $\phi_L$  will decrease for larger diameter pipes in accordance with the surface roughness effect. References also indicate that the displacements appertaining to the onset of fully mobilised lateral frictional resistance decrease with an increase in pipe diameter.<sup>(53,54)</sup> In respect of these factors, suggested values for the full scale pipeline parameters given in Table 1.2 are 1.0 for the lateral friction coefficient and 30 mm for the displacement corresponding to full mobilisation. It is to be noted that the suggested  $\phi_L$  value of 1.0 is higher than those assumed in the former fully mobilised analyses; that is,  $0.1 \leq \phi_L \leq 0.7$ . Validation of these values is detailed in the ensuing design consideration. Anand and Agarwal<sup>(54)</sup> give similar values for  $\phi_A$  ( $\theta = \pi/2$ ) with respect to model tests. Corresponding large scale tests result in  $\phi_A$  increasing with pipe diameter although the displacement corresponding

to the onset of full mobilisation appears to be largely independent of scale effects. (Results for clay media<sup>(52,55,56,57)</sup> are not considered to be applicable to the present study.) In view of these observations, therefore, indicated full scale values for the axial friction coefficient and the corresponding displacement for full mobilisation are 0.7 and 5 mm respectively. Further validation of these values will be given in the design discussions.

With regard to orientations  $0 < \theta < \pi/2$ , the interpolation loci given in Fig. 2.14 afford useful insight with respect to the corresponding full scale values. The differing scaling factors involved in the lateral and axial orientations would indicate, for example, the necessity of a change in the gradient of the loci given in Fig. 2.14 (a). The effect of trenching has been demonstrated to lie primarily with the magnitude of the friction coefficient rather than with the corresponding fully mobilised displacements. Again, Fig. 2.14 affords useful data from which full scale values could be deduced. Given the nature of the computations delineated in Section 1.4, however, present concern lies with the rather more crucial lateral and axial cases, and the means by which the appropriate parametric values deduced in this experimental study can be incorporated

within the design process appertaining to the possible in-service buckling of submarine pipelines.

## 2.6 AXIAL AND LATERAL FRICTION FORCE CHARACTERISTICS - ASSIMILATION

Noting the small scale experimental loci previously given in Figs. 2.7 ( $\bar{R}$ ) and 2.13 ( $\bar{R}$ ) for the lateral and axial cases respectively and the foregoing experimental discussion, then the small scale values for parameters  $\phi_A$ ,  $u_\phi$ ,  $\phi_L$  and  $w_\phi$  take the form

$$\phi_A = 0.53 \quad (2.11)$$

$$u_\phi = 20 \text{ mm} \quad (2.12)$$

$$\phi_L = 1.21 \quad (2.13)$$

$$w_\phi = 180 \text{ mm} \quad (2.14)$$

with the corresponding loci being reproduced, in non-dimensional form, in Figs. 2.15 (axial) and 2.16 (lateral). Given the preceding scaling factor discourse, the suggested full scale values for  $\phi_A$ ,  $u_\phi$ ,  $\phi_L$  and  $w_\phi$  for the submarine pipeline parameters

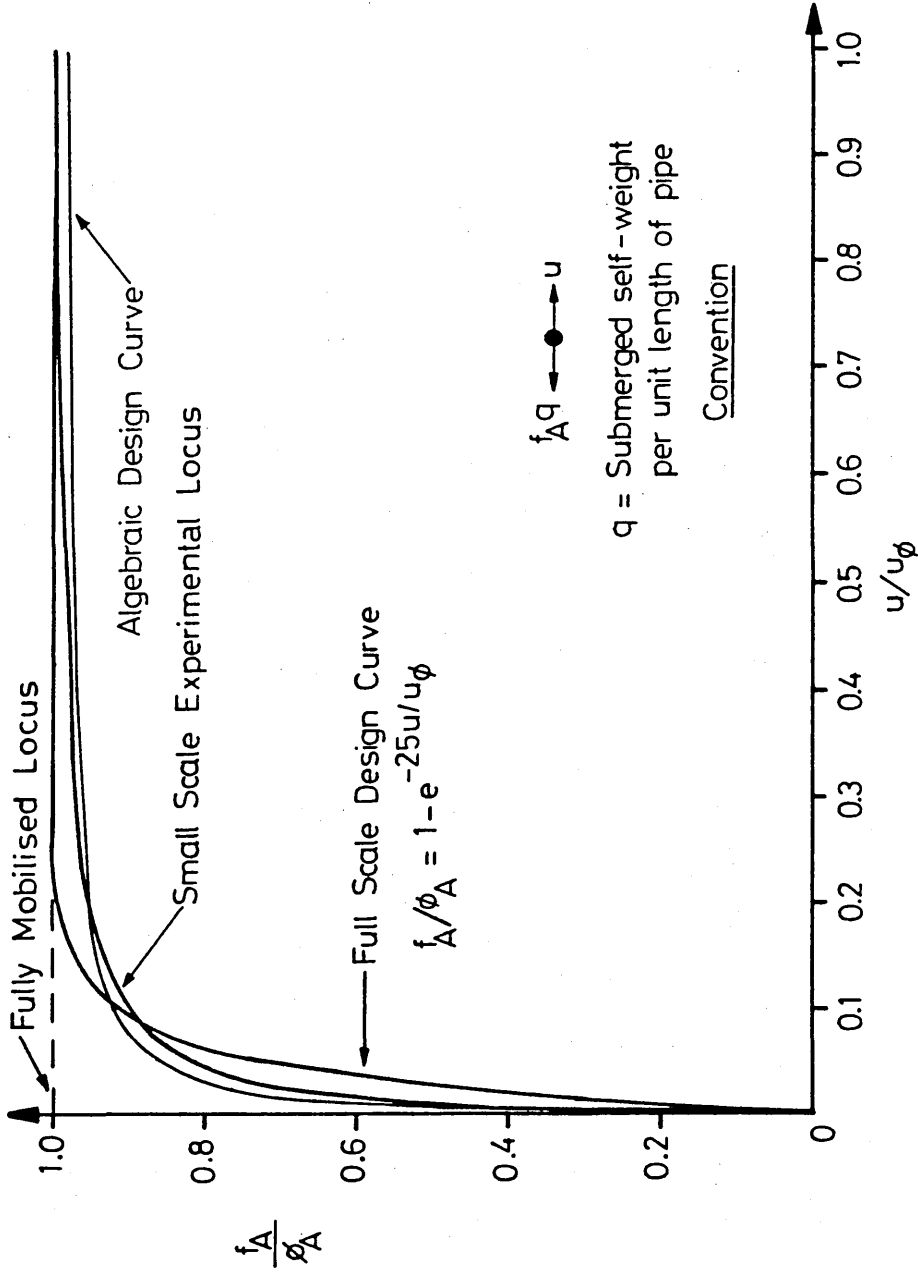


Fig. 2.15 Generalised Axial Friction Characteristics

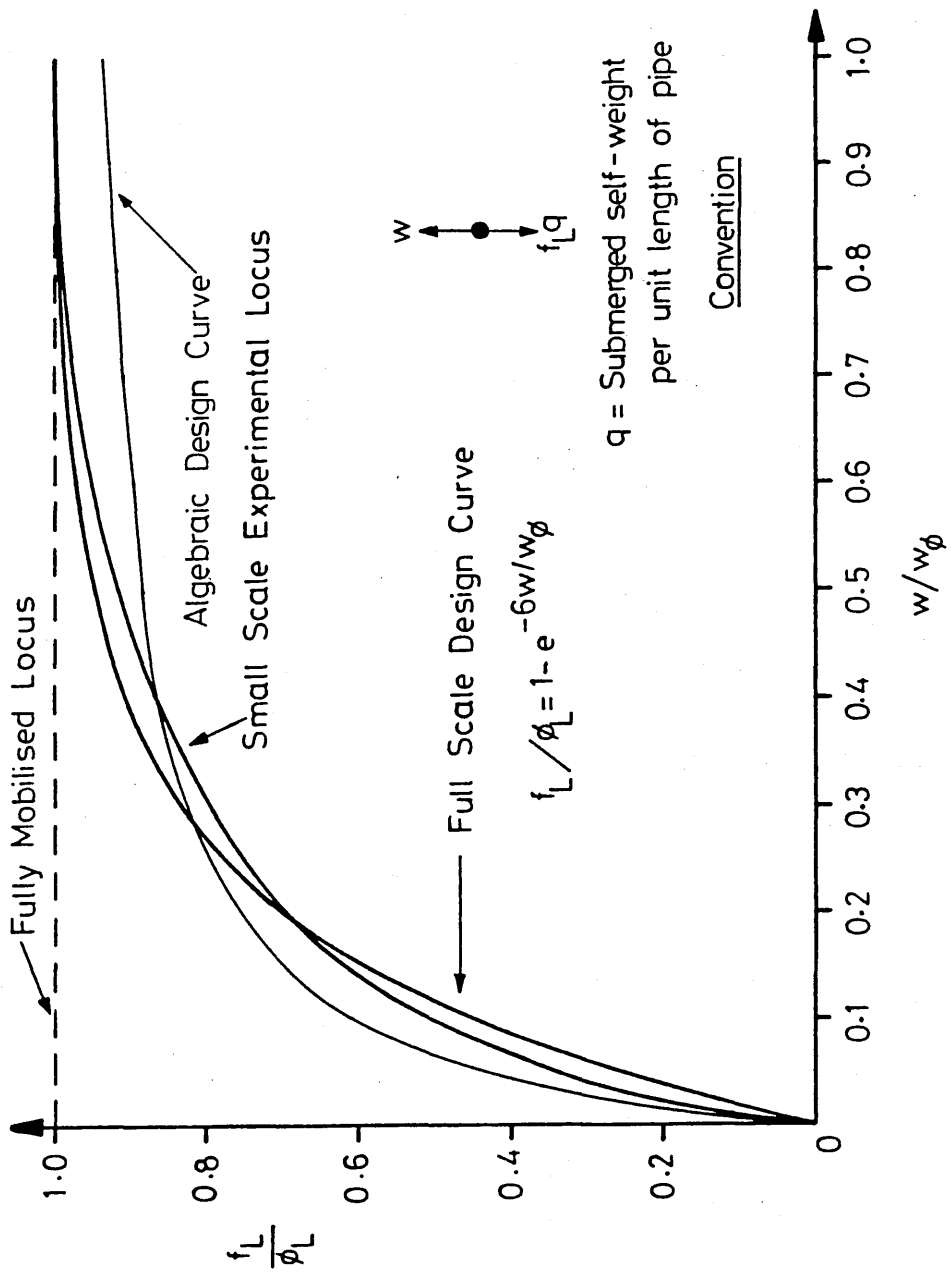


Fig. 2.16 Generalised Lateral Friction Characteristics

given in Table 1.2 are

$$\phi_A = 0.7 \quad (2.15)$$

$$u_\phi = 5 \text{ mm} \quad (2.16)$$

$$\phi_L = 1.0 \quad (2.17)$$

$$w_\phi = 30 \text{ mm} \quad (2.18)$$

Employing an exponential curve-fit, then suggested full scale design loci employ

$$f_A/\phi_A = 1 - e^{-25u/u_\phi} \quad (2.19)$$

and

$$f_L/\phi_L = 1 - e^{-6w/w_\phi} \quad (2.20)$$

These loci are superimposed on the respective experimental curves in Figs. 2.15 and 2.16 accordingly. The correlation between the numerical and experimental loci can be seen to be satisfactory.

Alternatively, algebraic functions can be employed to produce design curves of the following form

$$f_A/\phi_A = u/(u+\delta_A) \quad (2.21)$$

and

$$f_L/\phi_L = w/(w+\delta_L) \quad (2.22)$$

where parameters  $\delta_A$  and  $\delta_L$  can be determined through the mathematical modelling<sup>(52,58)</sup> of basic parameters such as the angle of internal friction of the supporting medium. In the present instance, parameters  $\delta_A$  and  $\delta_L$  are determined using equations (2.15)-(2.18) in conjunction with the necessary limitations

$$f_A/\phi_A|_{u=u_\phi} = 139/140 \approx 0.993 \quad (2.23)$$

and

$$f_L/\phi_L|_{w=w_\phi} = 0.94 \quad (2.24)$$

Employing equation (2.23) with equation (2.21) and equation (2.24) with (2.22) affords, upon manipulation, the appropriate axial and lateral full scale algebraic design curves

$$f_A/\phi_A = 1 - 1/(139u/u_\phi + 1) \quad (2.25)$$

and

$$f_L/\phi_L = 1 - 1/(15.67w/w_\phi + 1) \quad (2.26)$$

The respective design loci are also depicted in Figs. 2.15 and 2.16. It can be seen that the full scale exponential-type design curves give better agreement with the designated non-dimensionalised experimental curves and, in addition, accord with the appropriate fully mobilised asymptotes with  $f_A/\phi_A \approx 1$  at  $u/u_\phi = 1$  and  $f_L/\phi_L = 0.998$  at  $w/w_\phi = 1$  respectively. With regard to the full scale algebraic design curves, noting equations (2.23) and (2.24), the respective values at the onset of full mobilisation are inferior with  $f_A/\phi_A = 0.993$  at  $u/u_\phi = 1$  and  $f_L/\phi_L = 0.94$  at  $w/w_\phi = 1$ . Further consideration of these designated design curves will be given following the determination of the appropriate sea bed recovery characteristics.

## 2.7 SEA BED RECOVERY

With regard to the vertical buckling mode as depicted in Fig. 2.1, it can be envisaged that as the pipe lifts off the sea bed, some component of the self-weight is taken up by the recovery, on unloading, of the sea bed medium. The required effect can be obtained by expressing the effective or acting

$$f_M q = (1 - e^{-v/c}) q \quad (2.27)$$

in which  $f_M$  is a non-dimensionalised parameter  $0 \leq f_M \leq 1$  and  $c$  is dependent upon the geotechnical characteristics of the sea bed. The desired transition curve is therefore given by

$$f_M = 1 - e^{-v/c} \quad (2.28)$$

this function being graphically represented in Fig. 2.17. The sea bed recovery (unloading) locus is taken to be, under idealised circumstances, a skew-symmetric form of the loading locus with respect to axis a-b. Whilst imperfect conditions would detract from this assumption, it is considered that the initial tangent ( $1/c$ ) of the unloading locus would be the same as that of the loading locus and it is with this particular characteristic that the immediate study is concerned. The vector ratio  $v/c$  is the same for both the loading and unloading loci. It should be noted that the preceding axial and lateral friction-response loci can be considered to display similar characteristics. An exponential-type transition curve is chosen in view of the previous experience with the frictional loci. The constant  $c$  can be seen to be the vertical displacement corresponding to the intercept of the initial tangent with the asymptote  $f_M = 1$  which

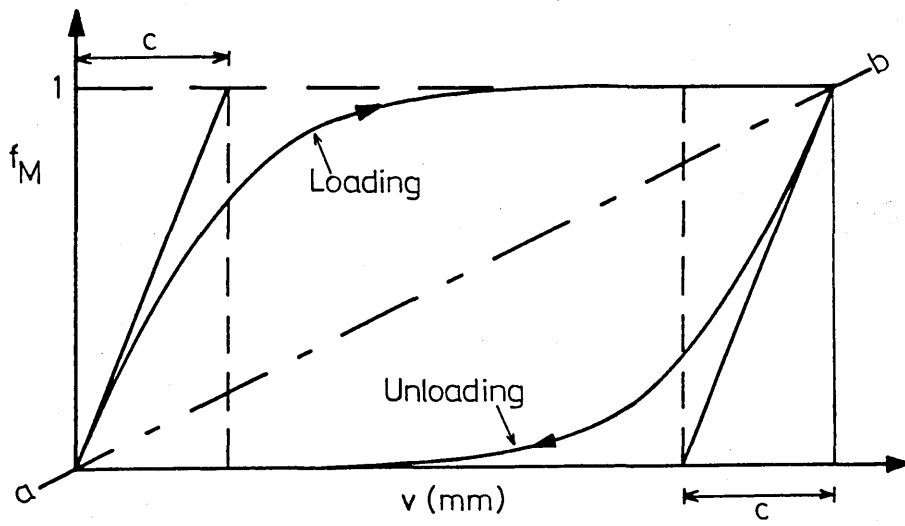


Fig. 2.17 Sea Bed Loading and Unloading Loci

denotes the onset of fully mobilised self-weight  
( $f_M q = q$ ).

Sample data relating to the determination of initial tangent and secant moduli from three typical drained triaxial tests is given in Appendix II (C) whilst the appropriate deviator stress/strain loci are shown in Fig. 2.18 which afford the average initial tangent modulus

$$E_t = \frac{\text{Deviator Stress}}{\text{Strain}} = 39,000 \text{ kN/m}^2 \quad (2.29)$$

An initial assumption is made regarding the lie of the pipe section; the pipe is taken to be semi-buried, affording an effective bearing width of diameter  $d$ . Further, based upon geotechnical engineering judgment, the effective depth at which the appropriate bearing stress and strain become zero - that is, the sea bed is effectively rigid - is taken to be twice the bearing width or pipe diameter, that is  $2d$ . This is a familiar feature with regard to geotechnical footings. (60)

The sea bed foundation stiffness topology is illustrated in Fig. 2.19. The maximum bearing stress  $\sigma_b$  is given by

$$\sigma_b = q/d \quad (2.30)$$

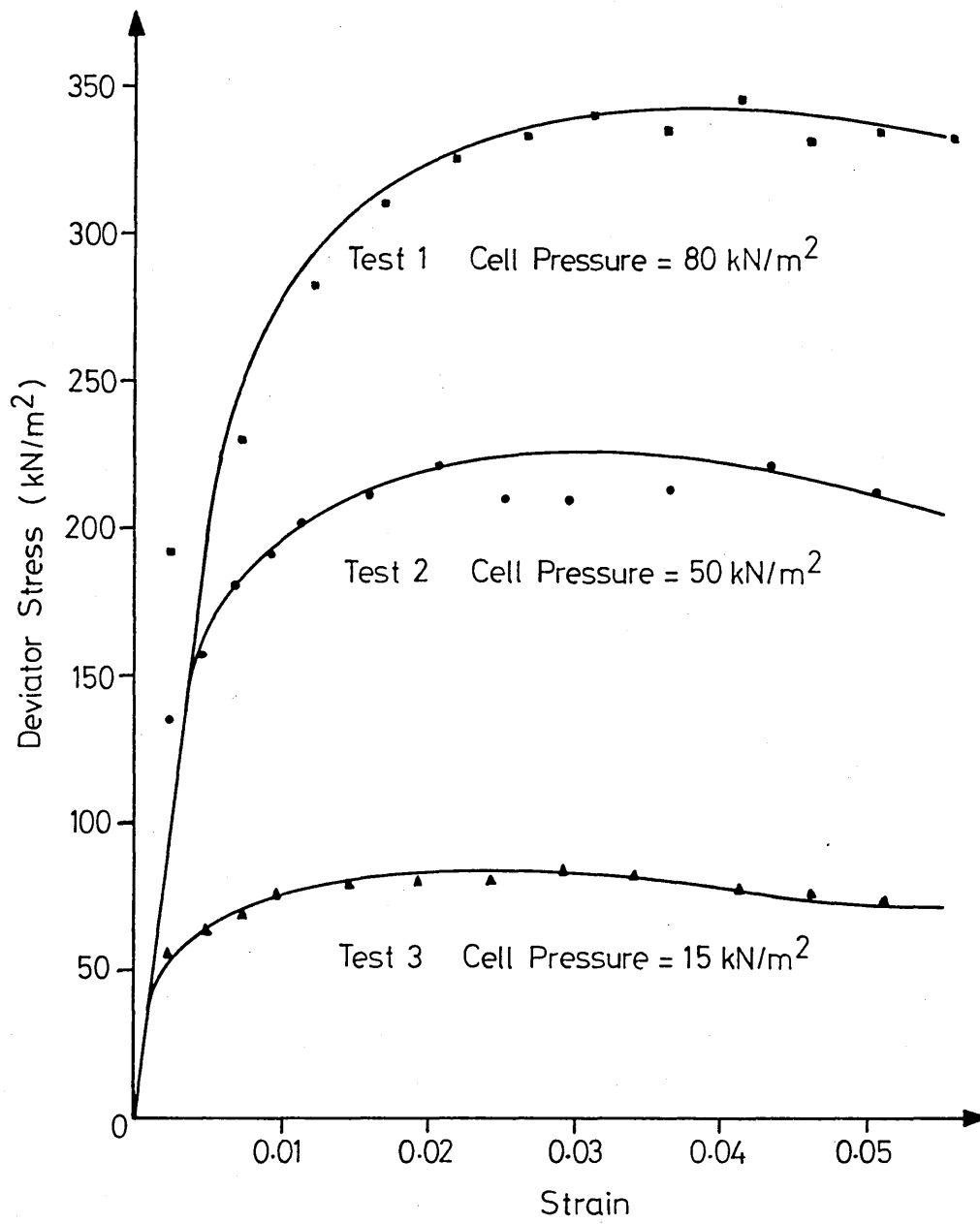


Fig. 2.18 Stress-Strain Loci

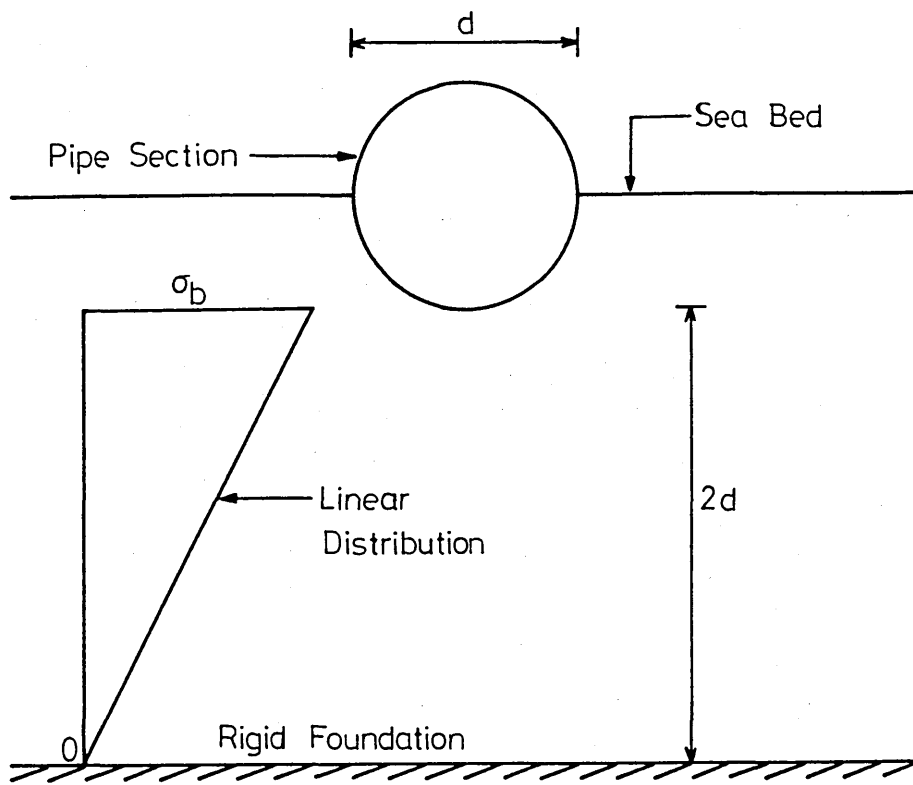


Fig. 2.19 Sea Bed Foundation Stiffness Topology

where  $q$  is the pipeline's submerged self-weight per unit run. Noting the pipeline parameters given in Table 1.2,  $q$  takes the value of 3.8 kN/m. Assuming that the bearing stress distribution is of linear form, the average bearing strain yields

$$\text{Average Bearing Strain} = \sigma_b / (2E_t) \quad (2.31)$$

The appropriate vertical displacement of the pipe can thereby be given by

$$c = 2d \times \text{Average Bearing Strain} \quad (2.32)$$

which affords, noting equations (2.30) and (2.31),

$$c = q/E_t \quad (2.33)$$

Based on the average  $E_t$  obtained from the drained triaxial tests, then upon substitution of equation (2.29) into equation (2.33), yields

$$c = 0.1 \text{ mm} \quad (2.34)$$

as illustrated in Fig. 2.20.

However, triaxial tests tend to over-estimate the field value of secant modulus,  $E_s$ , since any confining pressure 'stiffens' the soil so that a larger initial tangent modulus,  $E_t$  is obtained.<sup>(60)</sup>

A suggested realistic modulus value would perhaps be of the order 20,000 kN/m<sup>2</sup> ('loose' sand, 10,000-24,000 kN/m<sup>2</sup>; 'dense' sand, 48,000-81,000 kN/m<sup>2</sup><sup>(60)</sup>).

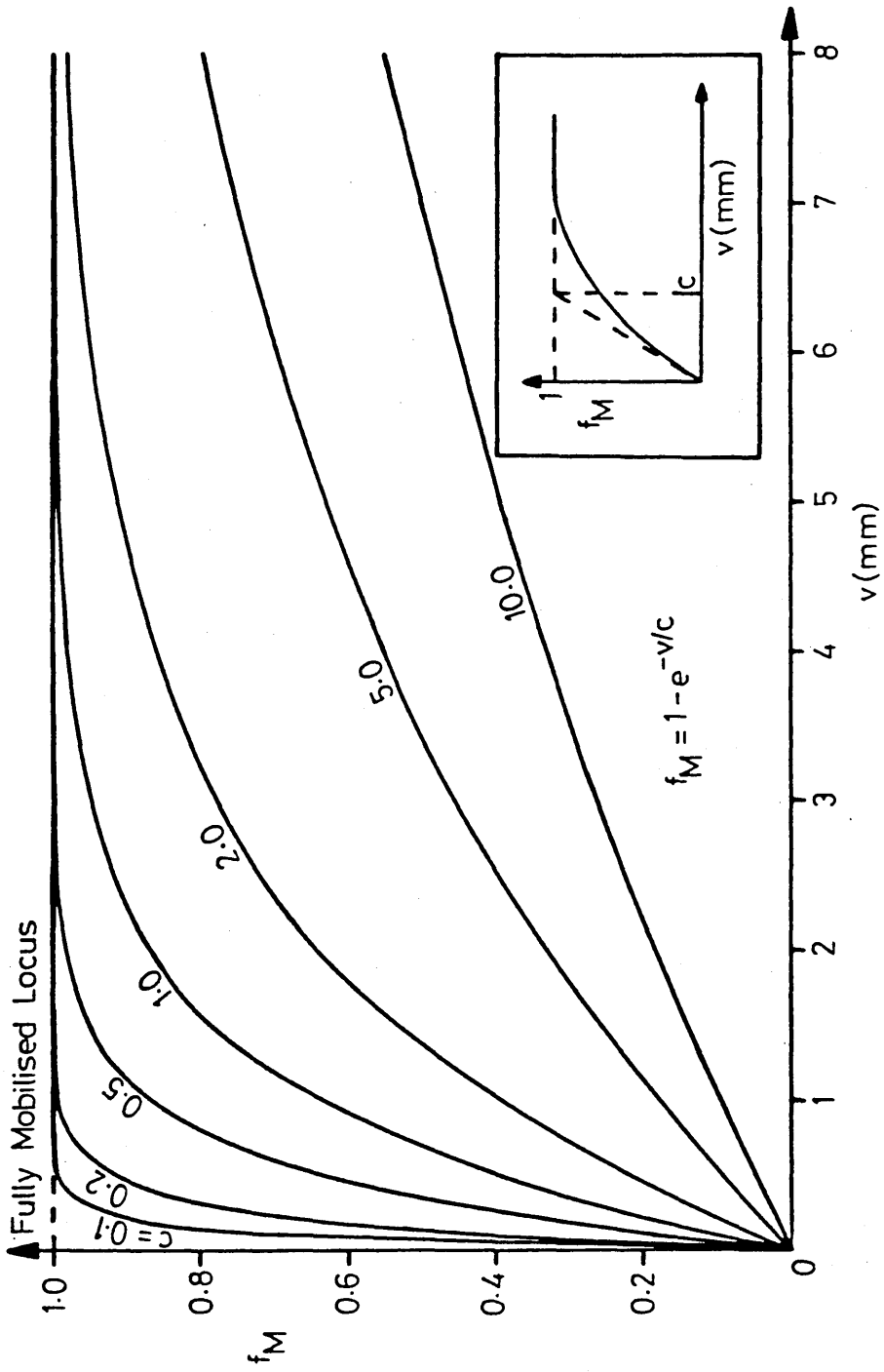


Fig.2.20 Sea Bed Recovery Loci

which gives a value for  $c$  of 0.2 mm. Studies in a related field indicate values of  $c$  to lie in the range 0.1-1.0 mm<sup>(61)</sup>, lending support to the above figures. Accordingly, a family of curves corresponding to equation (2.28) are included in Fig. 2.20. The larger values of  $c$ , 2.0, 5.0 and 10.0 mm, are an order of magnitude higher than those discussed above; they relate to a soft foundation; for example, soft clay.<sup>(61)</sup>

## 2.8 PRELIMINARY DESIGN CONSIDERATIONS

It was decided that a limited numerical assessment of the effects of the foregoing empirical parameters,  $f_A$ ,  $f_L$ ,  $f_M$  upon the structural modelling of the pipeline system should be undertaken in order to provide preliminary data. To this end, the effects of the sea bed/pipeline frictional behaviour delineated in Section 2.6 can be suitably demonstrated by considering the nature of the axial friction resistance force,  $F_A$ , generated through slip length  $L_S$ . This force is common to both the vertical and lateral buckling modes (except lateral mode  $\infty$ ). Recalling Fig. 2.3 and equation (2.4), the relatively cruder algebraic axial friction-response locus given in equation (2.25) is employed instead of the superior exponential-type modelling of equation (2.19)

so as to avoid complicated numerical integration of equation (2.4) for the determination of the axial friction resistance force,  $F_A$ . Therefore, employing equation (2.25) with equation (2.4), the revised modelling then takes the form

$$F_A = \int_L^{L+L_s} \phi_A^q [1 - 1/(1 - 139u/u_\phi)] dx \quad (2.35)$$

noting that the sign of the  $u/u_\phi$  term has been adapted to allow for  $u$  and  $f_A$  being co-oriented within the slip length region - note that Fig. 2.3 employs a different convention from Fig. 2.15. It is necessary to assume an axial displacement function for this deformation-dependent force. Utilising a cubic function, then

$$u = a_0 + a_1x + a_2x^2 + a_3x^3 \quad (2.36)$$

where  $a_i$ ,  $i = 0,1,2,3$ , represents some unprescribed coefficients - compare with fully mobilised quadratic function of equations (1.52) and (1.172). With regard to the topology of Fig. 2.3, the appropriate boundary conditions, noting Table 1.1 and Section 1.3.5, take the form

$$u|_{L+L_s} = 0 \quad (2.37)$$

$$u_{,x}|_{L+L_s} = 0 \quad (\text{transversality}) \quad (2.38)$$

$$u_{,xx}|_{L+L_s} = 0 \quad (2.39)$$

$$u|_L = u_s \quad (2.40)$$

It is to be noted that the field/boundary condition given in equation (2.39) has not previously been defined. This condition can, however, be shown to be valid by substituting equations (2.25) and (2.37) into the linearised field equation delineated in equation (1.27). Substituting the boundary conditions given in equations (2.37) through (2.40) into equation (2.36) yields the axial displacement expression

$$u = u_s \left[ \frac{L+L_s-x}{L_s} \right]^3 \quad (2.41)$$

The integration of equation (2.35), noting equation (2.41), can be simplified by introducing a change of variable based on  $(L + L_s - x)$ . Letting

$$z = L + L_s - x \quad (2.42)$$

with

$$dz = -dx \quad (2.43)$$

results in equation (2.35) being replaced by

$$F_A = \int_0^{L_S} \phi_A q [1 - 1/(1 - 139u/u_\phi)] dz \quad (2.44)$$

and the boundary conditions given in equation (2.37) through (2.40) taking the new form

$$u|_0 = 0 \quad (2.45)$$

$$u, z|_0 = 0 \quad (\text{transversality}) \quad (2.46)$$

$$u, zz|_0 = 0 \quad (2.47)$$

$$u|_{L_S} = u_S \quad (2.48)$$

Substituting equation (2.42) into equation (2.41) affords

$$u = u_S (z/L_S)^3 \quad (2.49)$$

Equation (2.44) can now be expressed in the form

$$\frac{F_A}{\phi_A q L_s} = 1 - \frac{1}{6J^{1/3}} \left[ \ln \frac{1+J^{2/3}+2J^{1/3}}{1+J^{2/3}-J^{1/3}} \right. \\ \left. 2\sqrt{3} \left( \tan^{-1} \left[ 2J^{1/3}/\sqrt{3} - 1/\sqrt{3} \right] + \tan^{-1} 1/\sqrt{3} \right) \right] \quad (2.50)$$

in which

$$J = -139 u_s / u_\phi \quad (2.51)$$

Equations (2.50) and (2.51) can be compared with the established fully mobilised modelling, as denoted by equation (2.1),

$$\frac{F_A}{\phi_A q L_s} = 1 \quad (2.52)$$

The two modelling systems are compared in Fig. 2.21 where the total axial friction resistance force  $F_A$  is related to overall movement of the slip length ( $u_s$ ). The improvement in modelling, utilising deformation-dependent axial friction behaviour, is important in that the employment of sub-fully mobilised friction resistance forces is necessary if a critical temperature rise,  $T_c$ , is to be established together with the appropriate post-buckling behaviour. The established fully mobilised modelling can be seen to overestimate the axial friction resistance.

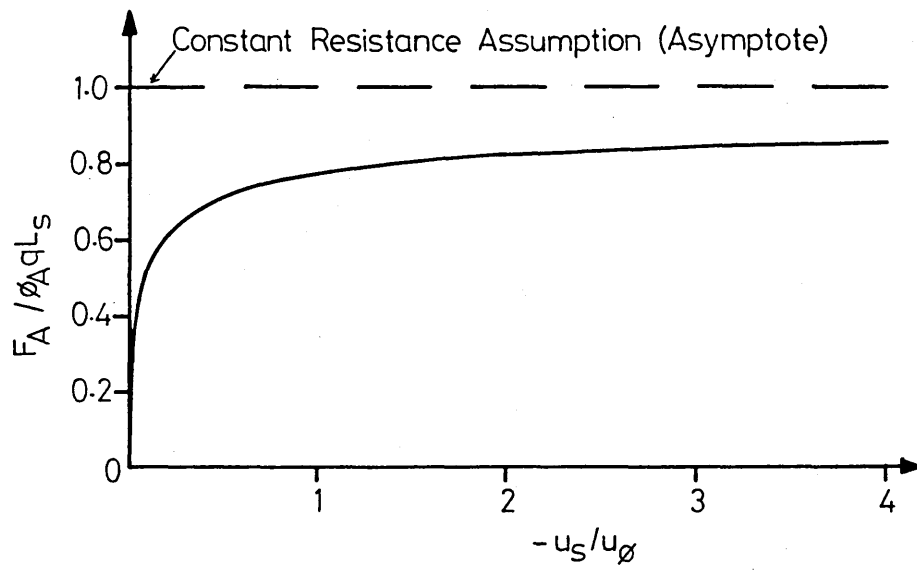


Fig. 2.21 Axial Force-Displacement Characteristics

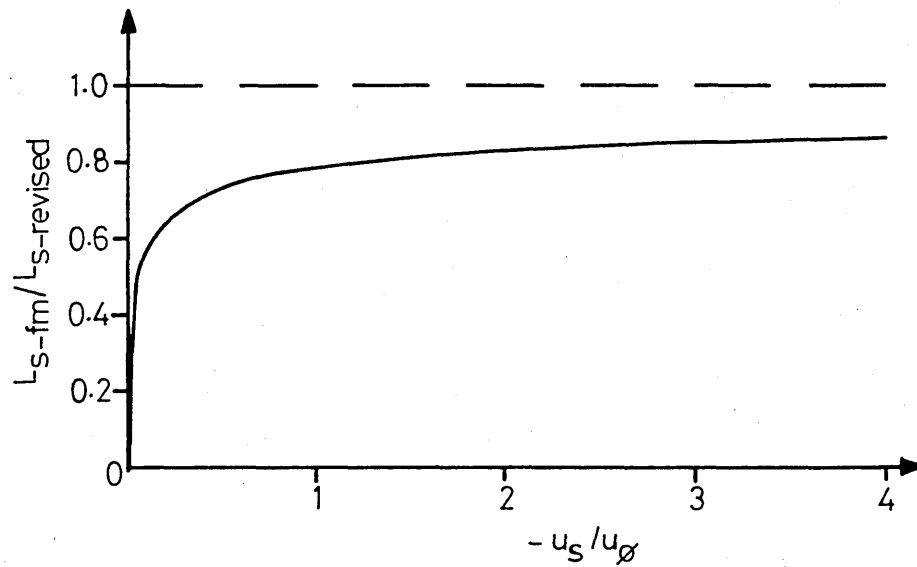


Fig. 2.22 Slip Length Ratio Characteristics

Preliminary buckling design computations can be undertaken employing the foregoing findings. Combining the linearised slip length field equation given in equation (1.27) with equation (2.49), noting the change of variable in equations (2.42) and (2.43), affords

$$u_{,zz} = -\frac{\phi_A q}{AE} [1 - 1/(1 - 139u/u_\phi)] \quad 0 \leq z \leq L_S \quad (2.53)$$

which yields, upon integration and noting equation (2.46),

$$u_{,z} = -\frac{\phi_A q}{AE} \left[ z - \frac{L_S}{6J^{1/3}} \left( \ln \frac{1 + J^{2/3} (z/L_S)^2 + 2J^{1/3} (z/L_S)}{1 + J^{2/3} (z/L_S)^2 - J^{1/3} (z/L_S)} \right. \right. \\ \left. \left. + 2\sqrt{3} \left[ \tan^{-1} \left( 2J^{1/3} (z/L_S) / \sqrt{3} - 1/\sqrt{3} \right) + \tan^{-1} 1/\sqrt{3} \right] \right) \right] \quad (2.54)$$

It is to be noted that this expression affords, upon incorporation of the condition  $u_{,z}|_{L_S} = -F_A/AE$ , the total axial friction resistance force ( $F_A$ ) expression given in equation (2.50). Integrating equation (2.54), noting equation (2.48), yields

$$u_s = -\frac{\phi_A q L_s^2}{2AE} \left[ 1 - \frac{1}{3J^{1/3} L_s} \int_0^{L_s} \left( \ln \frac{1+J^{2/3} (z/L_s)^2 + 2J^{1/3} (z/L_s)}{1+J^{2/3} (z/L_s)^2 - J^{1/3} (z/L_s)} + 2\sqrt{3} \left[ \tan^{-1} (2J^{1/3} (z/L_s) / \sqrt{3} - 1/\sqrt{3}) + \tan^{-1} 1/\sqrt{3} \right] \right) dz \right] \quad (2.55)$$

The second part of the above expression requires numerical treatment. This expression can be compared with the fully mobilised equivalent,

$$u_s = -\frac{\phi_A q L_s^2}{2AE} \quad (2.56)$$

Equations (2.53) to (2.56) apply to all modes (trivial for lateral mode  $\infty$ ,  $L_s = 0$ ). Accordingly, the above results are depicted in Fig. 2.22 which illustrates the axial slip length ratio appertaining to the revised ( $L_{s\text{-revised}}$ ) and established fully mobilised ( $L_{s\text{-fm}}$ ) friction models. The latter is shown to underestimate the length of slip.

Full buckling analyses have been undertaken employing the foregoing revised axial friction model in the slip length region and fully mobilised lateral

revised slip length analysis can be combined with the appropriate established (fully mobilised) buckling length analysis delineated in Section 1.4 using the compatibility expression given in either equation (1.29) or equation (1.30). The procedure of the numerical evaluation can be outlined by considering, for example, lateral mode 1. Employing the pipeline parameters given in Table 1.2,  $L_s$  can be determined in terms of any discrete (negative) values of  $u_s$  (mm) from equation (2.55), noting equation (2.51).  $F_A$  (ie;  $P_o - P$ ) can then be obtained from equation (2.50) by substituting the appropriate values of  $u_s$  and  $L_s$ . Employing the above mentioned compatibility expression given in equation (1.29) which yields equations (1.55) and (1.56),  $L$  can now be determined by solving the seventh order polynomial. Finally, the temperature rise  $T$  can be obtained from equation (1.6).

A similar procedure can be employed for the remaining lateral modes except lateral mode  $\infty$  in which axial friction resistance does not exist (ie;  $L_s = 0$ ). In the case of the vertical mode, the procedure of numerical evaluation is similar to those of lateral modes except that  $F_A$  is now  $(P_o - P - f_A qL)$  - note equation (2.2). The revised action-response loci are of similar nature to those depicted in Figs. 1.12-1.17.

They differ only slightly from their fully mobilised equivalents; the respective minimum safe temperature rises ( $T_{\min}$ ) are reduced by less than  $0.1^{\circ}\text{C}$  employing this particular modelling of variable axial resistance. The above findings can be explained by the fact that whilst the established fully mobilised modelling overestimates the axial friction resistance, it also similarly underestimates the length of slip and, thus, any significant difference between the fully mobilised and revised modellings is thereby greatly reduced. With respect to Figs. 2.21 and 2.22, for example, then the value of  $u_s/u_{\phi}$  corresponding to the minimum safe temperature rise,  $T_{\min}$ , state is of the order of 14.3 (lateral mode 1). Further, critical temperature rise values are not obtained due to the inclusion of fully mobilised lateral friction force and self-weight characteristics. Clearly, superior modelling to this briefly described procedure is to be anticipated from the ensuing work.

## 2.9 SUMMARY

In all, some eighty-four individual geotechnical tests have been undertaken and the appropriate resistance force-displacement loci produced. A published article<sup>(62)</sup> concerning the geotechnical experimentation is given in Appendix I (B). In

particular, information on friction coefficients has been determined for a variety of force-displacement orientations and interface configurations; appropriate interpolation formulae have been produced. Full scale values for the primary friction coefficients, that is for the axial and lateral cases, have been deduced upon the basis of the model tests. The displacements at which these friction resistance forces become fully mobilised have been similarly identified. The appropriate axial and lateral friction-response design loci have been produced using two types of semi-empirical formulae; that is, a superior exponential-type curve and the corresponding algebraic curve. The latter has been employed in the preliminary design calculations in order to avoid complicated double integral numerical analysis. Further, these preliminary calculations have afforded additional insight into the requirements demanded of the enhanced analyses that ensue.

Finally, using the superior exponential-type curve, a novel interpretation of the pipeline's submerged self-weight inertial characteristics associated with the vertical buckling mode has also been made available. The three exponential-type design curves discussed above will be employed in the rational modelling of submarine pipeline buckling behaviour given in Chapter 3.

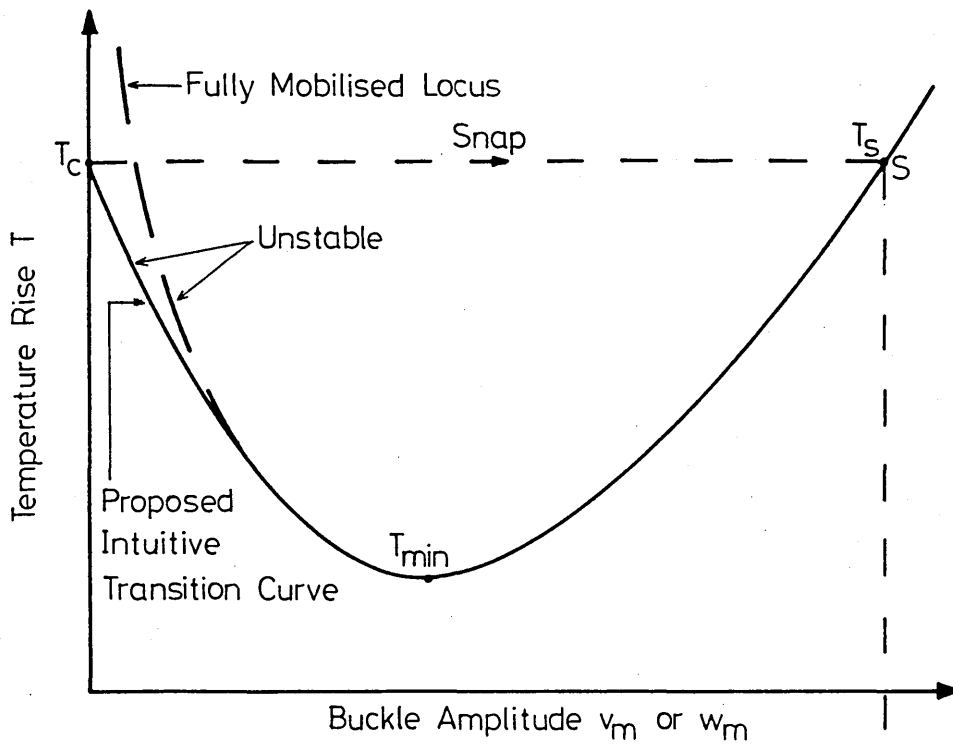
## 3.1 INTRODUCTION

A crucial part of stability studies relates to the establishment of the critical state - the bifurcation point at which, in the present context, the system response changes from axial to predominantly flexural behaviour. As noted in Chapter 1, analyses to-date with regard to the buckling of submarine pipelines have employed the simplifying non-conservative assumptions that the axial and lateral friction forces together with the vertical submerged self-weight characteristics are fully mobilised throughout. It is the inclusion of fully mobilised lateral friction resistance and fully mobilised submerged self-weight characteristics with regard to the lateral and vertical buckling modes respectively that precludes the ability to define the appropriate critical temperature rise at which idealised axial-flexural bifurcation occurs. The work set out in Chapter 2 is designed to overcome the above limitations and enable, for the first time, definition of critical state temperature rises, and thereby afford more realistic buckling analyses to be undertaken. Further, and equally important, quantitative evaluation of the respective post-

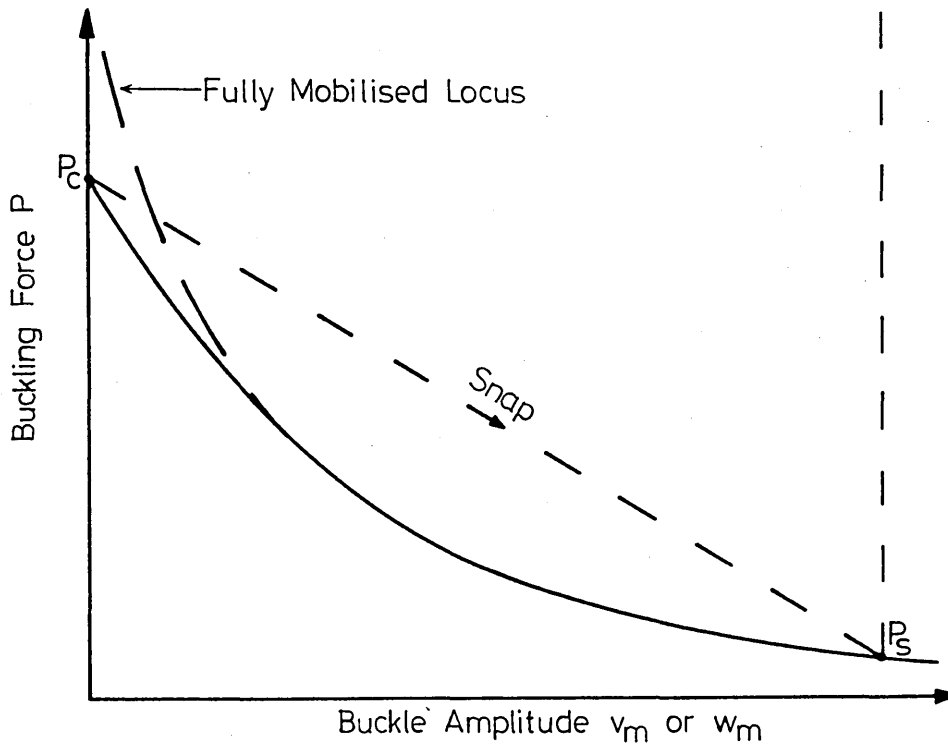
buckling characteristics should be similarly afforded for the first time. That is, a rational modelling of submarine pipeline buckling is to be made available.

Fig. 3.1 illustrates a diagrammatic interpretation of the desired, appropriate action-response loci. By determining the critical state in thermal and axial force terms, denoted by  $T_c$  and  $P_c$  respectively, the associated snap phenomenon will lead to definition of the critical post-buckling state denoted by  $T_s$  and  $P_s$  in the figure. Ensuing post-buckling behaviour can also then be defined. The falling paths given in the figure are of unstable form. Should  $T_c < T_{min}$ , a completely stable post-buckling path will be incurred in the absence of snap. Determination of the post-buckling path is important to the design engineer in so far as it will afford location of the pipe should buckling occur. Knowledge of both the  $T_c$  and  $T_{min}$  states will also enable the design engineer to take preventative measures at the design stage.

With regard to the lateral modes, the following analyses present a rational modelling of the deformation-dependent friction forces which employ the axial and lateral friction-response loci obtained from the geotechnical experimentation delineated in Chapter 2. The appropriate axial and lateral



(a) Thermal



(b) Buckling Force

Fig. 3.1 Post-Buckling Characteristics

friction design curves are given in Figs. 2.15 and 2.16 and employ

$$f_A/\phi_A = 1 - e^{-25u/u_\phi} \quad (3.1)$$

in which

$$\phi_A = 0.7 \quad , \quad u_\phi = 5 \text{ mm} \quad (3.2)$$

and

$$f_L/\phi_L = 1 - e^{-6w/w_\phi} \quad (3.3)$$

with

$$\phi_L = 1.0 \quad , \quad w_\phi = 30 \text{ mm} \quad (3.4)$$

With respect to the vertical mode, inclusion of the appropriate axial friction-response locus given in equation (3.1) overcomes the inherent limitation with regard to the established fully mobilised modelling, noting equations (1.180) and (1.181), which is shown to be invalid at small values of vertical displacement. Further, by incorporating the vertical lift-off characteristics discussed in Section 2.7, an attempt is made to model the gradual nature by means of which the pipeline's submerged self-weight is incurred at the onset of buckling. Effectively, this feature enables the ability to define a critical

temperature rise. The appropriate sea bed recovery loci represented in Fig. 2.20 employ the transition curve

$$f_M = 1 - e^{-v/c} \quad (3.5)$$

where  $c$  is shown to lie in the range of 0.1-1.0 mm for a sand sea bed foundation. The larger values of  $c$ , 2.0, 5.0 and 10.0 mm, are an order of magnitude higher than those above; they relate to a soft foundation (eg; soft clay<sup>(61)</sup>). Further, their employment assists in determining the sensitivity of critical temperature rise to the sea bed geotechnical characteristics constant  $c$ . Buckling studies are thereby to be carried out for this range of values.

Notwithstanding the foregoing attention being paid to the conceptual aspects of the problem, it is to be noted that practical buckling studies require consideration to be made of physical imperfections as denoted in Chapter 1. This important feature will be studied once the conceptual idealised factors regarding critical state analyses have been established. In view of the importance of imperfection studies, however, the rational modelling to be presently undertaken will concentrate on showing the important features concerned rather than attempting to deal in detail with each mode in formal terms.

Prior to incorporation of equations (3.1) to (3.5) within the proposed analyses, it is useful to list all the essential structural relationships, based on the established fully mobilised analyses delineated in Section 1.4. Noting the constants given in Table 3.1, the buckling force set up in the  $L_1$  region is given by

$$P = k_1 EI / L_1^2 \quad (3.6)$$

where  $L_1$  is as denoted in Fig. 1.5 et al.

The maximum amplitude of the buckle takes the form

$$w_m = k_2 \frac{\phi_L q L_1^4}{EI} \quad (3.7)$$

where constant  $k_2$  relates to the differing general displacement expressions, noting equations (1.39), (1.64), (1.76), (1.106) and (1.141). The resultant longitudinal movement at each buckle/slip length interface is given by

$$u_s = k_3 \frac{(P_o - P)L_1}{AE} - k_4 \left( \frac{\phi_L q}{EI} \right)^2 L_1^7 \quad (3.8)$$

whilst the relationship between the pre-buckling force  $P_o$ , given by equation (1.6), and the buckling force  $P$  for lateral modes 1 to 4 is derived to be

Mode	$k_1$ (Eq. 3.6)	$k_2$ (Eq. 3.7)	$k_3$ (Eq. 3.8)	$k_4$ (Eq. 3.8)	$k_5$ (Eq. 3.9)	$k_6$ (Eq. 3.9)
1	20.19	$3.8512 \times 10^{-2}$	1.0	$1.0225 \times 10^{-3}$	1.0	$2.045 \times 10^{-3}$
2	$4\pi^2$	$5.532 \times 10^{-3}$	1.0	$8.715 \times 10^{-5}$	1.0	$1.743 \times 10^{-4}$
3	8.515	0.16512	2.588	$1.7878 \times 10^{-2}$	2.588	$5.3397 \times 10^{-3}$
4	28.20	$1.048 \times 10^{-2}$	1.608	$2.7716 \times 10^{-4}$	1.608	$2.143 \times 10^{-4}$
$\infty$	$\pi^2$	$7.1192 \times 10^{-2}$	N/A	N/A	See Eq. (3.10)	
Vert.	20.19	$3.8512 \times 10^{-2}$	1.0	$1.0225 \times 10^{-3}$	See Eq. (3.11)	

Table 3.1 Constants for All Buckling Modes

$$P_o = P + k_5 \phi_A q L_1 \left[ \left( 1 + k_6 \frac{AE}{\phi_A q} \left[ \frac{\phi_L q}{EI} \right]^2 L_1^5 \right)^{\frac{1}{2}} - 1 \right] \quad (3.9)$$

For lateral mode  $\infty$ , equation (3.9) is replaced by

$$P_o = P + 3.0112 \times 10^{-3} AE \left( \frac{\phi_L q}{EI} \right)^2 L_1^6 \quad (3.10)$$

In the case of the vertical mode, subject to  $w_m$  and  $\phi_L q$  being replaced by  $v_m$  and  $q$  respectively, equations (3.6), (3.7) and (3.8) remain valid with equation (3.9) being replaced by

$$P_o = P + \frac{q L_1}{EI} \left[ 2.045 \times 10^{-3} AE \phi_L q L_1^5 - (\phi_A EI)^2 \right]^{\frac{1}{2}} \quad (3.11)$$

As in the lateral modes, constant  $k_2$  for the vertical mode relates to the vertical displacement expression given in equation (1.158). It should be noted that expressions for  $L_s$  are also available from equation (1.153) for lateral modes 1 to 4 and equation (1.73) for the vertical mode.

As a corollary, it is instructive to assess the degree of full mobilisation actually involved in the

established analyses above. With regard to the lateral buckling modes, noting the values for  $\phi_A$ ,  $\phi_L$ ,  $u_\phi$  and  $w_\phi$  given in equations (3.2) and (3.4), then Table 3.2 affords the appropriate information with respect to the state corresponding to the respective minimum safe temperature rise,  $T_{\min}$ . The most obvious deduction is that, employing the fully mobilised criterion, the axial friction modelling is relatively cruder than the lateral friction modelling throughout. In the case of the vertical buckling mode, 72.9% of the slip length is subject to fully mobilised axial friction force at the  $T_{\min}$  state whilst the appropriate degree of full mobilisation of the submerged self-weight in the buckling (lift-off) region ranges from 90% for  $c = 10$  mm to 97.8% for  $c = 0.1$  mm. Initially, therefore, it is proposed to re-define the axial friction resistance employing the locus given in Fig. 2.15 as designated by equation (3.1). Lateral friction resistance and submerged self-weight with regard to the lateral modes and the vertical mode respectively remain fully mobilised. Such analyses will serve to introduce the rational modelling techniques employed and overcome the inherent error in the established vertical mode modelling. It is to be noted that the proposed rational axial friction force modelling involves an additional procedure to the inclusion of equation (3.1). Treatment of the governing linearised slip

Mode	% of buckle length L wherein $w \geq w_\phi$ ( $w_\phi = 30 \text{ mm}$ )	% of slip length $L_s$ wherein $u \geq u_\phi$ ( $u_\phi = 5\text{mm}$ )
1	85.5	76.6
2	88.0	75.7
3	98.5	74.1
4	98.0	73.7
$\infty$	95.8	N/A

Table 3.2 Percentage of Region Subjected to Fully Mobilised Resistance Employing the Fully Mobilised Friction Force Criterion

length field equation given in equation (1.27) apparently requires the assumption of some function  $u = f(x)$  and ensuing double integration. The problems associated with this approach have already been discussed in Section 2.8. These problems, however, can be overcome by employing the regularity slip length boundary condition

$$\lim_{x \rightarrow \infty} [ u , u_{,x} ] = 0 \quad (3.12)$$

and the identity

$$2u_{,xx} = [ (u_{,x})^2 ]_{,u} \quad (3.13)$$

The former assists in precluding the prejudicial requirement of assuming some function  $u = f(x)$  whilst the latter avoids double integration of the slip length field equation. In addition, noting the regularity boundary condition in equation (3.12),  $L_s$  is effectively of infinite length, indeterminate and no longer an unknown. This particular feature will be further considered in due course.

### 3.3 LATERAL MODE ANALYSES: Deformation-Dependent Axial Resistance in Conjunction with Fully Mobilised Lateral Resistance

#### 3.3.1 Lateral Mode 1

The essential features of lateral mode 1 are shown in Figs. 3.2 (a) and (b) which depict the revised topology and axial force distribution respectively. The formulation of the buckling region is the same as that undertaken in Section 1.4.2 in view of the fact that the lateral friction force remains fully mobilised; that is,  $f_L = \phi_L$ . Equations (3.6), (3.7) and (3.8), together with the appropriate values given in Table 3.1, thereby remain valid.

With regard to the slip length region, combining equations (3.1) and (1.27) affords the slip length field equation

$$AEu_{,xx} = -\phi_A q (1 - e^{25u/u\phi}) \quad L \leq x \leq L+L_S \quad (3.14)$$

noting that the change of sign of the exponent is due to  $u$  and  $f_A$  being co-oriented within the slip length region - note that Fig. 3.2 (a) employs a different convention from Fig. 2.15. Apart from the regularity slip length boundary condition given in

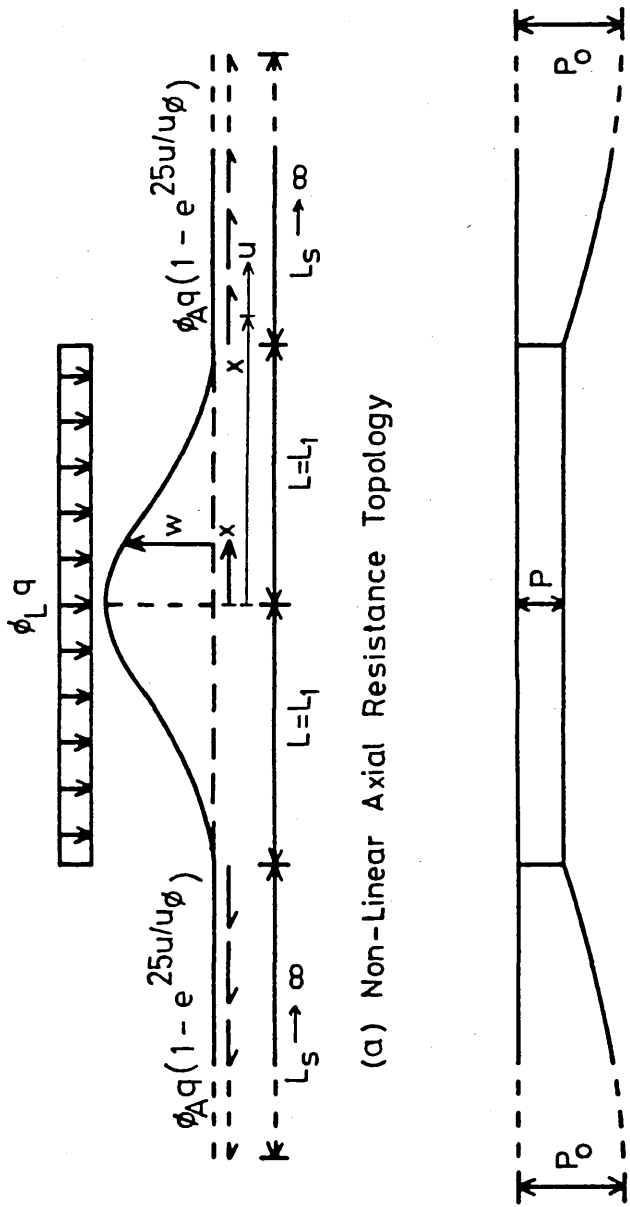


Fig. 3-2 Revised Buckling Topology - Lateral Mode 1

equation (3.12), there is, noting Table 1.1, an additional boundary condition at the buckle slip length interface

$$u, x|_{L_1} = \frac{(P_0 - P)}{AE} \quad (3.15)$$

Employing the identity given in equation (3.13), then equation (3.14) becomes

$$(u, x)^2 = \frac{2\phi_A q}{AE} \left( \frac{e^{25u/u\phi}}{5} - u \right) + k \quad (3.16)$$

where k is a constant of integration. Substituting equation (3.12) into equation (3.16) for the evaluation of k gives

$$u, x = \left[ \frac{2\phi_A q}{AE} \left( \frac{e^{25u/u\phi}}{5} - 1 - u \right) \right]^{\frac{1}{2}} \quad (3.17)$$

Equating this expression with the boundary condition given in equation (3.15), and noting  $u|_{L_1} = u_s$ , yields

$$(P_0 - P) = \left[ 2\phi_A q AE \left( \frac{e^{25u_s/u\phi}}{5} - 1 - u_s \right) \right]^{\frac{1}{2}} \quad (3.18)$$

Accepting that equation (3.8) remains valid in view of the fact that the lateral friction force is fully

mobilised, then, noting the values given in Table 3.1,

$$u_s = \frac{(P_0 - P)L_1}{AE} - 1.0225 \times 10^{-3} \left( \frac{\phi_L q}{EI} \right)^2 L_1^7 \quad (3.19)$$

Solutions for  $(P_0 - P)$  and  $u_s$  are thereby obtained in terms of discrete values of  $L_1$  employing a computerised non-linear iterative algorithm involving equations (3.18) and (3.19). The pipeline parameters employed are given in Table 1.2 and the geotechnical data given in equation (3.2) completes the requisite numerical definition. Again noting that equations (3.6) and (3.7) together with the respective values given in Table 3.1 remain valid, then locus 1, depicted in Fig. 3.3 is produced by substituting the results for  $(P_0 - P)$  into equations (1.6), (3.6) and (3.7). The dashed portions of the locus denote computations involving buckling slopes in excess of 0.1 radians. Prior to discussing the implications of this analysis, it is proposed to briefly consider the equivalent analyses of the remaining lateral modes.

### 3.3.2 Lateral Modes 2, 3 and 4

Equations (3.12) through (3.18) remain valid for these three modes. Equation (3.8) is again employed in conjunction with Table 3.1 to generate equivalent expression to that of equation (3.19). The analysis

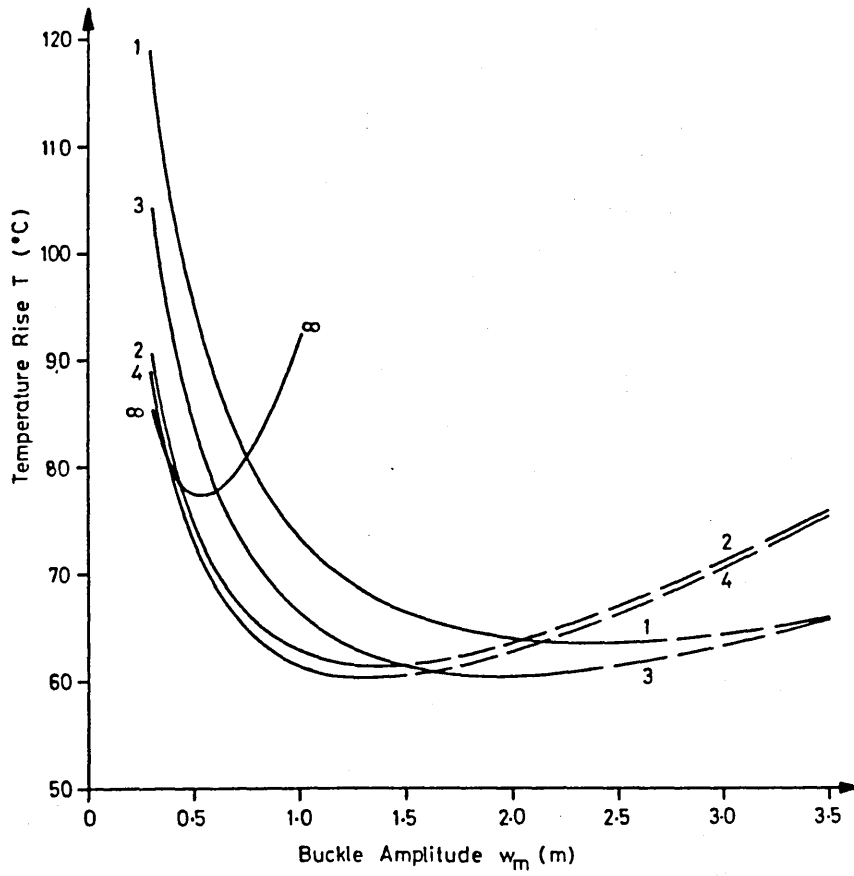


Fig.33 Comparison of Lateral Buckling Modes

of lateral mode  $\infty$ , in which there is no generation of axial friction force, remains as in Section 1.4.6. The appropriate behavioural loci are depicted in Fig. 3.3.

### 3.3.3 Assimilation - Lateral Modes

The action-response loci for lateral modes 1, 2, 3 and 4 in Fig. 3.3 differ only slightly from their fully mobilised equivalents - lateral mode  $\infty$  remains unchanged. For example, with regard to lateral mode 1, the minimum safe temperature rise ( $T_{\min}$ ) is reduced by only  $0.03^{\circ}\text{C}$  whilst the corresponding buckle amplitude ( $w_m$ ) remains virtually unchanged employing deformation-dependent axial resistance. This should not detract from the study, however, in as much as the effect of employing the simplifying fully mobilised assumption, with respect to defining the  $T_{\min}$  state ( $w_m = 2.4 \text{ m}$ ,  $T_{\min} = 63.6^{\circ}\text{C}$ ), has been shown to be reasonable from the findings of a semi-rational model. Further, the ordering of the lateral modes in terms of their respective minimum safe temperature rise is also shown to remain unchanged.

It should be noted that the solutions for the respective  $w = f(x)$  remain the same as in Section 1.4. As illustrated in Fig. 3.3, the behavioural loci

approach the thermal axis asymptotically; this is a consequence of assuming the lateral friction resistance to be fully mobilised even for vanishingly small displacements.

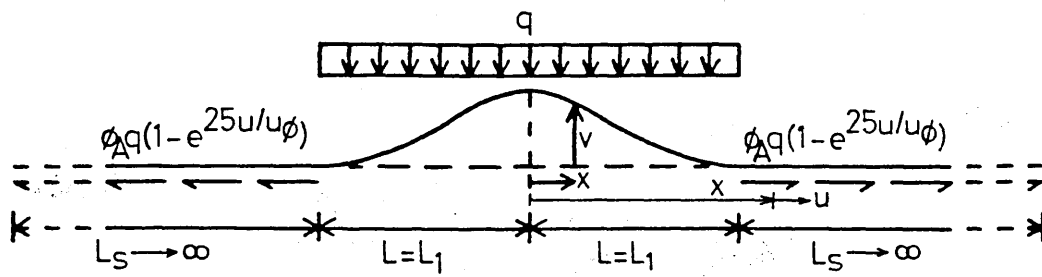
### 3.4 VERTICAL MODE ANALYSIS: Deformation-Dependent Axial Resistance in Conjunction with Fully Mobilised Submerged Self-Weight

The essential features of the vertical mode are depicted in Figs. 3.4 (a) and (b) which illustrate the revised topology and axial force distribution respectively. The analysis is similar to that of lateral mode 1 given in Section 3.3.1. Equations (3.12) through (3.17) remain valid except that equation (3.15) is replaced by

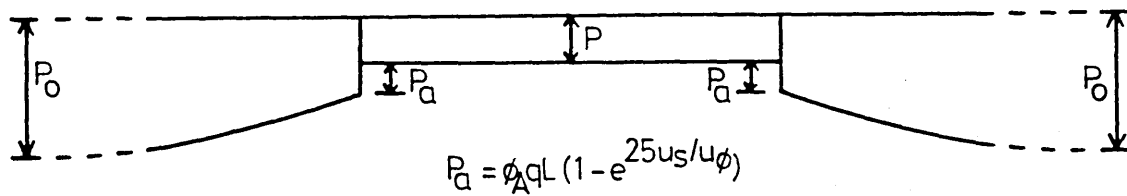
$$u_{,x}|_{L_1} = \frac{(P_o - P) - P_a}{AE} \quad (3.20)$$

where  $P_a$  is the axial force component frictionally induced in the pipe by the vertical shear reaction at the buckle/slip length interface. Noting Fig. 3.4 and  $u|_{L_1} = u_s$ , this force can be represented by

$$P_a = \phi_A q L_1 (1 - e^{25u_s/u\phi}) \quad (3.21)$$



(a) Non-Linear Axial Resistance Topology



(b) Axial Force Distribution

Fig. 3.4 Revised Buckling Topology - Vertical Mode

Substituting equations (3.20) and (3.21) into equation (3.17) and noting  $u|_{L_1} = u_s$  yields

$$(P_o - P) = \left[ 2\phi_A q A E \left( \frac{e^{25u_s/u\phi} - 1}{5} - u_s \right) \right]^{\frac{1}{2}} + \phi_A q L_1 (1 - e^{25u_s/u\phi}) \quad (3.22)$$

It is to be recalled that equations (3.6), (3.7) and (3.8), subject to  $w_m$  and  $\phi_L q$  being replaced by  $v_m$  and  $q$  respectively, remain valid in view of the fact that the submerged self-weight is fully mobilised. Employing equation (3.8) together with the appropriate value given in Table 3.1 yields

$$u_s = \frac{(P_o - P)L_1}{AE} - 1.0225 \times 10^{-3} \left( \frac{q}{EI} \right)^2 L_1^7 \quad (3.23)$$

The solution procedure for  $(P_o - P)$  and  $u_s$  is as previously; equations (3.22) and (3.23) are solved iteratively in terms of discrete values of  $L_1$ . It should be recalled that the inherent limitation on the established fully mobilised axial friction modelling elucidated in Section 1.4.7 - note equations (1.180) and (1.181) - requires, for the pipeline parameters employed,  $v_m \geq 68.2$  mm. In the present

revised analysis there is no such restriction upon equations (3.22) and (3.23) due to the variable, deformation-dependent axial friction modelling; that is, equation (1.179) is valid for all values of  $P_o$ ,  $P$  and  $P_a$ . The appropriate revised action-response characteristics are depicted in Fig. 3.5 in the form of the dashed 'rigid' locus. As with its lateral mode equivalents, the action-response locus differs only slightly from its fully mobilised equivalent with its  $T_{\min}$  value reduced by only  $0.03^\circ\text{C}$  whilst the corresponding buckle amplitude  $v_m$  remains virtually unchanged. The asymptotic nature of the locus is due to assuming fully mobilised submerged self-weight; that is, the sea bed is effectively rigid ( $c = 0$ ).

In order to define the critical temperature rise, therefore, it is necessary to model the lateral friction force and the pipeline's submerged self-weight, with regard to the lateral and vertical modes respectively, in a rational manner. Further, this will serve to provide an appropriate fully rational modelling of the buckling problem.

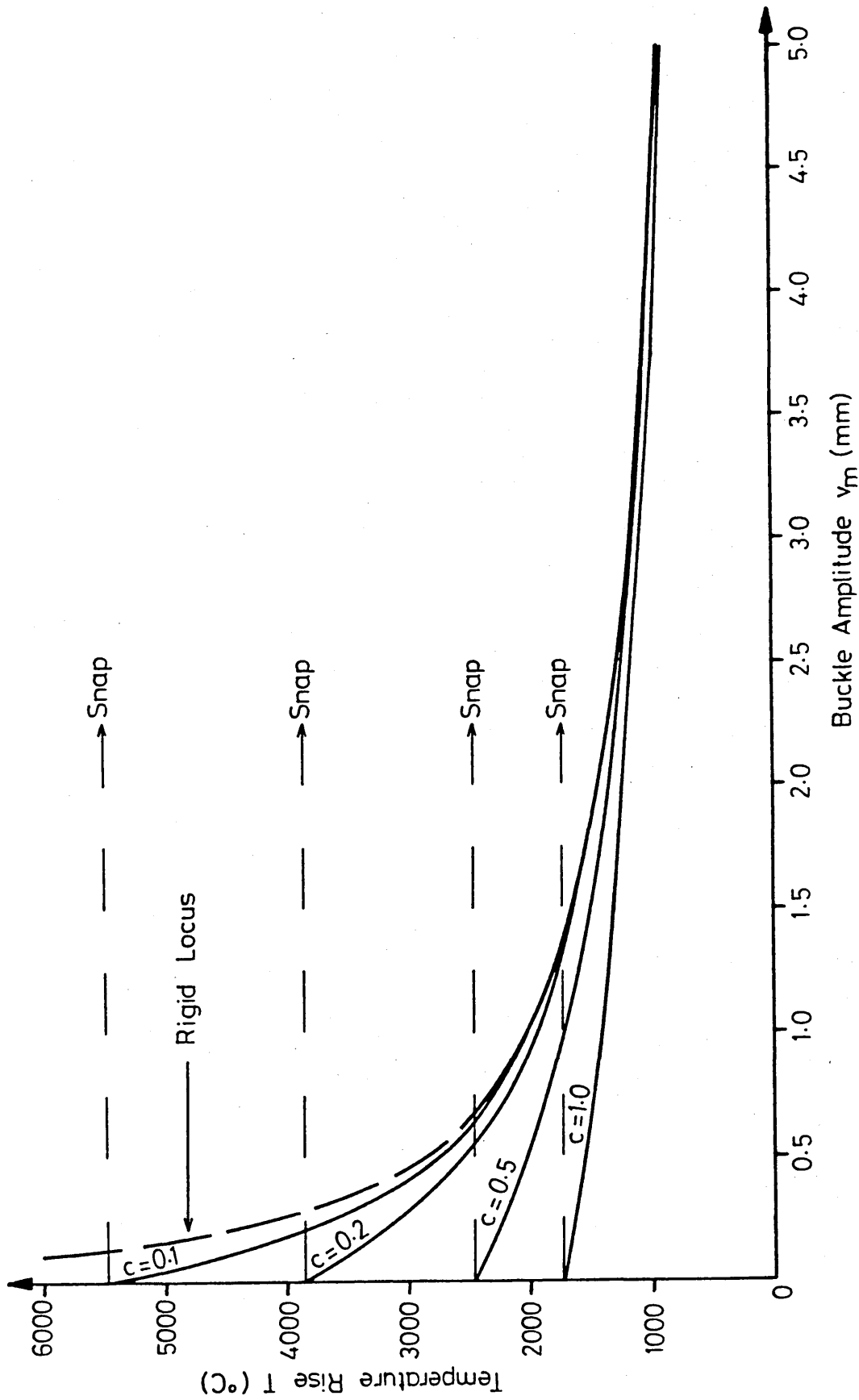


Fig.3.5 Individual Rational Modelling Loci - Vertical Mode

### 3.5 LATERAL MODE 1: Deformation-Dependent Axial and Lateral Friction Resistances

In order to establish a critical temperature rise,  $T_c$ , it is necessary to incorporate the lateral friction-response locus given in Fig. 2.16 and designated by equations (3.3) and (3.4). The appropriate topology and axial force distribution are depicted in Figs. 3.2 (a) and (b) except that the lateral resistance,  $\phi_L q$ , is now replaced by  $\phi_L q(1 - e^{-6w/w\phi})$ .

With regard to the formulation in the buckling region, noting equation (3.3), the flexural field equation given in equation (1.23) can be rewritten

$$EIw_{,xxxx} + Pw_{,xx} = -\phi_L q(1 - e^{-6w/w\phi}) \quad 0 \leq x \leq L \quad (3.24)$$

The complexity of this field equation prevents a closed form solution being obtained. A boundary collocation procedure is therefore instituted employing the assumed series

$$\frac{w}{w_m} = \sum_{i=0}^{i=4} a_i (x/L)^{2i} \quad (3.25)$$

where  $a_i$  denotes a typical unprescribed coefficient. The symmetry of the buckling mode is incorporated directly in equation (3.25). Accepting that

relationships are sought between  $P$ ,  $L$  and  $w_m$  as indicated by equations (3.6) and (3.7) with regard to the previous study, then a seven point collocation procedure is required. Employing the following five conditions and identities

$$\begin{aligned}
 w|_L &= 0 \\
 w_{,x}|_L &= 0 \\
 w_{,xx}|_L &= 0 \quad (\text{transversality}) \\
 w|_0 &= w_m \\
 (EIw_{,xxxx} + Pw_{,xx})|_L &= -\phi_L q(1 - e^{-0}) = 0
 \end{aligned}
 \tag{3.26}$$

the respective coefficients of  $a_i$  can be defined, such that

$$w = \frac{w_m}{7} [7 - 24(x/L)^2 + 30(x/L)^4 - 16(x/L)^6 + 3(x/L)^8] \tag{3.27}$$

Further, equilibrium demands that the shear force at the ends of the buckle length takes the form

$$-EIw_{,xxx}|_L = \phi_L q \int_0^L (1 - e^{-6w/w\phi}) dx \tag{3.28}$$

which gives

$$w_m = \frac{7\phi_L q L^3}{192EI} \int_0^L (1 - e^{-6w/w\phi}) dx \quad (3.29)$$

and that the central bending moment affords

$$\begin{aligned} EIw_{,xx}|_0 &= \phi_L q L \int_0^L (1 - e^{-6w/w\phi}) dx - Pw_m \\ &\quad - \phi_L q \int_0^L (1 - e^{-6w/w\phi}) x dx \end{aligned} \quad (3.30)$$

resulting in, given equation (3.29),

$$P = \frac{192EI}{7L^2} \left[ \frac{5}{4} - \frac{\int_0^L (1 - e^{-6w/w\phi}) x dx}{L \int_0^L (1 - e^{-6w/w\phi}) dx} \right] \quad (3.31)$$

Slip length considerations are incorporated as previously - note Section 3.3.1 - employing equation (3.18). The matching compatibility condition at the buckle/slip length interface, recalling equation (1.29), takes the form

$$u|_L = u_s = \frac{(P_o - P)L}{AE} - 0.5 \int_0^L (w_{,x})^2 dx \quad (3.32)$$

which yields, noting equations (3.27) and (3.29),

$$u_s = \frac{(P_o - P)L}{AE} - 9.102 \times 10^{-4} L^5 \left( \frac{\phi_L q}{EI} \right)^2 \left[ \int_0^L (1 - e^{-6w/w_m \phi}) dx \right]^2 \quad (3.33)$$

This represents the rational equivalent of the fully mobilised expression given in equation (3.19). The solution procedure is as previously; equations (3.18) and (3.33) are solved iteratively, the integral steps being carried out numerically for any specific value for  $w_m$  (mm).

Fig. 3.6 depicts the resulting action-response locus together with the formerly defined locus given in Fig. 3.3. As detailed in Fig. 3.6, a critical temperature rise has been established ( $T_c = 774^\circ\text{C}$ ); this enables, in formal terms, superior definition of the post-buckling state. Scaling factors preclude inclusion of those parts of the locus in the vicinity of the minimum safe temperature rise ( $w_m = 2.4$  m as per Fig. 3.3). The rational curve becomes effectively, or graphically, indistinguishable from the former locus well before the minimum safe temperature rise ( $T_{\min}$ ) state. At this state, the rational value for  $T_{\min}$  is  $63.1^\circ\text{C}$ , 0.8% lower than that for the previous analysis ( $63.6^\circ\text{C}$ ) whilst the corresponding buckle amplitude  $w_m$  again remains virtually unchanged ( $w_m = 2.4$  m). The fully mobilised

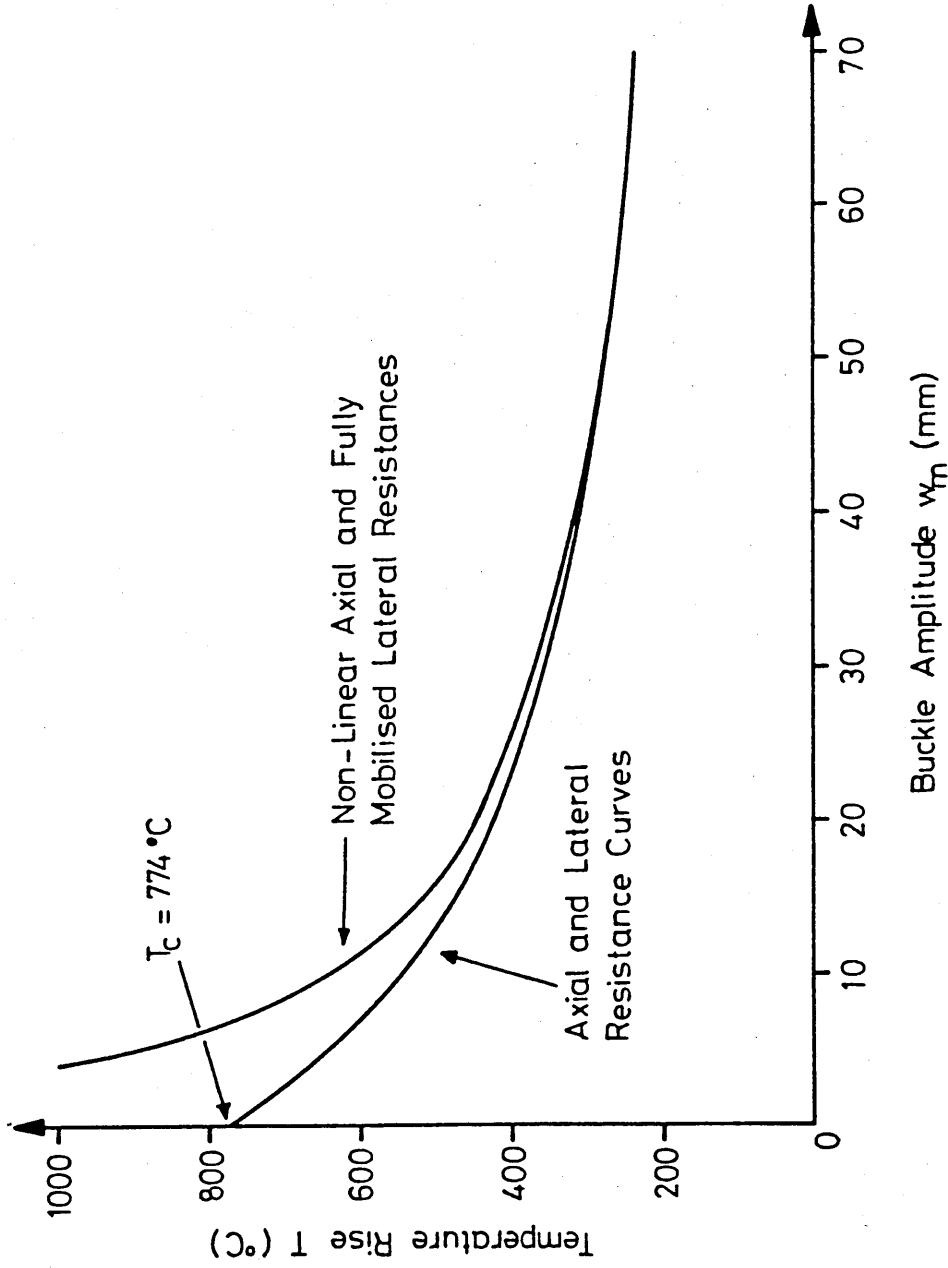


Fig.3.6 Rational Modelling for Lateral Mode 1

assumptions with respect to defining the  $T_{\min}$  state ( $w_m = 2.4$  m,  $T_{\min} = 63.6^\circ\text{C}$ ) again appear to be essentially acceptable. However, post-buckling characteristics can now be delineated. Further discussion will follow establishment of a fully rational vertical mode study.

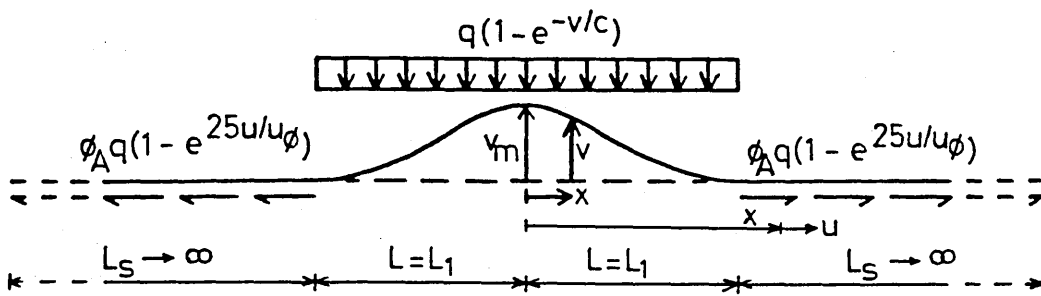
### 3.6 VERTICAL MODE: Deformation-Dependent

#### Axial Resistance in Conjunction with Sea Bed Recovery Characteristics

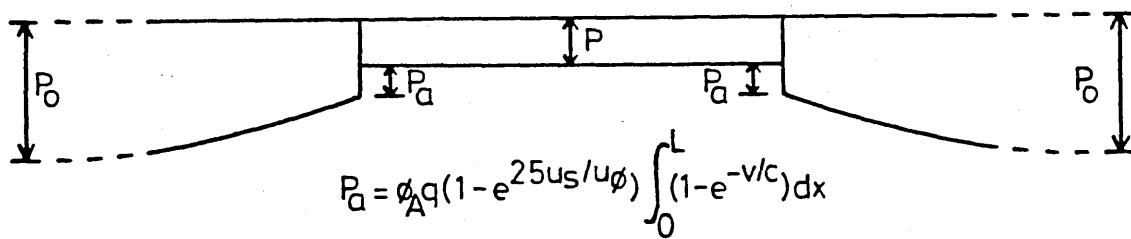
The appropriate topology and axial force distribution of the proposed rational modelling are depicted in Figs. 3.7 (a) and (b) respectively. The analysis is similar to the rational modelling of lateral mode 1 as denoted in Section 3.5. With regard to the formulation in the buckling (lift-off) region, noting the sea bed recovery loci illustrated in Fig. 2.20 and designated in equation (3.5), the flexural field equation given in equation (1.24) can be rewritten

$$EIv'''' + Pv'' = -q(1 - e^{-v/c}) \quad 0 \leq x \leq L \quad (3.34)$$

Equations (3.25) and (3.26) remain valid except that  $w$ , together with its related components, and  $\phi_L q$  are now replaced by  $v$  and  $q$  respectively. Hence, the



(a) Topology



(b) Axial Force Distribution

Fig.3.7 Vertical Mode - Details of Rational Model

vertical displacement expression can be determined, such that

$$v = \frac{v_m}{7} [7 - 24(x/L)^2 + 30(x/L)^4 - 16(x/L)^6 + 3(x/L)^8] \quad (3.35)$$

Further, equilibrium demands that the shear force at the ends of the buckle takes the form

$$-EIv_{,xxx}|_L = q \int_0^L (1 - e^{-v/c}) dx \quad (3.36)$$

which gives

$$v_m = \frac{7qL^3}{192EI} \int_0^L (1 - e^{-v/c}) dx \quad (3.37)$$

and that the central bending moment affords

$$\begin{aligned} EIv_{,xx}|_0 &= qL \int_0^L (1 - e^{-v/c}) dx - Pv_m \\ &\quad - q \int_0^L (1 - e^{-v/c}) x dx \end{aligned} \quad (3.38)$$

resulting in, noting equation (3.37),

$$P = \frac{192EI}{7L^2} \left[ \frac{5}{4} - \frac{\int_0^L (1 - e^{-v/c}) x dx}{L \int_0^L (1 - e^{-v/c}) dx} \right] \quad (3.39)$$

Slip length considerations are incorporated as previously - note Section 3.4 - except that the axial

force component is now

$$P_a = \phi_A q (1 - e^{25u_s/u\phi}) \int_0^L (1 - e^{-v/c}) dx \quad (3.40)$$

which results in equation (3.22) being replaced by

$$(P_o - P) = \left[ 2\phi_A q A E \left( \frac{e^{25u_s/u\phi} - 1}{5} - u_s \right) \right]^{\frac{1}{2}} + \phi_A q (1 - e^{25u_s/u\phi}) \int_0^L (1 - e^{-v/c}) dx \quad (3.41)$$

whilst the matching compatibility condition at the buckle/slip length interface, given equations (1.175), (3.35) and (3.37), takes the form

$$u_s = \frac{(P_o - P)L}{AE} - 9.102 \times 10^{-4} L^5 \left( \frac{q}{EI} \right)^2 \left[ \int_0^L (1 - e^{-v/c}) dx \right]^2 \quad (3.42)$$

The solution procedure is as previously; equations (3.41) and (3.42) are solved iteratively, the integral steps being carried out numerically for any specific value for  $v_m$  (mm). The numerical evaluations have been carried out for a series of values of  $c$  from 0.1 through to 10.0 (mm) as previously mentioned, although Fig. 3.5 only shows the appropriate loci for  $c$

in the fine to medium sand range ( $0.1 \leq c \leq 1.0$  mm). The rational action-response loci depicted in Fig. 3.5 display the respective critical temperature rises,  $T_c$ , and the relevant idealised post-buckling characteristics; the 'rigid' locus is asymptotic due to the submerged self-weight of the pipe being taken to be fully mobilised throughout the buckling (lift-off) region even for vanishingly small vertical displacements. Scaling factors preclude inclusion of those parts of the loci in the vicinity of the important minimum safe temperature rise state ( $T_{min}$ ). The rational loci become effectively indistinguishable from the fully mobilised locus well before the minimum safe temperature rise state; a composite locus is accordingly illustrated in Fig. 3.8. The rational values for  $T_{min}$  are lower than the fully mobilised value ( $65.3^\circ\text{C}$ ) but lie within 1% of this value. Clearly, the rational values for the vertical amplitude corresponding to the  $T_{min}$  state ( $v_{mm}$ ) are also indistinguishable from the appropriate fully mobilised value ( $v_{mm} = 2.35$  mm). With regard to Fig. 3.8, the onset of buckling slopes in excess of 0.1 radians is indicated. The appropriate limitation with regard to the fully mobilised modelling is also indicated in Fig. 3.8.

Table 3.3 shows the effect geotechnical parameter  $c$  has upon the critical temperature rise  $T_c$  for all values

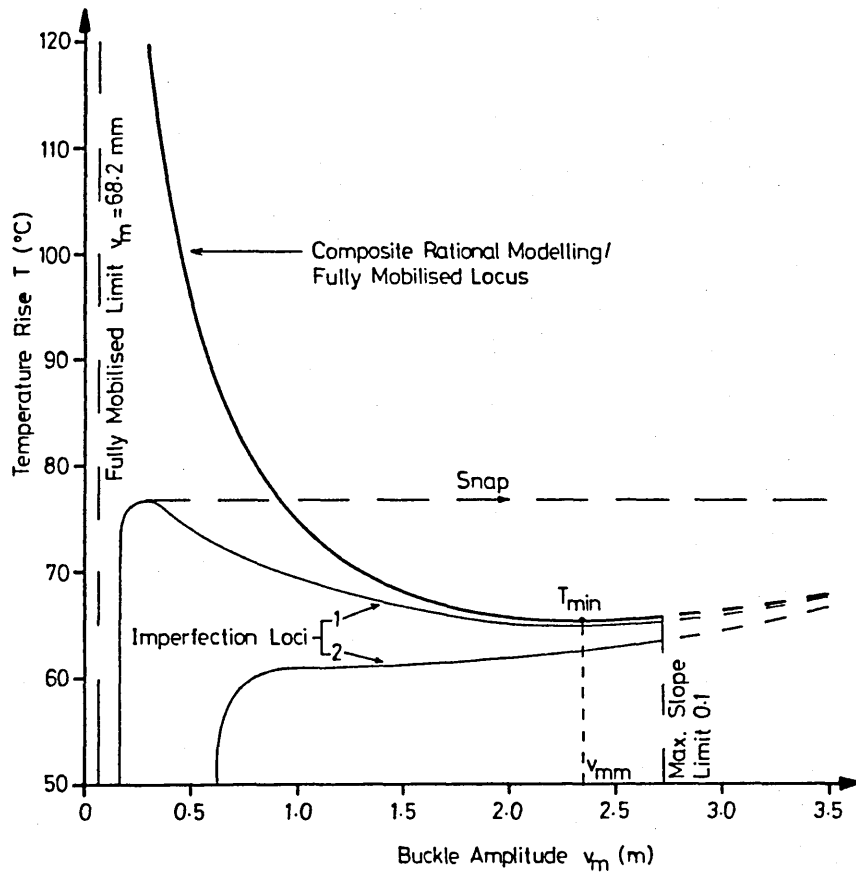


Fig.3.8 Composite Rational Modelling Locus - Vertical Mode

c (mm)	T <sub>c</sub> (°C)	Vertical deflection, v (mm), at		
		f <sub>M</sub> = 0.9	f <sub>M</sub> = 0.95	f <sub>M</sub> = 0.99
0.1	5470	0.230	0.300	0.461
0.2	3868	0.461	0.599	0.921
0.5	2446	1.151	1.498	2.303
1	1730	2.303	2.996	4.605
2	1223	4.605	5.991	9.210
5	774	11.513	14.979	23.026
10	547	23.026	29.957	46.052

Table 3.3 c - Dependent Output Data

of  $c$  considered. The higher values of  $c$  correspond to soft clay type sea bed conditions.<sup>(61)</sup> These higher  $c$ -value critical temperature rise values would be applicable to such conditions for the pipeline parameters considered; the appropriate post-buckling loci would not be applicable, however, due to the differing values of axial friction coefficient  $\phi_A$  and the corresponding fully mobilised axial deformation  $u_\phi$  required for clay studies. Accordingly, such loci for  $c > 1.0$  mm are omitted from Fig. 3.5. The relationship between  $T_c$  and  $c$  (all values) is graphically represented in Fig. 3.9. A linear relationship between  $T_c$  and  $c^{-\frac{1}{2}}$  is therefore available, the explicit relationship being

$$T_c = \frac{3.4124}{AE\alpha} \left( \frac{EIq}{c} \right)^{\frac{1}{2}} \quad (3.43)$$

The above enables rapid evaluation of the critical temperature rise for any relevant set of data.

Further to this, it is necessary to review the effect, in readily understandable physical terms, of the values of  $c$  considered. This can be done by evaluating the vertical displacement at which the submerged self-weight of the pipeline becomes fully mobilised. Given the asymptotic nature of the geotechnical loci illustrated in Fig. 2.20, full mobilisation is deemed to onset at some prescribed proportion of

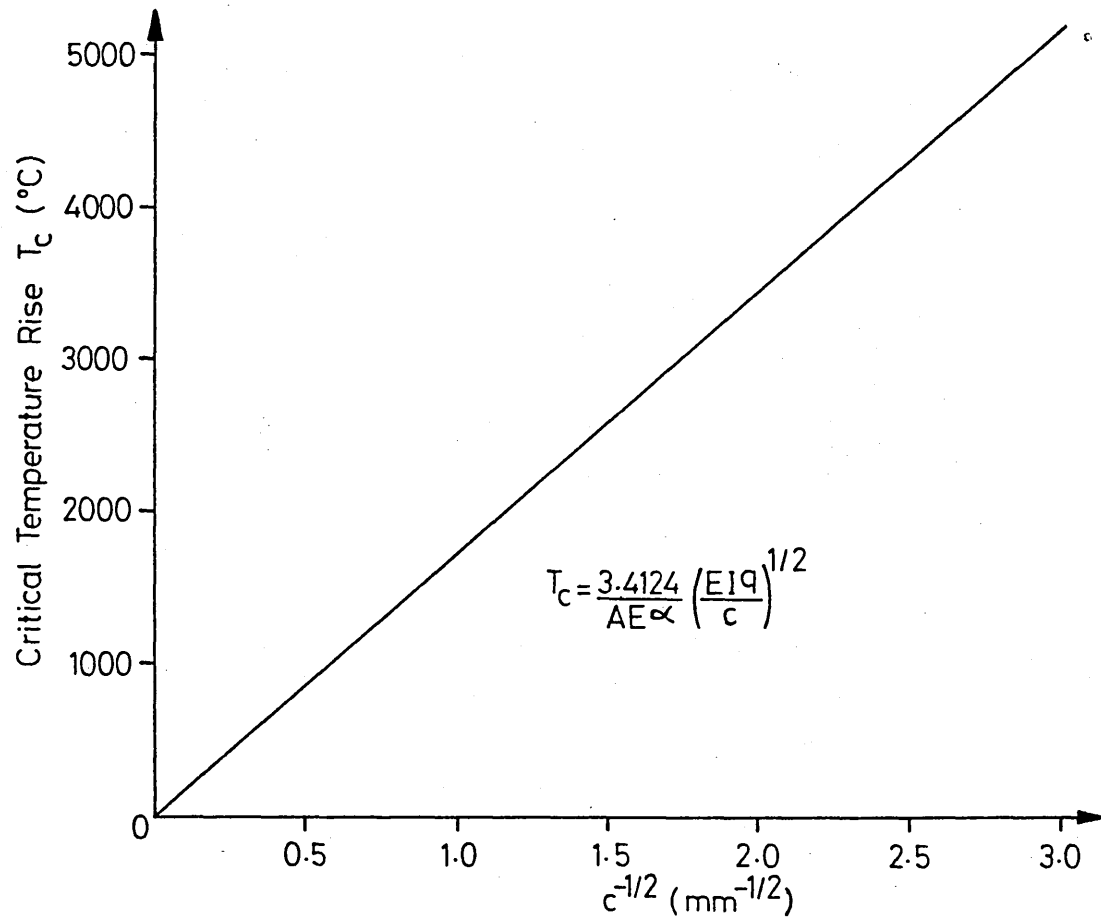


Fig.3.9 Critical Temperature Rise Assessment

the actual submerged self-weight. Table 3.3 therefore gives the appropriate values of vertical displacement for the onset of 90%, 95% and 99% of the actual fully mobilised submerged self-weight. Given the pipe diameter to be 650 mm, the values given in Table 3.3 correspond to vertical displacements of between 0.035% and 7.08% of the pipe diameter. It is considered that the trend of these values is of a valid nature, particularly in view of the minimal effect of their incorporation upon the  $T_{\min}$  values obtained. It can also be seen from Table 3.3 that the critical temperature rise  $T_c$  appropriate to the fine to medium sand range of  $c$  varies by a factor of three as the vertical displacement corresponding to the onset of fully mobilised submerged self-weight varies from 0.035% to 0.708% of the pipe diameter.

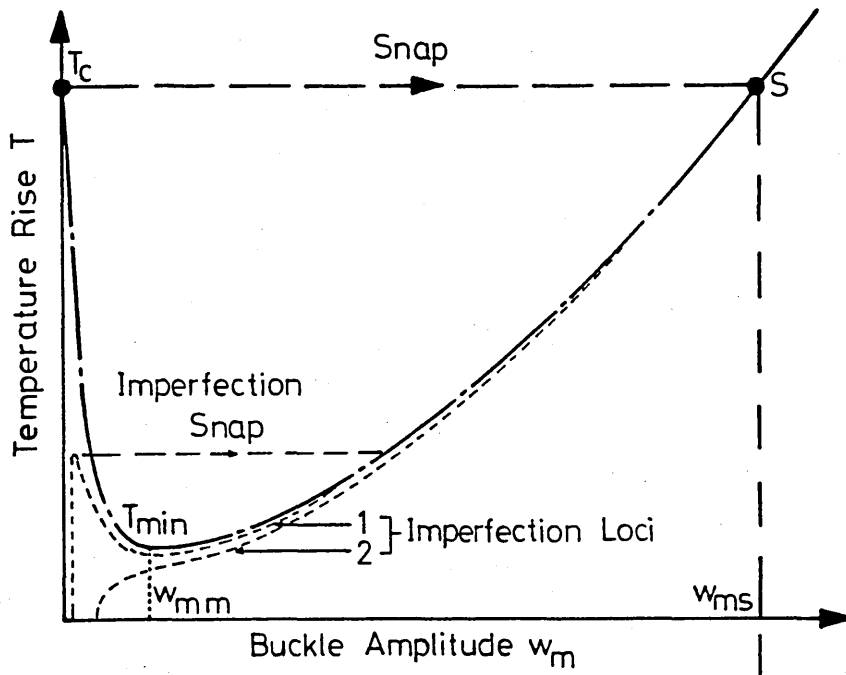
It should, perhaps, be noted that the present study considers the sea bed to exhibit flexibility only within the buckling (lift-off) region,  $2L$ ; parameter  $L$  is unprescribed and variable. Clearly, some penetration of the sea bed, additional to that existing in the pre-buckling state, could occur during buckling, particularly in the vicinity of the buckle/slip length interfaces,  $x = \pm L$ , due to the development of the vertical reaction at these locations. This feature has been neglected, support for this decision being available from related

studies.<sup>(61)</sup> The present analysis relates to sea bed recovery and takes the form of a limited sea bed flexibility study. The post-buckling characteristics of both the vertical and lateral mode 1 models can now be considered.

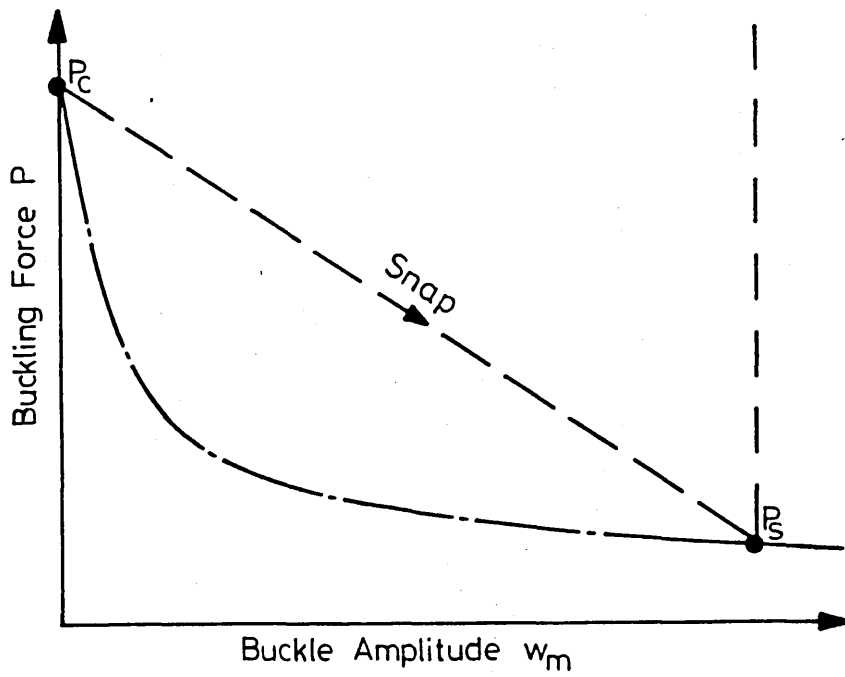
### 3.7 SUMMARY

The fully rational modelling of lateral mode 1 and the vertical mode has achieved two objectives. First, it supports the validity of the established simplified fully mobilised studies denoted in Chapter 1. Second, the appropriate critical temperature rise state has been established which is important, in formal or idealised terms, in that post-buckling characteristics can now be assessed.

Fig. 3.10 depicts the typical post-buckling mechanism in qualitative terms. Corresponding values for the primary parameters indicated in Fig. 3.10 are summarised in Table 3.4. That is, an idealised pipeline will not buckle until the critical temperature rise,  $T_c$  as denoted in Fig. 3.10 (a), is reached. The pipe then snap buckles to point S. The static topologies defined in Figs. 3.2, 3.4 and 3.7 only relate to this and ensuing states. Fig. 3.10 (b) depicts the corresponding buckling force characteristics. At the critical state denoted by  $P_c$ , the



(a) Thermal Characteristics



(b) Buckling Force Characteristics

Fig.3.10 Post Buckling Mechanism

Mode	T <sub>c</sub> (°C)	P <sub>C</sub> <sup>*</sup> (N)	T <sub>min</sub> (°C)	w <sub>mm</sub> or v <sub>mm</sub> (mm)	P <sub>S</sub> <sup>*</sup> (N)	w <sub>ms</sub> or v <sub>ms</sub> (m)
Lateral 1	3868	2.623x10 <sup>8</sup>	64.8	2.35	1.538x10 <sup>5</sup>	783.6
Vertical c=0.2mm	774	5.248x10 <sup>7</sup>	63.1	2.4	3.858x10 <sup>5</sup>	124.6

Notes; (1) \* denotes slopes > 0.1 radians

(2) Quasi-idealised studies only; material properties limit validity in practical terms

Table 3.4 Quasi-Idealised Post-Buckling Data

force in the pipeline is given by  $P_c = P_o$ . After snap, the force in the buckle reduces to the unique static value  $P = P_s$ ,  $P_s$  and location  $S$  being prescribed by the statically unique buckling amplitude  $w_m = w_{ms}$ . The chain-dotted locus defines a path which the quasi-idealised system cannot, in principle, follow due to snap at temperature rise  $T_c$ . This locus is important, however, in that it forms an upper bound to corresponding imperfection studies, particularly the theoretically stable portion between  $T_{min}$  and state  $S$ . State  $S$  (noting  $P_s$ ) has not previously been reported and is of considerable importance to the design engineer. Care in interpretation must be taken, however, at high values of temperature because of the associated effects upon the mechanical quantities involved.

In view of the importance of imperfections upon realistic pipeline buckling performance and the general agreement of the rational loci with their fully mobilised equivalents, fully rational modelling of the remaining lateral modes has been left to further study. With regard to the vertical mode, the inherent limitation of the fully mobilised approach denoted in Section 1.4.7 has been overcome. The effect of variations in sea bed recovery, that is variations in geotechnical parameter  $c$ , has also been discussed.

A number of further observations can be briefly noted. First, given the validity of the fully mobilised analyses in predicting generalised behaviour, the finite length of slip,  $L_S$ , can be determined, if required, from  $L_S = (P_0 - P)/\phi_A q$  for the lateral modes and  $L_S = (P_0 - P - \phi_A qL)/\phi_A q$  for the vertical mode, at any post-buckling state denoted by buckling force  $P$ . Should the total length of pipe be less than the overall affected length, that is  $2(L + L_S)$ , the required temperature rise will increase. (33)

Further, post-buckling behaviour may be subject to modal interaction. For example, a pipeline may be subject to lateral buckling once a trenched pipeline has buckled, initially, in the vertical plane. This feature is left to further study, but, must be borne in mind in considering the foregoing work.

Finally, the influence of imperfections must be noted. Diagrammatic representations given elsewhere (20) indicate the importance of the minimum safe temperature rise state. Typical qualitative imperfection loci are illustrated in Figs. 3.8 and 3.10 (a), one locus displaying snap buckling (type 1), the other affording a stable post-buckling path (type 2). Of particular interest with respect to such loci is the fact that recovery upon subsequent cooling would not be total, due to the non-conservative nature of the frictional forces involved. However, the

effect of this with respect to the vertical mode would not be as significant as it is in the case of lateral buckling in which lateral friction forces exist in the buckling region. This leads to the realisation that, upon recovery, any initial imperfection would be increased with a consequent change in post-buckling characteristics should thermal buckling recur. For example, an imperfection locus type 1 could degenerate into a locus type 2.

Finally, the specific parametric values determined from the foregoing quasi-idealised studies are of extreme form. However, the appropriate data trends established lead to the necessary inclusion of imperfections in order that realistic or practical structural behaviour is determined. Consequently, imperfection studies will be undertaken in Chapter 4.

A technical article<sup>(63)</sup> with regard to the rational modelling of lateral buckling modes has been accepted for publication and is included in Appendix I (C).

## CHAPTER 4

### IMPERFECTION STUDIES

#### 4.1 INTRODUCTION

Submarine pipelines can be safely assumed to suffer structural imperfections under field conditions. Initial lack-of-straightness will occur during laying operations and sea bed conditions will also generally preclude a perfect lie. The present study concentrates attention on the vertical mode and lateral modes 1 and 2. With regard to the five lateral modes depicted in Fig. 1.5, it is considered that lateral modes 1 and 2 are more susceptible than the remaining lateral modes to the most basic initially deformed pipeline topologies, these imperfections taking the form of fundamental symmetric and skew-symmetric modal deviations from the idealised lie. Further support for this choice of modes comes from the quasi-idealised analyses' stress trends. That is, values of  $T_{\min}$  for all six identified submarine pipeline buckling modes are given in Table 4.1 together with the corresponding buckle amplitudes and maximum compressive stresses; attention is also drawn to Fig. 1.5. It can be seen that on the basis of  $T_{\min}$  (quasi-idealised), lateral modes 3 and 4 are more critical than lateral modes 1 and 2. This ordering is indicated parenthetically

MODE	$T_{\min}$ (°C)	$v_m$ or $w_m _{T_{\min}}$ (m)	$\sigma_m _{T_{\min}}$ (N/mm <sup>2</sup> )
Vertical	65.3 (5)	2.35	597
Lateral 1	63.6 (4)	2.4	606
Lateral 2	61.6 (3)	1.4	495
Lateral 3	60.6 (2)	1.9	547
Lateral 4	60.5 (1)	1.3	479
Lateral $\infty$	77.5 (6)	0.5	261

Table 4.1 Quasi-Idealised / Fully Mobilised  
Analyses - Stress Trends at  $T_{\min}$

adjacent to the respective  $T_{\min}$  values. However, the corresponding stress levels are consistent with an underlying and alternative interpretation with the vertical mode and lateral mode 1 generating the highest stress levels. That is, accepting that imperfections will be present in practice, lateral mode 1 is notable for generating the highest stress trend of all the lateral modes. Taken in conjunction with the basic nature of the physical imperfection concerned, it is considered that, in practical terms, lateral mode 1 is the most significant symmetric lateral mode with respect to imperfection considerations. Similar reasoning suggests lateral mode 2 is the most significant skew-symmetric mode, lateral modes 3 and 4 being, in engineering terms, subordinate forms of lateral modes 1 and 2 respectively. All four modes can be considered to be localised versions of lateral mode  $\infty$ , this feature being reinforced by the presence of a particular imperfection in a particular locality.

In the three cases studied, the variable or deformation-dependent axial resistance forces introduced in the previous chapter are incorporated in the respective analyses; this feature is of particular importance with respect to the vertical mode study as the established modelling - note equations (1.180) and (1.181) - has been shown to be

invalid at small values of vertical displacement. The refined axial friction-response locus obtained from the geotechnical experimentation in Chapter 2, noting Fig. 2.15 and equations (2.15), (2.16) and (2.19), accordingly takes the form

$$f_A/\phi_A = 1 - e^{-25u/u_\phi} \quad (4.1)$$

where

$$\phi_A = 0.7 \quad , \quad u_\phi = 5 \text{ mm} \quad (4.2)$$

In view of the fact that the boundary collocation analyses associated with the variable or deformation-dependent nature of the lateral friction resistance and submerged self-weight with regard to lateral mode 1 and the vertical mode studies respectively support the validity of the simplified fully mobilised studies denoted in Chapter 1, it is proposed to employ the appropriate fully mobilised characteristics of the above features in the ensuing analyses. This will enable a set of formal analyses, using the Principle of Stationary Potential Energy Approach, together with the incorporation of structural imperfections, to be undertaken in a concise manner.

Briefly, the total potential energy of a system is given by<sup>(25)</sup>

$$V = U - W \quad (4.3)$$

where  $V$  is the total potential energy function,  $U$  is the generalised strain energy and  $W$  is the external potential work function. The corresponding equilibrium state equation takes the form

$$\delta V = 0 \quad (4.4)$$

This Potential Energy Approach can be demonstrated by considering the well-established pin-ended Euler strut, typified in Fig. 1.2 (b), with an initial imperfection as shown in Fig. 4.1. The transverse displacement expression obtained from the corresponding idealised equilibrium analysis can be shown to be<sup>(51)</sup>

$$w = w_m \sin(\pi x/L) \quad (4.5)$$

For imperfection studies regarding the pin-ended strut, the initially deformed shape can be assumed to take the 'sympathetic' form

$$w_0 = w_{0m} \sin(\pi x/L) \quad (4.6)$$

in which  $w_0$  and  $w_{0m}$  denote the respective transverse displacement and maximum amplitude of the imperfection topology. The total potential energy relating to the deformed state, noting equation (4.3), affords

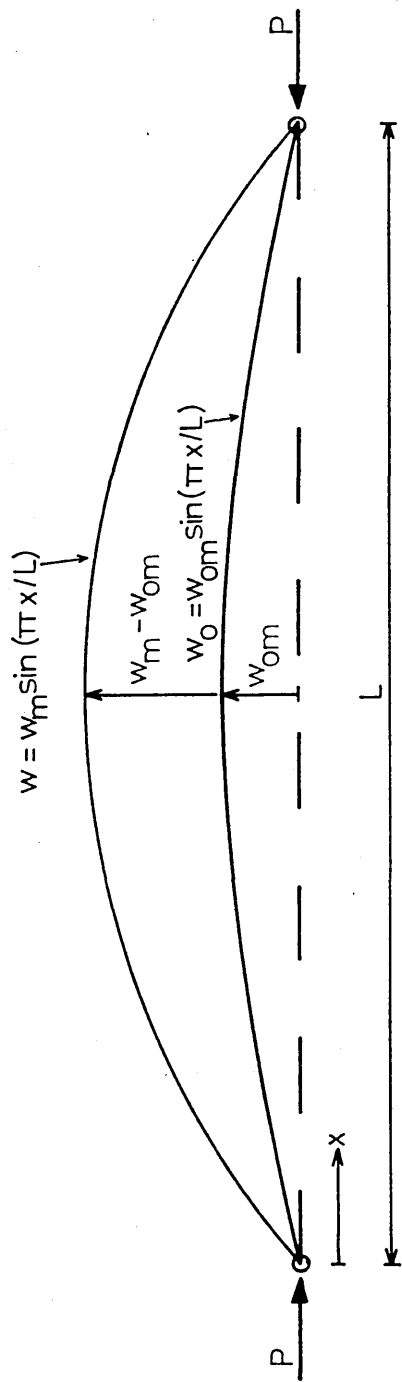


Fig.4.1 Pin-ended Strut – Imperfection Topology

$$V = \int_0^L 0.5EI(w_{,xx} - w_{o,xx})^2 dx - \int_0^L 0.5P[(w_{,x})^2 - (w_{o,x})^2] dx \quad (4.7)$$

Incorporating the equilibrium state equation (4.4) in terms of kinematic generalised coordinate  $w_m$  (25) such that

$$\frac{dV}{dw_m} = 0 \quad (4.8)$$

the buckling force  $P$  can be derived, noting equations (4.5), (4.6) and (4.7), to be

$$P = \frac{\pi^2 EI}{L^2} (1 - w_{om}/w_m) \quad (4.9)$$

This expression is graphically represented as imperfection locus type 2 in Fig. 1.2 (c).

#### 4.2 LATERAL MODE 1 ANALYSIS

The essential features of lateral mode 1 are shown in Figs. 4.2 (a) and (b). The former figure details the topology whilst the latter depicts the axial force distribution within the pipe. Regarding the imperfection parameters,  $w_o$  and  $w_{om}$  represent the respective lateral displacement and maximum amplitude whilst the appropriate buckling length parameter is denoted by  $L'_o$ , where  $L'_o = 2L_o$ . Given that the buckling length is a variable, then  $w_{om}/L'_o$  forms

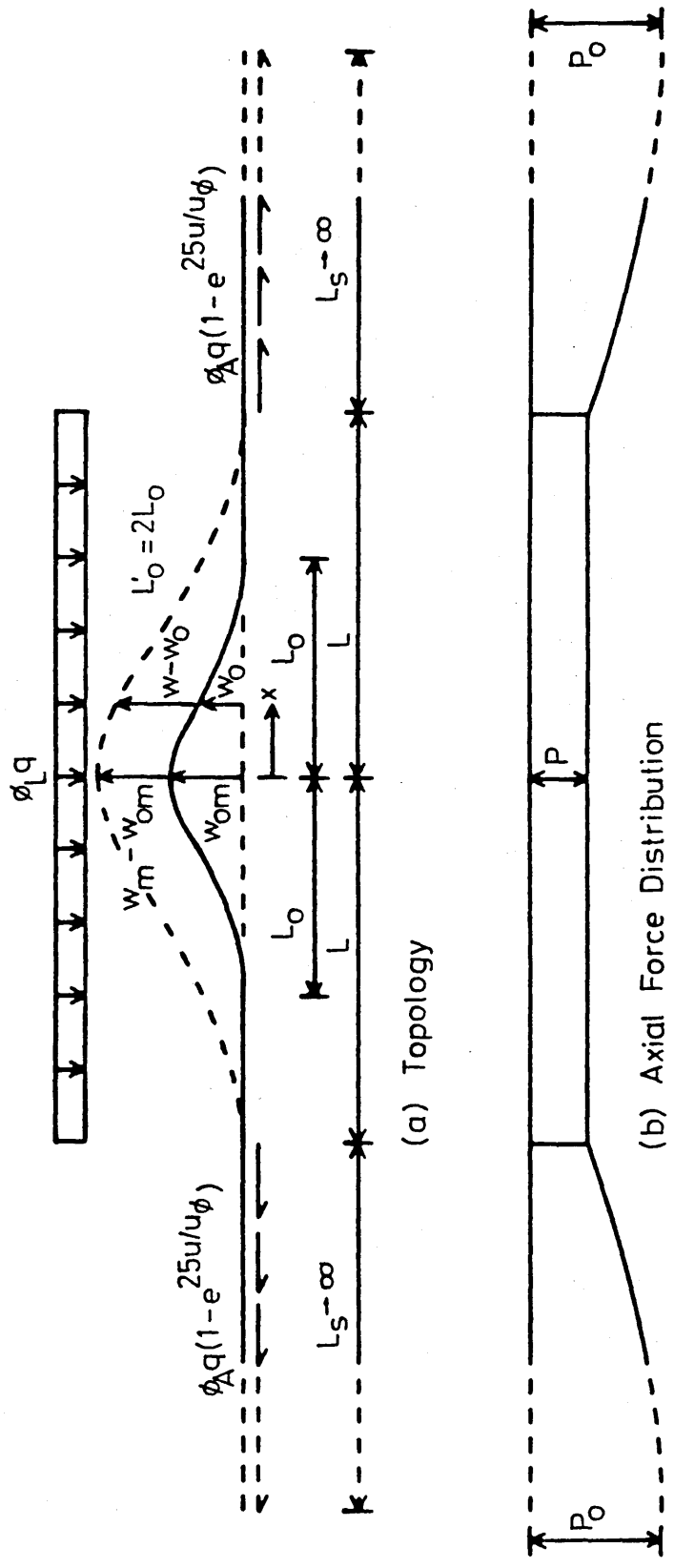


Fig.4.2 Details of Lateral Mode 1

the quintessential imperfection parameter. This parameter is unique in as much as  $w_{om}$  and  $L_0$  or  $L'_0$  are dependent. In the absence of submarine pipeline data relating to practical or field values for this imperfection ratio, data trends were to be sought on the basis of the ratio varying from 0.003 through to 0.010; it was noted that BS 4848 : Part 2 : 1975 stipulates a limit of 0.002 for structural steelwork. The linearised lateral displacement equation appertaining to quasi-idealised pipelines involving fully mobilised lateral resistance and given in equation (1.39), can be rewritten

$$w = \frac{\phi_L q}{EI n^4} (1 + n^2 L^2 / 2 - n^2 x^2 / 2 - \cos nx / \cos nL) \quad 0 \leq x \leq L \quad (4.10)$$

where

$$nL = 4.4934 \quad (4.11)$$

The maximum amplitude of the buckle, at  $x = 0$ , can then be given by

$$w_m = \frac{K_1 \phi_L q}{EI n^4} = 3.8512 \times 10^{-2} \frac{\phi_L q L^4}{EI} \quad (4.12)$$

where  $L$  is the unprescribed buckling length and  $K_1 = (1 + n^2 L^2 / 2 - 1 / \cos nL) = 15.698465$ , such that substituting equation (4.12) into equation (4.10)

yields the transverse displacement expression

$$w = \frac{w_m}{K_1} (1 + n^2 L^2 / 2 - n^2 x^2 / 2 - \cos nx / \cos nL) \quad (4.13)$$

From the foregoing, the imperfection displacement expression can be 'sympathetically' assumed to be

$$w_o = \frac{w_{om}}{K_1} (1 + n_o^2 L_o^2 / 2 - n_o^2 x^2 / 2 - \cos n_o x / \cos n_o L_o) \quad (4.14)$$

$$0 \leq x \leq L_o$$

where

$$n_o L_o = 4.4934 \quad (4.15)$$

and,  $w_{om}$ , the maximum imperfection amplitude, noting equation (4.12), takes the form

$$w_{om} = 3.8512 \times 10^{-2} \frac{\phi_L q L_o^4}{EI} \quad (4.16)$$

This equation displays the previously denoted dependence of  $w_{om}$  and  $L_o$ . The physical imperfection corresponding to equations (4.14), (4.15) and (4.16) takes the form of a basic symmetric wave and relates, in practical terms, to a lateral deviation from the intended or idealised lie. Employing symmetry, the total potential energy relating to the deformed state is given by

$$\begin{aligned}
V &= \int_0^{L_0} 0.5EI(w_{,xx} - w_{0,xx})^2 dx \\
&+ \int_{L_0}^L 0.5EI(w_{,xx} - w_{0,xx})^2 dx \\
&+ \int_0^{L_0} q(w - w_0) dx + \int_{L_0}^L q(w - w_0) dx \\
&- \int_0^{L_0} 0.5P[(w_{,x})^2 - (w_{0,x})^2] dx \\
&- \int_{L_0}^L 0.5P[(w_{,x})^2 - (w_{0,x})^2] dx
\end{aligned} \tag{4.17}$$

the corresponding equilibrium state equation being written

$$\frac{dV}{dw_m} = 0 \tag{4.18}$$

It can be seen from Fig. 4.2 that

$$\begin{aligned}
\int_{L_0}^L 0.5EI(w_{0,xx})^2 dx &= \int_{L_0}^L qw_0 dx \\
= \int_{L_0}^L 0.5P(w_{0,x})^2 dx &= 0
\end{aligned} \tag{4.19}$$

and, further, with

$$\begin{aligned}
\frac{d}{dw_m} \int_0^{L_0} 0.5EI(w_{0,xx})^2 dx &= \frac{d}{dw_m} \int_0^{L_0} qw_0 dx \\
= \frac{d}{dw_m} \int_0^{L_0} 0.5P(w_{0,x})^2 dx &= 0
\end{aligned} \tag{4.20}$$

then equation (4.18) becomes, upon substitution from equation (4.17)

$$\frac{dV}{dw_m} = \frac{d}{dw_m} \left[ \int_0^L 0.5EI(w,_{xx})^2 dx - \int_0^{L_0} EI(w,_{xx})(w_0,_{xx}) dx \right. \\ \left. + \int_0^L qw dx - \int_0^L 0.5P(w,_{xx})^2 dx \right] = 0 \quad (4.21)$$

Upon substitution from equations (4.13) and (4.14) and integrating, equation (4.21) becomes

$$\frac{dV}{dw_m} = \frac{d}{dw_m} \left[ 22.68130 EIn^3 w_m^2 / K_1^2 - R_1 EI w_m w_{om} n n_0^2 / K_1^2 \right. \\ \left. + 30.24174 qw_m / (nK_1) - 37.80217 Pn w_m^2 / K_1^2 \right] = 0 \quad (4.22)$$

where

$$R_1 = 4.60314 \left[ \sin(4.4934 L_0/L) \right. \\ \left. + 2.30157 \left( \frac{\sin 4.4934(1+L_0/L)}{(L/L_0+1)} + \frac{\sin 4.4934(1-L_0/L)}{(L/L_0-1)} \right) \right] \quad (4.23)$$

Differentiating, equation (4.22) becomes

$$45.36260 EIn^3 w_m / K_1^2 - R_1 EI w_{om} n n_0^2 / K_1^2 + 30.24174 q / (nK_1) \\ - 75.60434 Pn w_m / K_1^2 = 0 \quad (4.24)$$

which upon simplification, noting equations (4.11), (4.12), (4.15) and (4.16), yields the buckling force

$$P = 20.19 \frac{EI}{L^2} \left[ 1 - \frac{R_1}{75.60} \left( \frac{L_0}{L} \right)^2 \right] \quad (4.25)$$

Bending moment is afforded by

$$M = EI (w''_{,xx} - w''_{o,xx}) \quad (4.26)$$

which gives the maximum moment, at  $x = 0$ , upon substitution from equations (4.13) and (4.14), to be

$$M_m = -0.27751 \phi_L q (L^2 - L_0^2) \quad (4.27)$$

the negative sign correctly indicating flexural compression to be acting on the lower part of the pipeline section. The maximum compressive stress  $\sigma_m$  induced in the pipe is thereby, noting equations (1.31), (4.25) and (4.27), obtained to be

$$\sigma_m = \frac{20.19EI}{AL^2} \left[ 1 - \frac{R_1}{75.60} \left( \frac{L_0}{L} \right)^2 \right] + 0.27751 \phi_L q r (L^2 - L_0^2) / I \quad (4.28)$$

Having established the relationships between  $w$ ,  $L$ ,  $M_m$ ,  $\sigma_m$  and the buckling force  $P$ , it is now necessary to determine the dependence of  $P$  upon  $T$ , the temperature rise. This is achieved by considering the slip length characteristics. It is proposed to

employ a deformation-dependent axial friction force modelling as denoted in Figs. 2.15 and 4.2. The formulation of the slip length region is the same as that given in Section 3.3.1; that is, equations (3.14) through (3.18) remain valid.

It is now necessary to set up a matching compatibility expression at the interface of the slip and buckling lengths,  $x = L$ . Incorporating the presence of the imperfection  $w_0/L_0$ , equation (1.29) gives

$$u_s = \frac{(P_0 - P)L}{AE} - 0.5 \left[ \int_0^L (w',_x)^2 dx - \int_0^{L_0} (w_0',_x)^2 dx \right] \quad (4.29)$$

which yields, noting equations (4.13) and (4.14),

$$u_s = \frac{(P_0 - P)L}{AE} - 1.0225 \times 10^{-3} \left( \frac{\phi_L q}{EI} \right)^2 (L^7 - L_0^7) \quad (4.30)$$

Solutions for  $(P_0 - P)$  and  $u_s$  are thereby obtained in terms of discrete values of  $L$  employing a computerised non-linear iterative algorithm involving equations (3.18) and (4.30). The numerical evaluations have been carried out, noting equation (4.16), for a series of eleven imperfection ratios  $w_{0m}/L'_0$ , noting that  $L'_0 = 2L$ , from 0.003 through to 0.010. The pipeline parameters employed are again as denoted in Table 1.2. Results for  $(P_0 - P)$  are then

substituted into equations (1.6), (4.12), (4.23) and (4.25) to produce the loci depicted in Figs. 4.3 and 4.4 (a). Only those loci for  $w_{om}/L'_0$  of 0.003, 0.007 and 0.010 are shown for reasons of clarity. The loci in Fig. 4.4 (b) are obtained by substituting the respective values of L into equation (4.28).

#### 4.3 LATERAL MODE 2 ANALYSIS

The topology and axial force distribution depicted in Figs. 4.5 (a) and (b) respectively represent the essential features of lateral mode 2. The linearised lateral displacement equation, relating to idealised pipelines based on fully mobilised lateral resistance, is given by, noting equations (1.64) and (1.65),

$$w = \frac{\phi_L q L^4}{16\pi^4 EI} [1 - \cos(2\pi x/L) + \pi \sin(2\pi x/L) + 2\pi^2 (1-x/L)x/L] \quad 0 \leq x \leq L \quad (4.31)$$

The maximum amplitude of the buckle, at  $x = 0.3464L$ , is

$$w_m = \frac{K_2 \phi_L q L^4}{16\pi^4 EI} = 5.532 \times 10^{-3} \frac{\phi_L q L^4}{EI} \quad (4.32)$$

where L is the unprescribed length and  $K_2 = 8.6211496$ .

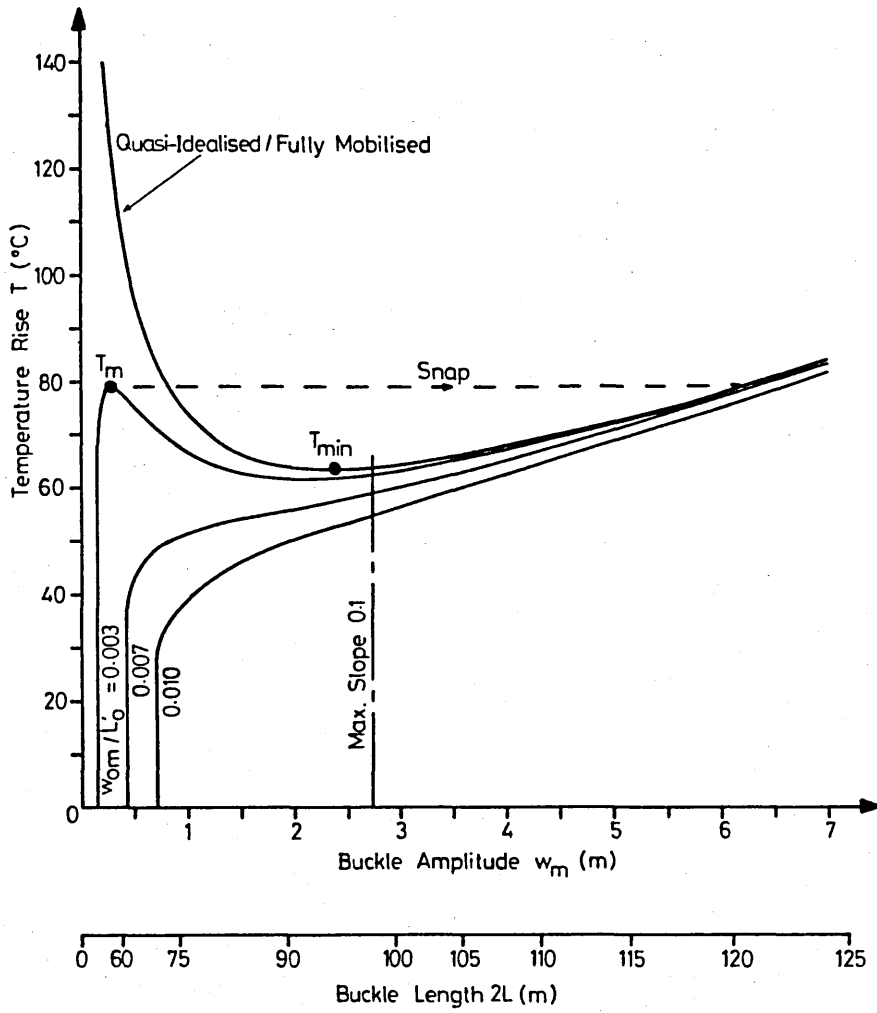


Fig.4.3 Thermal Action Characteristics - Lateral Mode 1

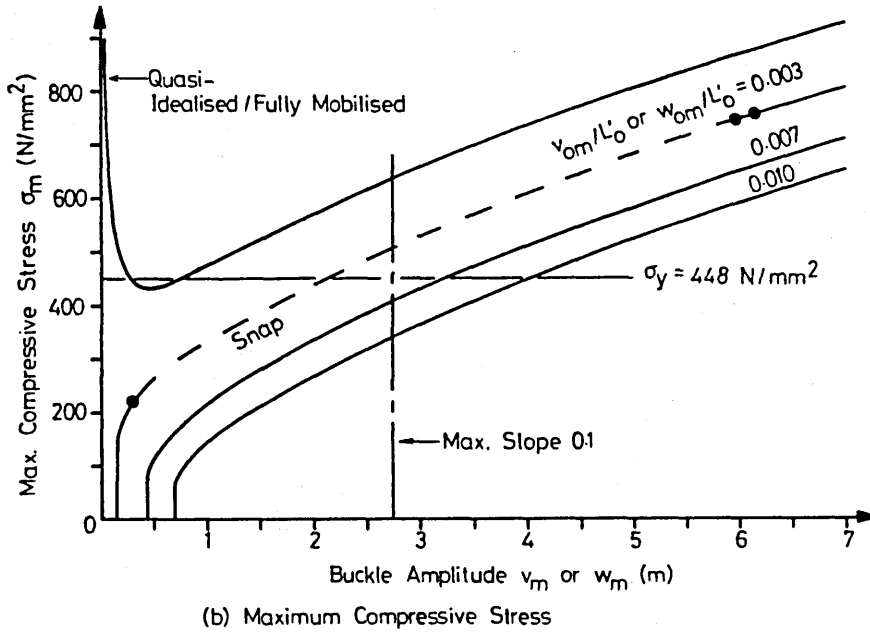
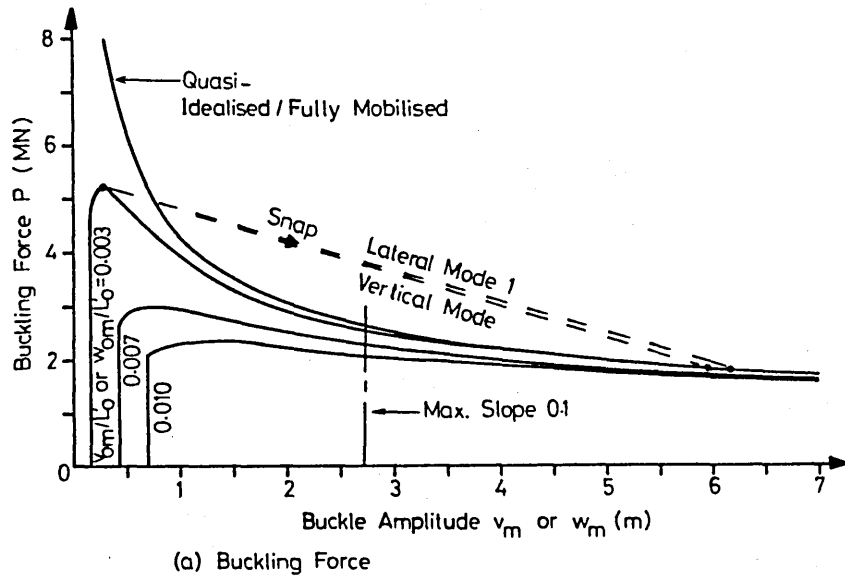


Fig.4.4 Dependent Parameter Characteristics  
- Vertical Mode and Lateral Mode 1

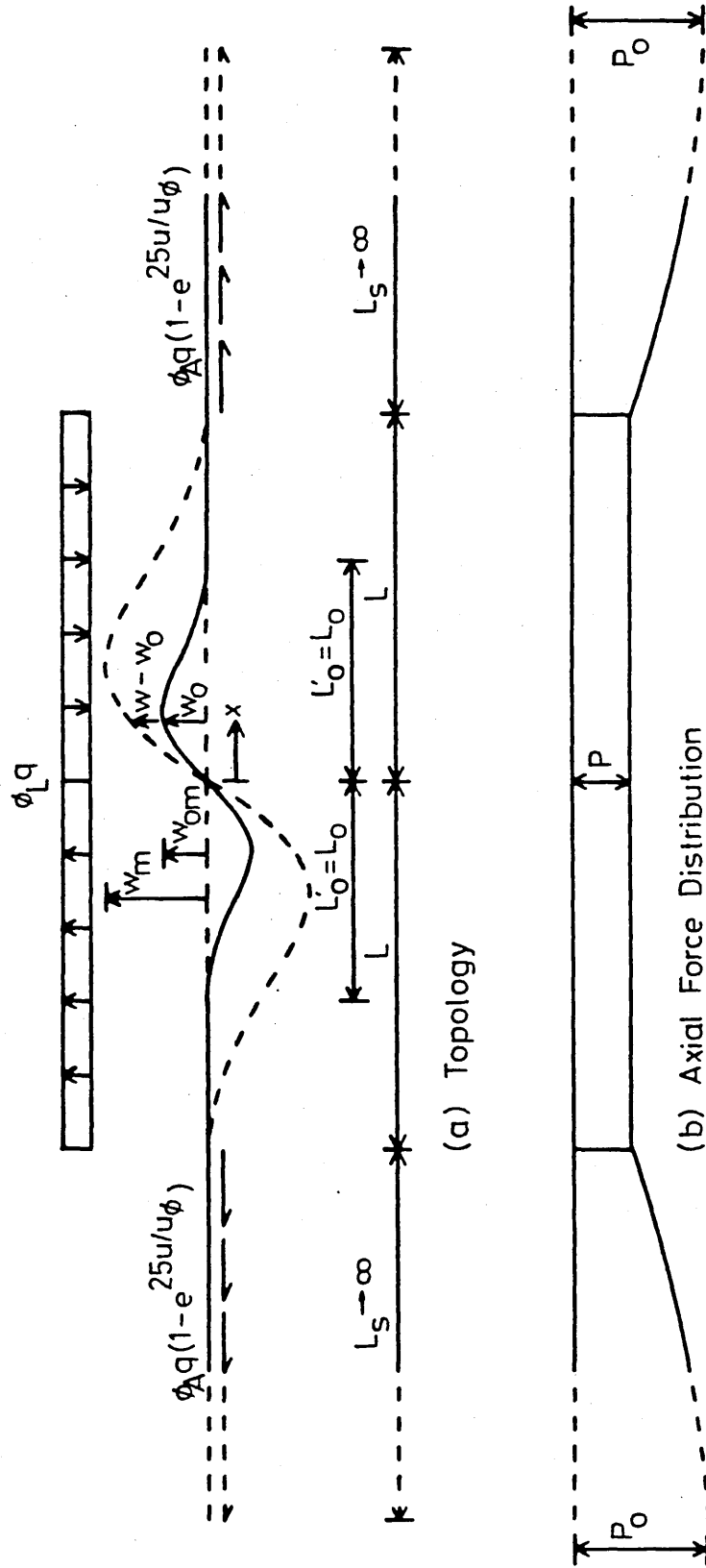


Fig.4.5 Details of Lateral Mode 2

Substituting equation (4.32) into equation (4.31) yields the lateral displacement expression

$$w = \frac{w_m}{K_2} [1 - \cos(2\pi x/L) + \pi \sin(2\pi x/L) + 2\pi^2(1-x/L)x/L] \quad (4.33)$$

From the foregoing, the imperfection displacement expression can be assumed to be

$$w_o = \frac{w_{om}}{K_2} [1 - \cos(2\pi x/L_o) + \pi \sin(2\pi x/L_o) + 2\pi^2(1-x/L_o)x/L_o] \quad 0 \leq x \leq L_o \quad (4.34)$$

where  $w_{om}$  represents the maximum imperfection amplitude which, noting equation (4.32), takes the form

$$w_{om} = 5.532 \times 10^{-3} \frac{\phi_L q L_o^4}{EI} \quad (4.35)$$

The physical imperfection corresponding to equations (4.34) and (4.35) therefore takes the form of a basic skew-symmetric wave. Employing skew-symmetry, the energy formulation is similar to that of lateral mode 1 analysis. Accordingly, equations (4.17) through (4.21) can again be employed. Upon substitution from equations (4.33) and (4.34) and integrating, equation (4.21) becomes

$$\frac{dV}{dw_m} = \frac{d}{dw_m} \left[ \frac{(12\pi^4 + 4\pi^6)EIw_m^2}{K_2^2 L^3} - \frac{8\pi^3 EIw_m w_{om} R_2}{K_2^2 L_o^2 L} \right. \\ \left. + \frac{\phi_L q w_m L}{K_2} (1 + \pi^2/3) - \frac{Pw_m^2}{K_2^2 L} (10\pi^2 + 10\pi^4/3) \right] = 0 \quad (4.36)$$

where

$$R_2 = \sin(2\pi L_o/L) \left( \frac{(L/L_o)(\pi^2 + L/L_o)}{1 - (L/L_o)^2} \right) + 2\pi L_o/L \\ + \pi [1 - \cos(2\pi L_o/L)] \left( \frac{L}{L + L_o} \right) \quad (4.37)$$

Differentiating, equation (4.36) affords

$$\frac{(24\pi^4 + 8\pi^6)EIw_m}{K_2^2 L^3} - \frac{8\pi^3 EIw_{om} R_2}{K_2^2 L_o^2 L} + \frac{\phi_L q}{K_2} (1 + \pi^2/3) \\ - \frac{Pw_m}{K_2^2 L} (10\pi^2 + 10\pi^4/3) = 0 \quad (4.38)$$

which upon simplification, noting equations (4.32) and (4.35), yields the buckling force

$$P = 4\pi^2 \frac{EI}{L^2} \left[ 1 - \frac{3}{5} \left( \frac{R_2}{3\pi + \pi^3} \right) \left( \frac{L_o}{L} \right)^2 \right] \quad (4.39)$$

Noting equation (4.26), the maximum bending moment  $M_m$  at  $x = 0.299L$ , upon substitution from equations (4.33) and (4.34), is given by

$$M_m = -0.10884 \phi_L q (L^2 - L_0^2) \quad (4.40)$$

Further, the maximum compressive stress  $\sigma_m$  induced in the pipe is thereby, noting equations (1.31), (4.39) and (4.40), obtained to be

$$\sigma_m = \frac{4\pi^2 EI}{AL^2} \left[ 1 - \frac{3}{5} \left( \frac{R_2}{3\pi + \pi^3} \right) \left( \frac{L_0}{L} \right)^2 \right] + 0.10884 \phi_L q r (L^2 - L_0^2) / I \quad (4.41)$$

Having established the essential relationships appertaining to the buckling region, those concerning the slip length are now determined. The formulation is similar to that given in the lateral mode 1 analysis; that is, equations (3.14) through (3.18) again remain valid. The matching compatibility expression at the interface of the slip and buckling lengths,  $x = L$ , noting equations (4.29), (4.33) and (4.34), takes the form

$$u_s = \frac{(P_0 - P)L}{AE} - 8.715 \times 10^{-5} \left( \frac{\phi_L q}{EI} \right)^2 (L^7 - L_0^7) \quad (4.42)$$

The solution procedure for  $(P_0 - P)$  and  $u_s$  is as previously; equations (3.18) and (4.42) are solved iteratively in terms of discrete values of  $L$ . Numerical evaluations have been carried out, noting equations (4.35) and Table 1.2, for the previously denoted range of eleven imperfection ratios  $(w_{om}/L'_0)$ ,  $L'_0 = L_0$ . Results for  $(P_0 - P)$  are then substituted into equations (1.6), (4.32), (4.37) and (4.39) to produce the loci depicted in Figs. 4.6 and 4.7 (a). The loci in Fig. 4.7 (b) are obtained by substituting the respective values of  $L$  into equation (4.41).

#### 4.4 VERTICAL MODE ANALYSIS

The essential features of the vertical mode are shown in Fig. 4.8 (a) and (b) which depict the respective topology and axial force distribution. With regard to the imperfection parameters,  $v_0$  and  $v_{om}$  represent the respective vertical displacement and maximum amplitude. The analysis for the buckling region is identical to that of lateral mode 1. Equations (4.10) through (4.28) remain valid except that  $w$ , together with its related components, and  $\phi_L q$  are now replaced by  $v$  and  $q$  respectively. The physical imperfection corresponding to equations (4.14), (4.15) and (4.16) therefore takes the form of a basic symmetric wave; this will act as a potential 'pop-up' trigger.

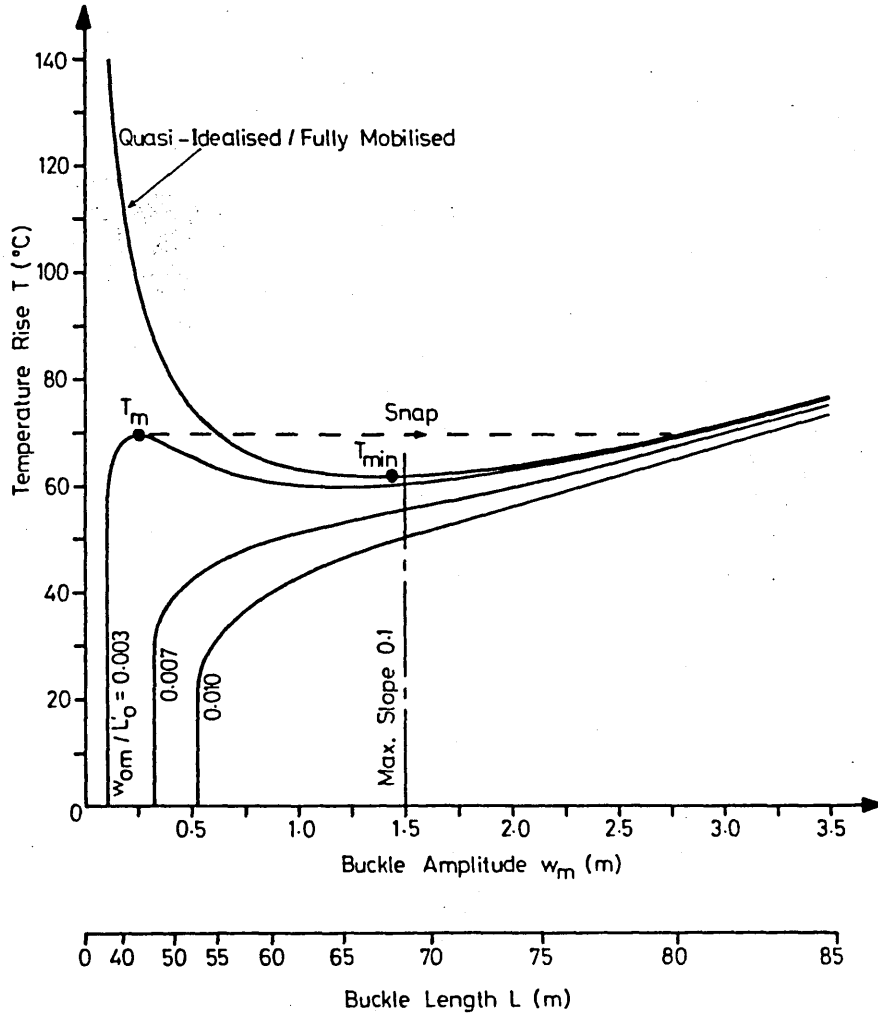
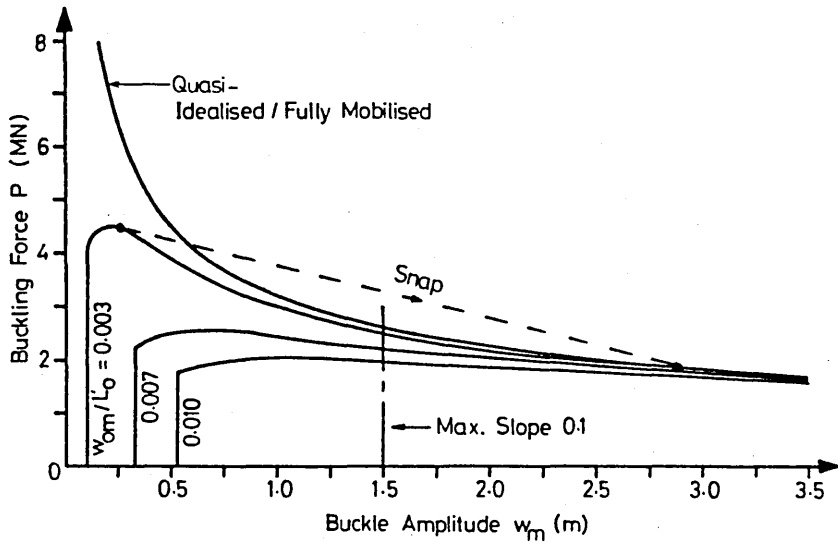
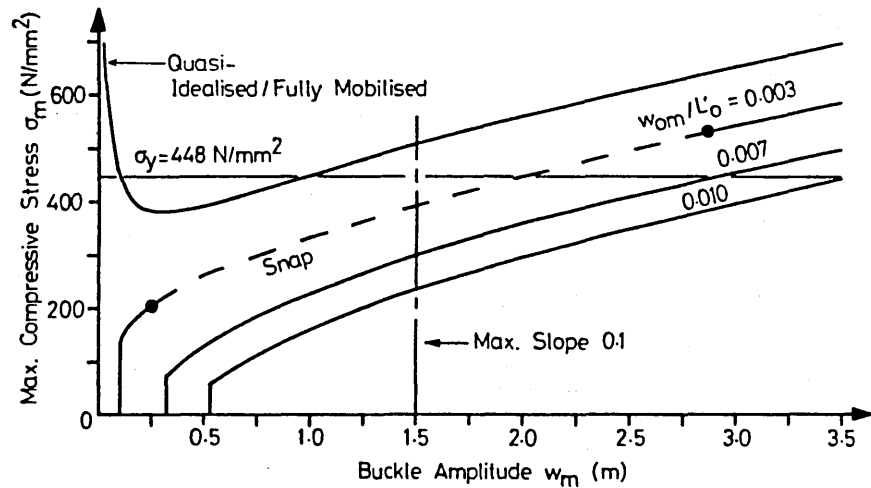


Fig.4.6 Thermal Action Characteristics - Lateral Mode 2



(a) Buckling Force



(b) Maximum Compressive Stress

Fig.4.7 Dependent Parameter Characteristics - Lateral Mode 2

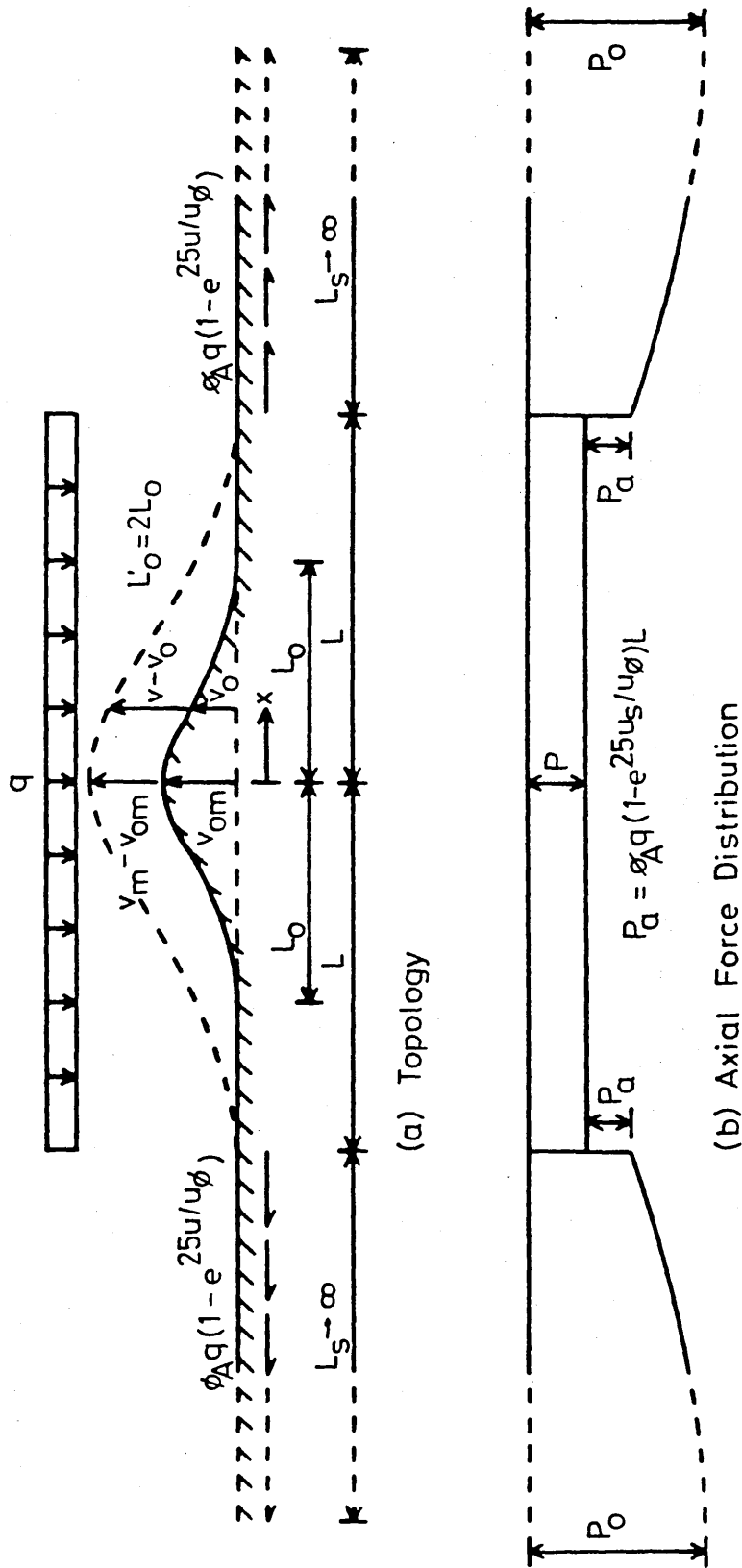


Fig.4.8 Details of Vertical Mode

The formulation of the slip length region is similar to that of Section 3.4; equations (3.20), (3.21) and (3.22) remain valid. The matching compatibility condition at the ends of the buckle remains as given previously for the lateral mode 1 analysis, subject to the appropriate replacement of  $w$  and  $\phi_L q$  by  $v$  and  $q$ . That is, equations (4.13), (4.14) and (4.29), so modified, generate

$$u_s = \frac{(P_0 - P)L}{AE} - 1.0225 \times 10^{-3} \left( \frac{q}{EI} \right)^2 (L^7 - L_0^7) \quad (4.43)$$

this expression being analogous to that given in equation (4.30).

The solution procedure for  $(P_0 - P)$  and  $u_s$  is as previously employed for the lateral mode 1 analysis, equations (3.22) and (4.43) being solved iteratively in terms of discrete values of  $L$ . It is to be noted that since  $\phi_L = 1.0$  (Chapter 2), the revised equations are actually the same as equations (4.10) through (4.28) apart from  $w$  being replaced by  $v$ . Numerical evaluations have been undertaken, noting equation (4.16) and Table 1.2, for the previously denoted range of eleven imperfection ratios (herein  $v_{om}/L'_0$ ),  $L'_0 = 2L_0$ . Results for  $(P_0 - P)$  are then substituted into equations (1.6), (4.12), (4.23) and

(4.25) to produce the v-loci depicted in Fig. 4.9. The loci in Figs. 4.4 (a) and (b), noting equation (4.28), are also valid since  $\phi_L = 1.0$ .

#### 4.5 ASSIMILATION

The imperfection ratios explicitly considered are denoted in Tables 4.2 and 4.3 together with the appropriate permissible temperature rise values, based upon the onset of first yield, and the corresponding buckling amplitudes. It is to be noted that the squash load for the pipeline parameters considered, denoted in Table 1.2 is 13.4 MN, which corresponds to a temperature rise of 197.7°C. Perusal of Tables 4.2 and 4.3 therefore shows that buckling action will occur in practice. Prior to further consideration of Tables 4.2 and 4.3, and the ensuing implications, it is pertinent to assess the behaviour associated with the three imperfection ratios identified in detail previously - that is, with  $v_{om}/L'_0$  and  $w_{om}/L'_0$  taking the values 0.003, 0.007 and 0.010.

With regard to the respective temperature rise/buckling amplitude loci given in Figs. 4.3, 4.6 and 4.9, it can be seen that only the relatively small imperfection ratio case (0.003) displays a maximum temperature rise,  $T_m$ , together with the associated snap buckling

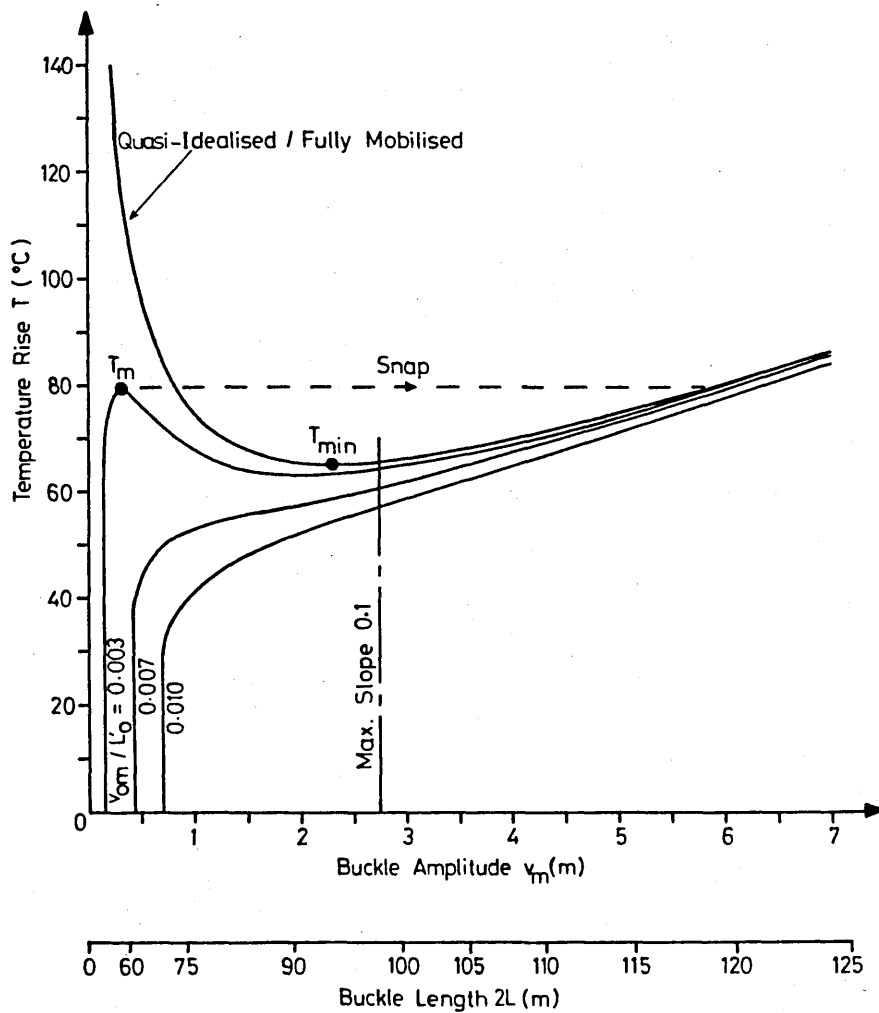


Fig.4-9 Thermal Action Characteristics - Vertical Mode

MODE		VERTICAL	LATERAL 1	LATERAL 2	
IMPERFECTION RATIO $v_{om}/L'_o$ or $w_{om}/L'_o$	0.003	$T_m$ (°C)	79.6	78.9	69.7
		$v_m$ or $w_m$ (m)	0.30	0.30	0.25
		$v_m$ or $w_m$ (m)	5.95 ↓	6.21 ↓	2.86 ↓
	0.0035	$T_m$ (°C)	72.9	72.1	64.1
		$v_m$ or $w_m$ (m)	0.38	0.37	0.32
		$v_m$ or $w_m$ (m)	4.79 ↓	5.03 ↓	2.21 ↓
	0.004	$T_m$ (°C)	67.8	66.9	*60.0
		$v_m$ or $w_m$ (m)	0.48	0.47	*0.42
		$v_m$ or $w_m$ (m)	3.83 ↓	4.05 ↓	*1.64 ↓
	0.0045	$T_m$ (°C)	63.9	62.8	*57.1
		$v_m$ or $w_m$ (m)	0.60	0.59	*0.60
		$v_m$ or $w_m$ (m)	2.99 ↓	3.20 ↓	*1.02 ↓
	0.005	$T_m$ (°C)	*60.9	*59.8	NA
		$v_m$ or $w_m$ (m)	*0.77 ↓	*0.74 ↓	NA
		$v_m$ or $w_m$ (m)	*2.18 ↓	*2.41 ↓	NA
	0.0055	$T_m$ (°C)	NA	*57.5	NA
		$v_m$ or $w_m$ (m)	NA	*1.06 ↓	NA
		$v_m$ or $w_m$ (m)	NA	*1.43 ↓	NA

\* Non-crucial values on basis of yield - refer to Table 4.3  
↓ Indicates snap

Table 4.2 Maximum Temperature Rise,  $T_m$

MODE		VERTICAL	LATERAL 1	LATERAL 2	
IMPERFECTION RATIO $v_{om}/L_o$ or $w_{om}/L_o$	0.004	$T_y$ ( $^{\circ}C$ )	NA	NA	*64.2
		$v_m$ or $w_m$ (m)	NA	NA	*2.26
	0.0045	$T_y$ ( $^{\circ}C$ )	NA	NA	*64.9
		$v_m$ or $w_m$ (m)	NA	NA	*2.37
	0.005	$T_y$ ( $^{\circ}C$ )	*62.3	*60.5	65.6
		$v_m$ or $w_m$ (m)	*2.67	*2.67	2.49
	0.0055	$T_y$ ( $^{\circ}C$ )	62.3	*60.5	66.3
		$v_m$ or $w_m$ (m)	2.81	*2.81	2.60
	0.006	$T_y$ ( $^{\circ}C$ )	62.4	60.6	67.0
		$v_m$ or $w_m$ (m)	2.95	2.95	2.71
0.007	$T_y$ ( $^{\circ}C$ )	62.8	60.9	68.6	
	$v_m$ or $w_m$ (m)	3.22	3.22	2.93	
0.008	$T_y$ ( $^{\circ}C$ )	63.3	61.4	70.1	
	$v_m$ or $w_m$ (m)	3.48	3.48	3.14	
0.009	$T_y$ ( $^{\circ}C$ )	64.0	62.0	71.8	
	$v_m$ or $w_m$ (m)	3.74	3.74	3.35	
0.010	$T_y$ ( $^{\circ}C$ )	64.7	62.7	73.4	
	$v_m$ or $w_m$ (m)	4.00	4.00	3.55	

\*Snap followed by yield, refer to \* on Table 4.2

Table 4.3 Temperature Rise at First Yield,  $T_y$

phenomenon. The remaining two cases (0.007 and 0.010) generate stable post-buckling paths. In all three modes, the respective loci are of converging form as is to be anticipated; indeed, the modes afford characteristics which are in general agreement with those reported in the related field of rail track buckling<sup>(30,34,38)</sup>, although in the present study it is to be recalled that the buckling length  $L$  is unprescribed. It is to be noted that the results obtained relate to small deformation studies, the onset of slopes in excess of 0.1 radians being indicated in the three figures concerned. The loci are therefore conservative in this larger deformation range. (20,28)

The general characteristics for the respective buckling force/buckling amplitude and maximum compressive stress/buckling amplitude loci for all three modal studies, given in Figs. 4.4 and 4.7, are again of common form. Fig. 4.4 is directly applicable to both the vertical mode and lateral mode 1 ( $\phi_L = 1.0$ ) studies. As illustrated in Figs. 4.4 (a) and 4.7 (a), all imperfection ratio cases generate maximum buckling force states; it should be noted that in the low imperfection ratio case, this state does not exactly coincide with the corresponding maximum temperature rise state. This feature is again in agreement with studies in the

related field of rail track buckling.<sup>(38)</sup> Figs. 4.4 (b) and 4.7 (b), read in conjunction with Figs 4.3, 4.6 and 4.9, suggest that for the stable configurations, the temperature rise required for the onset of first yield increases with increasing imperfection ratio. This feature will be discussed further when consideration is given to all the imperfection ratios studied. Care must be taken with the small imperfection ratio snap buckling cases, however, as the first yield state is incurred during snap. This implies that yield is first incurred with the onset of the respective maximum temperature rise, this feature being indicated by use of the dashed locus.

The corresponding quasi-idealised/fully mobilised buckling loci are included in Figs. 4.3, 4.4, 4.6, 4.7 and 4.9. The inclusion of imperfections can be seen to result in a significant reassessment of 'safe temperature rise'<sup>(20,21,50)</sup>, identified in quasi-idealised terms in Figs. 4.3, 4.6 and 4.9 by  $T_{min}$ . Credibility with regard to the quasi-idealised/fully mobilised loci given in Figs. 4.3, 4.4, 4.6, 4.7 and 4.9 is also to be restricted given the possible snap phenomenon associated with such studies. Noting this, it is deemed appropriate to employ 'permissible' rather than 'safe' with respect to the design interpretation of limiting temperature

rise.

Considering the whole set of imperfection ratios studied, then Tables 4.2 and 4.3 present data relating to the establishment of permissible temperature rises  $T_p$ . The cases given in Table 4.2 are those involving a maximum temperature rise state ( $T_m$ ) - recall the 0.003 imperfection ratio loci given in Figs. 4.3, 4.6 and 4.9 - whilst those cases in which the first yield state is incurred statically, at temperature rise  $T_y$  with or without a prior snap, are listed in Table 4.3. There is some overlap between the tables due to the fact that there are essentially three possible configurations dependent upon the magnitude of the delineated imperfection ratio. First, there are those cases involving a  $T_m$  state in which the ensuing snap buckling results in achievement of a stable state which involves stresses in excess of first yield. These cases are associated with relatively low imperfection ratios and are given in Table 4.2 with  $T_p = T_m$ .

Second, there are those cases involving a  $T_m$  state in which snap buckling occurs but the post-snap stable state is sub-yield; these cases, involving middle-order imperfection ratios, are denoted in Tables 4.2 and 4.3 by an asterisk, with  $T_p = T_y > T_m$ . It should be noted

that from the design aspect, for the medium range imperfection ratios in which the post-snap state is sub-yield, it could be argued that the maximum temperature rise  $T_m$  should be taken as the permissible temperature rise  $T_p$ . This assumes snap to be undesirable in practice. However, for such cases involving a relatively large discrepancy in the respective  $T_p$  values (eg 10%) the degree of snap is small; cases in which the degree of snap is more substantial show only small discrepancies in the respective values of  $T_p$ . Design would involve the application of safety factors, however, and such matters could be simply resolved by their appropriate application.

Third, there are the cases relating to higher imperfection ratios which involve a fully stable path such that  $T_p = T_y$ ; these cases are given in Table 4.3. The pairs of deformation values ( $v_m$  or  $w_m$ ) given in conjunction with each  $T_m$  value in Table 4.2 correspond to the amplitudes associated with the temperature rise  $T_m$  pre- and post-snap. The single-valued amplitudes given in Table 4.3 simply denote the first yield state.

It can therefore be suggested that there are three imperfection range classifications, low, medium and high. Low imperfection ratios are associated

with permissible temperature rises restricted, subject to safety factors, by maximum temperature rises associated with snap buckling. Medium ratios will involve careful consideration of sub-yield snap buckling whilst high ratios will afford the most stable and predictable basis for yield stress based permissible temperature rises. The imperfection ratio ranges associated with these classifications vary between the different modes and will be subject to individual pipeline parameters; note Table 1.2. The above considerations are illustrated in Fig. 4.10 and shown qualitatively in Fig. 4.11. A possible fourth classification, wherein snap and yield occur simultaneously, is also denoted in Fig. 4.11.

Fig. 4.10 is, subject to the imposition of safety factors, effectively a design chart for thermal submarine pipeline buckling with respect to the particular pipeline parameters employed. The general trends are that for low imperfection ratios, the permissible temperature rise decreases with increasing imperfection ratio, whilst for high ratios, the permissible temperature rise increases with increasing imperfection ratio. Intermediate ratios require due consideration to be made regarding the conflicting requirements of snap buckling and yield stress onset. With regard to the range

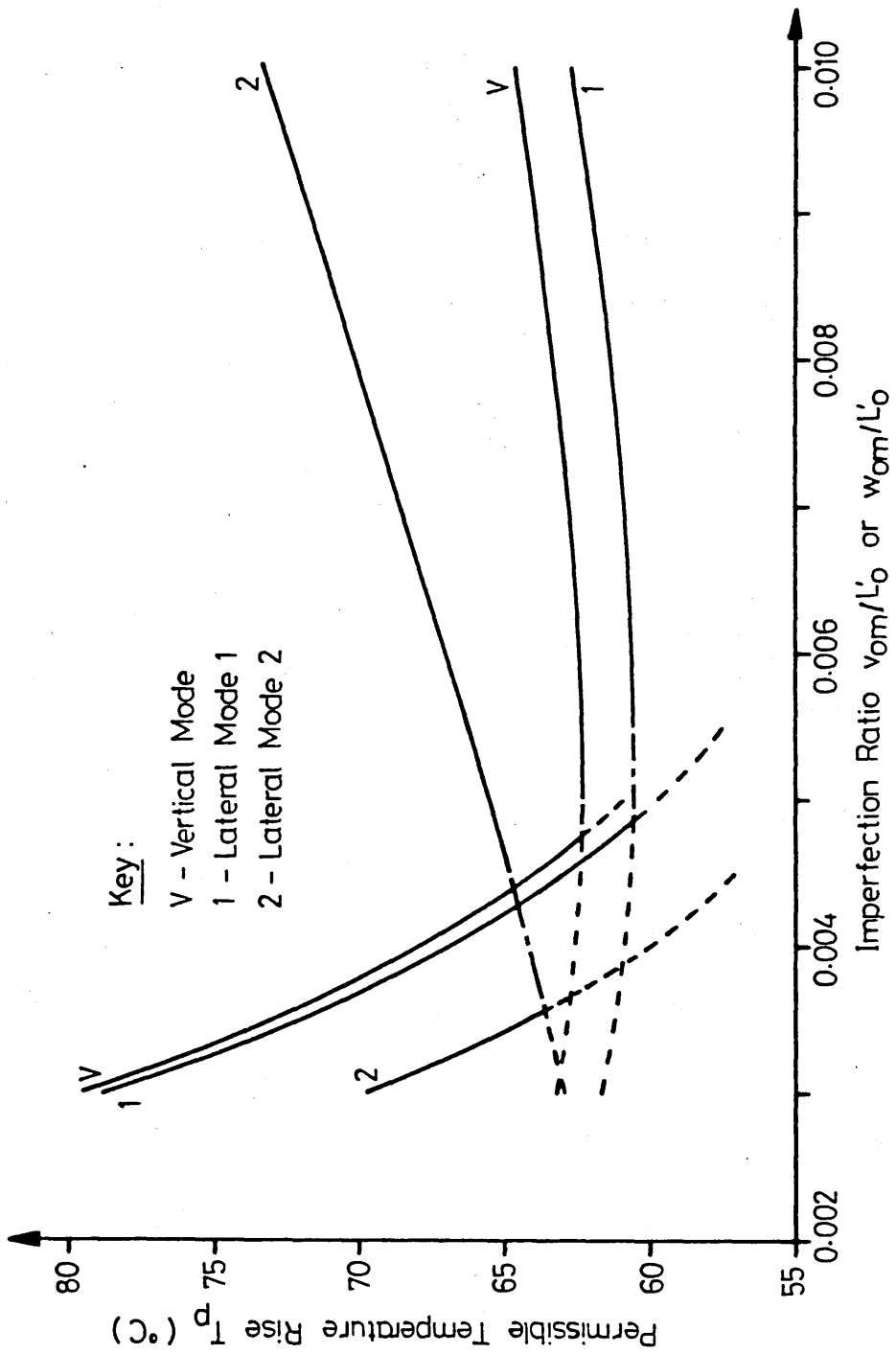


Fig.4.10 Permissible Temperature Rise / Imperfection Ratio Graph

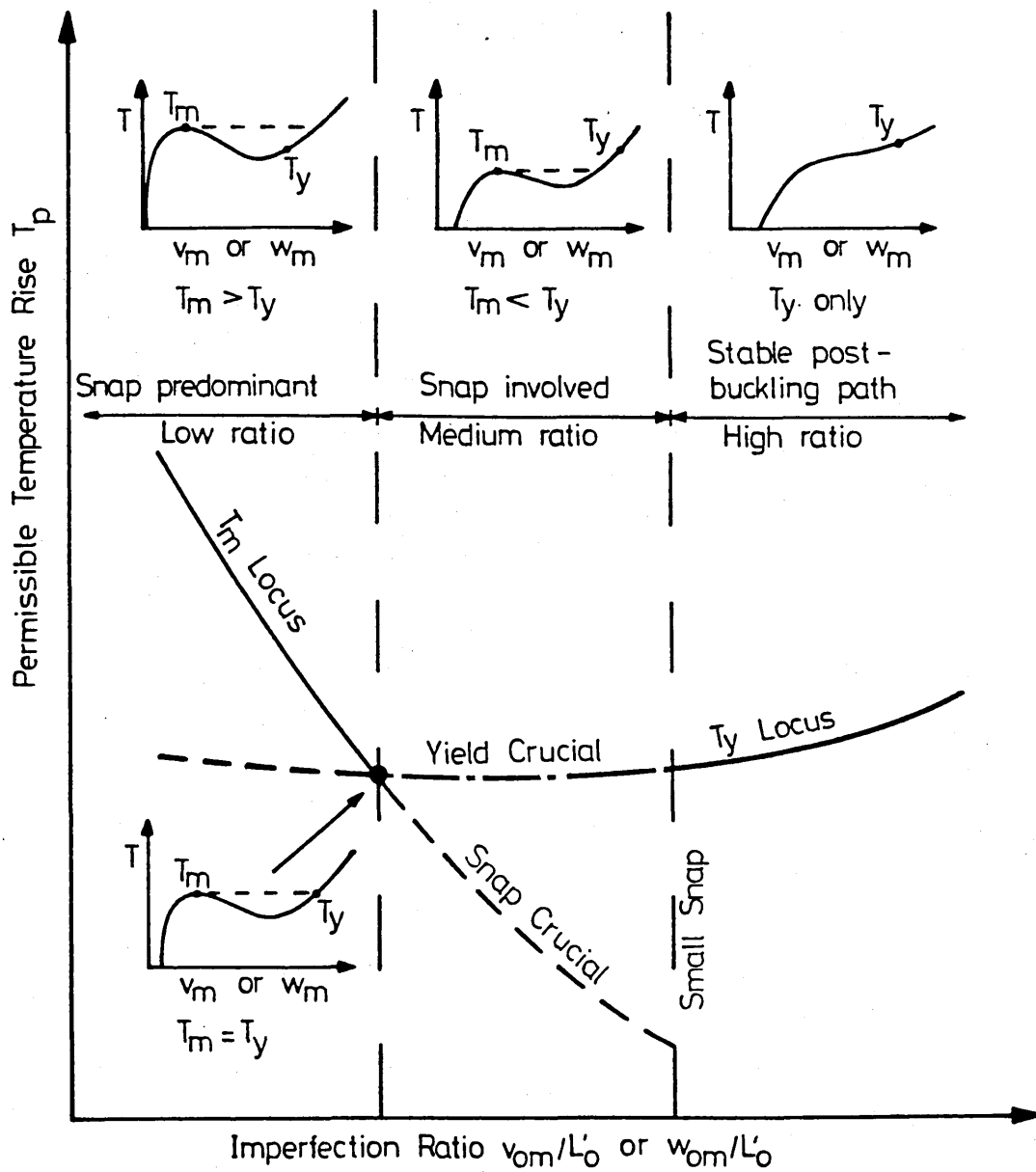


Fig.4.11 Qualitative Imperfection Ratio Relationships

of imperfection ratios chosen (0.003-0.010), it can be seen that it allows for treatment of each of the three possible snap/yield configurations. Further, effective length has been deemed in each mode to lie between non-transversely-displaced adjacent nodes of contraflexure. It is felt that each of the three modes generate related characteristics, note Fig. 4.10, on this basis.

Finally, noting the previous argument relating to the role of the respective quasi-idealised modal maximum compressive stress levels in determining the relative importance of the various lateral modes, it is suggested that for high imperfection ratios, the (stable) curves appertaining to lateral modes 3 and 4 appropriate to Fig. 4.10 will lie between those given for lateral modes 1 and 2 and above that for lateral mode 2 respectively. The corresponding infinity mode locus will then lie above that corresponding to lateral mode 4.

#### 4.6 SUMMARY

An archetypal design chart for use in thermal submarine pipeline buckling has been produced. Clearly, such a chart could be prepared for alternative pipeline parameter and imperfection ratio data. The study has illustrated the effects of basic

physical imperfections appropriate to the problem involved. The modes investigated have been considered upon the basis of their being the most sympathetic and susceptible to such localising physical 'triggers'. The permissible temperature rise values obtained demand that careful attention must be paid to these studies for, as already stated, oil and gas temperatures under field conditions could be as high as 100°C above that of the water environment.

A yield stress based permissible temperature rise criterion, suited to both the design of new pipelines and the assessment of existing pipelines, has been suggested. This is considered to be superior to the somewhat vague fully mobilised safe temperature rise concept previously delineated despite the absence of quantitative knowledge of the probable idealised critical state snap. That is, the quasi-idealised criterion offered little help in determining the appropriate post-buckling characteristics, making identification of the location of the pipeline, should buckling occur, impossible. The proposed approach affords formal post-buckling displacement characteristics, including information on the onset, or otherwise, of plasticity during buckling. Whilst it is not suggested that the present study totally overcomes such problems, difficulty lying with identifying any given physical imperfection,

data trends can now be determined. Basing permissible temperature rise upon the maximum temperature rise state for low imperfection ratios causes such cases to be imperfection sensitive, a feature not experienced with the medium and high imperfection ratio cases; note Figs. 4.10 and 4.11.

Of additional interest is the possibility that recovery upon subsequent cooling would not be total, due to the non-conservative nature of the frictional forces involved. This leads to the realisation that, upon recovery, the imperfection ratio would have increased with a consequent change in post-buckling characteristics should thermal buckling recur. Such post-buckling considerations are perhaps particularly important with regard to trenched pipelines undergoing vertical buckling - 'pop-ups' - in view of the possibility of raised pipelines fouling, for example, anchor cables.

Finally, it must be recalled that the effects of residual stresses remain to be considered, although their effects could perhaps be interpreted in terms of equivalent initial lack-of-straightness. Further, the eccentricity of the frictional forces with respect to the pipe centreline has been neglected. Both features require further study. It should also be noted that the initial assumption that the material response be deemed to be elastic has been

shown to be appropriate although medium and high imperfection ratios lead to yield criteria involving slopes in excess of 0.1 radians. That is, the appropriate data is conservative<sup>(20,28)</sup> with a non-linear kinematic study being required to improve this situation.

# CHAPTER 5

## COMMENTS AND CONCLUSIONS

### 5.1 PRIMARY ASSESSMENTS

Of particular importance to submarine pipeline buckling behaviour is the necessity of determining not only permissible design parametric values in order that buckling be avoided but also the probable location of the pipeline should buckling occur. Construction methods and pipelaying techniques are both sophisticated and expensive; investment is substantial and failure of a pipeline is costly both in terms of lost production and repair costs. Submarine pipelines therefore require the utmost care in engineering design.

At the commencement of the research programme, submarine pipeline buckling studies were essentially limited to the simplified fully mobilised analyses detailed in Chapter 1. Indeed, they were not so succinctly presented, and relied heavily upon associated rail track studies. Not only have errors and limitations contained within these studies been determined and delineated, two enhanced sets of analyses have been developed employing a variety of mathematical techniques. These revised analyses can be considered to consist of two complementary computational suites or programmes of study, one

other oriented quite specifically about the requirements of engineers in practice. The former programme of study deals with critical state studies, the latter with imperfection loci. Both programmes make quantitative post-buckling loci available for the first time with regard to submarine pipeline buckling. Taken together, these programmes of study afford a previously unavailable insight into the nature of submarine pipeline buckling. Design implications, based upon these analyses, have been delineated.

Given that the idealised and imperfection studies are dealt with in Chapters 3 and 4 respectively, it has to be recalled that the associated geotechnical factors developed in Chapter 2 are of crucial importance in establishing the relevant geotechnical parameters involved in the aforementioned buckling computations. These empirical parameters were established by experimentation and are of novel form in their own right. Economics determined that model testing be employed with engineering judgment being used for extrapolation to full scale field values.

A concise overview of the research programme is presented by means of Figs. 5.1 and 5.2 wherein the established and enhanced behavioural loci concerned are presented in terms of variable scale

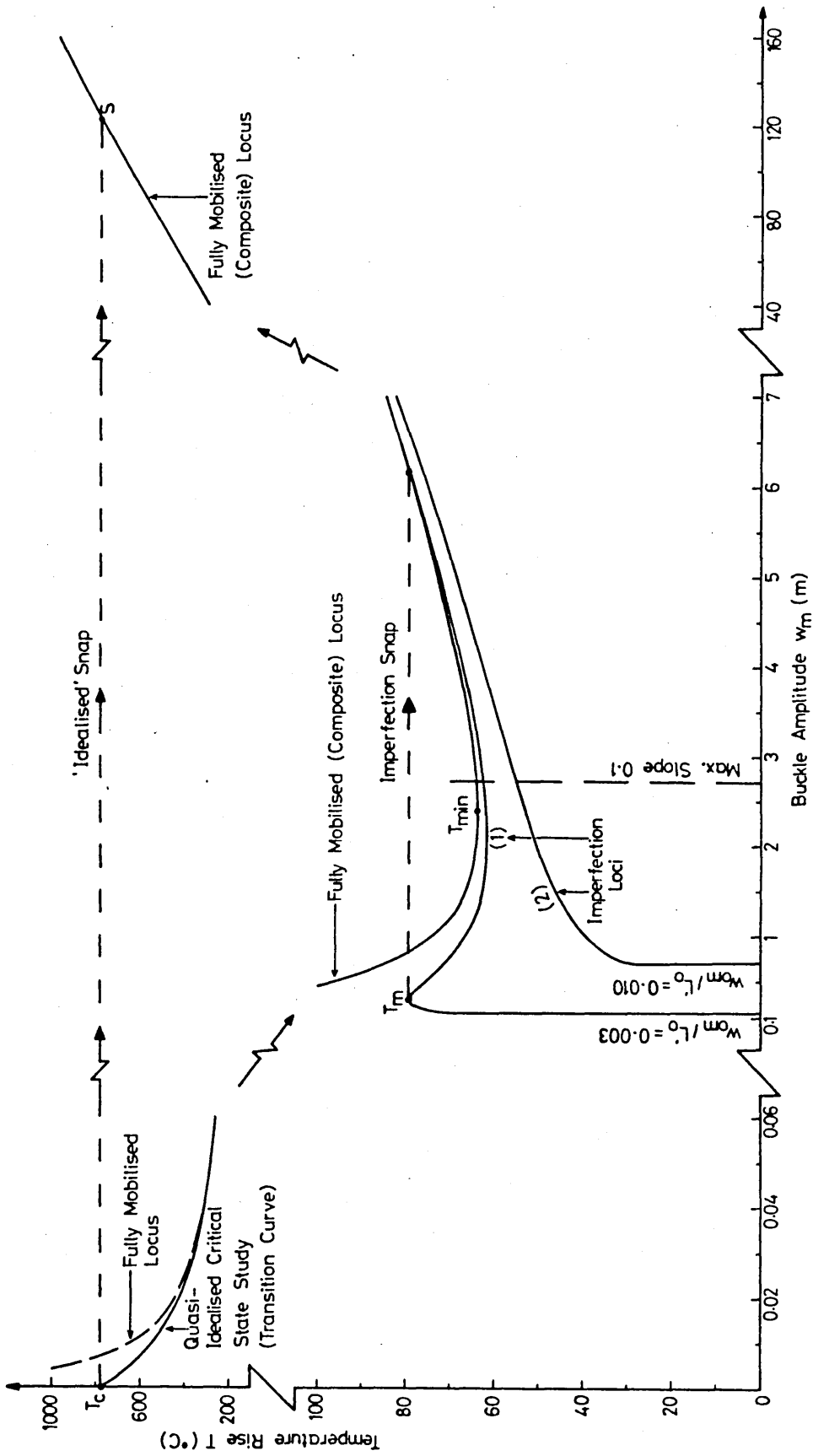


Fig. 5.1 Lateral Submarine Buckling - Enhanced Action-Response Loci (Mode 1)

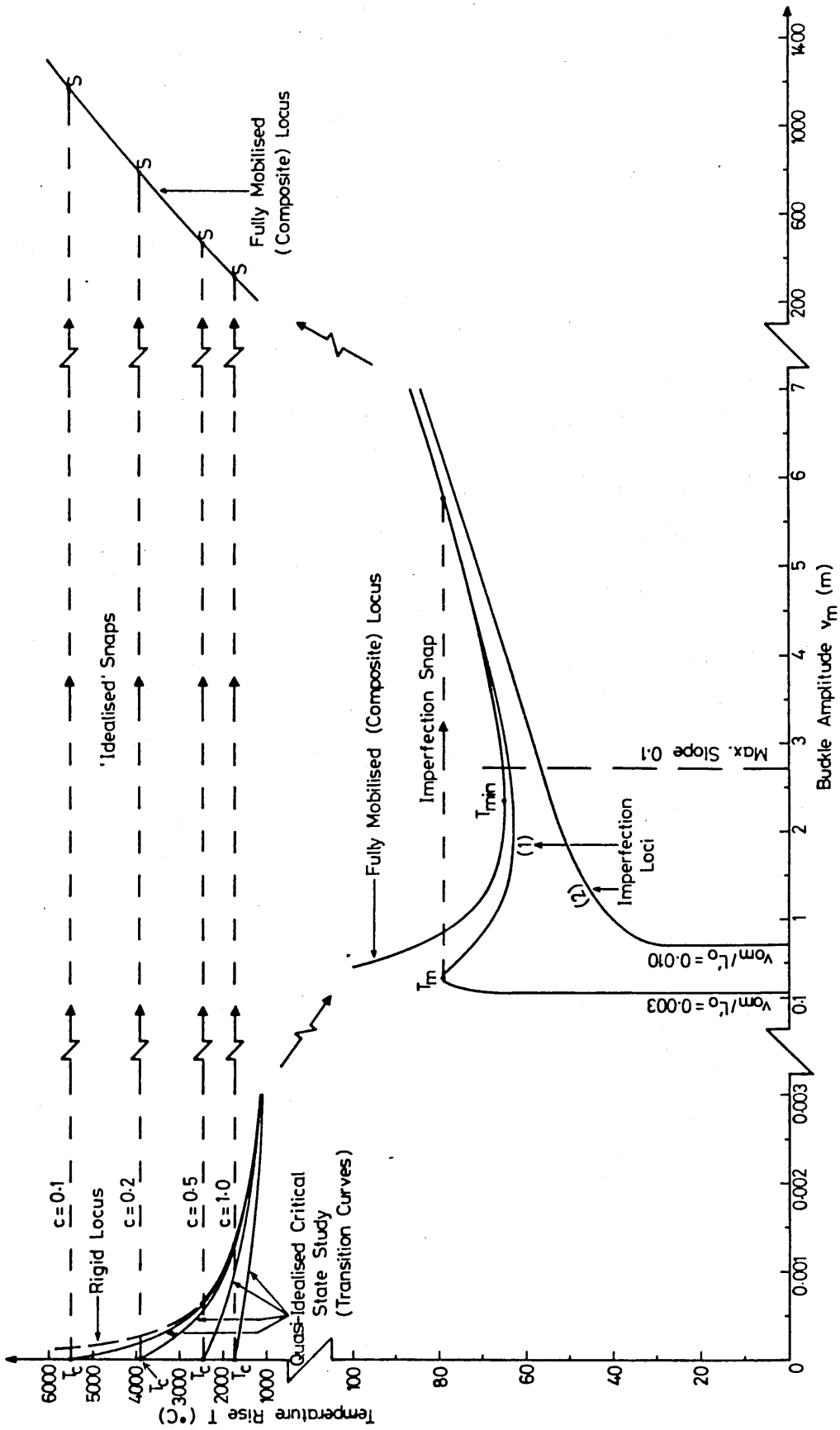


Fig. 5.2 Vertical Submarine Buckling - Enhanced Action-Response Loci

graphs for both lateral (mode 1) and vertical submarine pipeline buckling. Clearly, the analyses presented could be employed with alternative pipeline, material and geotechnical parametric values; application to submarine pipeline buckling involving pressure gradients is readily available.

## 5.2 ASSOCIATED FACTORS

There is widespread use of numerical techniques in advanced engineering problems where formal solutions are unavailable; the present study is no exception. Numerical integrations have been undertaken employing Simpson's Rule to solve complex integral functions. In cases involving highly non-linear simultaneous equations, an in-house developed iterative solution procedure has been employed using a computerised non-linear iterative algorithm. Further, relationships between geotechnical parameters  $\phi$  and  $e$  have been determined by means of computer generated linear and cubic interpolation curves using the Least Squares method. Several methods of analysis, each suited to a particular problem, have been employed. Fully mobilised studies have been analysed in closed form using formal continuum analysis involving linearised differential equations. In the critical state studies, the boundary collocation method has been employed in view of the complex

non-linear field equations which prevent closed form solutions being obtained. Lastly, imperfection studies have been carried out by means of the Principle of Stationary Potential Energy Approach.

All numerical evaluations have been carried out on the IBM 4341 8 Megabyte mainframe computer under the VM/CMS virtual system using Fortran programming with the appropriate computer graphics being obtained employing the Gino graphics suite routines. Indeed, numerical evaluations of the analyses would have been virtually impossible without access to a digital computer. In order that some appreciation of this feature be made available, a concise set of typical programme listings is included in Appendix III.

Recourse was made as necessary to experimentation particularly with regard to the geotechnical parameters relating to friction resistance and sea bed recovery characteristics. This experimentation provided the means for the appropriate development of the research programme. Employment of empiricism and engineering judgment has been necessary in order to apply the aforementioned mathematical techniques.

### 5.3 SUGGESTIONS FOR FURTHER STUDIES

Perfect elasticity and small deformations (slopes  $< 0.1$

radians) have been assumed throughout the present study. Should plasticity and/or finite deformation occur, the analyses presented cease to be effective. Further, on unloading, yielding will result in permanent set of the pipe and this will act as an additional imperfection on subsequent reloading. Consequently, more complex kinematic non-linear analyses would provide for a better definition of the post-buckling paths involving buckling slopes in excess of 0.1 radians whilst elasto-plastic analyses would be appropriate to paths exceeding the elastic limit. An investigation into definitive imperfection ratios would also be apposite. This would involve assessment of sea bed topologies and the manner in which a pipeline's sea bed lie is actually achieved in practice.

In view of the non-conservative nature of the sea bed recovery and friction characteristics, recovery upon subsequent cooling (unloading) would not be total, this also leading, as in the case above, to a revised imperfection topology should thermal buckling recur. Better understanding of this feature would require full scale tests, involving heating and cooling the pipeline, in order to determine the appropriate sea bed recovery and friction parameters. Again, in-situ assessment would appear necessary.

Finally, post-buckling behaviour may be subject to modal interaction. A pipeline may be subject to lateral (or inclined) buckling once a trenched pipeline has buckled, initially, in the vertical plane. More importantly, a combination of both lateral and vertical (ie inclined) movements may occur throughout the buckling process, particularly in cases where the pipeline is initially resting in a wide trench. In-depth study of this behaviour could involve a complex three-dimensional analysis combining both lateral and vertical buckling behaviours.

The foregoing suggested developments would lead to the institution of highly complex analyses. However, the assessment of definitive imperfection ratios is felt to be the most urgent of the proposals given in view of the fact that, in quantitative terms, this is the most contentious issue incurred in this study.

APPENDIX I  
PUBLICATIONS

I(A) Reference (21)

TAYLOR,N. and GAN,A.B. 'Regarding the buckling of pipelines subject to axial loading.' Journal of Constructional Steel Research, Vol.4, Jan, 1984, 45-50.

I(B) Reference (62)

TAYLOR,N. RICHARDSON,D. and GAN,A.B. 'On submarine pipeline frictional characteristics in the presence of buckling.' Proceedings of the 4th International Symposium on Offshore Mechanics and Arctic Engineering, American Society of Mechanical Engineers, Dallas, Texas, 17-21 Feb, 1985, 508-515.

I(C) Reference (63)

TAYLOR,N. and GAN,A.B. 'A refined modelling for the lateral buckling of submarine pipelines.' Journal of Constructional Steel Research.  
(Accepted for publication.)

## Regarding the Buckling of Pipelines Subject to Axial Loading

Neil Taylor and Aik Ben Gan

Department of Civil Engineering, Sheffield City Polytechnic, Pond Street, Sheffield  
S1 1WB, UK

### SYNOPSIS

*The buckling of submarine pipelines subject to axial loading has received attention in the form of linearised study.<sup>1</sup> Both vertical and lateral deflection modes have been analysed. This paper concentrates on two crucial factors which must be considered further before any formal non-linear predictive analyses can be meaningfully undertaken.*

### NOTATION

$m$	$p/EI$
$n$	$(P/EI)^{1/2}$
$p$	Submerged weight of pipeline per unit length.
$v$	Vertical displacement of the pipe
$w$	Lateral displacement of the pipe.
$x$	Cartesian coordinate with $d^2w/d^2x$ as second derivative.
$A$	Cross-sectional area.
$E$	Young's modulus.
$I$	Second moment of area of cross-section.
$L$	Buckle length.
$L_s$	Slip length.
$P$	Axial force in buckled pipe.
$P_0$	Prebuckling axial force.
$T$	Temperature increment.
$\alpha$	Coefficient of linear thermal expansion.

- $\phi_A$  Axial coefficient of friction.  
 $\phi_l$  Lateral coefficient of friction.

## 1 INTRODUCTION

A uniform temperature increase,  $T$ , in a perfectly straight submarine pipeline will create an axial compression force due to constrained thermal expansion. Within the elastic range of the pipeline response, this force can be represented by:

$$P_0 = AE\alpha T \quad (1)$$

where  $AE$  is the axial rigidity at the pipe and  $\alpha$  is the respective coefficient of linear thermal expansion. During buckling, part of the constrained thermal expansion is released in the buckled region,  $L$ , which, taken together with the frictional resistance of the sea-bed/pipeline interface, results in a reduction in the axial compression to some buckling force  $P$ . The situation, with particular reference to the vertical mode, is illustrated in Fig. 1. Key parameters include  $L_s$ , the slip length over which axial

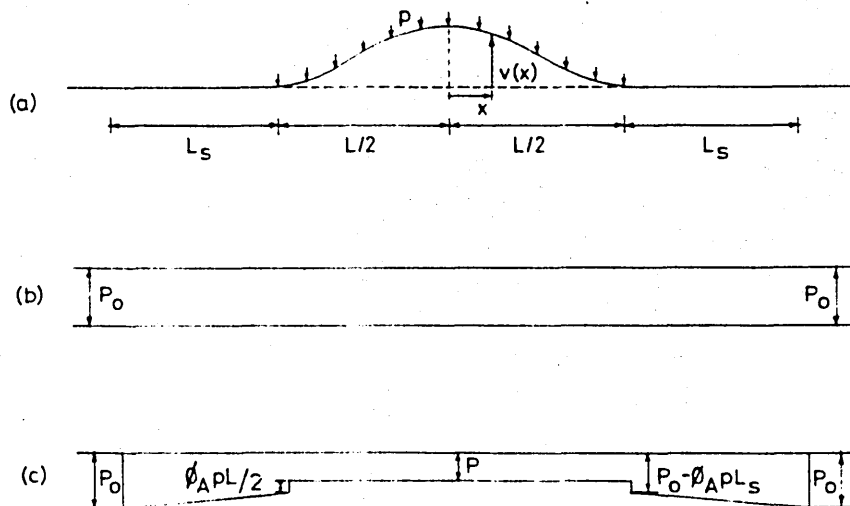


Fig. 1. (a) Vertical buckling mode; (b) distribution of axial force before buckling; (c) distribution of axial force after buckling.

friction resistance acts;  $\phi_A$ , the axial coefficient of friction; and  $p$ , the submerged weight of the pipeline per unit length.

## 2 VERTICAL DEFLECTION MODE

Noting the related study of the buckling of rail track<sup>2</sup> and referring to Fig. 1, the linearised differential equation is said to take the form:<sup>1</sup>

$$d^2v/dx^2 + n^2v + m(4x^2 - L^2)/8 = 0 \quad (2)$$

where  $v$  is the vertical displacement,  $n^2 = P/EI$  and  $m = p/EI$ ,  $EI$  being the flexural rigidity of the pipe. Ensuing analysis leads to the evaluation of the critical load and explicit values of deformation, apparently offering a basis for more refined non-linear study. However, particular care would be required as such a study, surely incorporating some initial geometric imperfection parameter, would need to overcome the fact that eqn (2) is not valid at

$$v = 0 \quad (3)$$

as the corresponding curvature implies

$$d^2v/dx^2 = -m(4x^2 - L^2)/8 \neq 0 \quad (4)$$

## 3 LATERAL DEFLECTION MODES

Again noting the related studies in the field of rail track stability,<sup>3</sup> the five basic modes are as illustrated in Fig. 2. For the given problem of pipeline stability, it could be argued that as action (i.e., temperature rise) is of distributive form, a distributive response is to be anticipated. This leads to the logical conclusion that the infinity mode should be afforded as the critical response. Localisation would presumably then ensue as an elasto-plastic phenomenon.<sup>4</sup> The analyses of Modes 1 to 4 are available from rail track studies<sup>3</sup> whilst the infinity mode has been separately established.<sup>1</sup> This latter analysis indeed claims the infinity mode to be the critical case (i.e., that corresponding to the lowest temperature at which buckling will occur). However, closer inspection shows this claim to be erroneous, leading to realisation that either the above logical deduction relating to the infinity mode is incorrect or that the modelling employed<sup>1</sup> is invalid.

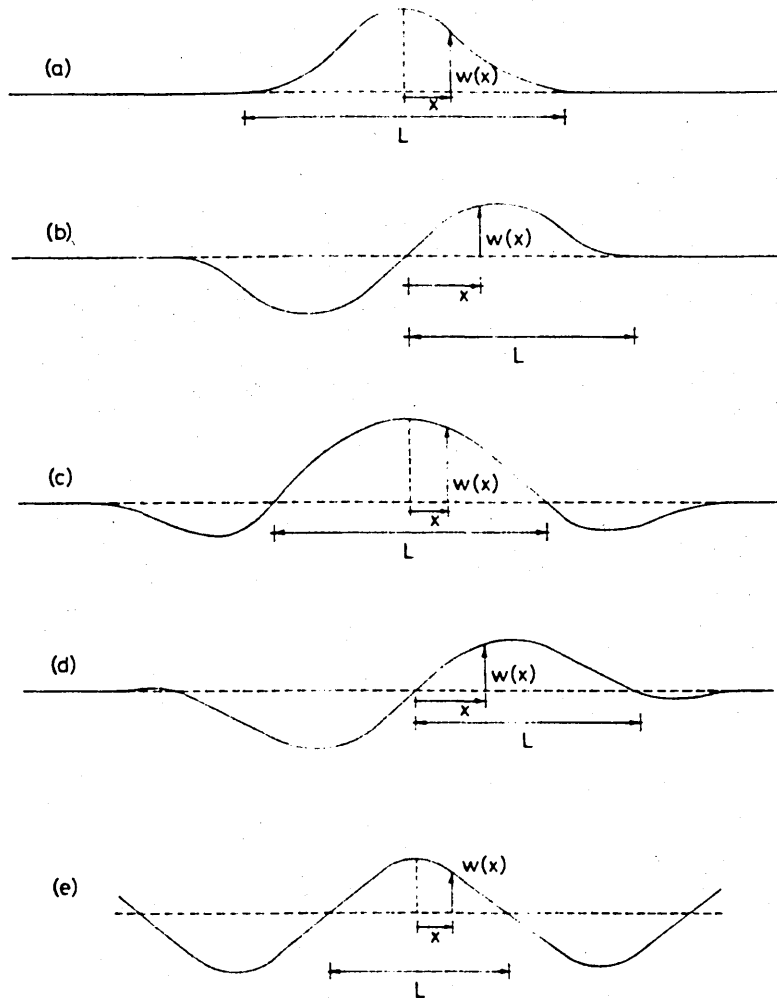


Fig. 2. Details of lateral buckling modes (a) Mode 1; (b) Mode 2; (c) Mode 3; (d) Mode 4; (e) Mode  $\infty$ .

Noting Fig. 2, the linearised differential equation appertaining to the infinity mode is given as:<sup>1</sup>

$$d^2w/dx^2 + n^2w + \phi_1 \frac{p(4x^2 - L^2)}{8EI} = 0 \quad (5)$$

where  $w$  is the lateral displacement and  $\phi_1$  is the lateral coefficient of

friction. Incorporation of the respective boundary conditions leads to the determination of the buckling load as:

$$P = 4\pi^2 EI/L^2 \tag{6}$$

The buckle length  $L$  is then determined from the compatibility expression:<sup>1</sup>

$$P_0 - P = AE/L \int_{-L/2}^{L/2} \frac{1}{2} (dw/dx)^2 dx \tag{7}$$

which affords:

$$P_0 = P + (47.05 \times 10^{-6}) AE \left[ \frac{\phi_{1,P}}{EI} \right]^2 L^6 \tag{8}$$

Importantly, this is not in agreement with the previous work in this field,<sup>1</sup> although it is supported by analogous computations.<sup>5,6</sup> The crucial consequence is that the infinity mode, employing the established modelling,<sup>1</sup> is not the critical mode.

This can be illustrated by referring to Fig. 3 which depicts the essential relationships between the various lateral modes for a typical set of

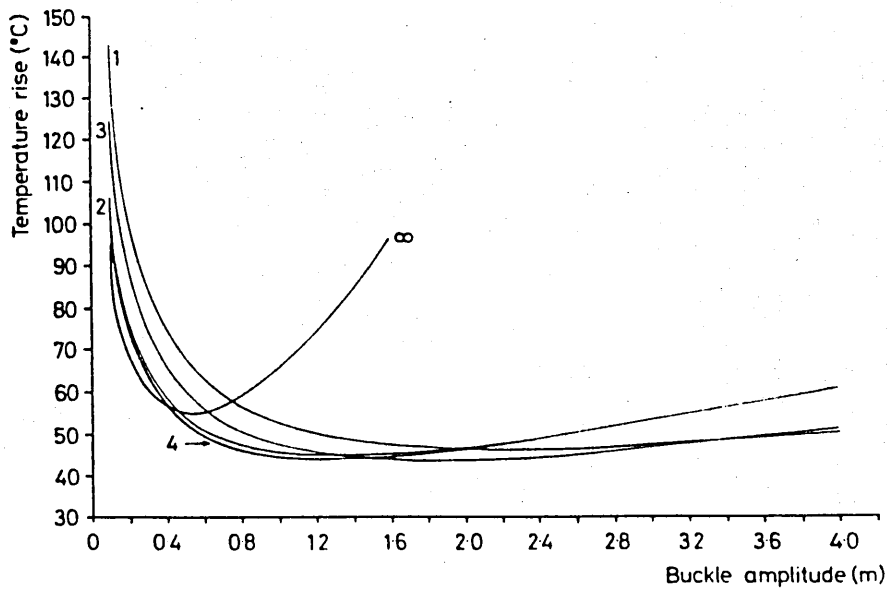


Fig. 3. Comparison of lateral buckling modes.

parametric values.<sup>1</sup> It can be seen that Mode 4 is the critical mode; it could, perhaps, be argued that this is a 'semi-infinite' mode. (Further, it should be noted that the vertical mode can be shown to be non-critical unless the pipeline is laid in a trench.)

#### 4 CONCLUSIONS

Essential information is provided in this paper to allow prediction of the behaviour of submarine pipelines subject to axial loading, should this be desired. However, it would seem that a distinct improvement in the respective modelling assumptions is required if the buckling and large deflection behaviour is to be fully understood. The established approach<sup>1</sup> offers very little information on structural behaviour with regard to definitive load-displacement characteristics; further, the inherent small deformation assumption raises the problem of whether sea-bed resistance is indeed likely to be fully mobilised at the critical state. It should be noted that the relationships between pipeline and rail-track buckling studies are subject to the considerable differences between the respective ground/structure interfaces. Perhaps a relatively crude non-linear modelling would serve as a better introduction to this area of work, offering a higher degree of consistency.

#### REFERENCES

1. Hobbs, R. E., Pipeline buckling caused by axial loads, *J. Construct. Steel Res.*, **1**(2) (January 1981) 2-10.
2. Kerr, A. D., On the stability of the railroad track in the vertical plane, *Rail International*, **2** (February 1974) 131-42.
3. Kerr, A. D., Analysis of thermal track buckling in the lateral plane, *Acta Mech.*, **30** (1978) 17-50.
4. Tvergaard, V. and Needleman, A., On the localization of buckling patterns, *J. Appl. Mech., Trans. ASME*, **47** (September 1980) 613-19.
5. Marek, P. J. and Daniels, J. H., Behaviour of continuous crane rails, *J. Struct. Div., ASCE*, **ST4** (April 1971) 1081-95.
6. Granstrom, A., Behaviour of continuous crane rails, *J. Struct. Div., ASCE*, **ST1** (January 1972) 360-1.

Contributions discussing this paper should be received by the Editor before 1984.

# Appendix I (B)

## ON SUBMARINE PIPELINE FRICTIONAL CHARACTERISTICS IN THE PRESENCE OF BUCKLING

N. Taylor, Senior Lecturer in Structural Engineering  
 D. Richardson, Senior Lecturer in Geotechnical Engineering  
 A. Ben Gan, Research Student  
 Department of Civil Engineering  
 Sheffield City Polytechnic  
 Sheffield, England

### ABSTRACT

An important aspect of submarine pipeline behaviour relates to the possible incursion of structural buckling during routine operation. An integral part of this area of study involves the resistance to movement provided by the supporting medium. It is with the nature of these frictional resistance forces that this study is primarily concerned. Sand was chosen as the supporting medium in view of North Sea conditions. The relative dearth of information available on this subject led to the institution of an experimental investigation involving some eighty-four small scale tests. Data trends are presented and scaling factors discussed; semi-empirical design formulae are then proposed.

### NOMENCLATURE

A cross-sectional area  
 E Young's modulus  
 E interface configuration (entrenched)  
 f friction parameter  
 I second moment of area of cross-section  
 L buckle length  
 P pressure difference across pipe wall  
 P buckling force  
 F interface configuration (compacted)  
 q submerged weight of pipeline per unit length  
 r pipe radius  
 R interface configuration (resting)  
 t wall thickness of pipe  
 T temperature thickness  
 u axial displacement of the pipe  
 w lateral displacement of the pipe  
 x spatial coordinate  
 $\alpha$  coefficient of linear thermal expansion  
 $\gamma$  theoretical friction locus coefficient  
 $\theta$  horizontal angle between the direction of pull and an axis normal to the pipe centre line  
 $\nu$  Poisson's ratio  
 $\phi$  generalised friction coefficient  
 $\phi_1$  generalised coordinate  
 $F_A$  axial frictional resistance force  
 $L_S$  slip length

$P_0$  prebuckling axial force  
 $u_s$  overall extension of slip length  
 $u_\phi$  fully mobilised axial displacement  
 $w_\phi$  fully mobilised lateral displacement  
 $\phi_A$  axial friction coefficient  
 $\phi_L$  lateral friction coefficient

### INTRODUCTION

The cost of failure with regard to submarine pipelines is prohibitive both in terms of repair and lost production. As a result, the design and construction of such pipelines require the highest degree of rigour. Amongst the contingencies for which the offshore engineer must be prepared is that concerned with the effects of some axial compression being set up within the pipeline during routine operation. These compressive forces are induced by the frictional restraint of axial extensions due to change in temperature or internal pressure. With oil temperatures up to 100°C above that of the water environment and operating pressures over 10N/mm<sup>2</sup>, these forces can be substantial given the ability of the pipeline-sea bed interface to generate the necessary resistance. Clearly, this gives rise to the risk of structural buckling.

Analyses concerned with the buckling behaviour of submarine pipelines caused by axial compression have been carried out in the form of linearised studies (1), (2). Both lateral and vertical modes have been identified, Figure 1 illustrating a typical lateral mode, wherein the pipeline snakes across the sea bed, together with the respective axial force distribution. Both axial and lateral frictional resistance forces, identified by distributed forces  $\phi_{Aq}$  and  $\phi_{Lq}$  respectively, are involved; vertical buckling only involves axial frictional resistance forces as typified by  $\phi_{Aq}$ . In order to identify the role of these frictional forces, it is instructive to briefly consider the essential mathematics concerned.

Initially, the axial force generated in a pipeline due to restrained thermal expansion can be given by

$$P_0 = EA\alpha T \quad (1)$$

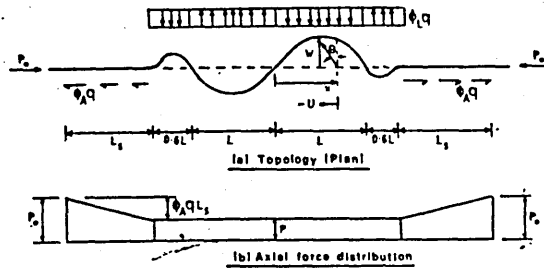


Figure 1 Typical lateral buckling mode

where  $AE$  is the axial rigidity of the pipe,  $\alpha$  is the respective coefficient of linear thermal expansion and  $T$  represents the temperature increase. Alternatively, the axial force generated due to restrained pressure expansion can be given by

$$P_0 = \frac{AE\alpha T}{L} (0.5 - \nu) \quad (2)$$

where  $A$  is the cross-sectional area,  $p$  is the increase in internal pressure,  $r$  and  $t$  are the pipe radius and wall thickness and  $\nu$  denotes the respective Poisson's ratio. Assuming pipeline response to be elastic and employing the appropriate equilibrium and compatibility relationships, then, for the mode illustrated in Figure 1, either Eq. (1) or Eq. (2) is equated with

$$P_0 = \frac{28.2EI}{L^2} + 1.608\phi_A qL \left[ 1 + 2.144 \times 10^{-4} \left( \frac{\phi_L^2}{\phi_A} \frac{AEqL^5}{EI^2} \right)^{1/2} - 1 \right] \quad (3)$$

where  $EI$  represents the flexural rigidity of the pipe,  $q$  is the submerged weight of the pipe per unit length,  $\phi_A$  and  $\phi_L$  are the fully mobilised axial and lateral friction coefficients respectively, and  $L$  is the variable buckling length (1), (2). Following the solution for  $L$ , associated expressions afford knowledge of the critical state and the ensuing post-buckling path. However, three major assumptions are involved; both the lateral and axial frictional resistance forces are taken to be fully mobilised throughout, linearised curvature is employed and physical imperfections are of symbolic form only. Whilst information on the latter pair of structural assumptions can be said to be readily available (3), (4) (gross sectional distortion as associated with laying operations (5) is not a factor here), little information is available with regard to the nature of the frictional forces involved.

The established modelling employs, for example, a resultant axial frictional force  $F_A$  given by

$$F_A = \phi_A q L_S \quad (4)$$

where  $L_S$  represents the slip length (6), (7) over which the axial frictional resistance force is taken to be developed; this feature is incorporated in Figure 1 and is more specifically detailed in Figure 2. The frictional force is denoted therein by  $f q$  per unit

length where parameter  $f$  is, in formal terms, some variable in  $x$  for  $0 \leq x \leq L_S$ .

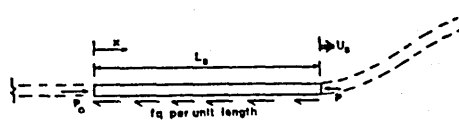


Figure 2 Slip length detail

Equilibrium affords the slip length frictional resistance force to be more formally given by

$$\int_0^{L_S} f q dx = P_0 - P \quad (5)$$

where  $P$  is the buckling force in the pipeline. It can be seen from Eq. (4) and Eq. (5) that the established modelling therefore assumes  $f$  to be a constant ( $\phi_A$ ) throughout the slip length, surely a simplification of some extent. It is with the behaviour of  $f$ , therefore, that this study is primarily concerned. Although there is data available on the nature of the frictional forces involved in the related field of rail track instability (6), (7), the corresponding data for submarine pipelines is very limited (8), (9), (10), (11), particularly with regard to the essentially hydrostatic environment appertaining to relatively deep-water pipelines.

It was therefore determined to undertake an experimental investigation into the nature of the frictional forces involved. Accepting that displacements of the pipeline can occur in arbitrary orientations due to the interaction of the axial and lateral displacement components denoted by  $u$  and  $v$  respectively, this feature being denoted by the angle  $\theta$  in Figure 1, then the experimental programme also sought to include this aspect of the problem. That is, values for  $f$  were to be determined for arbitrary force-displacement orientations. Further, three frictional interface configurations were to be considered as trenching will clearly affect buckling response. The configurations chosen were that with the pipe simply resting on the supporting medium ( $\bar{R}$ ), a basic entrenched topology ( $\bar{E}$ )

and an entrenched arrangement involving compaction of the supporting medium (F). Trenching constituted a quarter pipe diameter penetration of the supporting medium and compaction studies were primarily for qualitative purposes. Model or small scale tests were deemed to be the appropriate manner in which, at least initially, to proceed. Quasi-static behaviour is stipulated throughout.

**EXPERIMENTAL PROGRAMME**

The objective was, therefore, to obtain the frictional force-displacement loci for arbitrary orientations of disturbing force subject to a variety of frictional interface configurations. Of particular interest were the corresponding values of friction coefficient together with the magnitudes of the displacements at which these coefficients become effective. Sand was chosen as the supporting medium in view of North Sea conditions (12), and a sieve analysis enabled the requisite medium to fine sand to be identified; the sieve analysis results are given in Figure 3. Dry testing was employed for convenience, noting that a Coulomb medium was involved.

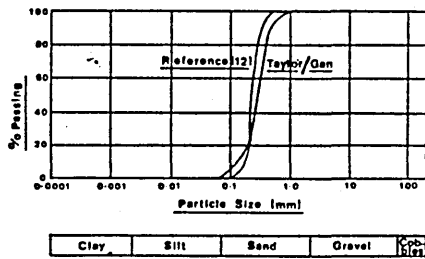
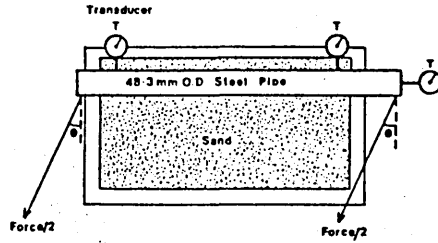


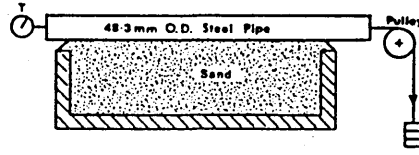
Figure 3 Sieve Analysis

The experimental topology is illustrated in Figures 4 and 5. A discrete element of pipeline was represented by a 1 m long steel tube of outer diameter 48.3 mm, wall thickness 3.2 mm and self-weight 34.92 N/m. The pipe possessed a 150 mm overhang with respect to the sand flume employed in order to prevent the pipe from digging into the sand when undergoing axial movement. Further equipment included transducers for measuring the longitudinal and transverse displacement components of the pipe, weights, wires and pulleys. The disturbing force was applied to the pipe in the horizontal plane at values of  $\theta$  ranging from zero through to  $\pi/2$  in increments of  $\pi/12$ . The three interface configurations were thereby considered in each of these seven orientations. The disturbing force was applied in the form of two equal component forces acting at the ends of the pipe except in the axial case studies in which the disturbing force was applied only to the respective end of the pipe. It was considered that a long pipeline on the sea bed would slide rather than roll along its longitudinal axis under lateral force. Hence the transducer readings were subject to the prevention of any significant rolling movement. The onset of full mobilisation for each of the twenty-one cases considered was taken as being the state at which displacement continued



Schematic (Plan) View of Pipe under Arbitrary/Lateral Force  
 $10^\circ \leq \theta < 90^\circ$

Figure 4



Schematic (Side) View of Pipe under Axial Force  $\theta = 90^\circ$

Figure 5

without any further increase in the respective disturbing force. Each test case was undertaken four times, average results being finally recorded.

**EXPERIMENTAL OBSERVATIONS AND RESULTS**

The results are given in Figures 6 to 12 in the form of resistance force-displacement loci. For the lateral ( $\theta = 0$ ) cases, a sand wedge was formed in front of the pipe as the force was applied, the wedge gradually growing in height. Full mobilisation was preceded by the pipe rising over the respective wedge.

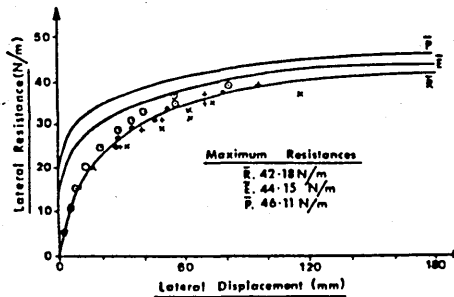


Figure 6 Force-Displacement Relationships -  $\theta = 0^\circ$

Both trenched cases initially required the pipe to rise out of the respective trench, and this effect is clearly displayed in Figure 6 by virtue of the appropriately stiffer force-displacement loci obtained. Further, the maximum resistance values obtained, also denoted in Figure 6, reflect the greater inertia possessed by the trenched cases. With regard to both of these characteristics, and as is to be anticipated given the respective degrees of sand compaction involved, the compacted case is to be particularly noted. Experimental data points, included in Figure 6 (R) for information, are suppressed for clarity in the remaining force-displacement figures. Axial movement was negligible throughout.

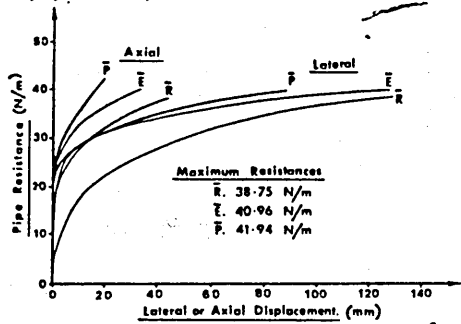


Figure 7 Force - Displacement Relationships  $\theta = 15^\circ$

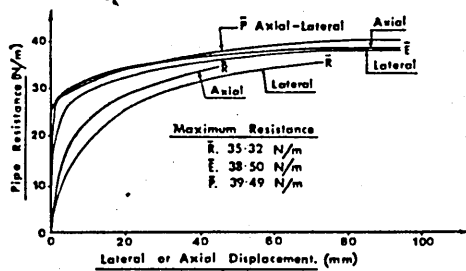


Figure 8 Force - Displacement Relationships  $\theta = 30^\circ$

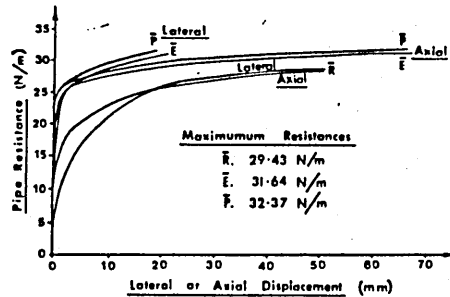


Figure 9 Force - Displacement Relationships  $\theta = 45^\circ$

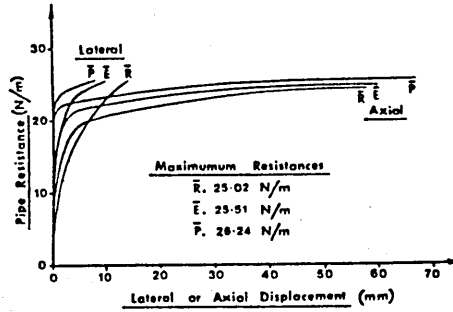


Figure 10 Force - Displacement Relationships  $\theta = 60^\circ$

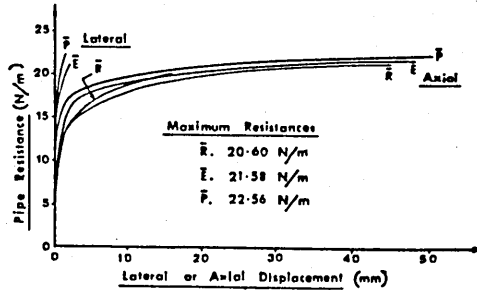


Figure 11 Force - Displacement Relationships  $\theta = 75^\circ$

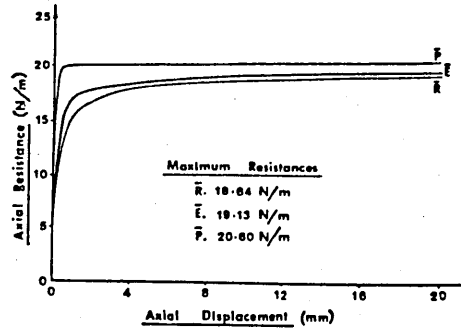


Figure 12 Force - Displacement Relationships  $\theta = 90^\circ$

For each of the remaining force orientation cases, illustrated in Figures 7 to 12, maximum frictional resistance was again attributable to the depressed

configuration. All but the axial case set generated a sand wedge, this being, relatively, of decreasing magnitude as  $\theta$  was increased. For the resting configuration, full lateral mobilisation signified maximum resistance for values of  $\theta < \pi/4$ , whilst full axial mobilisation signified maximum resistance for values of  $\theta > \pi/4$ . Simultaneous mobilisation occurred for  $\theta = \pi/4$ . The trenching effect caused simultaneous mobilisation to occur as precipitately as  $\theta = \pi/6$ , full axial mobilisation governing maximum resistance thereafter. For each interface configuration set, values of the maximum resistance force decreased as orientation was increased through to  $\theta = \pi/2$ , at which state lateral movement became negligible. In the cases governed by full axial mobilisation, the maximum resistance state occurred more abruptly with significantly less displacement.

Table 1 Friction Coefficients

$\phi$ (DEGREES)	FRICTION COEFFICIENT ( $\phi$ )		
	R	E	P
0	1.21	1.26	1.32
15	1.11	1.17	1.20
30	1.01	1.10	1.13
45	0.84	0.91	0.93
60	0.72	0.73	0.75
75	0.59	0.62	0.65
90	0.53	0.55	0.59

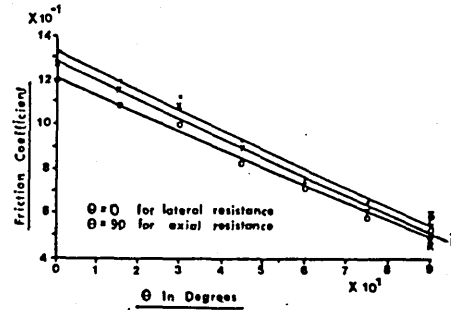
Table 1 summarizes the values of friction coefficient determined from the force-displacement loci. The resting configuration, involving a relatively small interface area, exhibits the lowest value of friction coefficient for each force orientation, whilst the compacted configuration, involving a higher angle of internal friction, exhibits the highest value of friction coefficient for each force orientation. The respective friction coefficients decrease as the disturbing force orientation  $\theta$  increases. The relationships between force orientation, interface configuration and friction coefficient are displayed by means of computer graphics in Figure 13, together with the appropriate linear and cubic interpolation curves. The equations of these least squares fit computer-generated formulae, written in terms of  $\theta$  and  $\phi$  the pertinent abscissa and ordinate parameters, take the form:

$$\begin{aligned} \phi &= 1.220 - 8.024 \times 10^{-3} \theta & (6) \\ \phi &= 1.291 - 8.571 \times 10^{-3} \theta & (7) \\ \phi &= 1.332 - 8.738 \times 10^{-3} \theta & (8) \end{aligned}$$

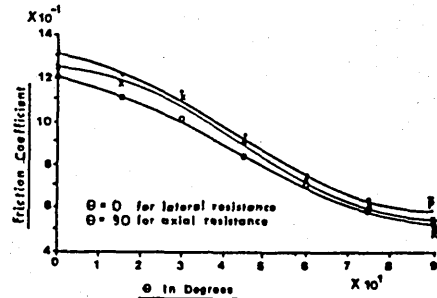
for the linear resting ( $\bar{R}$ ), entrenched ( $\bar{E}$ ) and compacted ( $\bar{P}$ ) cases respectively with:

$$\phi = 1.208 - 4.094 \times 10^{-3} \theta - 1.312 \times 10^{-4} \theta^2 + 1.030 \times 10^{-6} \theta^3 \quad (9)$$

$$\phi = 1.252 - 6.105 \times 10^{-3} \theta - 2.315 \times 10^{-4} \theta^2 + 1.682 \times 10^{-6} \theta^3 \quad (10)$$



a) Linear interpolation



b) Cubic interpolation

Figure 13 Graphs of Friction Coefficient against  $\theta$

$$\phi = 1.311 - 2.428 \times 10^{-3} \theta - 2.062 \times 10^{-4} \theta^2 + 1.061 \times 10^{-6} \theta^3 \quad (11)$$

for the cubic resting ( $\bar{R}$ ), entrenched ( $\bar{E}$ ) and compacted ( $\bar{P}$ ) cases respectively.

The maximum variation between interface configuration friction coefficient values for any of the orientations considered is of the order of 10%. The displacements corresponding to the attainment of fully mobilised resistance do not show great variation with interface configuration. These values range from 180 mm in the lateral orientation to 5 mm in the axial orientation. It is to be noted that the frictional resistance-displacement loci produced are of inelastic form.

Clearly, the foregoing data relates to model tests. In practice, submarine pipelines possess, typically, diameters in excess of 200 mm. With regard to this matter, the values for  $\phi_L$  ( $\theta = 0$ ) follow the trend set by Lyons (8) and Gulhati et al (9), indicating that values for  $\phi_L$  will decrease for larger diameter pipes in accordance with the surface roughness effect. References also indicate that the displacements appertaining to the onset of fully mobilised lateral frictional resistance decrease with an increase in pipe diameter (8), (9). In respect of these factors, suggested values for full scale pipelines are 1.0 for

the lateral friction coefficient and 30 mm for the displacement corresponding to full mobilisation. Validation of these values is detailed in the ensuing design consideration. Anand and Agarwal (10) give similar values for  $\phi_A$  ( $\theta = \pi/2$ ) with respect to model tests. Corresponding large scale tests result in  $\phi_A$  increasing with pipe diameter although the displacement corresponding to the onset of full mobilisation appears to be largely independent of scale effects. (Results for clay media (8), (11) are not considered to be applicable to the present study.) In view of these observations, therefore, indicated full scale values for the axial friction coefficient and the corresponding displacement for full mobilisation are 0.7 and 5 mm respectively. Further validation of these values will be given in the design discussions.

With regard to orientations  $0 < \theta < \pi/2$ , the interpolation loci given in Figure 13 afford useful insight with respect to the corresponding full scale values. The differing scaling factors involved in the lateral and axial orientations would indicate, for example, the necessity of a change in the gradient of the loci given in Figure 13(a). The effects of trenching have been demonstrated to lie primarily with the magnitude of the friction coefficient rather than with the corresponding fully mobilised displacements. Again, Figure 13 affords useful data from which full scale values could be deduced. Given the nature of the computations exemplified by Eq. (1) to Eq. (5), however, present concern lies with the rather more crucial lateral and axial cases, and the means by which the appropriate parametric values deduced in this experimental study can be incorporated within the design process appertaining to the possible in-service buckling of submarine pipelines.

#### DESIGN CONSIDERATIONS

The effects of the foregoing can be suitably demonstrated by considering the nature of the axial frictional resistance force generated through slip length  $L_S$ ; this force is common to both the vertical and lateral buckling modes. Recalling Figure 2 and Eq. (5), the initial requirement is to produce a mathematical function for parameter  $f$ . Noting Figure 12 and the foregoing discussion with regard to scaling effects, then a suitable inelastic force locus is given by

$$f = \frac{u \phi_A}{u \gamma} \quad (12)$$

where  $\gamma$  is some parameter to be fixed for any given (empirical) values of the respective friction coefficient  $\phi_A$  and the corresponding fully mobilised displacement  $u_s$ . Alternatively,  $\gamma$  can be related through the mathematical modelling (8), (13) of basic parameters such as the angle of internal friction of the supporting medium.

The suggested full scale values  $\phi_A = 0.7$  and  $u_s = 5$  mm are therefore to be incorporated into Eq. (12), with regard to  $f$  and  $u$  respectively, in order to evaluate  $\gamma$ . However, use of Eq. (12) demands an approximation of the form

$$f \Big|_{u=5\text{mm}} = 0.695 \quad (13)$$

be actually employed, involving a modest 0.7% error, in order that asymptotic behaviour be observed with  $f$  never exceeding  $\phi_A$ . Employing Eq. (13) with Eq. (12) affords, upon manipulation

$$f = 0.7 \left( 1 - \frac{1}{28u + 1} \right) \quad (14)$$

where  $u$  is in mm units. Eq. (14) is thereby plotted as a design curve in non-dimensional form in Figure 14, together with the experimental locus previously given in Figure 12 (R). The correlation is clearly depicted, noting that the small scale values for  $\phi_A$  and  $u_s$  are 0.53 and 20 mm respectively.

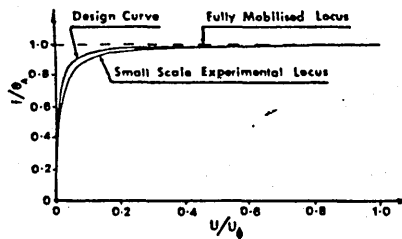


Figure 14 Generalised Axial Frictional Characteristics

Employing Eq. (5), the revised modelling then takes the form

$$P_o - P = \int_0^{L_S} 0.7q \left( 1 - \frac{1}{28u + 1} \right) dx \quad (15)$$

It is necessary to assume an axial displacement function for this non-linear force. Utilising a cubic function, then

$$u = a_0 + a_1 x + a_2 x^2 + a_3 x^3 \quad (16)$$

where  $a_1, 0 < i < 3$ , represents some unspecified coefficient. Noting the topology of Figure 2, the boundary conditions take the form (1), (2), (7)

$$\left. \begin{aligned} u \Big|_0 &= 0 \\ \frac{du}{dx} \Big|_0 &= 0 \\ \frac{d^2u}{dx^2} \Big|_0 &= 0 \\ u \Big|_{L_S} &= u_s \end{aligned} \right\} \text{(transversality)} \quad (17)$$

Upon substitution, Eq. (16) thus becomes

$$u = \frac{u_s x^3}{L_S^3} \quad (18)$$

Eq. (15) can now be expressed in the form

$$\frac{P_A}{0.7qL_S} = \frac{P_o - P}{0.7qL_S} \quad \text{(continued over)}$$

$$= 1 - \frac{0.05489}{u_s^{1/3}} \left[ \ln \left( \frac{1+9.22087u_s^{2/3} + 6.07318u_s^{1/3}}{1+9.22087u_s^{2/3} + 3.03659u_s^{1/3}} \right) + 3.46410 \left[ \tan^{-1} (3.50635u_s^{1/3} - 3^{-4}) - \tan^{-1} (-3^{-4}) \right] \right] \quad (19)$$

with implied millimetre units. This compares with the established simplified modelling, as denoted by Eq. (4),

$$\frac{P_0 - P}{0.7qL_s} = 1 \quad (20)$$

Eq. (19) can now be incorporated into the appropriate set of analytical expressions in which unknown displacement  $u_s$  already exists by means of compatibility expressions. Further, this equation relates total frictional resistance  $(P_0 - P)$  to overall movement of the slip length ( $u_s$ ); this is graphically represented in Figure 15. This improvement in modelling is important in that the employment of sub-fully mobilised frictional resistance forces is necessary if accurate post-buckling behaviour is to be determined for vanishingly small displacements (14), (15).

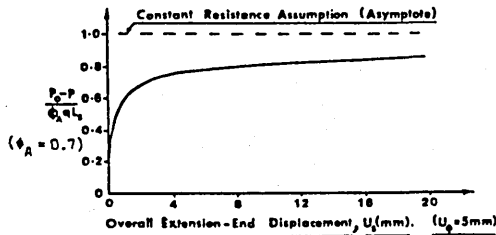


Figure 15 Axial Force-Displacement Characteristics

Further, the established simplified modelling can be seen to overestimate the frictional resistance and thereby resistance to buckling; this is a crucial design factor.

An equivalent procedure can be adopted for the lateral frictional behaviour. Noting Eq. (12), a suitable inelastic resistance force locus is given by

$$f = \frac{wL}{w + \gamma} \quad (21)$$

Incorporation of the suggested full scale values  $\phi_L = 1.0$  and  $w_\phi = 30$  mm with regard to  $f$  and  $w$  respectively is achieved employing the approximation

$$f \Big|_{w=30\text{mm}} = 0.94 \quad (22)$$

in order to prevent  $f$  exceeding the appropriate fully mobilised value ( $\phi_L$ ). Employing Eq. (22) with Eq. (21) to evaluate  $\gamma$  affords, upon manipulation

$$f = 1 - \frac{1}{0.52w+1} \quad (23)$$

where  $w$  is in mm units. Eq. (23) is thereby plotted as a design curve in non-dimensional form in Figure 16,

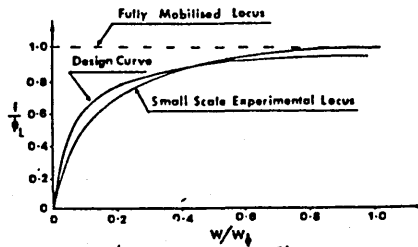


Figure 16 Generalised Lateral Frictional Characteristics

together with the experimental locus previously given in Figure 6 (R), subject to the small scale values for  $\phi_L$  and  $w_\phi$  of 1.21 and 180 mm respectively. Again, the quality of correlation is to be noted. Eq. (23) is now capable of absorption into the corresponding analytical expressions (1), (2). Further, enhanced structural modelling could employ the remaining orientation and interface frictional characteristics deduced in this study though such modelling should, perhaps, also include finite curvature and physical imperfection studies (3), (4). Preliminary buckling design computations have been undertaken employing the foregoing findings. Figure 17 typifies the results obtained to date with regard to the axial slip length ratios appertaining to the revised and established fully mobilised friction models. The latter is shown to underestimate the length of slip by up to 30%.

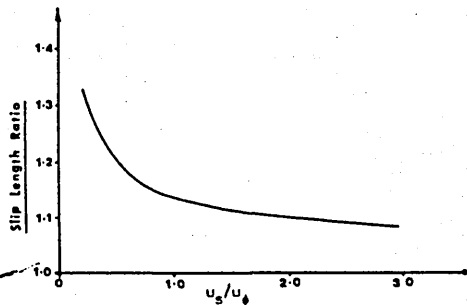


Figure 17 Axial Deformation Characteristics - Preliminary Findings

Finally, notwithstanding the benefits of generalisation afforded by mathematical modelling, already exemplified in related areas of study (8), (13), some thought should perhaps now be given to the undertaking of appropriate large scale tests.

#### CONCLUSIONS

In all, some eighty-four individual tests have been undertaken and the appropriate resistance force-displacement loci produced. In particular, information on friction coefficients has been determined for a variety of force-displacement orientations and interface configurations; appropriate interpolation formulae have been produced. Full scale values for the primary friction coefficients, that is for the axial and lateral cases, have been deduced upon the basis of the model tests. The displacements at which these frictional resistance forces become fully mobilised have been similarly identified. A semi-empirical formula has thereby been produced for use in design practice and suggestions made regarding possible further studies. It should perhaps be noted that extrapolation of the geotechnical findings contained herein for use with dynamic systems would a priori require careful consideration to be made of the manner in which the respective interface movements occur.

#### ACKNOWLEDGEMENT

The authors wish to thank Professor A C Walker, Surrey University, for advice afforded with regard to the foregoing study.

#### REFERENCES

1. Hobbs R E, 'Pipeline Buckling Caused by Axial Loads', Journal of Constructional Steel Research, Vol. 1, No. 2, January 1981, 2-10.
2. Taylor N and Gan A B, 'Regarding the Buckling of Pipelines Subject to Axial Loading', Journal of Constructional Steel Research, Vol. 4, No. 1, 1984, 45-50.
3. Taylor N and Hirst P B, 'Regarding Flexural Curvature', Proc. Instn. Civ. Engrs., Part 2, 77, 1984, 399-400.
4. Croll J G A and Walker A C, Elements of Structural Stability, Macmillan, 1972.
5. Palmer A C and Martin J H, 'Buckle Propagation in Submarine Pipelines', Nature, 254, March 1975, 46-48.
6. Kerr A D, 'On the Stability of the Railroad Track in the Vertical Plane', Rail International, 2, February 1974.
7. Kerr A D, 'Analysis of Thermal Track Buckling in the Lateral Plane', Acta Mechanica, 30, 1978, 17-50.
8. Lyons C G, 'Soil Resistance to Lateral Sliding of Marine Pipelines', 5th Offshore Technology Conference, OTC 1876, Vol. II, 1973, 479-484.
9. Gulhati S K, Venkatapparao G and Varadarajan A, 'Positional Stability of Submarine Pipelines', I.G.S. Conference on Geotechnical Engineering, Vol. 1, 1978, 430-434.
10. Anand S and Agarwal S L, 'Field and Laboratory Studies for Evaluating Submarine Pipeline Frictional Resistance', Transactions of the ASME, Journal of Energy Resources Technology, Vol. 103, September 1981, 250-254.
11. Agarwal S L and Malhotra A K, 'Frictional Resistance for Submarine Pipeline in Soft Clays', I.G.S. Conference on Geotechnical Engineering, Vol. 1, 1978, 373-379.
12. Bjerrum L, 'Geotechnical Problems Involved in Foundations of Structures in the North Sea', Geotechnique, 23, No. 3, 1973, 319-358.
13. Keral K, 'Lateral Stability of Submarine Pipelines', 9th Offshore Technology Conference, OTC 2967, Vol. IV, 1977, 71-78.
14. Kerr A D, 'On Thermal Buckling of Straight Railroad Tracks and the Effect of Track Length on the Track Response', Rail International, 9, September 1979, 759-768.
15. Kerr A D, 'The Effect of Lateral Resistance on Track Buckling Analyses', Rail International, 1, January 1976, 30-38.

## Refined Modelling for the Lateral Buckling of Submarine Pipelines

Neil Taylor and Aik Ben Gan

Department of Civil Engineering, Sheffield City Polytechnic,  
Pond Street, Sheffield S1 1WB, UK

(Received 00 ?????, 1985; final version accepted (X) ?????, 1985)

### ABSTRACT

*In-service buckling of submarine pipelines can occur due to the institution of axial compressive forces caused by the constrained expansions set up by thermal and internal pressure actions. An integral part of this area of study involves the resistance to movement provided by the supporting medium. Previous attempts at modelling the appropriate behaviour have employed fully mobilised friction forces. Herein presented is a set of analyses which incorporate consistent deformation-dependent resistance forces. This feature enables a more rational interpretation of submarine pipeline buckling behaviour to be established.*

### NOTATION

$A$	Cross-sectional area.
$a_i$	Unprescribed coefficient.
$C_x$	Axial compression of pipe element.
$E$	Young's modulus.
$F$	Shear force.
$f_A$	Axial friction parameter.
$f_L$	Lateral friction parameter.
$I$	Second moment of area of cross-section.
$k$	Constant of integration.
$k_1-k_6$	Constants in Table 1.
$L, L_1$	Buckle lengths.

$L_s$	Slip length.
$M$	Bending moment.
$P$	Buckling force.
$P_0$	Prebuckling axial force.
$P_s$	Post-buckling axial force at state $S$ .
$q$	Submerged weight of pipeline per unit length.
$T$	Temperature rise.
$T_c$	Critical temperature rise.
$T_{\min}$	Minimum safe temperature rise.
$u$	Axial deformation of the pipe.
$u_s$	Resultant longitudinal movement at buckle/slip length interface.
$u_\phi$	Fully mobilised axial displacement.
$w$	Lateral deformation of the pipe.
$w_m$	Maximum amplitude of the buckled pipe.
$w_{mm}$	Buckle amplitude at $T_{\min}$ .
$w_{ms}$	Post-buckling amplitude at state $S$ .
$w_\phi$	Fully mobilised lateral displacement.
$x$	Spatial co-ordinate.
$\alpha$	Coefficient of linear thermal expansion.
$\phi_A$	Axial friction coefficient.
$\phi_L$	Lateral friction coefficient.

## 1 INTRODUCTION

The circumstances concerning the means by which the in-service buckling of submarine pipelines can occur have been discussed at length elsewhere.<sup>1-4</sup> Analyses have been primarily oriented about thermal action with oil and gas temperatures potentially ranging up to 100°C above that of the water environment. That is, a uniform temperature increase,  $T$ , in a perfectly straight submarine pipeline will create an axial compression force due to constrained thermal expansion. Within the elastic range of the pipeline response, this force can be represented by

$$P_0 = AE\alpha T \quad (1)$$

where  $AE$  is the axial rigidity of the pipe and  $\alpha$  is the respective coefficient of linear thermal expansion. Should buckling occur, part of the constrained thermal expansion is released in a buckled region which, taken

*Lateral buckling of submarine pipelines*

together with the friction resistance of the sea-bed/pipeline interface, results in a reduction in the axial compression to some buckling force  $P$ .

Studies to date have employed the simplifying non-conservative assumption that the friction forces are fully mobilised throughout. Further, this precludes the ability to define a critical temperature rise at which idealised axial-flexural bifurcation occurs. In the following analyses a rational modelling of the deformation-dependent friction

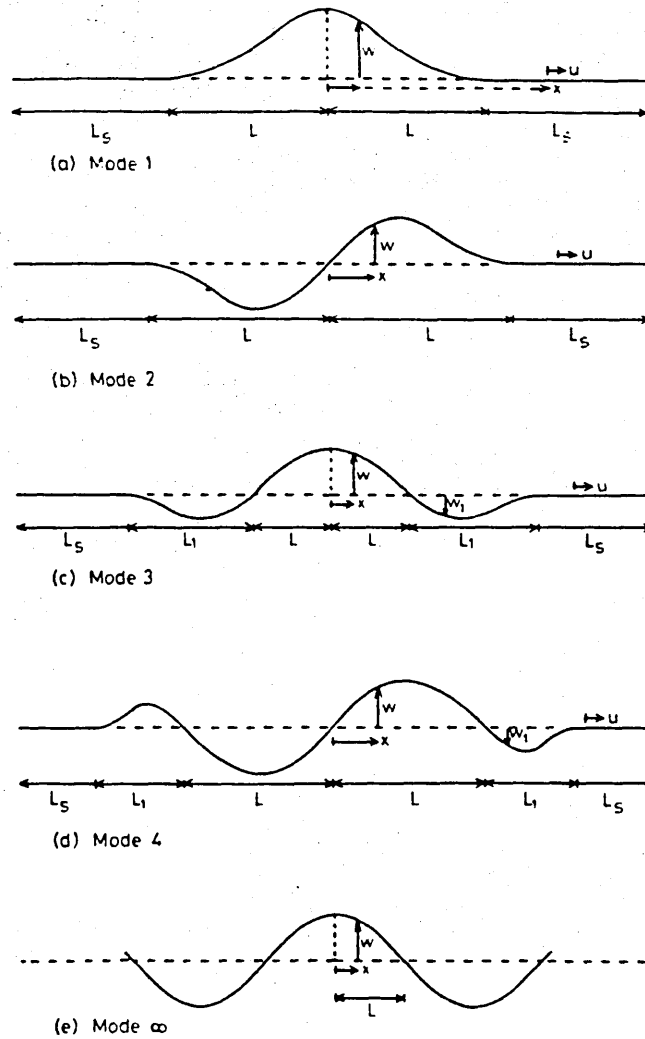


**Fig. 1.** Lateral buckling mode topologies.

forces is undertaken employing recently established axial and lateral friction response loci.<sup>4</sup> As a result, a more logical interpretation of the submarine pipeline buckling problem is made available. In addition, this will assist in the development of non-linear analyses involving physical imperfections.

The five established lateral buckling modes which relate to snaking movements across the sea bed are illustrated in Fig. 1.<sup>1,3</sup> Attention is restricted to these lateral modes given the less critical nature of vertical buckling except in cases where trenching is involved.<sup>1,3</sup> Axial and lateral deformations are denoted by  $u$  and  $w$  respectively. The appropriate buckling lengths are denoted by  $L$  and  $L_1$  whilst  $L_s$  represents the slip length. Axial friction resistance is generated through the slip length whilst lateral friction resistance occurs through the buckling lengths. To date, these friction forces have been assumed to be fully mobilised throughout their respective regions.<sup>1-3</sup> Material behaviour is taken to be elastic; gross sectional distortion as associated with laying operations<sup>5</sup> is not a factor here.

## 2 GEOTECHNICAL FACTORS

Recent geotechnical experimentation<sup>4</sup> with respect to North Sea conditions<sup>6</sup> has provided information relating to the nature of the deformation-dependent friction force behaviour with regard to typical submarine pipeline parameters. Based upon these findings, refined friction force characteristics are depicted in Figs 2 and 3 for axial ( $u$ ) and lateral ( $w$ ) pipeline movements respectively. The appropriate fully mobilised axial and lateral friction coefficients are given by  $\phi_A$  and  $\phi_L$ . The movements corresponding to the attainment of full mobilisation are denoted by  $u_\phi$  and  $w_\phi$ . The friction force parameters  $f_A$  and  $f_L$ , discussed in detail in the ensuing analyses, serve to complete the requisite loci definitions. Suggested values for the parameters  $\phi_A$ ,  $u_\phi$ ,  $\phi_L$  and  $w_\phi$  for submarine pipelines take the form<sup>4,7-9</sup>

$$\left. \begin{array}{l} \phi_A = 0.7 \\ u_\phi = 5 \text{ mm} \\ \phi_L = 1.0 \\ w_\phi = 30 \text{ mm} \end{array} \right\} \quad (2)$$

Lateral buckling of submarine pipelines

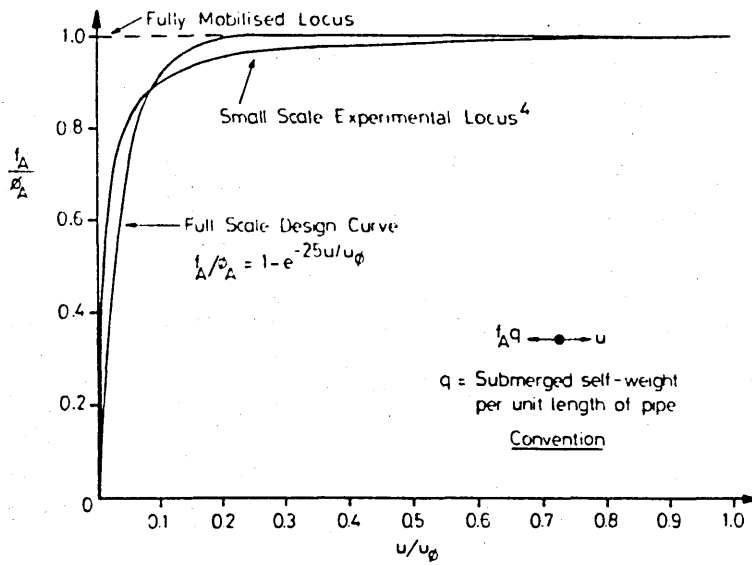


Fig. 2. Generalised axial friction characteristics.

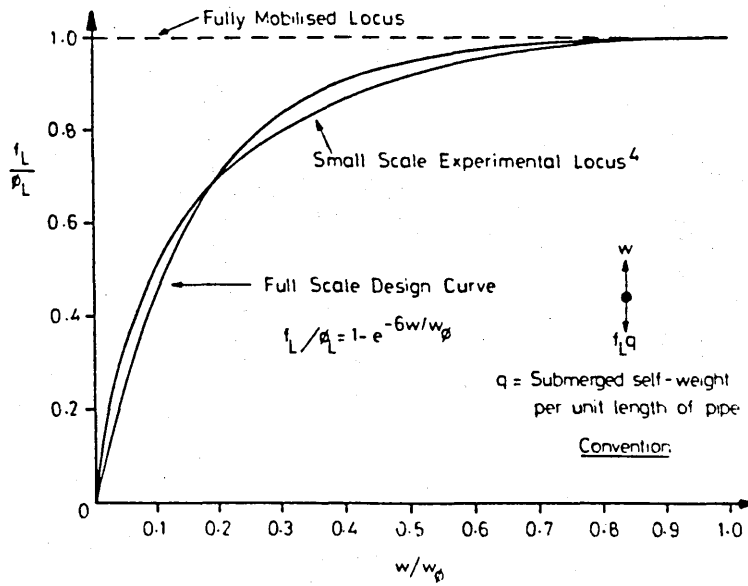


Fig. 3. Generalised lateral friction characteristics.

and the design curves given in Figs 2 and 3 thereby employ

$$f_A/\phi_A = 1 - e^{-25u/u_\phi} \quad (3)$$

and

$$f_L/\phi_L = 1 - e^{-6w/w_\phi} \quad (4)$$

noting the appropriate conventions given in the figures. These expressions give good agreement with the designated non-dimensionalised experimental curves and, in addition, accord with the appropriate fully mobilised asymptotes with  $f_A/\phi_A \cong f_L/\phi_L \cong 1$  at  $u/u_\phi = 1$  and  $w/w_\phi = 1$  respectively. It is to be noted that eqns (3) and (4) offer superior modelling characteristics to their precursors given elsewhere.<sup>4</sup>

### 3 ESSENTIAL STRUCTURAL RELATIONSHIPS

Prior to the incorporation of eqns (3) and (4) within the proposed analyses, it is useful to list all the essential structural relationships, based on fully mobilised friction resistance assumptions, obtained from previous submarine pipeline<sup>1-3</sup> and related rail track<sup>10</sup> studies. Noting the constants given in Table 1, the buckling force set up in the  $L, L_1$  regions is given by

$$P = k_1 \frac{EI}{L^2} \quad (5)$$

**TABLE 1**  
Constants for Lateral Buckling Modes

Mode	$k_1$ (eqn (5))	$k_2$ (eqn (6))	$k_3$ (eqn (7))	$k_4$ (eqn (7))	$k_5$ (eqn (8))	$k_6$ (eqn (8))
1	20.19	$3.8512 \times 10^{-2}$	1.0	$1.0225 \times 10^{-3}$	1.0	$2.045 \times 10^{-3}$
2	$4\pi^2$	$5.532 \times 10^{-3}$	1.0	$8.715 \times 10^{-5}$	1.0	$1.743 \times 10^{-4}$
3	8.515	0.165 12	2.588	$1.7878 \times 10^{-2}$	2.588	$5.3397 \times 10^{-3}$
4	28.20	$1.048 \times 10^{-2}$	1.608	$2.7716 \times 10^{-4}$	1.608	$2.143 \times 10^{-4}$
$\infty$	$\pi^2$	$7.1192 \times 10^{-2}$	NA	NA	see eqn (9)	

NA = not applicable

*Lateral buckling of submarine pipelines*

where  $EI$  is the flexural rigidity of the pipe. The maximum amplitude of the buckle takes the form

$$w_m = k_2 \frac{\phi_L q L^4}{EI} \quad (6)$$

where  $q$  is the submerged self-weight of the pipe per unit length. The resultant longitudinal movement at each buckle/slip length interface is given by

$$u_s = k_3 \frac{(P_0 - P)L}{AE} - k_4 \left( \frac{\phi_L q}{EI} \right)^2 L^7 \quad (7)$$

whilst the relationship between the pre-buckling force  $P_0$ , given by eqn (1), and the buckling force  $P$  for modes 1 to 4 is derived to be

$$P_0 = P + k_5 \phi_A q L \left\{ \left[ 1 + k_6 \frac{AE}{\phi_A q} \left( \frac{\phi_L q}{EI} \right)^2 L^5 \right]^{1/2} - 1 \right\} \quad (8)$$

For mode  $\infty$ , eqn (8) is replaced by

$$P_0 = P + 3.0112 \times 10^{-3} AE \left( \frac{\phi_L q}{EI} \right)^2 L^6 \quad (9)$$

As a corollary, it is instructive to assess the degree of full mobilisation actually involved in the above submarine pipeline studies.<sup>1-3</sup> Noting the values for  $\phi_A$ ,  $\phi_L$ ,  $u_\phi$  and  $w_\phi$  given in eqn (2), then Table 2 affords the

**TABLE 2**  
Percentage of Region Subjected to Fully Mobilised Resistance Employing the Fully Mobilised Friction Force Criterion

<i>Mode</i>	<i>% of buckle length L wherein <math>w \geq w_\phi</math> (<math>w_\phi = 30 \text{ mm}</math>)</i>	<i>% of slip length L, wherein <math>u \geq u_\phi</math> (<math>u_\phi = 5 \text{ mm}</math>)</i>
1	85.5	76.6
2	88.0	75.7
3	98.5	74.1
4	98.0	73.7
$\infty$	95.8	NA

NA = not applicable

appropriate information with regard to the state corresponding to the respective minimum safe temperature rise.<sup>1,3</sup> The most obvious deduction is that, employing the fully mobilised criterion, the axial friction modelling is relatively cruder than the lateral friction modelling throughout. Initially, therefore, it is proposed to re-define the axial friction force resistance employing the locus given in Fig. 2 as designated by eqn (3).

#### 4 MODE 1 ANALYSIS: Non-Linear Axial Resistance in Conjunction with Fully Mobilised Lateral Resistance

The essential features of mode 1, with regard to established studies,<sup>1-3</sup> are shown in Figs 4(a) and (b). The former figure details the topology whilst the latter depicts the axial force distribution within the pipe. Figures 4(c) and (d) depict the corresponding revised topology and axial force distribution.

Noting the non-linear axial force distributions in the slip length regions, the nature of  $f_A$  is detailed in Fig. 5(a) which illustrates a typical element of pipe within the slip length region ( $x > L$ ). Axial compression is denoted by  $C_x$ . Considering the longitudinal equilibrium of the elemental pipe  $\delta x$ , then

$$\delta C_x = f_A q \delta x \quad (10)$$

so that

$$\frac{dC_x}{dx} = f_A q \quad (11)$$

Incorporating the appropriate thermal effect detailed in Fig. 5(b), compatibility gives

$$-u + \int_x^{L_s+L} \left( \frac{C_x}{AE} \right) dx = \alpha T(L_s + L - x) \quad (12)$$

Differentiating with respect to  $x$  gives

$$C_x = AE \left( \alpha T - \frac{du}{dx} \right) \quad (13)$$

Lateral buckling of submarine pipelines

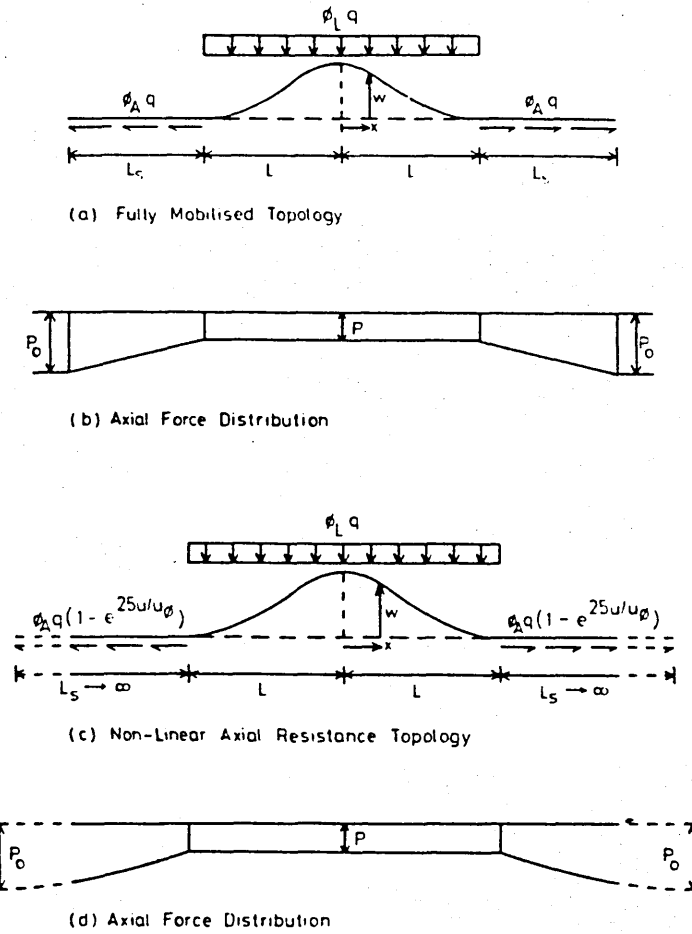


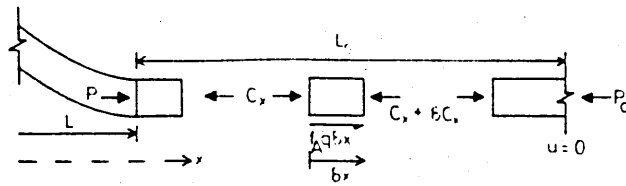
Fig. 4. Fully mobilised and revised buckling topologies.

Substituting eqn (13) into eqn (11) yields the field equation within the slip length region

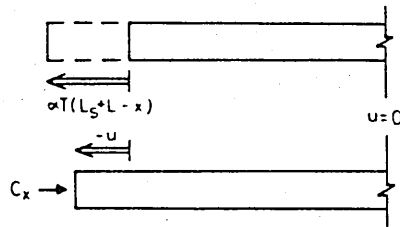
$$AE \frac{d^2 u}{dx^2} = -f_A q \quad L \leq x \leq L + L_s \quad (14)$$

The associated slip length boundary conditions take the form

$$\lim_{x \rightarrow \pm \infty} [u, du/dx] = 0 \quad (15)$$



(a) Equilibrium



(b) Compatibility

**Fig. 5.** Slip length detail.

and

$$\left. \frac{du}{dx} \right|_L = \frac{(P_0 - P)}{AE} \quad (16)$$

Equation (15) can be considered to be a regularity condition which assists in precluding the prejudicial requirement of assuming some function  $u = f(x)$ .

Combining eqns (3) and (14) affords the non-linear slip length field equation

$$AE \frac{d^2 u}{dx^2} = -\phi_A q (1 - e^{2Su/\mu\phi}) \quad (17)$$

noting that the change of sign of the exponent is due to  $u$  and  $f_A$  being co-oriented within the slip length region—note that Fig. 5 employs a different convention from Fig. 2. Employing the identity

$$\frac{2d^2 u}{dx^2} = \frac{d}{du} \left( \left[ \frac{du}{dx} \right]^2 \right) \quad (18)$$

then eqn (17) becomes

$$\left(\frac{du}{dx}\right)^2 = \frac{2\phi_{\Lambda}q}{AE} \left(\frac{e^{25u/\mu\phi}}{5} - u\right) + k \quad (19)$$

where  $k$  is a constant of integration.

Substituting eqn (15) into eqn (19) for the evaluation of  $k$  gives

$$\frac{du}{dx} = \left[ \frac{2\phi_{\Lambda}q}{AE} \left(\frac{e^{25u/\mu\phi} - 1}{5} - u\right) \right]^{1/2} \quad (20)$$

Equating this expression with the boundary condition given in eqn (16), and noting  $u|_L = u_s$ , yields

$$(P_0 - P) = \left[ 2\phi_{\Lambda}qAE \left(\frac{e^{25u_s/\mu\phi} - 1}{5} - u_s\right) \right]^{1/2} \quad (21)$$

Accepting that eqn (7) remains valid in view of the fact that the lateral friction force is fully mobilised, then, noting the values given in Table 1,

$$u_s = \frac{(P_0 - P)L}{AE} - 1.023 \times 10^{-3} \left(\frac{\phi_L q}{EI}\right)^2 L^7 \quad (22)$$

Solutions for  $(P_0 - P)$  and  $u_s$  are thereby obtained in terms of discrete values of  $L$  employing a computerised non-linear iterative algorithm involving eqns (21) and (22). Again noting that eqns (5) and (6) together with the respective values given in Table 1 remain valid, then locus 1, depicted in Fig. 6, is produced by substituting the results for  $(P_0 - P)$  into eqns (1), (5) and (6). For this action-response locus, the external pipe diameter was taken to be 650 mm, the wall thickness 15 mm, the submerged self-weight  $3.8 \text{ kN m}^{-1}$ , the Young's modulus  $206 \text{ kN mm}^{-2}$  and the coefficient of linear thermal expansion  $11 \times 10^{-6} \text{ }^\circ\text{C}^{-1}$ ; the data given in eqn (2) complete the requisite numerical definition. The dashed portions of the locus denote computations involving buckling slopes in excess of 0.1 radians. Prior to discussing the implications of this analysis, it is proposed to briefly consider the equivalent analyses of the remaining lateral modes.

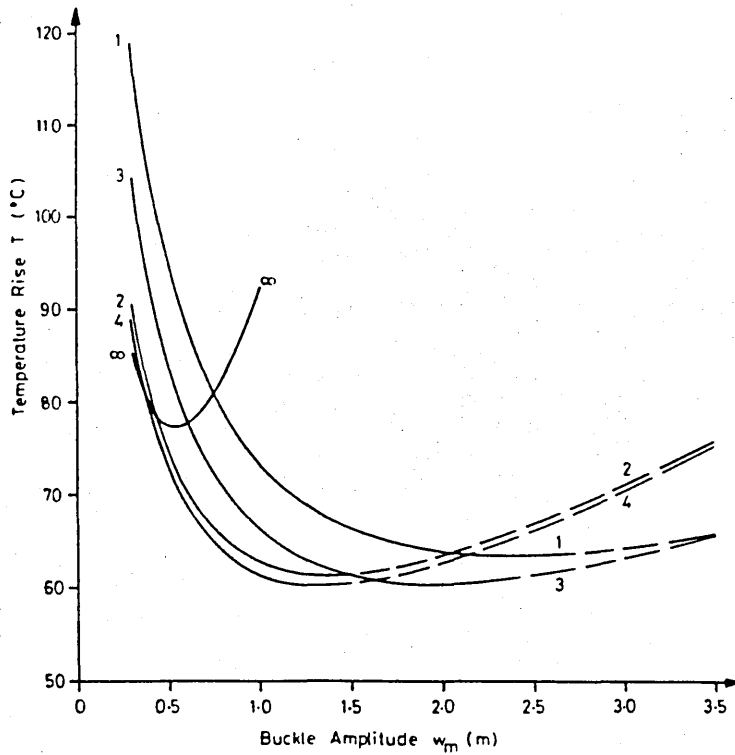


Fig. 6. Comparison of lateral buckling modes.

### 5 MODES 2, 3 AND 4: Non-Linear Axial Resistance in Conjunction with Fully Mobilised Lateral Resistance

Equations (10) through (21) remain valid for these three modes. Equation (7) is again employed in conjunction with Table 1 to generate an equivalent expression to that of eqn (22). The analysis of mode  $\infty$ , in which there is no generation of axial friction force, remains as previously.<sup>1,3</sup> The appropriate behavioural loci are depicted in Fig. 6.

### 6 FURTHER CONSIDERATIONS

The action-response loci for modes 1, 2, 3 and 4 in Fig. 6 differ only slightly from their fully mobilised equivalents—mode  $\infty$  remains

unchanged. For example, with regard to mode 1, the minimum safe temperature rise ( $T_{\min}$ ) is reduced by only  $0.03^{\circ}\text{C}$  employing variable axial resistance. This should not detract from the study, however, in as much as the effect of employing the simplifying fully mobilised assumption has been shown to be reasonable from the findings of a rational model. Further, the ordering of the modes in terms of their respective minimum safe temperature rises is also shown to remain unchanged.<sup>3</sup>

It should be noted that the solutions for the respective  $w = f(x)$  remain as previously.<sup>1,3</sup> As illustrated in Fig. 6, the behavioural loci approach the thermal axis asymptotically; this is a consequence of assuming the lateral friction resistance to be fully mobilised even for vanishingly small displacements.<sup>11</sup> In order to define a critical temperature rise, therefore, it is necessary to model the lateral friction force in a rational manner. Further, this will serve to provide a fully rational modelling of the buckling problem.

#### 7 MODE 1: Non-Linear Axial and Lateral Friction Resistances

In order to establish a critical temperature rise,  $T_c$ , it is necessary to incorporate the lateral friction-response locus given in Fig. 3 and designated by eqn (4). The appropriate topology and axial force distributions are depicted in Figs 4(c) and (d) except that the lateral resistance,  $\phi_L q$ , is now replaced by  $\phi_L q (1 - e^{-6w/w_0})$ .

The flexural parameters are in accordance with the detail illustrated in Fig. 7. Bending moment and shear force are denoted by  $M$  and  $F$  respectively. Applying transverse and rotational equilibrium, noting the self-compensating flexural end-shortening effect, affords

$$\frac{dF}{dx} = f_L q \quad (23)$$

and

$$-F = \left( \frac{dM}{dx} + P \frac{dw}{dx} \right) \quad (24)$$

Further, incorporating the appropriate moment-curvature expression,<sup>12</sup>

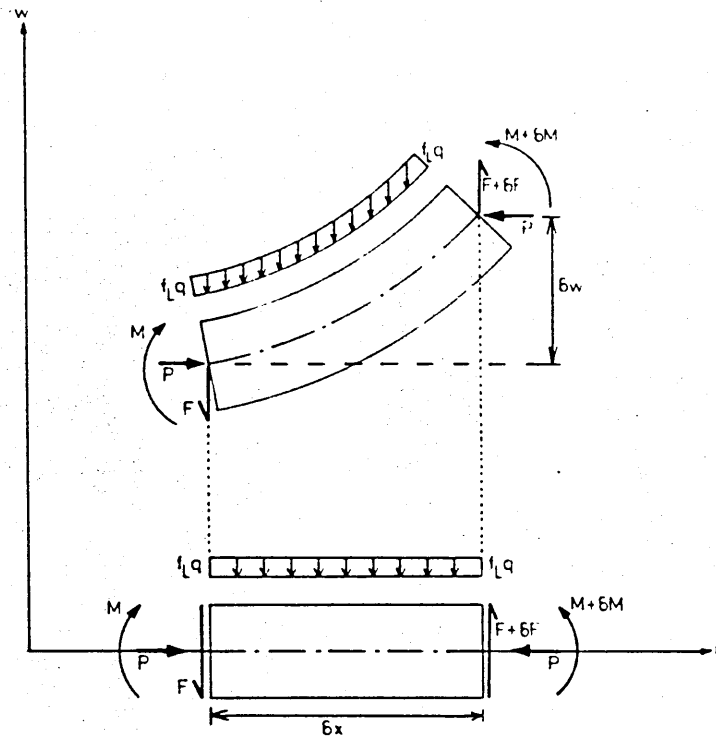


Fig. 7. Flexural topology.

differentiation of eqn (24) and combining with eqn (23) yields the linearised field equation

$$EI \frac{d^4 w}{dx^4} + P \frac{d^2 w}{dx^2} = -f_L q \quad (25)$$

Noting eqn (4), eqn (25) can be rewritten

$$EI \frac{d^4 w}{dx^4} + P \frac{d^2 w}{dx^2} = -\phi_L q (1 - e^{-6w/w_\phi}) \quad (26)$$

The complexity of this field equation prevents a closed form solution being obtained. A boundary collocation procedure is therefore instituted employing the assumed series

$$\frac{w}{w_m} = \sum_{i=0}^{i=4} a_i \left(\frac{x}{L}\right)^{2i} \quad 0 \leq x \leq L \quad (27)$$

*Lateral buckling of submarine pipelines*

where  $a_i$  denotes a typical unprescribed coefficient. The symmetry of the buckling mode is incorporated directly in eqn (27). Accepting that relationships are sought between  $P$ ,  $L$  and  $w_m$  as indicated by eqns (5) and (6) with regard to the previous study, then a seven point collocation procedure is required. Employing the following five conditions and identities

$$\left. \begin{aligned} w \Big|_L &= 0 \\ \frac{dw}{dx} \Big|_L &= 0 \\ \frac{d^2w}{dx^2} \Big|_L &= 0 \text{ (transversality}^{10}\text{)} \\ w \Big|_0 &= w_m \\ \left( EI \frac{d^4w}{dx^4} + P \frac{d^2w}{dx^2} \right) \Big|_L &= -\phi_L q (1 - e^0) = 0 \end{aligned} \right\} \quad (28)$$

the respective coefficients of  $a_i$  can be defined, such that

$$w = w_m \left[ 1 - \frac{24}{7} \left( \frac{x}{L} \right)^2 + \frac{30}{7} \left( \frac{x}{L} \right)^4 - \frac{16}{7} \left( \frac{x}{L} \right)^6 + \frac{3}{7} \left( \frac{x}{L} \right)^8 \right] \quad (29)$$

Further, equilibrium demands that the shear force at the ends of the buckle length takes the form

$$-EI \frac{d^3w}{dx^3} \Big|_L = \phi_L q \int_0^L (1 - e^{-6w/w\phi}) dx \quad (30)$$

which gives

$$w_m = \frac{7\phi_L q L^3}{192EI} \int_0^L (1 - e^{-6w/w\phi}) dx \quad (31)$$

and that the central bending moment affords

$$EI \frac{d^2 w}{dx^2} \Big|_0 = \phi_1 q L \int_0^L (1 - e^{-6w/w\phi}) dx - \phi_1 q \int_0^L (1 - e^{-6w/w\phi}) x dx - P w_m \quad (32)$$

resulting in, noting eqn (31),

$$P = \frac{192EI}{7L^2} \left[ \frac{5}{4} \frac{\int_0^L (1 - e^{-6w/w\phi}) x dx}{L \int_0^L (1 - e^{-6w/w\phi}) dx} \right] \quad (33)$$

Slip length considerations are incorporated as previously employing eqn (21). The matching compatibility condition at the ends of the buckle length takes the form<sup>10</sup>

$$u|_L = u_s = \frac{(P_0 - P)L}{AE} - \frac{1}{2} \int_0^L \left( \frac{dw}{dx} \right)^2 dx \quad (34)$$

which yields, noting eqns (29) and (31),

$$u_s = \frac{(P_0 - P)L}{AE} - 9.102 \times 10^{-4} L^5 \left( \frac{\phi_1 q}{EI} \right)^2 \left[ \int_0^L (1 - e^{-6w/w\phi}) dx \right]^2 \quad (35)$$

This represents the rational equivalent of the fully mobilised expression given in eqn (22). The solution is as previously; eqns (21) and (35) are solved iteratively, the integral steps being carried out numerically for any specified value for  $w_m$  (mm).

Figure 8 depicts the resulting action-response locus together with the formerly defined locus given in Fig. 6. Scaling factors preclude inclusion of those parts of the locus in the vicinity of the minimum safe temperature rise ( $w_m \cong 2.4$  m as per Fig. 6). The revised curve becomes effectively, or graphically, indistinguishable from the former locus well before the minimum safe temperature rise state ( $T_{min}$ ). At this state, the rational value is 1% lower than that for the previous analysis (63.6°C). However, whilst the fully mobilised assumptions again appear to be validated, the critical temperature rise has been established; this enables, in formal terms, superior definition of the post-buckling state.

### Lateral buckling of submarine pipelines

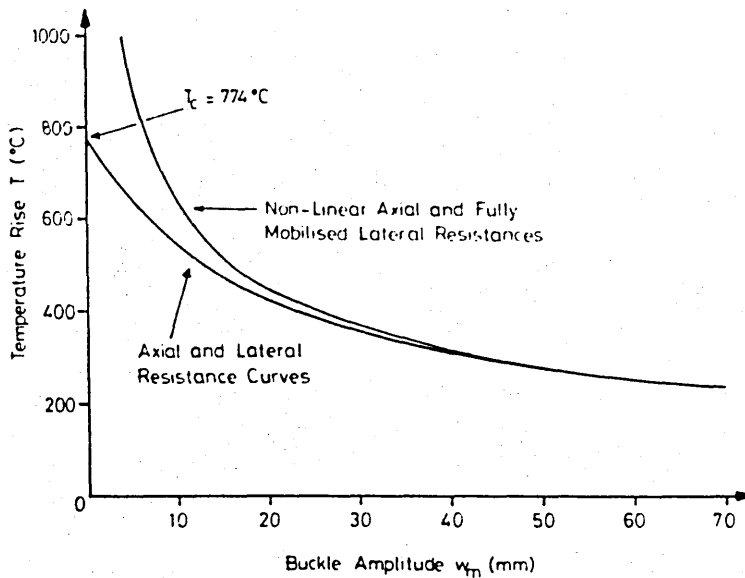
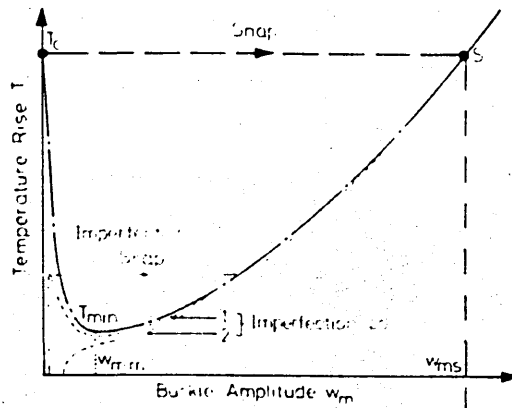


Fig. 8. Rational modelling for mode 1.

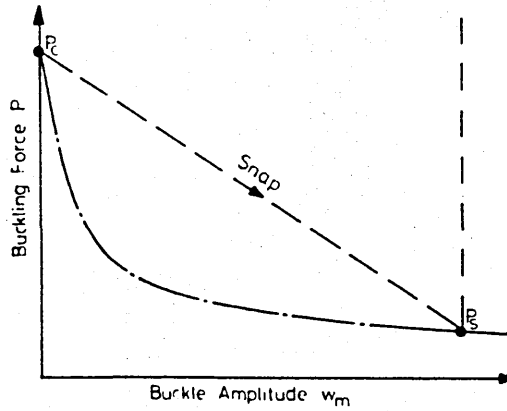
## 8 COMMENTS AND CONCLUSIONS

The rational modelling has achieved two objectives. First, it supports the validity of the simplified fully mobilised studies. Second, a critical temperature rise has been established which is important, in formal or idealised terms, in that post-buckling characteristics can be assessed.

Figure 9 depicts the post-buckling mechanism. That is, an idealised pipeline will not buckle until the critical temperature rise,  $T_c$  as denoted in Fig. 9(a), is reached. The pipe then snap buckles to point  $S$ . The static topologies defined in Figs 1 and 4 only relate to this and ensuing states. Figure 9(b) depicts the corresponding buckling force characteristics. At the critical state denoted by  $P_c$ , the force in the pipeline is given by  $P_c = P_0$ . After snap, the force in the buckle reduces to the unique static value  $P = P_s$ ,  $P$ , and location  $S$  being prescribed by the statically unique buckling amplitude  $w_m = w_{ms}$ . The chain-dotted locus defines a path which the idealised system cannot, in principle, follow due to snap at temperature rise  $T_c$ . This locus is, however, important in that it forms an upper bound to corresponding imperfection studies, particularly the theoretically stable portion between  $T_{min}$  and state  $S$ . States  $S$  and  $P$ , have



(a) Thermal Characteristics



(b) Buckling Force Characteristics

**Fig. 9.** Post-buckling mechanism.

not previously been reported. The values for  $P_c$ ,  $P_s$  and  $w_{ms}$  for mode 1 are 52.48 MN, 386 kN and 124.5 m respectively. ( $T_{min} = 63.1^\circ\text{C}$ ,  $w_{min} = 2.4$  m.)

In view of the importance of imperfections in realistic pipeline buckling performance, note below, and the general agreement of the rational loci with their fully mobilised equivalents, fully rational modelling of the remaining lateral modes has been left to further study. Further, such

study would benefit from the incorporation of geometric non-linearity as the point prescribed by  $w_{ms}$  involves relatively large slopes. That is, the general post critical state agreement between the two mode 1 loci depicted in Fig. 8 shows that the fully rational modelling will also incur the onset of slopes in excess of 0.1 radians shortly after theoretical attainment of the minimum safe temperature rise state  $T_{min}$  ( $w_{mm} \cong 2.4$  m)—note Figs 6 and 9. The locus is therefore conservative in this larger deformation range.<sup>1</sup> It should be noted that the value of  $T_c$  for any given analysis is sensitive to the lateral frictional curve employed; note the role of  $w_\phi$  in eqn (4). Such curves can be classified in terms of their respective fully mobilised displacements,  $w_\phi$ . As  $w_\phi$  increases, the critical temperature rise,  $T_c$ , will fall. Indeed,  $w_\phi$  can be such that  $T_c < T_{min}$ , affording a completely stable post-buckling path with no  $T_{min}$  turning point.

A number of further observations can be briefly noted. First, given the validity of the fully mobilised analyses in predicting generalised behaviour, the finite length of slip,  $L_s$ , can be determined, if required, from  $L_s = (P_0 - P_s)/\phi_A q$  for the post-buckling static state denoted by  $S$ . Associated studies<sup>4</sup> suggest that fully mobilised analyses underestimate the slip length at lower values of  $w_m$  (i.e.  $w_m < w_{mm}$ ). Should the total length of pipe be less than the overall affected length, that is  $2(L + L_s)$  with regard to the rational mode 1 modelling, the required temperature rise for state  $S$  will increase.<sup>11</sup> Further, post-buckling characteristics can be influenced by modal interaction. This is perhaps most important in cases where trenching is involved in which vertical buckling<sup>1,3</sup> might occur initially. Fully rational vertical buckling studies are in preparation.

Finally, the influence of imperfections must be noted. Diagrammatic representations given elsewhere<sup>1</sup> indicate the importance of the minimum safe temperature rise state. However, they also substantiate the importance of the  $w_{ms}$  state, to which all such imperfection loci should converge. Typical qualitative imperfection loci are illustrated in Fig. 9(a), one locus displaying snap buckling (type 1), the other affording a stable post-buckling path (type 2). Of particular interest with respect to such loci is the fact that recovery upon subsequent cooling would not be total, due to the non-conservative nature of the frictional forces involved. This leads to the realisation that, upon recovery, any initial imperfection would be increased with a consequent change in post-buckling characteristics should thermal buckling recur. For example, an imperfection locus type 1 could degenerate into a locus type 2. Imperfection studies are proceeding.

### ACKNOWLEDGEMENT

The authors wish to thank Professor Alastair Walker and Dr Charles Ellinas of J. P. Kenny and Partners, London, UK, for discussions held with regard to the contents of this article. However, the opinions expressed, and any errors incurred, are the authors' alone.

### REFERENCES

1. Hobbs, R. E., Pipeline buckling caused by axial loads, *J. Construct. Steel Res.*, **1** (1981) 2-10.
2. Hobbs, R. E., In-service buckling of heated pipelines, *J. Transport. Eng. Div., ASCE*, **110** (1984) 175-89.
3. Taylor, N. and Gan, A. B., Regarding the buckling of pipelines subject to axial loading, *J. Construct. Steel Res.*, **4** (1984) 45-50.
4. Taylor, N., Richardson, D. and Gan, A. B., On submarine pipeline frictional characteristics in the presence of buckling, *Proceedings of the 4th International Symposium on Offshore Mechanics and Arctic Engineering*, ASME, Dallas, Texas, 17-21 February 1985, 508-15.
5. Palmer, A. C. and Martin, J. H., Buckle propagation in submarine pipelines, *Nature*, **254** (1975) 46-8.
6. Bjerrum, L., Geotechnical problems involved in foundations of structures in the North Sea, *Geotechnique*, **231** (1973) 319-58.
7. Lyons, C. G., Soil resistance to lateral sliding of marine pipelines, *5th Offshore Technology Conference*, OTC 1876, Vol. 2, 1973, 479-84.
8. Gulhati, S. K., Venkatapparao, G. and Varadarajan, A., Positional stability of submarine pipelines, *IGS Conference on Geotechnical Engineering*, Vol. 1, 1978, 430-4.
9. Anand, S. and Agarwal, S. L., Field and laboratory studies for evaluating submarine pipeline frictional resistance, *Trans. ASME, J. Energy Resources Technol.*, **103** (1981) 250-4.
10. Kerr, A. D., Analysis of thermal track buckling in the lateral plane, *Acta Mech.*, **30** (1978) 17-50.
11. Kerr, A. D., On thermal buckling of straight railroad tracks and the effect of track length on the track response, *Rail International*, **9** (1979) 759-68.
12. Taylor, N. and Hirst, P. B., Regarding flexural curvature, *Proc. Instn Civ. Engrs.*, **77** (1984) 399-400.

APPENDIX II  
GEOTECHNICAL RESULTS

II(A) Sieve Analysis

II(B) Force-Displacement Relationships

$0 \leq \theta \leq 90^\circ$

II(C) Drained Triaxial Tests

B.S. SIEVE SIZE	WEIGHT RETAINED ON EACH SIEVE (g)							TOTAL WEIGHT PASSING EACH SIEVE (g)	PERCENTAGE PASSING EACH SIEVE
	1	2	3	4	5	AVE.			
2 mm	0	0	0	0	0	0	0	100	100
1.18 mm	0.5	0.5	0.5	0.5	1.0	0.6	0.6	99.4	99.4
600 µm	2.0	2.0	1.5	2.0	2.0	1.9	1.9	97.5	97.5
425 µm	10.0	10.0	9.5	10.0	10.0	9.9	9.9	87.6	87.6
300 µm	27.0	26.5	26.0	26.0	25.5	26.2	26.2	61.4	61.4
212 µm	31.5	31.5	31.5	31.5	31.5	31.5	31.5	29.9	29.9
150 µm	17.0	17.5	18.0	17.5	17.5	17.5	17.5	12.4	12.4
63 µm	11.0	11.0	12.0	11.5	11.5	11.4	11.4	1.0	1.0
SIEVE PAN	1.0	1.0	1.0	1.0	1.0	1.0	1.0		
TOTAL	100	100	100	100	100	100	100		

SIEVE ANALYSIS

Appendix II (A)

$$\theta = 0^\circ (\bar{R})$$

LOAD (N/m)	LATERAL DISPLACEMENT (mm)								
	A		B		C		D		AVE.
0.00	0.00	0.00	0.00	0.00	0.00	0.00	0.00	0.00	0.00
5.89	1.74	2.24	2.46	2.58	1.85	2.05	2.73	2.66	2.29
10.79	5.22	4.60	6.34	5.78	6.25	6.46	6.12	5.62	5.80
15.70	8.56	8.56	10.68	10.37	10.02	9.02	12.01	10.54	9.97
20.60	16.55	12.45	15.90	17.62	17.89	14.36	17.95	16.26	16.12
25.51	24.12	17.27	27.78	32.67	30.33	26.37	34.84	32.37	28.22
29.43	32.22	26.70	36.89	43.79	34.21	37.27	47.62	51.92	38.83
31.39	35.46	35.62	49.67	51.69	44.51	48.98	61.44	64.26	48.95
33.35	43.56	39.51	61.99	62.45	53.78	53.12	61.44	64.28	55.02
35.32	58.70	54.01	68.61	73.06	63.05	69.25	72.87	75.80	66.92
37.28	58.71	54.03	68.67	73.07	81.50	81.07	95.89	137.30	81.28
39.24	70.53	95.01	86.44	107.12	81.50	81.07	95.89	137.30	94.36
41.20	70.53	95.01	86.44	107.12	∞	∞	∞	∞	
43.16	∞	∞	∞	∞					

Appendix II (B)

$$\theta = 0^\circ (\bar{E})$$

LOAD (N/m)	LATERAL DISPLACEMENT (mm)								
	A		B		C		D		AVE.
0.00	0.00	0.00	0.00	0.00	0.00	0.00	0.00	0.00	0.00
10.79	0.13	0.11	0.10	0.04	0.08	0.06	0.04	0.03	0.07
15.70	0.28	0.24	0.20	0.15	0.20	0.19	0.10	0.13	0.19
20.60	1.41	1.84	1.85	1.07	1.17	1.26	1.32	1.41	1.42
25.51	6.24	8.02	6.76	6.11	5.96	6.32	5.96	6.41	6.47
30.41	15.56	19.33	18.02	16.23	15.33	16.79	15.55	19.14	16.99
34.34	39.98	34.63	36.31	31.88	29.14	30.44	26.11	34.23	32.84
36.30	56.14	54.12	51.39	38.10	39.76	46.10	32.34	41.99	44.99
40.22	90.04	82.37	69.34	69.52	62.11	79.10	79.10	84.32	76.99
42.18	132.61	116.24	119.34	121.51	88.27	93.24	79.10	84.32	103.43
43.16	132.61	116.24	140.51	159.67	131.36	147.21	∞	∞	
44.15	∞	∞	∞	∞	131.36	147.21			
45.13					∞	∞			

$$\theta = 0^\circ (\bar{P})$$

LOAD (N/m)	LATERAL DISPLACEMENT (mm)								
	A		B		C		D		AVE.
0.00	0.00	0.00	0.00	0.00	0.00	0.00	0.00	0.00	0.00
5.89	0.01	0.01	0.00	0.01	0.02	0.01	0.00	0.00	0.01
10.79	0.01	0.03	0.04	0.03	0.09	0.03	0.04	0.04	0.04
15.70	0.04	0.09	0.12	0.08	0.19	0.08	0.14	0.11	0.11
20.60	0.07	0.26	0.23	0.19	0.34	0.17	0.20	0.29	0.22
25.51	1.82	0.99	0.42	0.48	0.60	0.38	3.20	11.87	2.47
30.41	7.66	2.54	0.99	1.23	9.29	11.46	3.20	11.87	6.03
34.34	15.11	6.74	19.80	20.21	9.29	11.46	13.80	26.14	15.32
36.30	20.34	12.67	19.80	20.21	23.75	34.08	40.49	41.59	26.62
38.26	34.61	22.78	40.51	43.66	44.52	51.75	40.49	41.59	39.99
40.22	34.61	22.78	70.51	73.67	44.52	51.75	61.27	64.59	52.96
42.18	66.77	54.32	70.51	73.67	72.52	73.76	95.27	99.80	75.80
44.15	112.56	89.76	99.81	103.44	140.56	142.34	95.27	99.80	110.47
45.13	156.21	132.11	99.81	103.44	∞	∞	∞	∞	
46.11	156.21	132.11	130.51	103.66					
47.09	∞	∞	∞	∞					

$\theta = 15^\circ (\bar{R})$

LOAD (N/m)	A		B		C		D		AVERAGE	
	DISPLACEMENT (mm)		DISPLACEMENT (mm)		DISPLACEMENT (mm)		DISPLACEMENT (mm)		DIS. (mm)	
	LONG.	LATERAL	LONG.	LATERAL	LONG.	LATERAL	LONG.	LATERAL	LONG.	LATERAL
0.00	0.00	0.00	0.00	0.00	0.00	0.00	0.00	0.00	0.00	0.00
5.89	0.01	0.03	0.01	0.63	0.91	0.00	1.66	1.73	0.00	1.36
10.79	0.04	0.47	0.14	1.94	2.86	0.10	4.17	4.68	0.15	4.98
15.70	0.86	5.07	1.01	5.39	8.07	1.00	8.12	10.86	1.06	9.82
20.60	2.52	11.02	2.82	9.28	15.23	2.78	14.22	17.90	3.02	15.76
25.51	5.69	18.04	6.23	16.61	25.28	7.62	27.07	34.21	7.51	29.11
27.47	10.18	29.34	9.55	22.62	35.88	10.91	35.20	44.31	9.39	33.89
29.43	14.37	38.58	15.61	35.90	55.78	14.57	44.00	58.26	13.51	44.70
31.39	17.36	45.47	15.61	35.91	55.78	16.33	57.37	61.89	13.52	44.71
33.35	17.37	45.49	21.72	47.88	75.25	21.35	68.28	80.22	19.47	60.24
35.32	24.84	61.51	33.99	72.15	94.53	29.27	84.01	92.90	27.62	77.57
37.28	-	∞	33.99	72.15	94.53	29.28	84.03	92.91	27.62	77.57
39.24	-	∞	-	∞	∞	-	∞	∞	-	∞

$\theta = 15^\circ$  (E)

LOAD (N/m)	A		B		C		D		AVERAGE	
	DISPLACEMENT (mm)		DISPLACEMENT (mm)		DISPLACEMENT (mm)		DISPLACEMENT (mm)		DIS. (mm)	
	LONG.	LATERAL	LONG.	LATERAL	LONG.	LATERAL	LONG.	LATERAL	LONG.	LATERAL
0.00	0.00	0.00	0.00	0.00	0.00	0.00	0.00	0.00	0.00	0.00
5.89	0.00	0.00	0.00	0.04	0.07	0.00	0.00	0.00	0.01	0.00
10.79	0.00	0.14	0.00	0.53	0.50	0.00	0.35	0.00	0.08	0.00
15.70	0.00	0.67	0.00	1.17	1.10	0.00	1.27	0.00	0.30	0.00
20.60	0.14	1.82	0.06	2.24	1.99	0.09	2.58	0.00	0.64	0.07
25.51	0.99	8.27	0.18	3.38	2.86	0.66	5.01	0.10	1.04	0.48
29.43	3.26	14.94	2.37	15.01	7.06	3.38	14.75	0.33	1.79	2.34
33.35	13.27	40.69	3.96	17.94	12.38	9.07	28.13	3.77	11.36	7.52
37.28	31.27	139.43	121.21	17.72	55.27	22.10	78.16	9.87	23.99	20.24
39.24	31.27	139.43	121.21	37.72	100.10	22.10	78.16	19.37	48.11	27.62
40.22	31.27	139.43	121.21	37.72	100.10	-	-	19.37	48.11	51.12
41.20	-	-	-	-	-	-	-	-	-	-

$$\theta = 15^\circ (\bar{P})$$

LOAD (N/m)	A		B		C		D		AVERAGE	
	DISPLACEMENT (mm)		DISPLACEMENT (mm)		DISPLACEMENT (mm)		DISPLACEMENT (mm)		DIS. (mm)	
	LONG.	LATERAL	LONG	LATERAL	LONG.	LATERAL	LONG.	LATERAL	LONG.	LATERAL
0.00	0.00	0.00	0.00	0.00	0.00	0.00	0.00	0.00	0.00	0.00
5.89	0.00	0.01	0.00	0.00	0.00	0.00	0.01	0.00	0.02	0.01
10.79	0.00	0.03	0.00	0.01	0.01	0.00	0.07	0.00	0.03	0.04
15.70	0.00	0.09	0.00	0.07	0.06	0.00	0.23	0.00	0.11	0.11
20.60	0.00	0.19	0.00	0.16	0.14	0.00	0.54	0.01	0.23	0.25
25.51	0.01	0.40	0.02	0.36	0.27	0.17	1.33	0.68	1.44	1.35
29.43	2.63	19.07	5.75	12.94	3.80	4.00	17.50	5.10	21.46	13.22
33.35	5.08	27.25	12.99	3.85	16.81	7.49	45.70	11.20	40.95	27.99
37.28	13.61	77.59	49.20	13.35	41.78	36.40	68.59	25.20	67.97	60.08
39.24	13.61	77.59	49.20	16.05	87.97	57.91	68.59	25.20	67.97	68.54
41.20	-	∞	∞	16.05	87.97	57.91	68.59	25.20	67.97	82.56
42.18	-	-	-	∞	∞	∞	∞	-	∞	∞

$\theta = 30^\circ$  (R)

LOAD (N/m)	A		B		C		D		AVERAGE	
	DISPLACEMENT (mm)		DISPLACEMENT (mm)		DISPLACEMENT (mm)		DISPLACEMENT (mm)		DIS. (mm)	
	LONG.	LATERAL	LONG.	LATERAL	LONG.	LATERAL	LONG.	LATERAL	LONG.	LATERAL
0.00	0.00	0.00	0.00	0.00	0.00	0.00	0.00	0.00	0.00	0.00
5.89	0.00	0.80	0.10	1.19	1.24	0.00	0.59	0.66	2.30	1.23
9.81	0.23	2.68	0.37	3.13	3.08	0.22	3.78	2.81	5.68	3.72
13.73	1.08	5.77	4.97	1.14	6.20	5.22	0.71	5.69	9.28	6.23
17.66	3.19	10.15	8.38	2.91	10.12	9.32	2.91	10.47	14.43	10.47
19.62	6.05	14.62	11.89	4.98	13.81	10.96	5.32	14.36	18.83	14.10
21.58	9.05	14.62	11.89	7.90	17.38	16.08	8.53	18.57	23.64	17.29
23.54	10.85	21.56	16.98	13.10	24.83	22.00	8.55	18.58	26.83	21.22
25.51	20.95	34.89	28.88	13.11	24.86	22.02	15.81	26.90	34.27	28.33
27.47	20.95	34.89	28.89	19.28	32.51	29.43	22.32	34.98	34.28	32.10
29.43	29.30	45.09	39.53	30.84	45.96	43.54	22.32	35.34	52.39	42.19
31.39	46.79	64.43	59.38	30.87	46.21	43.56	28.12	42.10	52.42	48.75
33.35	46.82	64.44	59.38	30.87	46.21	43.56	56.36	71.69	52.42	65.28
35.32	-	$\infty$	-	$\infty$	$\infty$	-	$\infty$	$\infty$	$\infty$	$\infty$

$\theta = 30^\circ$  (E)

LOAD (N/m)	A		B		C		D		AVERAGE	
	DISPLACEMENT (mm)		DISPLACEMENT (mm)		DISPLACEMENT (mm)		DISPLACEMENT (mm)		DIS. (mm)	
	LONG.	LATERAL	LONG.	LATERAL	LONG.	LATERAL	LONG.	LATERAL	LONG.	LATERAL
0.00	0.00	0.00	0.00	0.00	0.00	0.00	0.00	0.00	0.00	0.00
5.89	0.00	0.04	0.00	0.01	0.00	0.00	0.00	0.01	0.00	0.05
9.81	0.00	0.26	0.00	0.23	0.00	0.00	0.00	0.30	0.00	0.22
13.73	0.12	0.83	0.10	0.74	0.00	0.00	0.00	0.66	0.07	0.66
17.66	0.36	1.43	0.34	1.57	0.08	0.08	0.08	1.15	0.20	1.22
21.58	0.92	2.47	0.69	2.84	0.34	0.34	0.34	1.83	0.43	2.06
25.51	1.78	4.16	1.65	5.65	0.85	0.85	0.85	2.84	0.83	3.41
29.43	6.55	12.08	11.26	19.31	7.82	7.82	7.82	16.78	10.76	12.87
31.39	14.76	22.94	19.98	28.91	7.82	7.82	7.82	16.78	10.76	17.65
33.35	14.76	22.94	19.98	28.91	13.21	13.21	13.21	34.15	26.80	23.22
35.32	33.03	42.73	38.48	46.03	20.86	20.86	20.86	73.20	66.45	42.78
36.30	33.03	42.73	38.48	46.03	20.86	20.86	20.86	73.20	66.45	42.78
37.28	73.03	92.67	98.53	96.05	42.74	42.74	42.74	∞	∞	
38.26	∞	∞	77.58	96.05	42.74	42.74	42.74	∞	∞	
39.24			∞	∞	∞	∞	∞	∞	∞	

$\theta = 30^\circ (\bar{P})$

LOAD (N/m)	A		B		C		D		AVERAGE	
	DISPLACEMENT (mm)		DISPLACEMENT (mm)		DISPLACEMENT (mm)		DISPLACEMENT (mm)		DIS. (mm)	
	LONG.	LATERAL	LONG.	LATERAL	LONG.	LATERAL	LONG.	LATERAL	LONG.	LATERAL
0.00	0.00	0.00	0.00	0.00	0.00	0.00	0.00	0.00	0.00	0.00
5.89	0.00	0.01	0.00	0.00	0.01	0.00	0.00	0.00	0.00	0.01
9.81	0.00	0.04	0.00	0.00	0.04	0.00	0.01	0.00	0.03	0.02
13.73	0.00	0.09	0.01	0.02	0.08	0.00	0.05	0.02	0.10	0.06
17.66	0.01	0.19	0.02	0.06	0.13	0.04	0.10	0.04	0.17	0.11
21.58	0.10	0.33	0.08	0.12	0.20	0.15	0.19	0.08	0.26	0.20
25.51	0.30	0.61	0.21	0.26	0.34	0.53	0.39	0.25	0.47	0.33
29.43	3.93	6.32	26.78	10.06	24.96	4.55	3.45	4.28	0.55	8.95
31.39	17.78	21.43	26.78	10.06	24.96	13.10	13.23	10.75	10.84	15.42
33.35	17.78	21.43	36.26	20.41	33.90	13.10	13.23	10.75	10.84	17.83
35.32	31.46	34.42	36.26	20.41	33.90	23.77	24.03	22.02	28.10	28.97
37.28	62.06	65.51	43.48	45.88	46.95	48.25	48.97	52.84	60.00	56.67
39.29	∞	∞	∞	∞	∞	48.25	48.97	52.84	∞	∞
40.22						∞	∞	∞		

$\theta = 45^\circ$  (R)

LOAD (N/m)	A		B		C		D		AVERAGE	
	DISPLACEMENT (mm)		DISPLACEMENT (mm)		DISPLACEMENT (mm)		DISPLACEMENT (mm)		DIS. (mm)	
	LONG.	LATERAL	LONG.	LATERAL	LONG.	LATERAL	LONG.	LATERAL	LONG.	LATERAL
0.00	0.00	0.00	0.00	0.00	0.00	0.00	0.00	0.00	0.00	0.00
5.89	0.00	1.19	0.00	0.03	0.14	0.02	0.18	0.05	0.08	0.43
9.81	0.25	4.47	0.09	0.72	0.70	0.15	0.79	0.30	0.78	1.68
13.73	0.96	7.48	0.41	1.83	1.76	0.54	1.96	0.90	2.37	3.31
17.66	2.99	11.05	0.85	6.27	5.15	1.39	3.70	4.16	7.22	6.47
19.62	6.55	14.96	12.94	5.06	8.81	7.22	6.80	7.05	10.13	9.10
21.58	11.96	19.52	17.02	10.84	13.74	11.18	10.94	11.70	13.99	12.98
23.54	27.57	32.10	27.33	19.48	19.37	17.07	15.34	18.85	18.91	19.41
25.51	27.59	32.12	27.34	19.52	19.41	17.09	21.16	36.05	30.88	23.62
27.47	50.49	46.89	43.27	46.37	44.22	43.61	39.31	54.57	43.15	41.99
29.43	∞	∞	∞	∞	∞	∞	∞	∞	∞	∞

$\theta = 45^\circ$  (E)

LOAD (N/m)	A		B		C		D		AVERAGE	
	DISPLACEMENT (mm)		DISPLACEMENT (mm)		DISPLACEMENT (mm)		DISPLACEMENT (mm)		DIS. (mm)	
	LONG.	LATERAL	LONG.	LATERAL	LONG.	LATERAL	LONG.	LATERAL	LONG.	LATERAL
0.00	0.00	0.00	0.00	0.00	0.00	0.00	0.00	0.00	0.00	0.00
5.89	0.00	0.00	0.00	0.02	0.03	0.00	0.13	0.00	0.02	0.00
9.81	0.01	0.10	0.00	0.05	0.05	0.00	0.62	0.00	0.20	0.00
13.73	0.07	0.31	0.00	0.13	0.14	0.05	1.16	0.07	0.51	0.05
17.66	0.26	0.58	0.04	0.22	0.27	0.27	1.75	0.29	1.00	0.22
21.58	0.69	0.98	0.18	0.37	0.50	0.68	2.36	0.73	1.66	0.57
23.54	1.10	1.27	0.36	0.50	0.73	1.12	2.83	1.00	1.92	0.90
25.51	1.99	1.84	0.60	0.66	1.00	2.75	3.78	7.31	6.08	3.16
27.47	15.93	8.77	3.41	1.61	2.08	16.12	10.03	18.86	11.70	13.58
29.43	44.71	20.13	38.32	13.13	13.57	47.10	19.93	47.42	21.67	44.39
30.41	44.71	20.13	38.32	13.13	13.57	47.10	19.93	47.42	21.67	44.39
31.39	∞	-	87.02	23.76	30.35	∞	-	∞	-	-
32.37			∞	-	-					

$\theta = 45^\circ$  ( $\bar{P}$ )

LOAD (N/m)	A				B				C				D				AVERAGE	
	DISPLACEMENT (mm)		DISPLACEMENT (mm)		DISPLACEMENT (mm)		DISPLACEMENT (mm)		DISPLACEMENT (mm)		DISPLACEMENT (mm)		DISPLACEMENT (mm)		DIS. (mm)			
	LONG.	LATERAL	LONG.	LATERAL	LONG.	LATERAL												
0.00	0.00	0.00	0.00	0.00	0.00	0.00	0.00	0.00	0.00	0.00	0.00	0.00	0.00	0.00	0.00	0.00	0.00	0.00
5.89	0.00	0.00	0.03	0.00	0.01	0.01	0.00	0.00	0.00	0.00	0.00	0.00	0.01	0.00	0.01	0.00	0.00	0.01
9.81	0.00	0.01	0.04	0.00	0.02	0.02	0.00	0.00	0.00	0.01	0.00	0.00	0.02	0.00	0.02	0.00	0.00	0.02
13.73	0.00	0.03	0.05	0.00	0.07	0.06	0.00	0.00	0.00	0.04	0.00	0.00	0.05	0.00	0.03	0.00	0.00	0.04
17.66	0.00	0.07	0.07	0.06	0.17	0.15	0.04	0.02	0.09	0.09	0.06	0.12	0.07	0.04	0.07	0.04	0.10	0.10
21.58	0.05	0.13	0.10	0.35	0.39	0.37	0.18	0.13	0.17	0.17	0.21	0.22	0.12	0.20	0.12	0.20	0.20	0.20
23.54	0.13	0.19	0.14	0.79	0.75	0.69	0.33	0.22	0.23	0.33	0.39	0.34	0.17	0.41	0.17	0.41	0.34	0.34
25.51	0.14	0.26	0.18	1.67	1.60	0.69	0.79	0.48	0.34	0.79	0.86	0.66	0.35	0.87	0.66	0.87	0.66	0.66
27.47	0.60	0.40	0.27	13.96	9.10	9.21	19.92	10.75	4.55	17.44	17.44	10.64	6.42	12.98	6.42	12.98	6.42	6.42
29.43	28.18	11.34	7.49	28.81	15.98	15.56	37.00	17.90	9.95	40.03	40.03	19.94	17.12	33.35	17.12	33.35	14.41	14.41
30.41	28.18	11.34	7.49	28.81	15.98	15.56	37.00	17.90	9.95	40.03	40.03	19.94	17.12	33.35	17.12	33.35	14.41	14.41
31.39	51.31	17.24	15.31	98.02	36.28	48.64	55.52	26.30	16.46	-	-	-	-	-	-	-	-	-
32.37	51.31	17.24	15.31	-	-	-	-	-	-	-	-	-	-	-	-	-	-	-
33.35	-	-	-	-	-	-	-	-	-	-	-	-	-	-	-	-	-	-

$\theta = 60^\circ$  (R)

LOAD (N/m)	A		B		C		D		AVERAGE			
	DISPLACEMENT (mm)		DISPLACEMENT (mm)		DISPLACEMENT (mm)		DISPLACEMENT (mm)		DIS. (mm)			
	LONG.	LATERAL	LONG.	LATERAL	LONG.	LATERAL	LONG.	LATERAL	LONG.	LATERAL		
0.00	0.00	0.00	0.00	0.00	0.00	0.00	0.00	0.00	0.00	0.00	0.00	0.00
5.89	0.00	0.06	0.06	0.62	0.96	0.02	0.17	0.09	0.52	0.04	0.38	0.38
9.81	0.12	0.46	0.42	2.14	2.43	0.15	0.85	0.45	1.87	0.29	1.34	1.34
13.73	0.70	1.76	1.44	4.58	4.18	1.00	3.36	2.04	4.59	1.30	3.34	3.34
17.66	5.55	7.58	4.95	5.36	6.83	6.09	8.80	7.14	6.76	5.94	7.54	7.54
19.62	11.72	11.37	7.70	10.22	12.12	11.58	11.92	9.99	14.19	11.93	10.56	10.56
21.58	11.72	11.37	7.70	10.22	12.12	11.58	11.92	9.99	14.19	11.93	10.56	10.56
23.54	24.60	16.35	12.06	26.73	18.74	35.66	19.64	17.76	-	-	-	-
25.51	∞	-	∞	-	-	∞	-	-	-	-	-	-

$$\theta = 60^\circ (\bar{E})$$

LOAD (N/m)	A		B		C		D		AVERAGE	
	DISPLACEMENT (mm)		DISPLACEMENT (mm)		DISPLACEMENT (mm)		DISPLACEMENT (mm)		DIS. (mm)	
	LONG.	LATERAL	LONG.	LATERAL	LONG.	LATERAL	LONG.	LATERAL	LONG.	LATERAL
0.00	0.00	0.00	0.00	0.00	0.00	0.00	0.00	0.00	0.00	0.00
5.89	0.00	0.03	0.03	0.02	0.03	0.00	0.02	0.00	0.02	0.01
9.81	0.00	0.13	0.03	0.08	0.09	0.03	0.17	0.00	0.08	0.02
13.73	0.17	0.49	0.13	0.25	0.26	0.18	0.44	0.07	0.22	0.14
17.66	0.51	0.95	0.35	0.53	0.52	0.44	0.78	0.31	0.49	0.34
19.62	0.81	1.22	0.61	0.74	0.71	0.84	1.12	0.60	0.71	0.72
21.58	1.83	1.63	3.68	1.35	1.38	3.14	1.78	3.74	1.26	3.10
23.54	46.67	5.05	41.50	3.34	2.94	43.33	3.73	49.10	2.32	45.15
24.53	46.67	5.05	41.50	3.34	2.94	93.30	5.07	119.02	4.25	75.14
25.51	∞	-	∞	-	-	∞	-	∞	-	-

$\theta = 60^\circ$  (E)

LOAD (N/m)	A		B		C		D		AVERAGE	
	DISPLACEMENT (mm)		DISPLACEMENT (mm)		DISPLACEMENT (mm)		DISPLACEMENT (mm)		DIS. (mm)	
	LONG.	LATERAL	LONG.	LATERAL	LONG.	LATERAL	LONG.	LATERAL	LONG.	LATERAL
0.00	0.00	0.00	0.00	0.00	0.00	0.00	0.00	0.00	0.00	0.00
5.89	0.00	0.01	0.00	0.01	0.01	0.00	0.01	0.00	0.01	0.01
9.81	0.00	0.01	0.00	0.02	0.01	0.01	0.02	0.00	0.01	0.02
13.73	0.02	0.03	0.02	0.05	0.01	0.02	0.04	0.00	0.03	0.04
17.66	0.22	0.10	0.11	0.10	0.11	0.05	0.05	0.00	0.07	0.11
19.62	0.49	0.17	0.22	0.15	0.23	0.07	0.07	0.22	0.18	0.29
21.58	2.12	0.55	0.40	0.21	0.51	0.11	0.08	0.62	0.18	0.91
23.54	14.24	4.93	0.98	0.33	3.41	1.57	0.53	36.99	1.92	13.91
24.53	63.42	7.45	56.21	4.11	56.36	3.55	1.52	74.92	3.39	62.73
25.51	∞	-	56.21	4.11	56.36	3.55	1.52	74.92	3.39	2.49
26.49			∞	-	∞	-	-	∞	-	-

$\theta = 75^\circ$  (R)

LOAD (N/m)	A		B		C		D		AVERAGE	
	DISPLACEMENT (mm)		DISPLACEMENT (mm)		DISPLACEMENT (mm)		DISPLACEMENT (mm)		DIS. (mm)	
	LONG.	LATERAL	LONG.	LATERAL	LONG.	LATERAL	LONG.	LATERAL	LONG.	LATERAL
0.00	0.00	0.00	0.00	0.00	0.00	0.00	0.00	0.00	0.00	0.00
5.89	0.01	0.02	0.10	0.15	0.15	0.00	0.02	0.01	0.02	0.03
9.81	0.12	0.25	0.23	0.42	0.46	0.10	0.21	0.07	0.14	0.13
11.77	0.25	0.62	0.59	1.15	1.16	0.23	0.41	0.15	0.25	0.31
13.73	0.68	1.04	0.97	1.69	1.67	0.55	0.86	0.40	0.58	0.67
15.70	3.44	3.50	2.98	2.78	2.59	3.75	3.53	4.90	4.60	3.57
17.66	7.12	7.68	5.87	7.60	7.01	10.78	6.70	12.81	7.97	4.92
18.64	28.77	13.77	10.21	12.89	7.60	10.78	6.70	31.69	13.68	8.11
19.62	28.77	13.77	10.21	12.89	7.60	10.78	6.70	31.69	13.68	8.11
20.60	∞	-	-	-	-	27.92	13.79	31.69	13.68	-
21.58	∞	-	-	-	-	27.92	13.79	31.69	13.68	-

$\theta = 75^\circ$  (E)

LOAD (N/m)	A		B		C		D		AVERAGE	
	DISPLACEMENT (mm)		DISPLACEMENT (mm)		DISPLACEMENT (mm)		DISPLACEMENT (mm)		DIS. (mm)	
	LONG.	LATERAL	LONG.	LATERAL	LONG.	LATERAL	LONG.	LATERAL	LONG.	LATERAL
0.00	0.00	0.00	0.00	0.00	0.00	0.00	0.00	0.00	0.00	0.00
5.89	0.00	0.01	0.00	0.00	0.00	0.00	0.00	0.00	0.00	0.00
10.79	0.00	0.02	0.03	0.00	0.03	0.04	0.01	0.01	0.00	0.02
15.70	0.14	0.05	0.21	0.03	0.00	0.11	0.08	0.18	0.06	0.19
17.66	0.32	0.08	0.47	0.05	0.00	0.18	0.10	0.43	0.09	0.41
19.62	10.80	0.09	1.00	0.08	0.00	58.88	1.26	20.56	0.40	22.81
20.60	47.12	0.09	13.02	0.25	0.00	58.88	1.26	36.99	0.87	39.00
21.58										

$\theta = 75^\circ (\bar{P})$

LOAD (N/m)	A		B		C		D		AVERAGE	
	DISPLACEMENT (mm)		DISPLACEMENT (mm)		DISPLACEMENT (mm)		DISPLACEMENT (mm)		DIS. (mm)	
	LONG.	LATERAL	LONG.	LATERAL	LONG.	LATERAL	LONG.	LATERAL	LONG.	LATERAL
0.00	0.00	0.00	0.00	0.00	0.00	0.00	0.00	0.00	0.00	0.00
5.89	0.00	0.00	0.00	0.01	0.00	0.01	0.00	0.00	0.00	0.00
10.79	0.03	0.01	0.00	0.02	0.01	0.00	0.00	0.05	0.01	0.04
15.70	0.13	0.02	0.00	0.10	0.04	0.01	0.00	0.06	0.02	0.11
17.66	0.23	0.04	0.01	0.20	0.05	0.01	0.00	0.21	0.04	0.22
19.62	0.48	0.08	0.01	2.35	0.10	0.04	0.00	0.34	0.07	0.91
21.58	1.96	0.15	0.03	2.35	0.10	0.04	1.87	2.97	0.11	2.29
22.56	∞	-	∞	-	-	-	∞	-	-	-

$\theta = 90^\circ (\bar{R})$

LOAD (N/m)	LONGITUDINAL DISPLACEMENT (mm)				
	A	B	C	D	AVE.
0.00	0.00	0.00	0.00	0.00	0.00
5.65	0.05	0.02	0.04	0.04	0.04
10.36	0.34	0.23	0.27	0.31	0.28
15.07	1.11	0.91	0.98	1.02	1.01
16.01	-	-	1.61	1.84	1.73
16.95	2.09	2.09	2.67	2.55	2.35
17.89	8.40	15.53	11.29	8.62	10.96
18.64	$\infty$	$\infty$	$\infty$	$\infty$	$\infty$

$\theta = 90^\circ (\bar{E})$

LOAD (N/m)	LONGITUDINAL DISPLACEMENT (mm)				
	A	B	C	D	AVE.
0.00	0.00	0.00	0.00	0.00	0.00
5.65	0.02	0.01	0.01	0.02	0.02
10.36	0.15	0.12	0.10	0.14	0.13
15.07	0.54	0.49	0.38	0.50	0.48
16.01	-	-	0.59	-	0.59
16.95	1.01	0.99	0.86	1.05	0.98
17.89	3.51	4.03	1.73	5.48	3.69
18.64	$\infty$	30.89	6.58	13.58	
19.13		$\infty$	6.58	$\infty$	
19.62			$\infty$		

$\theta = 90^\circ (\bar{P})$

LOAD (N/m)	LONGITUDINAL DISPLACEMENT (mm)				
	A	B	C	D	AVE.
0.00	0.00	0.00	0.00	0.00	0.00
5.65	0.00	0.00	0.01	0.00	0.00
10.36	0.01	0.01	0.02	0.01	0.01
15.06	0.07	0.06	0.08	0.08	0.07
16.95	0.13	0.14	0.18	0.16	0.15
18.84	0.26	0.30	0.36	0.37	0.32
19.78	0.46	0.52	-	-	0.49
20.60	$\infty$	$\infty$	$\infty$	$\infty$	$\infty$

TEST 1		TEST 2		TEST 3	
Deviator Stress (kN/m <sup>2</sup> )	Strain	Deviator Stress (kN/m <sup>2</sup> )	Strain	Deviator Stress (kN/m <sup>2</sup> )	Strain
0	0	0	0	0	
193	0.0024	135	0.0023	55	0.0024
230	0.0072	164	0.0046	62	0.0049
283	0.0121	182	0.0068	69	0.0073
310	0.0169	193	0.0091	75	0.0097
325	0.0217	203	0.0114	78	0.0146
334	0.0266	212	0.0160	79	0.0194
339	0.0314	221	0.0205	80	0.0243
335	0.0362	208	0.0251	83	0.0291
346	0.0411	209	0.0297	82	0.0340
332	0.0459	213	0.0365	77	0.0413
335	0.0507	222	0.0434	76	0.0461
333	0.0556	214	0.0502	75	0.0510

DRAINED TRIAXIAL TESTS

Appendix II (C)

APPENDIX III  
PROGRAMME LISTINGS

III(A) Quasi-Idealised / Fully Mobilised Analyses for  
All Lateral Modes - Computer Graphics

III(B) Quasi-Idealised Critical State Analysis  
- Lateral Mode 1

III(C) Imperfection Analysis - Lateral Mode 1

C  
C  
C  
C  
C  
C  
C  
C  
C

=====  
APPENDIX III (A)  
=====

QUASI-IDEALISED / FULLY MOBILISED ANALYSES FOR  
ALL LATERAL MODES - COMPUTER GRAPHICS

DIMENSION L(40),P(40),T(40),Y(40)  
DIMENSION KA(10),KB(10),KC(10),KD(10)  
REAL I,L,ML,KA,KB,KC,KD  
CALL NULIN (9)  
CALL T4010  
A=0.02992  
I=0.001509  
E=2.06E8  
W=3.8  
C=11.0E-6  
F=0.5  
CALL CHAMOD  
READ (9,10)  
10 FCKMAT (A4)  
CALL PICCLE

10

C  
C  
C

SETTING UP AXES AND SCALES

CALL AXIPCS (1,20.,20.,150.,1)  
CALL AXIPCS (1,20.,20.,105.,2)  
CALL AXISCA (1,16,0.,4.2,1)  
CALL AXISCA (1,12,30.,150.,2)  
CALL AXIDRA (2,1,1)  
CALL AXIDRA (-2,-1,2)  
CALL NOVTO2 (80.,5.)  
CALL CHAHOL (22HBUCKLE AMPLITUDE (M)\*.)  
CALL MOVTO2 (5.,140.)  
CALL CHAHOL (69HFIGURE 1.4 COMPARISON OF THE  
& LATERAL BUCKLING MODES (AFC=LFC=0.5)\*.)  
CALL NOVTO2 (5.,135.)  
CALL CHAHOL (69H=====\*)  
&=====\*)  
CALL MOVTO2 (5.,50.)  
CALL CHAANG (90.)  
CALL CHAHOL (22HTEMPERATURE RISE (C)\*.)

C  
C  
C  
C

CALCULATING AND DRAWING CURVES  
FOR VARIOUS LATERAL MODES

KA(1)=80.76  
KB(1)=6.391E-5  
KC(1)=0.5  
KD(1)=2.407E-3  
KA(2)=39.47842  
KB(2)=1.743E-4  
KC(2)=1.0

```

KD (2)=5.532E-3
KA (3)=34.06
KB (3)=1.668E-4
KC (3)=1.294
KD (3)=1.032E-2
KA (4)=28.20
KB (4)=2.144E-4
KC (4)=1.608
KD (4)=1.047E-2
DO 80 N=1,5
IF (N.NE.5) GOTO 75
DO 60 J=1,40
Y (J)=0.1*J
L (J)=((Y (J)*E*I)/(4.4495E-3*F*W))**0.25
P (J)=39.47842*E*I/L (J)**2+4.705E-5*A*E*((F*W)/
& (E*I))**2*L (J)**6
T (J)=P (J)/(E*A*C)
IF (T (J).GT.T (1)) GOTO 77
60 CONTINUE
GOTO 77
75 DO 76 J=1,40
Y (J)=0.1*J
L (J)=((Y (J)*E*I)/(KD (N)*F*W))**0.25
P (J)=KA (N)*E*I/L (J)**2+KC (N)*F*W*L (J)*((1.0+
& KB (N)*A*E*F*W*L (J)**5/(E*I)**2)**0.5-1.0)
T (J)=P (J)/(E*A*C)
IF (T (J).GT.T (1)) GOTO 77
76 CONTINUE
77 K=J
TK=T (K)
YK=Y (K)
T1=T (1)+1.0
Y1=Y (1)-0.04
CALL GRACUR (Y,T,K)
IF (N.EQ.5) GOTO 73
IF (N.EQ.1) GOTO 78
IF (N.EQ.3) GOTO 78
IF (N.EQ.2) GOTO 74
YK=YK+0.02
TK=TK-2.0
IF (N.EQ.4) GOTO 73
74 YK=YK+0.02
TK=TK+1.0
73 CALL GRAMOV (YK,TK)
CALL CHAANG (0.)
CALL CHAINT (N,1)
IF (N.NE.5) GOTO 80
78 CALL GRAMOV (Y1,T1)
CALL CHAANG (0.)
CALL CHAINT (N,1)
IF (N.NE.5) GOTO 80
YK=YK+0.12
CALL GRAMOV (YK,TK)
CALL CHAHOL (17H(INFINITY MODE)*.)
80 CONTINUE

```

CALL CHAMOD  
READ (9, 10)  
CALL PICCLE  
CALL DEVEND  
STOP  
END

C  
C  
C  
C  
C  
C  
C  
C  
C

=====  
APPENDIX III (B)  
=====

QUASI-IDEALISED CRITICAL STATE ANALYSIS  
LATERAL MODE 1

```
DIMENSION X(1000),WA(1000),W(1000)
REAL I,J,L
999 CONTINUE
WRITE (6,1)
1  FORMAT (//,2X,'INPUT WMAX(MM), OTHERWISE -1.0
& TC STOP')
READ (5,*)WC
IF(WC.LT.0.0) GOTO 3003
KK=999
CL=0.2
CA=5.0
E=2.0601E5
I=1.509E9
A=2.992E4
FA=2.66
FL=3.8
AL=1.1E-5
R1=0.0
DO 1000 JJ=1,2
K=KK

C
C  SIMPSON'S RULE
C
DO 100 N=1,K
S=1.0*N
ST=1.0*K-1.0
X(N)=(S-1.0)/ST
W(N)=(WC/7.0)*(7.0-24.0*X(N)**2+30.0*X(N)**4-
&16.0*X(N)**6+3.0*X(N)**8)
CC=-CL*W(N)
IF (JJ.EQ.2) GOTO 50
WA(N)=(1.0-EXP(CC))*X(N)
GOTO 60
50 CONTINUE
WA(N)=1.0-EXP(CC)
60 CONTINUE
100 CONTINUE
WA1=WA(1)+WA(K)
K=K-1
WA2=0.0
DO 200 N=2,K,2
WA2=WA2+WA(N)
200 CONTINUE
WA3=0.0
K=K-1
DO 300 N=3,K,2
```

```

      WA3=WA3+WA(N)
300  CONTINUE
      K=K+1
      TA=1.0/(3.0*K)*(WA1+4.0*WA2+2.0*WA3)
      IF(JJ.EQ.2) GOTO 333
      SS=TA
333  CONTINUE
1000 CONTINUE
      WRITE (6,*)SS,TA
      L=((192.0*WC*E*I)/(7.0*TA*FL))**0.25
      P=192.0*E*I*(1.25-SS/TA)/(7.0*L**2)
C
C   NON-LINEAR ITERATIVE ALGORITHM
C
1001 CONTINUE
      J=1.8204E-3*(IL*IA/(E*I))**2*L**7
      US=(R1*L)/(A*E)-0.5*J
      R=(2.0*FA*A*E*((EXP(CA*US)-1.0)/CA-US))**0.5
      R2=ABS(R-R1)
      IF(R2.LT.10.0) GOTO 2002
      R1=0.5*(R+R1)
      GOTO 1001
2002 CONTINUE
      T=(P+R)/(E*A*AL)
      WRITE (6,*)L,R,T
      RF=((1.0+(J*E*A)/(FA*L**2))**0.5-1.0)*FA*L
      TF=(P+RF)/(E*A*AL)
      WRITE (6,*)L,RF,TF
      GOTO 999
3003 CONTINUE
      STOP
      END

```

C  
C  
C  
C  
C  
C  
C  
C

=====  
APPENDIX III (C)  
=====

IMPERFECTION ANALYSIS - LATERAL MODE 1

```
REAL I,J,L,LO,LI,JO,L2,LCO,IR  
WRITE (6,1)  
1  FORMAT (//,2X,'INPUT IR, OTHERWISE -1.0 TO STOP')  
READ (5,*) IR  
IR=2.0*IR  
CA=5.0  
E=2.0601E5  
I=1.509E9  
A=2.992E4  
FA=2.66  
FL=3.8  
AL=1.1E-5  
RA=325.0  
LO=((IR*E*I)/(3.8512E-2*FL))**0.3333333  
WOC=3.8512E-2*FL*LO**4/(E*I)  
ROI=0.5*WOC/LO  
WRITE (6,*) WOC,ROI  
DO 111 II=1,100  
L=LO+1000.0*II-1000.0  
WC=3.8512E-2*FL*L**4/(E*I)  
L2=2.0*L  
WRITE (6,*) WC,L2  
DO 1111 JJ=1,2  
R1=0.0  
Z1=(SIN(4.4934-4.4934*LO/L))/(L/LO-1.0)  
Z2=(SIN(4.4934+4.4934*LO/L))/(L/LO+1.0)  
Z3=2.0*SIN(4.4934*LO/L)  
Z=((Z1+Z2)/COS(4.4934)-Z3)/CCS(4.4934)  
IF (JJ.EQ.2) GOTO 55  
P=20.19*E*I/L**2  
GOTO 555  
55  CONTINUE  
LL=LC+200.0  
IF (L.LI.LL) GOTO 44  
P=(20.19*E*I/L**2)*(1.0-(LC/L)**2*Z/151.2)  
GOTO 444  
44  CONTINUE  
P=0.4*20.19*E*I/L**2  
R=0.0  
GOTO 2002  
444  CONTINUE  
555  CONTINUE  
C  
C  NON-LINEAR ITERATIVE ALGORITHM  
C  
1001 CONTINUE  
JO=2.045E-3*(FL/(E*I))**2*LC**7
```

```

J=2.045E-3*(FL/(E*1))**2*L**7
IF (JJ.EQ.2) GOTO 66
US=(R1*L)/(A*E)-0.5*J
GOTO 666
66  CONTINUE
US=(R1*L)/(A*E)-0.5*(J-JC)
666 CONTINUE
IF (US.LT.30.0) GOTO 77
R=(2.0*FA*A*E*(-1.0/CA-US))**0.5
GOTO 777
77  CONTINUE
R=(2.0*FA*A*E*( (EXP(CA*US)-1.0)/CA-US))**0.5
777 CONTINUE
R2=ABS(E-R1)
IF (R2.LT.100.0) GOTO 2002
R1=0.5*(R+R1)
GOTO 1001
2002 CONTINUE
ICO=10
IF (JJ.EQ.2) GOTO 2004
LOC=0.0
2004 CONTINUE
BM=0.27752*FL*(I**2-LOC**2)
BS=P/A+BM*RA/I
T=(P+R)/(E*A*AL)
WRITE (6,*) P,R,T,BS
1111 CONTINUE
IF (L.GT.75100.0) GOTO 3003
WRITE (6,33)
33  FORMAT (//)
111 CONTINUE
3003 CONTINUE
STOP
END

```

# APPENDIX IV

## NOTATION

$a_i$	Unprescribed coefficient
$c$	Geotechnical parameter
$d$	Pipe diameter
$f_A$	Axial friction parameter
$f_L$	Lateral friction parameter
$f_M$	Submerged self-weight parameter
$k_1-k_6$	Constants in Table 3.1
$p$	Pressure
$q$	Submerged self-weight of pipeline per unit length
$r$	Pipe radius
$t$	Wall thickness of pipe
$u$	Axial displacement of the pipe
$u, x$	$du/dx$
$u, xx$	$d^2u/dx^2$
$u, z$	$du/dz$
$u, zz$	$d^2u/dz^2$
$u_a$	Tensile extension of the pipe
$u_f$	Compressive flexural end shortening of the buckle
$u_L$	Overall axial shortening
$u_s$	Resultant longitudinal movement at buckle/slip length interface
$u_\phi$	Fully mobilised axial displacement
$\bar{u}$	Flexurally induced end shortening

$v$	Vertical displacement of the pipe
$v, x$	$dv/dx$
$v, xm$	Maximum slope of vertical buckle
$v, xx$	$d^2v/dx^2$
$v, xxx$	$d^3v/dx^3$
$v, xxxx$	$d^4v/dx^4$
$v_m$	Maximum vertical amplitude of the buckled pipe
$v_{mm}$	Vertical buckle amplitude at $T_{min}$
$v_{ms}$	Post-buckling vertical amplitude at state S
$v_o$	Vertical displacement of the imperfection topology
$v_{om}$	Maximum vertical amplitude of the imperfection topology
$w, w_1, w_2$	Lateral displacements of the pipe
$w, x$	$dw/dx$
$w, xm$	Maximum slope of lateral buckle
$w, xx$	$d^2w/dx^2$
$w, xxx$	$d^3w/dx^3$
$w, xxxx$	$d^4w/dx^4$
$w_m$	Maximum lateral amplitude of the buckled pipe
$w_{mm}$	Lateral buckle amplitude at $T_{min}$
$w_{ms}$	Post-buckling lateral amplitude at state S
$w_o$	Lateral displacement of the imperfection topology
$w_{om}$	Maximum lateral amplitude of the imperfection topology

$w_\phi$	Fully mobilised lateral displacement
$x$	Spatial coordinate
$z$	Spatial coordinate
$A$	Cross-sectional area
$C_x$	Axial compression of pipe element
$C_{x'x}$	$dC_x/dx$
$E$	Young's modulus
$E_s$	Secant modulus
$E_t$	Initial tangent modulus
$\bar{E}$	Interface configuration (entrenched)
$F$	Shear force
$F'_{x'}$	$dF/dx$
$F_A$	Resultant axial friction force
$I$	Second moment of area of cross-section
$L, L_1, L_2$	Buckle lengths
$L_0, L'_0$	Buckle lengths of the imperfection topology
$L_s$	Slip length
$M$	Bending moment
$M'_{x'}$	$dM/dx$
$M_m$	Maximum bending moment
$P$	Buckling force
$P_a$	Axial force component
$P_c$	Critical buckling force
$P_o$	Pre-buckling axial force
$P_s$	Post-buckling axial force at state S
$\bar{P}$	Interface configuration (compacted)

$\bar{R}$	Interface configuration (resting)
T	Temperature rise
$T_c$	Critical temperature rise
$T_m$	Maximum temperature rise
$T_{min}$	Minimum safe temperature rise
$T_p$	Permissible temperature rise
$T_s$	Temperature rise at state S, $T_s = T_c$
$T_y$	Temperature rise at first yield
U	Generalised strain energy
V	Total potential energy
W	External potential work done
Z	Section modulus
$\alpha$	Coefficient of linear thermal expansion
$\delta_A$	Theoretical axial friction locus coefficient
$\delta_L$	Theoretical lateral friction locus coefficient
$\epsilon$	Free axial strain
$\theta$	Horizontal angle between the direction of pull and an axis normal to the pipe centreline
$\nu$	Poisson's ratio
$\sigma_A$	Axial stress
$\sigma_b$	Maximum bearing stress
$\sigma_m$	Maximum compressive stress
$\sigma_y$	Yield stress
$\phi$	Generalised friction coefficient
$\phi_A$	Axial friction coefficient
$\phi_L$	Lateral friction coefficient

## APPENDIX V

### REFERENCES

- (1) JINSI, B.K. 'Collapse and buckling-strength considerations are pinpointed for offshore pipeline design.' Oil and Gas Journal, 3 May 1982, 217-227.
- (2) BROWN, R.J. 'A more stable platform for deep, rough water pipelaying.' Pipe Line Industry, Dec 1973, 37-39.
- (3) BROWN, R.J. 'Application of aerospace systems for improving pipe laying in deep rough waters.' Oil and Gas Journal, 14 Oct 1974, 71-74, 79-80.
- (4) TIMMERMANS, W.J. 'Deepwater pipelaying techniques improve.' Oil and Gas Journal, 4 Nov 1974, 83-88.
- (5) BROWN, R.J. 'New methods needed for deepwater pipe-laying.' Oil and Gas Journal, 29 Aug 1977, 58-61.
- (6) BROWN, R.J. 'How deep should an offshore line be buried for protection?' Oil and Gas Journal, 11 Oct 1971, 90-98.

- (7) EWING, R.C. 'Seabed crawler to bury pipelines laid on sea bottom.' Oil and Gas Journal, 22 July 1974, 50-51.
- (8) STEVENINCK, J.V. 'Pipeline burial by fluidisation.' 7th Offshore Technology Conference, OTC 2276, 1975, 313-314.
- (9) MORTENSEN, P. and FREDSOE, J. 'Natural backfilling of pipeline trenches.' 10th Offshore Technology Conference, OTC 3073, Vol I, 1978, 225-232.
- (10) BROWN, R.J. 'Examining new burial methods.' Offshore, April 1978, 68-75.
- (11) WILHOIT, J.C. Jr. and MERWIN, J.E. 'Pipe stresses induced in laying offshore pipelines.' Transactions of the American Society of Mechanical Engineers, Journal of Engineering for Industry, 89, 1967, 37-43.
- (12) PALMER, A.C., HUTCHINSON, G. and ELLIS, J.W. 'Configuration of submarine pipelines during laying operations.' Transactions of the American Society of Mechanical Engineers, Journal of Engineering for Industry, 96, 1974, 1112-1118.

- (13) GIANESSI, F., JURINA, L. and MAIER, G.  
'Optimal excavation profile for a pipeline  
freely resting on the sea floor.' Engineering  
Structures, Vol 1, No 2, London, England,  
Jan 1979, 81-91.
- (14) MAIER, G. and ANDREUZZI, F. 'Elastic and  
elasto-plastic analysis of submarine pipelines  
as unilateral contact problems.' Computer and  
Structures, Vol 8, London, England, May 1978,  
421-432.
- (15) MOUSSELLI, A.H. 'Pipe stresses at the  
sea bed during installation and trenching  
operations.' Presented at the May 2-5, 1977,  
9th Annual Offshore Technology Conference,  
held at Houston, Texas.
- (16) HOBBS, R.E. 'The lifting of pipelines for  
repair of modification.' Proceedings of the  
Institution of Civil Engineers, Part 2, 67,  
Dec 1979, 1003-1013.
- (17) PALMER, A.C. and MARTIN, J.H. 'Buckle  
propagation in submarine pipelines.' Nature,  
254, March 1975, 46-48.

- (18) HOBBS, R.E. 'A beam bending problem with a free boundary.' Computers and Structures, Vol 10, London, England, Dec 1979, 915-920.
- (19) HOBBS, R.E. 'Solutions for pipeline tie-in and repair problems.' Proceedings Second Symposium on Offshore Mechanics and Arctic Engineering, American Society of Mechanical Engineers, Houston, Texas, 1983, 538-552.
- (20) HOBBS, R.E. 'Pipeline buckling caused by axial loads.' Journal of Constructional Steel Research, Vol 1, No 2, Jan 1981, 2-10.
- (21) TAYLOR, N. and GAN, A.B. 'Regarding the buckling of pipelines subject to axial loading.' Journal of Constructional Steel Research, Vol 4, Jan 1984, 45-50.
- (22) TODD, J.D. 'Structural Theory and Analysis.' Macmillan, 1974.
- (23) TAYLOR, N. and HIRST, P.B. 'Regarding flexural curvature.' Proceedings of the Institution of Civil Engineers, Part 2, 77, 1984, 399-400.
- (24) COATES, R.C., COUTIE, M.G. and KONG, F.K. 'Structural Analysis.' Nelson, 1975.

- (25) THOMPSON, J.M.T. and HUNT, G.W. 'A General Theory of Elastic Stability.' Wiley, 1973.
- (26) THOMPSON, J.M.T. 'Instabilities and Catastrophes in Science and Engineering.' Wiley, 1982.
- (27) THOM, R. 'Structural Stability and Morphogenesis.' Translated from the French by D.H. Fowler, Benjamin, Reading, 1975.
- (28) TIMOSHENKO, S.P. and GERE, J.M. 'Theory of Elastic Stability.' 2nd Edition, McGraw-Hill, Kogakusha, New York, 1961, 76-81.
- (29) WALKER, A.C. 'Interactive buckling of structural components.' Science Programme, Oxford, 62, 1975, 579-597.
- (30) KERR, A.D. 'A model study for vertical track buckling.' High Speed Ground Transportation Journal, Vol 7, No 3, 1973, 351-368.
- (31) KERR, A.D. 'On the stability of the railroad track in the vertical plane.' Rail International, No 2, Feb 1974, 131-142.
- (32) KERR, A.D. 'Analysis of thermal track buckling in the lateral plane.' Acta Mechanica, 30, 1978, 17-50.

- (33) KERR, A.D. 'On thermal buckling of straight railroad tracks and the effect of track length on the track response.' Rail International, Sep 1979, 759-768.
- (34) KERR, A.D. 'The effect of lateral resistance on track buckling analyses.' Rail International, Jan 1976, 30-38.
- (35) EL-AINI, Y.M. 'Effect of foundation stiffness on track buckling.' Proceedings of the American Society of Civil Engineers, Journal of the Engineering Mechanics Division, 102, EM3, 1976, 531-545.
- (36) MAREK, P.J. and DANIELS, J.H. 'Behaviour of continuous crane rails.' Proceedings of the American Society of Civil Engineers, Journal of the Structural Division, ST4, 1971, 1081-1095.
- (37) GRANSTRÖM, A. 'Behaviour of continuous crane rails.' Proceedings of the American Society of Civil Engineers, Journal of the Structural Division, ST1, 1972, 360-361.
- (38) TVERGAARD, V. and NEEDLEMAN, A. 'On localized thermal track buckling.' International Journal of Mechanical Science, Vol 23, No 10, 1981, 577-587.

- (39) KERR, A.D. 'Lateral buckling of railroad tracks due to constrained thermal expansions - A critical survey.' Railroad Track Mechanics and Technology, Proceedings of a symposium, A.D. Kerr Editor, Pergamon Press, 1975.
- (40) NUMATA, M. 'Buckling strength of continuous welded rail.' Bulletin International Railway Congress Association, English Edition, Jan 1960, 33-49.
- (41) KERR, A.D. 'Thermal buckling of straight tracks; fundamentals, analyses, and preventive measures.' Bulletin 669 - American Railway Engineering Association 80, 1978, 16-47.
- (42) KERR, A.D. and EL-AINI, Y. 'Determination of admissible temperature increases to prevent vertical track buckling.' Journal of Applied Mechanics, 45(3), 1978, 565-573.
- (43) KERR, A.D. 'An improved analysis for thermal track buckling.' International Journal of Non-Linear Mechanics, Vol 15, 1980, 99-114.
- (44) NUMATA, H. 'Buckling strength of rails.' Journal for Research in Railroad Technology, Japan, Nr. 7, 8, 9, 1957.

- (45) MARTINET, A. 'Flambement des voies sans joints sur ballast et rails de grande longueur. (Buckling of the jointless track on ballast and very long rails. - in French)' Revue Générale des Chemins de Fer, No 10, 1936, 212-230.
- (46) CASE, J. and CHILVER, A.H. 'Strength of Materials and Structures.' Edward Arnold, 2nd Edition, 1971, 100-103.
- (47) KERR, A.D. 'On the derivation of well posed boundary value problems in structural mechanics.' International Journal of Solids and Structures, Vol 12, 1976, 1-11.
- (48) KERR, A.D. 'On the unbonded contact between elastic and elastic-rigid media.' Acta Mechanica.
- (49) BREBBIA, C.A. 'The Boundary Element Method for Engineers.' Pentech Press, 2nd Edition, 1980, 6-45.
- (50) HOBBS, R.E. 'In-service buckling of heated pipelines.' Proceedings of the American Society of Civil Engineers, Journal of the Transportation Engineering Division, 110(2), March 1984, 175-189.

- (51) ALLEN, H.G. and BULSON, P.S. 'Background to Buckling.' McGraw-Hill, 1980, 82, 89.
- (52) LYONS, C.G. 'Soil resistance to lateral sliding of marine pipelines.' 5th Offshore Technology Conference, OTC 1876, Vol II, 1973, 479-484.
- (53) GULHATI, S.K., VENKATAPPARAO, G. and VARADARAJAN, A. 'Positional stability of submarine pipelines.' I.G.S. Conference on Geotechnical Engineering, Vol I, 1978, 430-434.
- (54) ANAND, S. and AGARWAL, S.L. 'Field and laboratory studies for evaluating submarine pipeline frictional resistance.' Transaction of the American Society of Civil Engineers, Journal of Energy Resources Technology, Vol 103, Sep 1981, 250-254.
- (55) AGARWAL, S.L. and MALHOTRA, A.K. 'Frictional resistance for submarine pipelines in soft clays.' I.G.S. Conference on Geotechnical Engineering, Vol I, 1978, 373-379.
- (56) GHAZZALY, O.I. and LIM, S.J. 'Experimental investigation of pipeline stability in very soft clay.' 7th Offshore Technology Conference, OTC 2277, Vol II, 1975, 315-326.

- (57) WANTLAND, G.M., O'NEILL, M.W., REESE, L.C. and KALAJIAN, E.H. 'Lateral stability of pipelines in clay.' 11th Offshore Technology Conference, OTC 3477, 1979, 1025-1034.
- (58) KARAL, K. 'Lateral stability of submarine pipelines.' 9th Offshore Technology Conference, OTC 2967, Vol IV, 1977, 71-78.
- (59) BJERRUM, L. 'Geotechnical problems involved in foundations of structures in the North Sea.' Geotechnique 23, No 3, 1973, 319-358.
- (60) BOWLES, J.E. 'Foundation Analysis and Design.' 3rd Edition, McGraw-Hill, 1982, 28,60,66,67, 188,189.
- (61) HOBBS, R.E. 'Soil modulus and longitudinal pipeline stresses.' Proceedings of the American Society of Civil Engineers, Journal of the Transportation Engineering Division, 106, TE6, Nov 1980, 775-786.
- (62) TAYLOR, N., RICHARDSON, D. and GAN, A.B. 'On submarine pipeline frictional characteristics in the presence of buckling.' Proceedings of the 4th International Symposium on Offshore Mechanics and Arctic Engineering, American Society of Mechanical Engineers, Dallas, Texas, 17-21 Feb 1985, 508-515.

(63) TAYLOR, N. and GAN, A.B. 'A refined modelling for the lateral buckling of submarine pipelines.' Journal of Constructional Steel Research. (Accepted for publication.)